Decision-Making for Utility Scale Photovoltaic Systems:

Probabilistic Risk Assessment Models for Corrosion of Structural Elements

and a Material Selection Approach for Polymeric Components

by

Abbas Chokor

A Dissertation Presented in Partial Fulfillment
of the Requirements for the Degree
Doctor of Philosophy

Approved April 2017 by the
Graduate Supervisory Committee:

Mounir El Asmar, Chair
Oswald Chong
James Ernzen

ARIZONA STATE UNIVERSITY

May 2017

ABSTRACT

The solar energy sector has been growing rapidly over the past decade. Growth in renewable electricity generation using photovoltaic (PV) systems is accompanied by an increased awareness of the fault conditions developing during the operational lifetime of these systems. While the annual energy losses caused by faults in PV systems could reach up to 18.9% of their total capacity, emerging technologies and models are driving for greater efficiency to assure the reliability of a product under its actual application. The objectives of this dissertation consist of (1) reviewing the state of the art and practice of prognostics and health management for the Direct Current (DC) side of photovoltaic systems; (2) assessing the corrosion of the driven posts supporting PV structures in utility scale plants; and (3) assessing the probabilistic risk associated with the failure of polymeric materials that are used in tracker and fixed tilt systems.

As photovoltaic systems age under relatively harsh and changing environmental conditions, several potential fault conditions can develop during the operational lifetime including corrosion of supporting structures and failures of polymeric materials. The ability to accurately predict the remaining useful life of photovoltaic systems is critical for plants ‘continuous operation. This research contributes to the body of knowledge of PV systems reliability by: (1) developing a meta-model of the expected service life of mounting structures; (2) creating decision frameworks and tools to support practitioners in mitigating risks; (3) and supporting material selection for fielded and future photovoltaic systems. The newly developed frameworks were validated by a global solar company.

ACKNOWLEDGMENTS

This research would not have been possible without the dedication and support of many people. First and foremost, I am thankful to my advisor, Dr. Mounir El Asmar, who guided me throughout my studies at Arizona State University. He has set an example of excellence as a researcher, mentor, and instructor. I am also very grateful to my committee members Drs. Oswald Chong and James Ernzen for their enthusiasm, guidance, and support. Collectively, their passion for education and academic research challenged me to pursue my research interests.

The work on this dissertation is the result of collaboration with many industry leaders and researchers. I gratefully acknowledge the funding received towards my PhD from First Solar, Inc. Many thanks to First Solar's Chief Commercial Officer – Georges Antoun – and Chief Operations Officer – Tymen DeJong – for sponsoring this research. I was privileged to work with Sumanth Lokanath and Azmat Siddiqi who were always ready to provide assistance when I faced challenges. Bryan Skarbek, Ferdinand Abella, and Andy Anderson provided all types of support throughout this journey.

I was very fortunate to be a member of the π-DEAS research team at ASU. I am particularly grateful for the numerous times the team members have reviewed my work and provided valuable suggestions; they have been phenomenal colleagues. Finally, I would like to acknowledge my family and friends for being my foundation of compassion, understanding, and courage. You each vicariously lived this journey with me and without you it would not have been half as much fun. Thank you all for your loving support.

TABLE OF CONTENTS

Page

LIST OF TABLES

Table Page

Table Page

Table Page

Table Page

LIST OF FIGURES

Figure Page

Figure Page

GLOSSARY

American Galvanization Association	AGA
American Society for Testing and Materials	ASTM
American Association of State Highway and Transportation Officials	AASHTO
American Water Works Association	AWWA
Arc-fault circuit interrupters	AFCI
Arizona State University	ASU
Artificial neural networks	ANN
California Department of Transportation	Caltrans
Capacitance	C
Chlorinated Polyethylene	CPE
Coefficient of determination	R^2
Corrosion current	I_{corr}
Corrosion potential	E_{corr}
Corrosion rate	CR
Current-Voltage	I-V
Differential thermal analysis	DTA
Direct Current	DC
Engineering, Procurement, and Construction	EPC
Ethylene Propylene Diene Monomers	EPDM
Ethylene propylene rubber	EPR
Equipment Grounding Conductor	EGC
Estimated service life	ESL
Ethylene vinyl acetate	EVA
Factor analysis	FA
Fault detection and diagnostics	FDD
Fault Tree Analysis	FTA
Federal Highway Administration	FHWA

Fourier transform infrared spectroscopy	FTIR
Gigawatts	GW
Ground fault protection devices	GFPD
High-density crosslinked polyethylene	XLPE
High-density polyethylene	HDPE
Inductance	L
International Organization for Standardization	ISO
Low-Density Polyethylene	LDPE
Magnesium chloride	$MgCl_2$
Maximum Likelihood Estimation	MLE
Millivolts	mV
Mils per year	mpy
National Association of Corrosion Engineers	NACE
National Bureau of Standards	NBS
National Cooperative Highway Research Program	NCHRP
National Electrical Code®	NEC
National Institute of Standards and Technology	NIST
New York State Department of Transportation	NYSDOT
Operations and Maintenance	O&M
Overcurrent protection devices	OCPD
Parts per million	ppm
Photovoltaic	PV
Principal Component Analysis	PCA
Polychlorotrifluoroethylene	PCTFE
Polyethylene	PE
Polypropylene	PP
Polystyrene	PS
Polyurethane	PUR
Polytetrafluoroethylene	PTFE

Polyvinyl Chloride	PVC
Prognostics and health management	PHM
Quality Assurance	QA
Quality Check	QC
Remaining useful life	RUL
Resistance	R
Return on Investment	ROI
Sodium chloride	NaCl
Temperature-relative humidity complex	T-RH complex
Thermal volatilization analysis	TVA
Thermogravimetric analysis	TG
Thermoplastic elastomers	TPE
Time of wetness	TOW
Total Cost of Ownership	TCO
Ultraviolet	UV
US Department of Agriculture	USDA

CHAPTER 1

INTRODUCTION

1.1. BACKGROUND

The solar energy sector has been growing rapidly over the past decade. In 2015, the U.S. installed 7.6 Gigawatts (GW) of solar generation facilities to reach 27.4 GW of total installed capacity, enough to power 5.4 million American homes (Zhou 2015). As the global energy demands increase, the photovoltaic PV industry is expected to continue to grow due to several factors such as the falling prices of silicon and PV modules, technological advancements in large scale manufacturing, many governmental incentives, maturation and proliferation of favorable interconnection agreements and continued technological improvement of power converter technologies (Obi and Bass 2016). While the annual energy losses caused by faults in those PV systems could reach up to 18.9% of their total capacity (Firth et al. 2010), emerging technologies and models are driving for greater efficiency to assure the reliability of these products under actual application conditions.

Fault detection and diagnostics (FDD) can help detect faults in systems and diagnose their reasons. Alongside FDD, failure prognostics is another area of research to predict performance over the remaining life and the eventual failure of systems. Together, FDD and failure prognostics methods make up Prognostics and health management PHM approaches, which link studies of failure mechanisms to system lifecycle management. PHM uses information to allow early detection of impending or incipient faults, remaining useful life (RUL) calculations, and logistical decision-making based on predictions. It aims to maximize the system return on investment (ROI) by optimizing

scheduled maintenance, predictive condition based maintenance, and non-predictive condition based maintenance to an operational objective (Pecht and Jaai 2010; Chokor et al. 2016).

As PV systems age under relatively harsh and changing environmental conditions, several potential fault conditions can develop during their operational lifetime. While some of these faults are expected, including the module degradation due to corrosion and failure of polymeric materials, other faults are catastrophic and unexpected such as ground faults, line-to-line faults, and arc faults resulting in electrical fires (Ancuta and Cepisca 2011; Alam et al. 2015). Various configurations and structures exist for PV systems, and different physics-based and data-driven monitoring models have been developed in previous studies.

First, degradation of driven posts due to corrosion is a major concern for many industries, including the solar industry. While it may seem easy to examine above-ground corrosion, driven posts are exposed to complex and infinitely variable external environments and are usually not readily accessible for inspection without pulling them over and affecting their ability to support the PV system. Above-ground corrosion, also known as the atmospheric corrosion, refers to the corrosive action that occurs on the surface of a metal in an atmospheric environment. It occurs when the surface is wet by moisture formed due to rain, fog, and condensation. Atmospheric corrosion is a complex process involving a large number of interacting and constantly varying factors, such as weather conditions, air pollutants, material conditions, etc. (Pierre 2008). The combined effect of these factors results in a great variations in corrosion rates.

Being less predictable than atmospheric corrosion, underground corrosion depends on the soil characteristics that can vary significantly within a single site. Soil corrosion, a complex phenomenon with a multitude of involved variables (Galvanizeit 2016), is a geologic hazard that affects buried metals and concrete that is in direct contact with soil or bedrock. Corrosive soils contain chemical constituents that can react with construction materials, which may damage foundations and buried structures. The electrochemical corrosion processes that take place on metal surfaces in soils occur in the groundwater that is in contact with the corroding structure (Wan et al. 2013). While the effects of corrosive soil can cause structural failure and financial burden, mitigating measures taken into account during design and construction, as well as an understanding of the corrosive potential in a particular soil, can minimize these issues.

Second, the long-term reliability of PV system components is highly affected by the degradation behavior of the polymeric components within the module, such as cables, module clips rubber, and connectors used in the tracker and fixed tilt systems. The degradation represents a change in the polymer properties, such as: tensile strength, shape, color, etc. Given the complexity of polymeric material composition and the different conditions of processing, storage and use, the types and mechanisms of polymer degradation are diverse (Emanuel and Buchachenko 1987). Multiple factors can lead to polymers degradation including Ultraviolet (UV) light, humidity, oxygen, heat, bacteria and stress. However, polymeric materials behave differently towards the acting agents and stresses which impact their stability and durability. As the recognition of polymer degradation improves, conservation guidelines and recommendations are emerging from

the materials selection process during the design phase to the maintenance process later when the polymeric material is in operation.

Along the fast growth of designed and installed PV technologies in different environmental conditions, a continuous progress toward low-cost and high-reliability systems is crucial. In addition to complying with international and local standards, developing predictive models for the failure of PV systems ensures a reliable operation over their intended life. Corrosion of driven posts and degradation of polymeric materials both lead to the failure of PV systems; hence, keeping in view these mechanisms, this dissertation investigates the research gaps, reviews the existing literatures, develops a research method and applies it on the used materials and components in tracker and fixed tilt systems.

1.2. RESEARCH GAPS AND OBJECTIVES

Reviewing the existing literature on predictive degradation models of PV systems shows a great need for prognostic models. The existing models have focused on the degradation of PV modules, without addressing the posts' corrosion and polymers degradation, which are equally important assets that are crucial for the plant operation. Moreover, different types of materials in PV systems require different studies. Knowing that the design life of PV systems is usually around 25 years, the availability of skilled feedback and real performance data over long periods highlights the opportunity to test such models in the future. Such data is also generally not publicly available, and solutions to address gaps for shared data streams are also needed. The large discrepancy between the existing models and the real measured values of estimated service life (ESL) presents a series of interesting research questions:

1. What is the state of the art and practice of prognostics and health management for the Direct Current (DC) side of photovoltaic systems? What are the current challenges and opportunities?
2. How to best assess the ESL of driven posts supporting PV structures?
3. How to choose the best polymeric materials for the different PV components?

The contributions of this research include answering these questions for the focused scope of materials used in tracker and fixed tilt systems, as illustrated in Figure 1 below. The primary objectives of this dissertation are to assess the probabilistic risk associated with the failure of driven posts associated with underground and above-ground corrosion, and to inform the selection of polymeric materials used as part of PV solar energy plants.

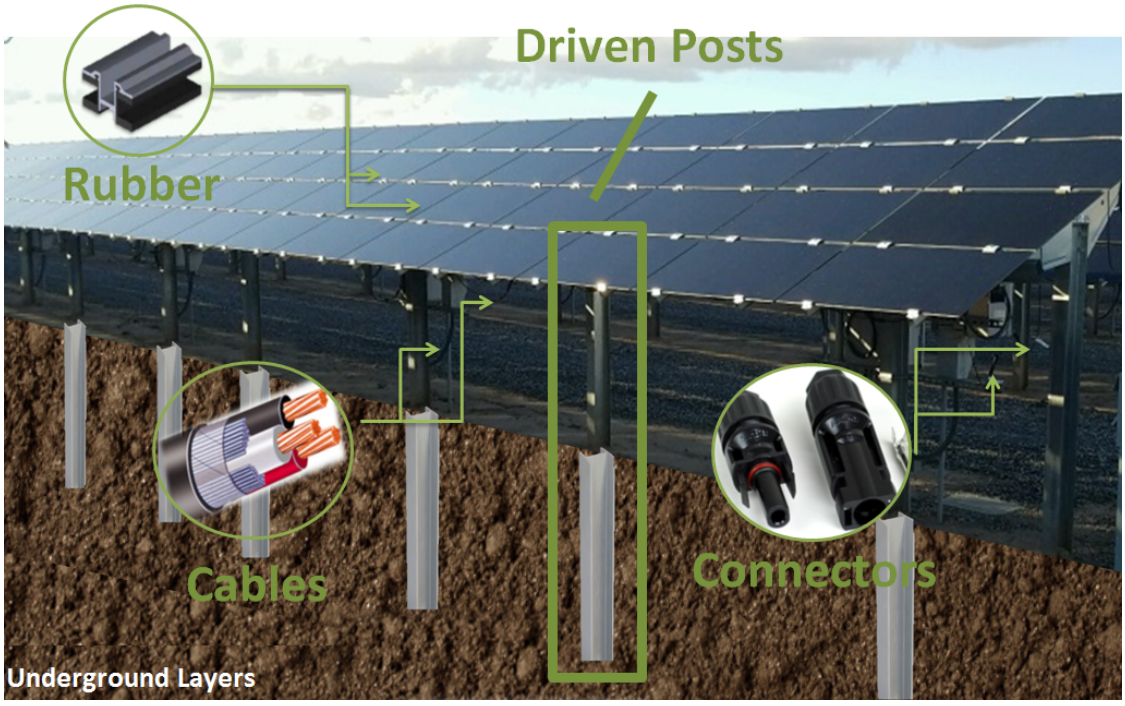

Figure 1. Research Scope: Driven Posts (Addressed in Chapter 3) and Cables, Connectors, and Rubber (Addressed in Chapter 4)

1.3. RESEARCH APPROACH

The research approach consists of three phases as shown in Figure 2. Next, each phase is introduced and discussed individually.

Research Phases	Contributions to the Body of Knowledge
Phase A: Literature Review • Classifying the different failure modes in the DC side of PV systems • Summarizing the main approaches for fault detection, diagnostics and prognostics	• Emphasizing the key research gaps and challenges in the current practice • Highlighting the available opportunities through a comprehensive understanding of the photovoltaic systems' current performance • Providing motivation for the following phases
Phase B: Corrosion Assessment of Driven Posts Supporting PV Structures • Investigating the factors affecting the corrosivity rate of a site • Conducting meta-analysis of corrosion modeling to highlight the current methods and practices to predict: - Underground corrosion rate - Above-ground corrosion rate • Developing new models based on the collected data from various sites to evaluate the corrosion rate and estimated service life of mounting structures	• Showing a noticeable discrepancy between the prediction of existing models and the real measured values of corrosion rates (CR). • Demonstrating the superiority of the newly developed approach, compared to existing methods, in predicting zinc and steel underground corrosion rates • Developing a comprehensive framework and tool to inform and support decision-makers in design and reliability applications • Providing several recommendations to improve the implementation of current practices and mitigate the risk associated with the corrosion of driven posts supporting PV structures
Phase C: Probabilistic Risk Assessment of Polymeric Materials Used in PV Systems • Investigating the factors affecting the degradation of polymeric materials • Conducting a meta-analysis of polymeric degradation modeling to highlight the current methods and practices for cables, connectors, and rubber insulation • Developing a decision framework to assist in the polymeric materials selection for the studied components	• Conducting a fault tree analysis to define the root cause failure factors and developing inspection checklists for each component • Ranking the different polymeric materials based on their cost, availability, and suitability against the acting stresses and the environment • Developing a comprehensive framework and tool to inform and support decision-makers in polymeric materials selection • Providing several recommendations to improve the implementation of current practices and highlighting future opportunities to mitigate the risk associated with the failure of polymeric materials.

Figure 2. Research Phases and Contributions

1.3.1. Phase A: Literature Review

Phase A reviews and discusses the array of PHM methods in the DC side of PV systems. Following a review of the photovoltaic industry's current status, the study classifies the different failure modes and outlines the corresponding approaches for fault detection, diagnostics and prognostics. This review paves the way to emphasize the key research gaps and challenges in the current practice. The available opportunities are also highlighted through a comprehensive understanding of the photovoltaic systems' current performance. Scholars and decision makers can use this review to integrate improvement strategies with promising directions for future research and practice. The findings of this first phase provide the motivation for the following phases. Out of the several identified factors that can lead to failures in photovoltaic plants infrastructure, this dissertation addresses the degradation of mounting systems due to corrosion, and the failure of polymeric materials, which continue to pose major challenges for practitioners.

1.3.2. Phase B: Corrosion Assessment of Driven Posts Supporting PV Structures

The objective of Phase B is to assess the corrosion of driven posts supporting PV panels. First, this phase details the factors affecting the corrosivity rate of a site. Second, a complete meta-analysis of corrosion modeling highlights the current methods and practices used in the industry to predict underground and above-ground corrosion rates. The research approach consists of developing a framework that integrates all the existing and applicable corrosion models in addition to newly-developed models based on the collected data to evaluate the corrosion rates and estimated service lives of assets.

Applying the underground corrosion models on current sites shows a noticeable discrepancy between the prediction of existing models and the real measured values of

corrosion rates. The results demonstrate the superiority of the newly developed approach, compared to existing methods, in predicting zinc and steel underground corrosion rates. The proposed approach is found to work best in highly corrosive environments.

1.3.3. Phase C: Probabilistic Risk Assessment of Polymeric Materials Used in PV Systems

Phase C investigates the probabilistic risk associated with the failure of polymeric materials that are used in tracker and fixed tilt systems. The long-term reliability of a photovoltaic module is highly affected by the degradation behavior of the polymeric components, such as cables, module clips rubber insulation, and connectors. After understanding the current practices and designs, this chapter details the factors and degradation modes leading to the failure of polymeric materials. Then, conducting a meta-analysis of polymeric degradation modeling and decision frameworks led to ranking the different polymeric materials based on their cost, availability, and suitability against the acting stresses and environments. Moreover, the research develops a comprehensive framework and tool to inform and support decision-makers in polymeric materials selection, and highlights future opportunities to mitigate the risk associated with the failure of polymeric materials. The identified factors are also used to develop inspection checklists for the different components at various lifecycle stages.

1.4. DISSERTATION FORMAT

The dissertation is organized around a line of work containing three connected studies. Each of the three subsequent chapters represents a stand-alone research phase. Therefore, each chapter will have its own abstract, introduction, objectives, methodology, findings, and conclusions.

A review of the state of the art and practice of PHM for the DC side of PV systems along the relevant challenges and opportunities is presented in Chapter 2, which showcases Phase A of the study. Then, Chapter 3 presents Phase B of the study. The chapter provides an in-depth investigation of the corrosion of driven posts supporting PV structures. Chapter 4, Phase C of the dissertation, assesses the probabilistic risk associated with the failure of polymeric materials that are used in tracker and fixed tilt systems.

The dissertation concludes with Chapter 5, which summarizes the overall contributions of this work to both theory and practice, and recommends a direction for future research. Following Chapter 5 are Appendices A (National Bureau of Standards (NBS) data analysis), B (sample size calculation), C (zinc quality analysis), and D (suppliers data).

CHAPTER 2

A REVIEW OF PHOTOVOLTAIC DC SYSTEMS PROGNOSTICS AND HEALTH MANAGEMENT: CHALLENGES AND OPPORTUNITIES

2.1. ABSTRACT

The surge in renewable electricity generation using PV systems was accompanied by an increased awareness of the fault conditions developing during the operational lifetime. Fault detection, diagnostics, and prognostics are such efforts to detect and classify a fault so the system operational expectations can be managed. Trending of the faults and prognostics also aid to evaluate expected remaining useful life so that mitigation actions can be evaluated and implemented. This chapter aims to review the state of the art and practice of PHM for the DC side of PV systems. Following a review of the PV industry current status, the study describes and classifies the different failure modes. Next, it summarizes the PV faults detection, diagnostics and prognostics approaches. A review of the PHM applications for PV systems paves the way to emphasize the key research gaps and challenges in the current practice. The available opportunities are also highlighted through a comprehensive understanding of the PV systems current performance, from where scholars and decision makers can integrate improvement strategies with promising directions for future research and practices

2.2. INTRODUCTION

The solar energy sector has been growing rapidly over the past decade. In 2015, the U.S. installed 7.6 GW of solar generation facilities to reach 27.4 GW of total installed capacity, enough to power 5.4 million American homes (Zhou 2015). As the global energy demand increases, the PV industry is expected to continue to grow due to several

factors such as the falling prices of PV modules and balance of systems, technological advancements in large scale manufacturing, many governmental incentives, maturation and proliferation of favorable interconnection agreements and continued technological improvement of power converter technologies (Obi and Bass 2016). While the annual energy losses caused by faults in those PV systems could reach up to 18.9% of their total capacity (Firth et al. 2010), emerging technologies and models are driving for greater efficiency to assure the reliability of a product under its actual application conditions.

FDD can help detecting faults in systems and diagnose their reasons. Alongside FDD, failure Prognostics is another area of research to predict the performance over the remaining life and the eventual failure of systems in the future. Together, FDD and failure prognostics methods make up PHM approaches. PHM methods provide numerous advantages, such as: (i) advance time-to-failure prediction; (ii) minimized unscheduled maintenance, extended maintenance cycles, effectiveness through timely repair actions; (iii) reduced life-cycle costs by decreasing downtime, inventory and refurbishment and; (iv) improved qualification and assistance in the design and logistical support of fielded and future systems (Pecht and Jaai 2010).

A typical grid-connected PV system mainly consists of a PV array, a grid-connected inverter, connection wiring, and protection devices, such as overcurrent protection devices (OCPD) and ground fault protection devices (GFPD). Figure 3 illustrates the setup of a simple PV system. Faults in PV systems damage the PV system components, as well as lead to electrical shock hazards and fire risk. For instance, two fire hazards caused by ground faults and line-line faults, respectively, in PV arrays have been demonstrated in case studies of a large PV power plant in California, US (Collier

and Key 1988). Additionally power inverters are ranked among the most critical components within PV systems whose faults affect the system performance and availability (Kaushik and Golnas 2011).

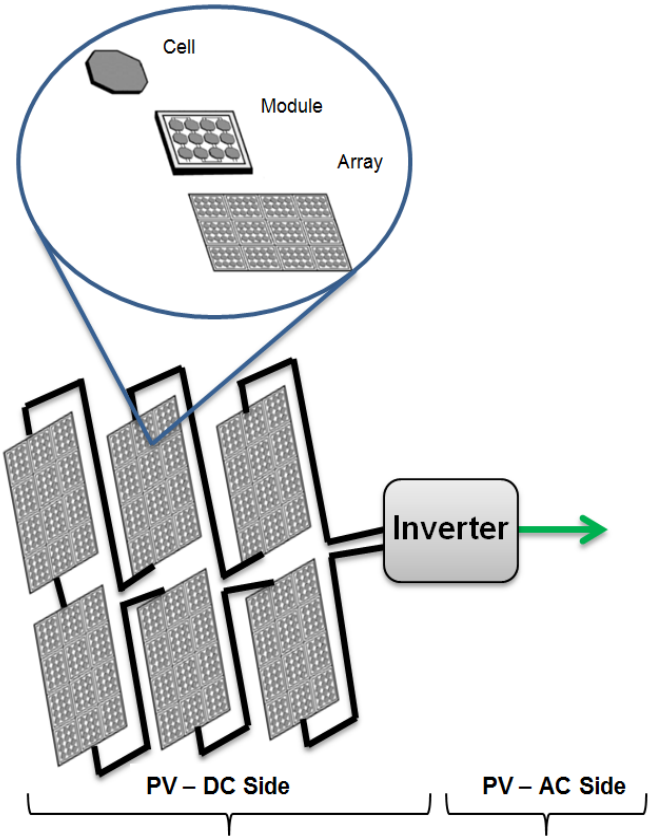

Figure 3. A Solar Photovoltaic System

This chapter reviews and discusses the array of PHM methods in the DC side of PV systems. Section 3 presents a comprehensive review of PV DC system failure modes. Such failure modes are also classified based on the system components between modules and cables. Section 4 describes the different physics-based and data-driven models used in the detection and diagnostics of PV DC side's failure. Section 5 presents the prognostics models used to estimate the RUL of PV DC systems based on the specific failure mechanisms. Section 6 outlines the key research gaps, challenges in the current

practice, as well as the opportunities for future studies. Finally, section 7 summarizes this review of the state of the art in PHM for the DC side of PV systems.

2.3. FAILURE MODES IN PV SYSTEMS

This section reviews the main failure modes occurring in the PV DC systems for discrete outdoor exposed components such as PV modules and cables. These components are expected to last the lifetime of the system by design. Failure modes for sub-assemblies or sub systems such as inverters or trackers are not covered. A description of the fault mechanism is presented below for PV modules and cables.

2.3.1. PV Module

Every type of PV module has variable characteristics inevitably caused by process variation; the optimal current and voltage will not be the same for each module in an array at a given point in time. These variations have the effect of reducing the output of the array, since the current and voltage of a module are constrained by the array's electrical configuration (Spertino and Akilimali 2009). Module mismatch causes each module to operate at a suboptimal point on the Current-Voltage (I-V) curve, reducing the array's power output (Manganiello et al. 2015). I-V mismatches are grouped, according to the causes, as permanent or temporary. Permanent mismatch is due to the effects of changes in one or more parameters of the PV module, such as the value of parallel resistance and/or series resistance (Sharma and Dalal 2015). In addition to the manufacturing tolerance, module degradation, hot spot, and bubbles mainly cause permanent mismatches. Temporary mismatches are affected by the temporal changes in the irradiance level received by PV modules (Katiraei and Agüero 2011). Such changes include cloud effects, soiling, snow covering, leaf and bird droppings, and the shading

from nearby PV arrays and structures. A review of the failure mechanisms occurring in the module level is presented below.

2.3.1.1.Degradation

The degradation and aging of a PV module is a continuous process, but several factors can influence its dynamics (Manganiello et al. 2015). In particular, environmental factors such as Sulphur, acidic fumes, or other pollutants can speed up the degradation process (Skoczek et al. 2009). The main degradation types taking place in PV modules are as follows:

- Discoloration: is the browning and yellowing of PV cells, mainly caused by the degradation of the ethylene vinyl acetate (EVA) encapsulant (Kaplani 2012). The main reasons of EVA degradation are UV rays combined with water under temperatures higher than 50 °C (Oreski and Wallner 2010). The changes in the color of the encapsulant material produce a variation of the transmittance of the light reaching the solar cells and, as a consequence, a reduction of the power generated (Skoczek et al. 2009; Jeong and Park 2013).
- Delamination: is defined as the breakdown of the bonds between material layers that constitute a module laminate. Delamination interrupts efficient heat dissipation and increases the possibility of reverse-bias cell heating (Quintana et al. 2002). The main causes of delamination are the movement of cells and cell interconnects due to environmental stresses, the expansion and the contraction of moisture and air that are trapped inside the layers of a PV module, the bond failure due to the combination of moisture and UV radiation, the cell overheating, and the consequent outgassing of the encapsulant (Dumas and Shumka 1982). In

addition, physical aging processes related to the application of high temperatures could provoke delamination of a PV module (Oreski and Wallner 2010).

- Cracking: is a common problem encountered in PV modules. It may develop in different stages of the module lifetime; however, it occurs in most of the cases during installation, maintenance, and especially during the transportation of modules to their sites (Wohlgemuth and Kurtz 2011). In addition, cracking is affected by the high-temperature thermal stresses of a cell and thermal cycling induced thermomechanical stresses (Dumas and Shumka 1982), mechanical loads due to wind (pressure and vibrations) and snow (pressure) (Cristaldi et al. 2014).
- Corrosion: attacks the metallic connection of PV cells causing a loss of performance by increasing leakage currents. The moisture that enters the module through the laminate edges mainly causes corrosion (Kempe 2005). The corrosion of the conductive parts of the cells and the interconnections through the encapsulant is responsible for the deterioration of the PV module (Ndiaye et al. 2013), which results in the increase of the series resistance and the decrease of the parallel resistance of the PV electrical model (Saly et al. 2002).

2.3.1.2.Hot Spot

The short-circuit current and the open circuit voltage are imposed by the PV cell showing the lowest electrical performance respectively in series and parallel montage. In short circuit conditions, when a PV cell is defective, its voltage is reversed and becomes equal and opposite to the voltage of the other cells in series. This defective cell becomes both a load for other cells and a place of a relatively high thermal dissipation constituting thus a hot spot (Rauschenbach and Maiden 1972). A hot spot is an area of a PV module that has

a very high temperature that could damage a cell or any other element of the module. It occurs in a PV module when the current capability of a particular cell or cells is lower than the operating current of the cell string. Over time, hot spots will permanently degrade the PV panels and decrease the overall performance of the PV plant (Molenbroek et al. 1991).

2.3.1.3.Bubbles

The bubbles are mainly due to the chemical reactions that emit gases trapped in the PV module. They form an air chamber in which the gas temperature is lower than in the adjacent cells. However, the air chamber worsens the heat dissipation capability of the nearby cell so that the latter overheats and therefore exhibits a temperature that is higher than in the adjacent cells (Ndiaye et al. 2013). Moreover, when bubbles appear on the front side, a reduction of the radiation reaching the PV cell occurs, thus creating a decoupling of light and increasing the reflection. Furthermore, bubbles can break, and can damage the back sealing surface that provokes humidity ingress (Kaplani 2012).

2.3.1.4.Shading and Soiling

Shading, the total or partial blockage of sunlight from a PV module surface, can bring serious concern in PV arrays (Quaschning and Hanitsch 1996; Nguyen and Lehman 2006; Patel and Agarwal 2008). This blockage can be caused by a number of different reasons, like shade from the building itself, light posts, trees, dirt, snow and other light blocking obstacles (Ancuta and Cepisca 2011). Shading causes large performance drops and can even damage modules if not properly controlled. Module soiling is the build-up of dirt on the surface of a PV module (Braun et al. 2012). Researchers have found that the effects of soiling are relatively small (2.3% loss of power) for directly incident light but

become more significant for larger angles: an 8.1% loss was observed in a soiled module when light is incident from an angle of 56° (Hammond et al. 1997). An experimental investigation on the reduction of PV output efficiency showed that the reduction of efficiency reached up to 11.6% when the dust deposition density was fixed at about 8 g/m^2 (Jiang et al. 2011). In addition, a single dust storm can reduce the output power by 20% and a reduction of 50% could be experienced if no cleaning is performed on modules for long time that exceeds six months (Adinoyi and Said 2013). The local soil and environmental conditions are key factors for severity impact.

2.3.2. Cabling

Cables are vital parts of a PV array. Similar to the rest of the PV system, cables are subjected to thermal, mechanical and external loads (Kalogirou and Tripanagnostopoulos 2007). Though the selection of cables is an important procedure, cable terminations and cables management thereafter can influence how the entire PV system will function. Three major catastrophic failure modes are common in the cabling of PV systems: ground faults, line-line faults, and arc faults.

2.3.2.1. Ground Faults

A ground failure mode occurs when the circuit develops an unintentional path to ground. This results in lowered output voltage and power, and can be fatal if the leakage currents are running through a person (Braun et al. 2012). If a ground fault remains undetected, it may generate a DC arc within the fault and cause a fire hazard (Alam et al. 2015). Previous research (Bower and Wiles 1994; Zhao et al. 2011) investigated the potential reasons that can lead to ground faults, and classified them into four categories:

- Cable insulation damage during the installation, due to aging, impact damage, water leakage, and corrosion;
- Ground fault within the PV modules (e.g., degraded sealant and water ingress);
- Insulation damage of cables due to chewing done by rodents and termites; and
- Accidental short circuit inside the PV source circuit combiners, often at the time of maintenance.

2.3.2.2.Line-Line Faults

A line-to-line failure mode in a PV system is defined as an unintentional connection between two points in a PV panel through a low resistance path (Zhao et al. 2011). However, if one of the points is on the equipment grounding conductor (EGC), the line-to-line fault is considered as a ground fault. A line-to-line fault may occur between two points on the same string or between two adjacent strings. The magnitude of the line-to-line fault current depends on the potential difference between the points before the fault occurs. The higher the potential difference, the higher the back feed current results, and the chance of tripping the OCPDs increases (Zhao et al. 2011; Johnson et al. 2011). Several studies (Gokmen et al. 2012; Zhao et al. 2013) summarize the reasons behind line-to-line faults in PV arrays as follows:

- Insulation failure of cables, i.e. UV degradation, animal chewing through cable insulation;
- Incidental short circuit between current carrying conductors, i.e. a nail driven through unprotected wirings; and

- Line-line faults within the DC junction box, which are caused by mechanical damage, water ingress or corrosion.

2.3.2.3.Arc Faults

Arc failure mode establishes a current path in the air, and this current path might be established due to any discontinuity in the current carrying conductors or insulation breakdown in adjacent current carrying conductors (Alam et al. 2013). Any type of arc fault is harmful for the PV system, and may introduce fire that may result in insulation burn-out and fire hazards in presence of any flammable substances in the vicinity of the PV plant (Johnson et al. 2011). The National Electrical Code (NEC)-2011 requires a series arc-fault protection device in a PV system if the DC operating voltage is equal to or higher than 80V. These devices are called as Arc-fault circuit interrupters (AFCIs) (Schimpf and Norum 2009). The causes of arc faults depend on their types, whether they are series or parallel. Series arc fault reasons include degradation in solder joints, wiring or connections inside the junction box, loosening of screws, and increased operating temperature that may result in thermal stress, leading to accelerated aging or complete disconnection (Hastings et al. 2011; Flicker and Johnson 2013). In addition to series arc-fault reasons, parallel arc faults can result from insulation damage due to mechanical damage, aging, or wildlife (Dini et al. 2011).

2.4.FAULT DETECTION AND DIAGNOSTICS METHODS IN THE DC SIDE OF PV SYSTEMS

This section presents a review of existing fault detection and classification methods in the DC side of PV modules and cables. The findings are presented in Table 1, summarizing

the fault detection models, measured system parameters, and the techniques used to validate the models.

Table 1. Fault Detection Models, Measured System Parameters, and Validation Techniques in the DC Side of PV Systems

References	Data-Driven Models									Physics-based Models					Measurement Devices							Validation	
	Regression	Decision Tree	Bayesian Networks	KNN Classification	Artificial Neural Networks	Support Vector Machines	Fuzzy Mathematics	Clustering	Graph based	Difference Calculation	Adjacent Comparison	Energy Loss	Heat Exchange and Temperature	External Devices	Current	Voltage	Irradiance	Temperature	Meteorological	Pulse generator	LCR Meter	Simulated	Experimental
Stellbogen (1993)										x					x	x	x	x				x	
Schirone et al. (1994)														x						x			x
Takashima et al. (2006)														x						x	x		x
Drews et al. (2007)												x			x	x	x	x	x			x	x
Chao et al. (2008)										x					x	x	x	x				x	
Takashima et al. (2008a)														x							x		x
Takashima et al. (2008b)														x						x			x
Vergura et al. (2008)												x			x	x						x	x
Zhiqiang and Li (2009)											x				x	x						x	
Houssein et al. (2010)										x					x	x	x	x				x	
Firth et al. (2010)												x			x	x	x	x					x
Chouder and Silvestre (2010)		x													x	x			x			x	x
Polo et al. (2010)												x			x	x			x			x	x
Xu et al. (2011)											x				x	x						x	
Zhao et al. (2011)										x					x	x						x	x

References	Data-Driven Models									Physics-based Models					Measurement Devices							Validation	
	Regression	Decision Tree	Bayesian Networks	KNN Classification	Artificial Neural Networks	Support Vector Machines	Fuzzy Mathematics	Clustering	Graph based	Difference Calculation	Adjacent Comparison	Energy Loss	Heat Exchange and Temperature	External Devices	Current	Voltage	Irradiance	Temperature	Meteorological	Pulse generator	LCR Meter	Simulated	Experimental
Syafaruddin and Karatepe (2011)				x											x	x	x	x				x	
Coleman and Zalweski (2011)			x												x	x	x	x				x	
Cheng et al. (2011)							x								x	x	x	x				x	
Ducange et al. (2011)							x								x	x	x	x				x	
Lin et al. (2012)										x					x	x	x	x				x	
Braun et al. (2012)										x					x	x						x	
Li et al. (2012)													x		x	x		x				x	
Zhao et al. (2012)		x													x	x	x	x				x	x
Braun et al. (2012)				x	x	x									x	x		x				x	
Zhao et al. (2013)										x					x							x	x
Gokmen et al. (2013)										x						x		x				x	x
Hu et al. (2013)													x		x	x		x				x	x
Solórzano and Egido (2013)												x			x	x						x	x
Ndiaye et al. (2013)										x					x	x	x	x				x	
Nilsson (2014)								x							x	x						x	x
Phinikarides et al. (2014)	x																						
Cristaldi et al. (2014)										x					x	x	x	x				x	
Zhao et al. (2015)									x						x	x	x	x				x	x
Jiang and Maskell (2015)					x												x	x				x	
Hare et al. (2016)				x	x	x	x			x													

The PV DC side fault detection and classification methods based on the type and method of measurement data can be classified into two main categories: physics-based models and data-driven models. Although most of the presented methods can be used for the different types of faults, some of them are more effective for specific system components.

2.4.1. Physics-based Models

Physics-based models employ system specific mechanistic knowledge, defect growth formulas, and condition monitoring data to detect and diagnose the faults (Heng et al. 2009). Five major FDD physics-based approaches for the DC side of PV systems are presented below.

2.4.1.1.Difference Calculation

This approach quantifies the difference between expected and measured current, voltage, or power. It is based on determining the expected values of PV parameters in varying environmental conditions and comparing real-time measurements with these expected values. This approach usually sets thresholds below or above where any fault signals arise both in modules and cables. For instance, in (Chao et al. 2008), an extended correlation function is used to identify faults between branches of the PV system. In (Braun et al. 2012), a statistical outlier detection method is employed. In (Gokmen et al. 2012), the expected output voltage value for different MPP is calculated and is used as a reference value for fault detection.

2.4.1.2.Adjacent Comparison

This approach uses the differences between measurements from adjacent strings as a reference to detect faults in PV cables, including ground, line-line, and arc faults. An

example of this method is a study by (Zhao et al. 2013), where statistical outlier detection methods such as Hampel Identifier, 3-sigma, and Box plot are used to identify the normal-operating PV strings by comparing all the individual string current measurements.

2.4.1.3.Energy Loss

This approach is based on the energy losses in the PV system. The fault detection and diagnostics are done based on the rate of energy losses in the PV system due to degradation, shading, and soiling. For instance, in (Drews et al. 2007), energy loss analysis based on monitored data from grid-connected PV systems and satellite-derived meteorological data is proposed. In (Chouder and Silvestre 2010) and (Silvestre et al. 2013), captured losses in a PV system, current, and voltage ratios are used for the fault-detection algorithm.

2.4.1.4.Heat Exchange and Temperature

Knowing that the PV module temperature changes in case of faults, this approach uses the heat exchange and module temperature during the faulted condition to detect and diagnose the faults, mainly due to hotspots as well as cables failure (Hu et al. 2013). For example, in (Vergura et al. 2008), using finite element methods, the physical defects of different types of PV cells are modeled based on the thermal behavior of the PV cells resulting from electrical faults.

2.4.1.5.External Devices

This method uses external devices such as signal generators, and LCR [inductance (L), capacitance (C), and resistance (R)] meters for most fault detection (Takashima et al.

2006). The response of the PV system to the injected signals is analyzed to detect and/or classify the type of faults in PV systems.

2.4.2. Data-Driven Models

This method uses machine-learning methods for fault detection and classification by analyzing the characteristics of streamed data. Machine-learning algorithms are used to learn the relation between some input and output parameters of the PV system and subsequently use the trained models to detect and classify faults.

Therefore, defining an appropriate threshold that is able to detect several types of faults in different conditions is a difficult task. However, training the model with input–output data helps overcoming the limitation of defining thresholds and aids in the detection and classification of faults. Some of the machine-learning techniques used by scholars for the DC side of PV systems are: modified artificial neural networks (ANN) with the extension theory (Chao 2010), evidence theory and Fuzzy mathematics (Cheng et al. 2011), TSK-FRBS Fuzzy estimator (Ducange et al. 2011), Bayesian belief networks (Coleman and Zalewski 2011), three-layered ANN (Katiraei and Agüero 2011), decision tree-based method (Zhao et al. 2012), and graph-based semi-supervised learning (Zhao et al. 2013). Although some techniques are preferred to detect a specific type of fault over the other, research of data-driven models is an ongoing task.

2.5. PROGNOSTICS METHODS IN THE DC SIDE OF PV SYSTEMS

This section presents a review of prognostics methods in the DC side of PV systems, which are used to estimate the RUL of such systems based on the specific failure mechanisms predominant in the module construction. Knowing that some of these models are stochastic, others are based on assumptions that emphasize a well-determined

factor, such as: radiation, temperature, and humidity. Although degradation models of PV systems are still few and further developments are needed, the main approaches found in the literature are summarized below.

2.5.1. Degradation Models

Several models were developed to estimate the degradation rate of solar modules and therefore their RUL. Vazquez and Ignacio (2008) found the module power *P* to be an indicator for the performance of the system. Moreover, their study identified the degradation of a PV to be relative to its initial power P_0. Such assumptions recall previous models that were developed to estimate the degradation of PV modules. From one side, some studies (Osterwald et al. 2003; Marion and Adelstein 2003; Raghuraman et al. 2006) considered P to decrease linearly in time:

$$\mu(t) = P_0 - At$$

where $\mu(t)$ and *A* are the average power at time t and the annual decrease in power, respectively. From the other side, other studies (Chuang et al. 1997; Xie and Pecht 2003) assumed the degradation rate to be exponential as a function of time:

$$\mu(t) = P_0 e^{-\alpha t}$$

where $\alpha = A/P_0$ is the annual degradation rate. Although these models estimate the PV module degradation over its lifetime, they are limited by many assumptions that do not consider the variation in weather conditions and relevant factors. Pan et al. (2011) proposed a degradation model of the PV module output power given by:

$$D(t) = 1 - e^{-b.t^a}$$

where a and b are parameters of the degradation model, that can be determined from accelerated testing (Charki et al. 2013). Knowing that such parameters change according

to the studied degradation mode (i.e., discoloration, delamination, corrosion, etc.), the overall degradation of the PV module is estimated as:

$$D_{PVmodule}(t) = 1 - \prod_{i=1}^{n}\left(1 - D_i(t)\right)$$

where $D_{PVmodule}(t)$ is the overall degradation of the PV module at time t, $D_i(t)$ is the mode i degradation at time t, and n is the number of considered degradation modes. One main limitation presented in this model is the dependency on the accelerated tests to determine *a* and *b*. For instance, Wohlgemuth and Kurtz (2011) have determined these parameters from damp heat tests assuming a temperature *T* of 85 °C and relative humidity *RH* of 85%. The study found $a_{corrosion}$ = 3.0868 and $b_{corrosion}$ = 5762.10^{-12}. Knowing that different temperature and humidity can lead to different results, the accuracy of this model is highly related to the test design.

2.5.2. UV Radiation Model

UV radiation is a major factor for the degradation of PV materials exposed to direct sunlight (Kojima and Yanagisawa 2004; Oreski and Wallner 2009; Wohlgemuth and Kurtz 2011). This is relevant for module constructions using an encapsulant between the glass and the PV cells. This degradation appears in the change of the encapsulating module transmittance that reflects a reduction in the PV module current and voltage. Zimmerman (2008) quantifies the UV degradation of PV module by:

$$D(t) = 1 - b_{cmx}.\ln(1 + a_{cmx}ct)$$

where a_{cmx} and b_{cmx} are parameters of material used for PV cell and c = $\int_{\lambda=0}^{\lambda=400} T_{cmx}(\lambda)P(\lambda)d\lambda$with $T_{cmx}(\lambda)$ the transmittance of the glass slide of PV cell, $P(\lambda)$ the spectral power density of the sun, and λ the wavelength belonging to the range

$[\lambda_{min}, \lambda_{max}]$ in which the spectral response of the PV cell is not zero. Yet, the challenge of this model consists of knowing the materials basic characteristics used in the PV cells, which can vary during the production phase.

2.5.3. Temperature Based Model

For temperature dependent processes, the Arrhenius law (Laidler 1984) is one of the most universally used models:

$$K = Ae^{\frac{-E_a}{RT}}$$

Where K is the rate constant of the process, A is an Arrhenius pre-exponential factor, E_a is the apparent activation energy, R is the gas constant, and T is the sample temperature. Cocca et al. (2011) used that law to develop a temperature based model predict the increase in rate resulting from an increase in temperature in PV modules:

$$AF_T = \frac{K1}{K2} = e^{\frac{E_a}{RT}(\frac{1}{T_2} - \frac{1}{T_1})}$$

where AF_T is the acceleration factor for thermal degradation (ratio of rate constants), K_1 and K_2 are the rate constants of the process at t_1 and t_2 respectively, and T_1 and T_2 are the sample temperatures at t_1 and t_2 respectively. Though this model can be used to quantify the effect of varying temperature and irradiance on the rate of PV module degradation, it does not provide the long-term degradation of PV modules or consider other factors including moisture, time of wetness, airborne pollutants and salinity, and electricity production.

2.5.4. Temperature and Humidity Based Model

The Peck model defines the acceleration of degradation with the capacity to take into account temperature and relative humidity (Escobar and Meeker 2006):

$$\tau = A.RH^{n}.e^{\frac{-E_a}{kT}}$$

where *Ea* is the effective activation energy of the degradation process; k is the Boltzmann's constant (=8.617.10-5 eV/°K), and A and n are two constants dependent on the failure mode. Later, Charki et al. (2013) developed an equation for acceleration factor for thermal and humidity degradation:

$$AF_{(T,RH)} = e^{n.\ln\left(\frac{RH}{RH0}\right) - \frac{E_a}{k}\left(\frac{1}{T} - \frac{1}{T0}\right)}$$

where $AF_{(T,RH)}$ is the acceleration factor for thermal and humidity degradation and RH_0 and T_0 are the relative humidity and temperature in the reference conditions. Although that model takes into account the effect of temperature and humidity on the degradation of PV module, its parameters are dependent on the design of the accelerated test. Defining the reference conditions for the temperature and relative humidity present some limits for the model.

2.6. RESEARCH GAPS AND CHALLENGES

While research in PHM for the DC side of PV systems active is ongoing, most of the previous work investigated the FDD in these systems. However, the endeavor to design and properly control a PV system to ensure it lifetime and reliability underline several challenges and technical gaps.

Although some of the reviewed FDD models are effective and reliable, almost all of them require the installation of external sensors to collect data. Further research is needed to determine the sensitivity, resolution, frequency and location of these sensors that might impose additional cost. Uncertainty in the collected data highly affects the uncertainty of FDD models. Studies investigating the sources of uncertainties and their

propagations through the whole system are needed. Moreover, the literature reveals a limited number of studies applying data-driven models. Future research can incorporate such models with the physics-based models to develop hybrid models.

A review of the literature shows the prognostics models of PV systems to be poorly studied by scholars and researchers. The reviewed models have solely studied the degradation of the PV modules. While additional studies and research are needed, cabling termination and connector degradation models are equally important and crucial. Moreover, different types of materials in PV systems require different studies. Another challenge for the development of PHM models is their verification and validation using experimental data. Knowing that the design life of PV systems is usually more than 30 years, the availability of experience feedback and real performance data over long periods highlights the opportunity to test such models in the future. Such data is also generally not publicly available and solutions to address gaps for shared and clean data streams are also needed.

Solar technologies are still evolving and new materials are being discovered to produce reliable and efficient systems. The surge of such technologies continues to challenge the researchers in developing new models and integrating them with operations and management planning and control. Accordingly, future studies can benefit from PHM models by developing online frameworks and algorithms to automatically detect and diagnose a fault and also predict the system RUL.

The importance and usefulness of PHM to inform decision-makers within time and different operational limitations requires an assessment for the ROI of PHM activities. A major gap that exists in the literature is a comprehensive assessment of the

additional costs that can be associated with the PHM models integration. Moreover, future studies that can support the decision-makers in selecting between different types of PHM and determining whether to adopt PHM versus more traditional maintenance approaches are crucial.

2.7. CONCLUSIONS

PHM applications are essential for the reliability of PV systems by facilitating condition based maintenance and minimization of cascading failures. This study provided an overview of the different types of failure modes in the DC side of PV system. Next, it summarized the PV fault detection, diagnostics and prognostics approaches. The presented methods presented showed the different approaches documented in literature to address the faults in the DC side of PV systems. However, depending on the monitoring technology, communication infrastructure, availability of physical models, and measured data, some solution approaches may perform better than the others due to the difference in the problem formulation. Through the integration of fault detection, diagnostics, and prognostics, future PV systems will possess the ability to sustain the power generation while increasing the reliability and resiliency of the system itself. A review of the PHM applications for PV systems paved the way to emphasize the key research gaps and challenges in the current practice as well as the available opportunities. Future studies are invited to fill the identified gaps by: (1) determining the parameters, location, resolution and precision of required sensors in the PV systems; (2) developing and testing new data-driven models; (3) generating new prognostics models for the different parts and materials of PV systems; (4) verifying and validating the developed models using experimental data; (5) designing online frameworks and algorithms to implement the

PHM models; and (6) assisting the decision-makers in their investigation of the ROI for PHM activities.

CHAPTER 3

CORROSION ASSESSMENT OF DRIVEN POSTS SUPPORTING PV STRUCTURES

3.1. ABSTRACT

Corrosion can lead to failures in solar PV plant infrastructure. Decisions regarding the future integrity of a structure or its components depend in large part on an accurate assessment of the site environment and conditions affecting its corrosion and rate of degradation. The objective of this research project is to curate the available approaches and identify the optimal approach to assess the corrosion of driven posts that are used in tracker and fixed tilt systems. As a result, this chapter develops a framework to inform and support decision-makers in design and reliability applications.

First, this chapter details the factors affecting the corrosivity rate of a site. Second, a complete meta-analysis of corrosion modeling, as it applies to PV solar support structures, highlights the current methods and practices used in industry to predict underground and above-ground corrosion rates. The research approach consists of developing a framework that integrates all the existing and applicable corrosion models in addition to newly-developed models based on the collected data to evaluate corrosion rates and estimated service lives of assets (structures).

Applying the underground corrosion models on current sites shows a noticeable discrepancy between the prediction of existing models and the real measured values of corrosion rates. The results demonstrate the superiority of the newly developed approach, compared to existing methods, in predicting zinc and steel underground corrosion rates. However, the application of the developed models is limited to the range of data found on

the available *First Solar* sites. Moreover, the proposed approach is found to work best in highly corrosive environments.

To bolster the proposed decision making framework, the research team provides the following four recommendations:

1. A solar company is recommended to request (and consultants are recommended to include) the critical soil electrochemical data in the commissioned geotechnical studies, in order to help predicting corrosion rates. Specifically, minimum, average, and maximum values of resistivity, pH, redox, chlorides, and sulfates need to be provided to the solar company. To improve the accuracy (and predictive power) of the newly-developed model, site data for a range of 41 to 78 projects are needed. The new data, originating from *First Solar* sites or other sites, should be used to strengthen the model and widen its range of application.
2. A solar company is recommended to continue its internal quality assurance testing and inspection of the 3 mils zinc coating thickness requirement, in compliance with American Society for Testing and Materials (ASTM) A123.
3. In addition to corrosion predictive models, accelerated testing is recommended to simulate underground and above-ground conditions to experimentally quantify the impact of corrosion. Further analysis of the air composition is recommended in specific microenvironments, where industrial emissions can include different types of contaminants boosting the atmospheric corrosivity of the site.
4. To plan for future studies and site monitoring, the study recommends including 5 to 10 additional benchmark/reference posts on each new site. One of these posts

will be unearthed every few years to reliably quantify the losses due to underground corrosion, without impacting operations.

3.2. INTRODUCTION

First Solar, Inc., incorporated on May 15, 2003 is a leading global provider of solar energy solutions. The company is the largest global manufacturer of thin film solar modules and is a vertically integrated PV energy solutions company spanning engineering, procurement, and construction (EPC) as well as operations and maintenance (O&M) operations.

To support the PV panels, *First Solar* uses galvanized steel driven posts as shown in Figure 4 below (First Solar Procurement and Construction Management 2016). As further evidence of *First Solar*'s foresight and leadership in the industry, the company developed an interest in studying the long-term corrosion degradation of driven posts, the most common foundation used for utility-scale PV applications. *First Solar* partnered with Arizona State University (ASU) to research this critical subject and to develop a decision-making framework dedicated to this topic.

Figure 4. First Solar Driven Posts (First Solar Procurement and Construction Management, 2017)

The objective of the research project consists of assessing the corrosion of driven posts that are used in tracker and fixed tilt systems. The scope of the research includes:

- The above-ground corrosion study to assess the atmospheric corrosion rate and the ESL of the driven posts' and PV super structure's zinc coating. The study entails:
  - Reviewing the atmospheric corrosion factors; and
  - Curating all the relevant models and methods.
- The underground corrosion study to evaluate the underground corrosion rate and the ESL of driven posts. The research steps include:
  - Summarizing the underground corrosion factors;
  - Gathering corrosion data;
  - Developing a meta-model based on the literature corrosion assessment methods for zinc coating and steel; and
  - Testing the model on various *First Solar* sites.

Posts have been widely used in a variety of oil and gas, marine, and construction applications. While they are made from a variety of materials, such as concrete and timber, steel posts are very common, due to their workability, strength and relatively low cost. Steel posts are often driven in undisturbed soils to support downward and lateral forces. In PV power plant applications, steel posts are usually hot-dip galvanized for above and below grade corrosion protection. Although hot dipping is very effective at reducing atmospheric corrosion (Galvanizeit 2016), it remains less effective against some types of soil corrosion.

Figure 5 summarizes the research method, which is thoroughly discussed in this study and implemented in a developed tool (Post Corrosion Assessment Tool (**πCAT**)).

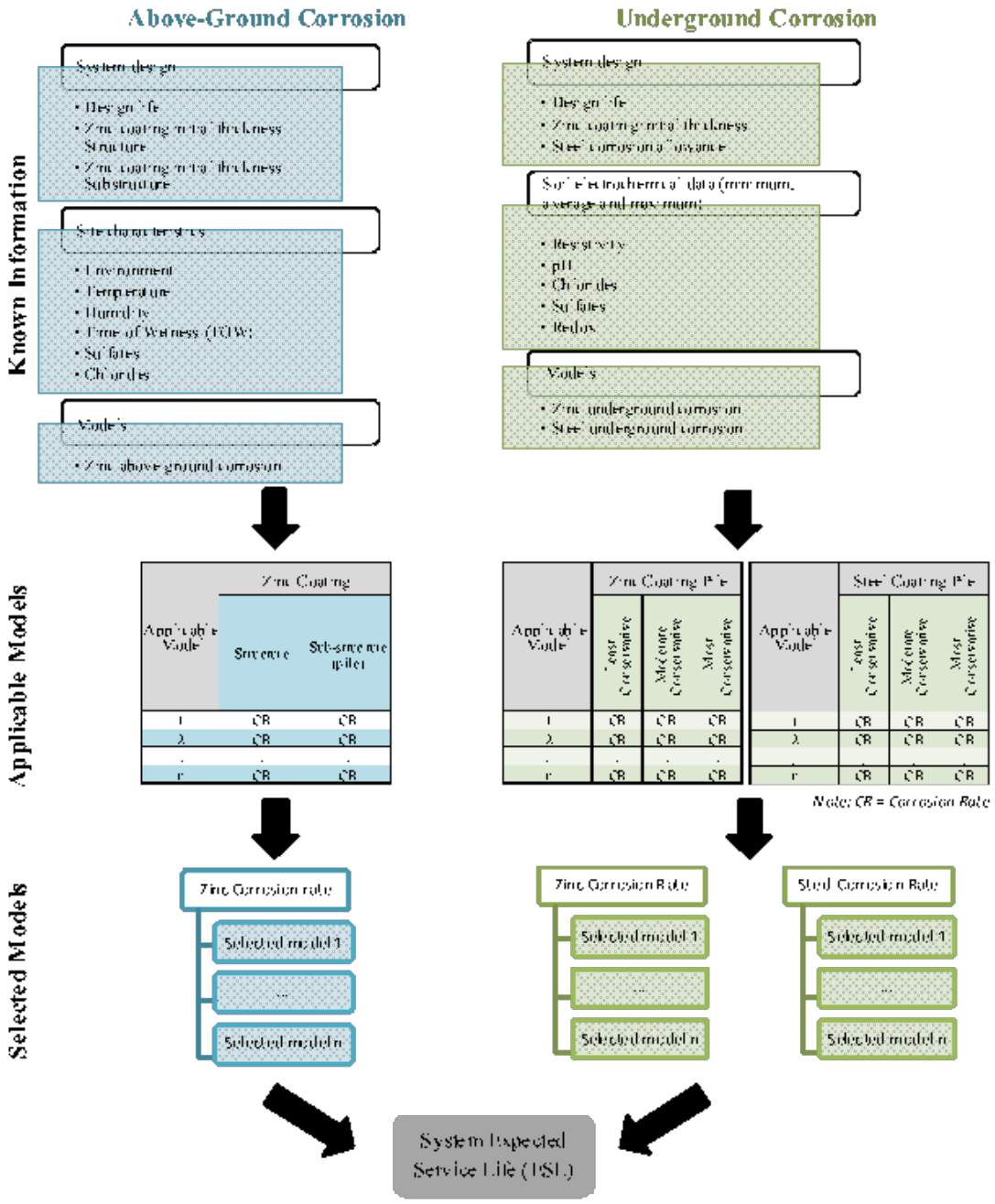

Figure 5. Research Method

First, the above-ground subsystem ESL of a structure is quantified by accounting for the above-ground zinc corrosion rate. Second, the underground subsystem ESL is calculated by adding the ESL of both steel and zinc. Third, the overall system ESL is defined to be the minimum of the underground and the above-ground subsystems ESL values.

This chapter presents a framework to assess the underground and above-ground corrosivity of galvanized steel posts used in different sites with different characteristics. Section 3 of this study describes the above-ground corrosion factors and related zinc corrosion models. Section 4 describes the underground corrosion factors, details the predictive models for zinc and steel, including a newly-developed model based on *First Solar* sites data, and applies the proposed framework on *First Solar* sites. Section 5 summarizes the conclusions, recommendations, and opportunities for future studies.

3.3. ABOVE-GROUND CORROSION

Above-ground corrosion, also known as the atmospheric corrosion, refers to the corrosive action that occurs on the surface of a metal in an atmospheric environment. It occurs when the surface is wet by moisture formed due to rain, fog, and condensation. Atmospheric corrosion is a complex process involving a large number of interacting and constantly varying factors, such as weather conditions, air pollutants, material conditions, etc. (Pierre 2008). The combined effect of these factors results in a great variations in corrosion rates.

Atmospheric corrosion is surely the most visible of all corrosion processes, e.g. rusty bridges, flagpoles, buildings and outdoor monuments. The large segment of the paint industry committed to the manufacture and application of products for the protection of metals, as well as the large-scale operations of the galvanizing industry

attest to the importance of controlling atmospheric corrosion. Economic losses caused by atmospheric corrosion are tremendous and therefore account for the disappearance of a significant portion of metal produced. Consider, for instance, agricultural machinery, steel structures, fences, exposed metals on buildings, automobile mufflers or bodies, and the myriad of other metal items, which are discarded when they become unusable as a result of corrosion. These constitute direct losses from corrosion.

This section describes the above-ground soil corrosion of driven posts. First, it discusses the factors contributing to the atmospheric corrosion. Second, it presents the potential methods used for the assessment and prediction of zinc atmospheric corrosion. Then, it details the proposed meta-model for the evaluation of driven posts underground corrosion.

3.3.1. Above-Ground Corrosion Factors

There are different factors that are essential to atmospheric corrosion. Such factors are the time of wetness including the temperature and the relative humidity, the airborne sulfur dioxide content (Leygraf et al. 2016), and the airborne chloride content (salinity). The following subsections describe the effect of these factors on the atmospheric corrosion rate.

3.3.1.1.Time of Wetness (TOW)

From the fundamental theory, the time of wetness of a corroding surface is a key parameter, directly determining the duration of the electrochemical corrosion processes. This is a complex variable, since all the means of formation and evaporation of the surface electrolyte solution must be considered. Time of wetness is the length of time during which the metal surface is covered by a film of water which renders atmospheric

corrosion possible (Bradford and Bringas 1993). It is influenced by factors such as metal mass, orientation, pollution, temperature, and relative humidity. Cyclic temperature can result in severe metal corrosion in tropical areas, especially in unheated warehouses, objects in plastic bags, metal tools and more. The combination of temperature and relative humidity is described as the Temperature-Relative Humidity (T-RH) complex, which can lead to the calculation of the time of wetness according to the International Organization for Standardization (ISO) 9223-92 (ISO Standard 9223-92 1992). TOW is quantified to sufficient accuracy by the number of hours per year that the relative humidity is above 80 percent for temperatures above 32° F (0° C).

3.3.1.2.Airborne Sulfur Dioxide Content

Sulfur dioxide, a product of the combustion of sulfur-containing fossil fuels, plays an important role in atmospheric corrosion in urban and industrial atmospheres. It is adsorbed on metal surfaces, has a high solubility in water, and tends to form sulfuric acid in the presence of surface moisture films. Sulfuric acid is corrosive to most metals, including zinc and common steels. Sulfur dioxide is usually measured in terms of its concentration in air in units of $\mu g/m^3$. Since it is the SO_2 deposited on the metal surface that affects the corrosion, it is also often measured in terms of deposition rate on the surface in units of $mg/m^2/day$.

3.3.1.3.Airborne Chloride Content

Airborne salinity refers to the content of gaseous and suspended salt in the atmosphere. It is measured by the concentration in the air in units of $\mu g/m^3$ or in terms of deposition rate in units of $mg/m^2/day$. The chloride levels can also be measured in terms of the concentration of the dissolved salt in rainwater. Atmospheric salinity distinctly increases

atmospheric corrosion rates. Apart from the enhanced surface electrolyte formation by hygroscopic salts such as Sodium chloride (NaCl) and Magnesium chloride ($MgCl_2$), direct participation of chloride ions in the electrochemical corrosion reactions is also likely. Metals such as zinc, whose chloride salts tend to be less soluble than those of iron, are less prone to chloride-induced corrosion than are common steels.

There are different factors that are essential to the above-ground corrosion including TOW, airborne sulfur dioxide content, and airborne chloride content. When metals are exposed to the aforementioned factors, above-ground corrosion may take place more rapidly and through various mechanisms. Thus, knowledge on these underlying factors could greatly help in managing corrosion and its harmful effects by providing the required inputs for the above-ground corrosion potential methods. The next section presents the four main approaches to assess the above-ground corrosion of galvanized driven posts.

3.3.2. Potential Methods for the Above-ground Corrosion Assessment

Galvanizing produces a zinc coating on the steel surface and is one of the most popular methods for corrosion protection of steel. This is attributed to the corrosion resistance of zinc coatings, particularly in atmospheric environments. This section describes potential methods for above-ground corrosion assessment of galvanized steel driven posts.

3.3.2.1. Traditional Method – American Galvanization Association

This method, initiated by the American Galvanization Association (AGA) (Galvanizeit 2016), uses a generalized value to represent the corrosion rates in each typical environment. As shown in Figure 6, it provides simplified corrosion life data for five predetermined atmospheric environments.

It can be easily seen that this method provides only a rough and non-specific estimation of product life since it uses only a few fixed values to account for the wide variation of real corrosion rates in one type of environment. For corrosion classification purposes, the AGA divides atmospheres into five groups:

- Industrial environments are generally the most aggressive in terms of corrosion. Air emissions may contain some sulfides and phosphates that cause coating consumption. Automobile, truck and plant exhaust are examples of these emissions. Such environments are: Pocatello, ID; Los Angeles, CA; Chicago, IL; Dallas, TX; New York, NY; and Knoxville, TN.
- Tropical Marine environments are found in climate regions where the temperature rarely, if ever, falls below the freezing point of water. The high humidity in combination with the chlorides in the air from the nearby water makes these climates almost as corrosive as industrial environments. The warmer temperatures of the tropical marine atmosphere raise the activity level of the corrosion elements on the surface of the zinc coating. Other factors that affect marine corrosion rates are wind speed and direction as well as proximity to the coast. Such atmospheres are: Miami, FL; Corpus Christi, TX; San Diego, CA; Cancun, Mexico; and Mazatlán, Mexico.

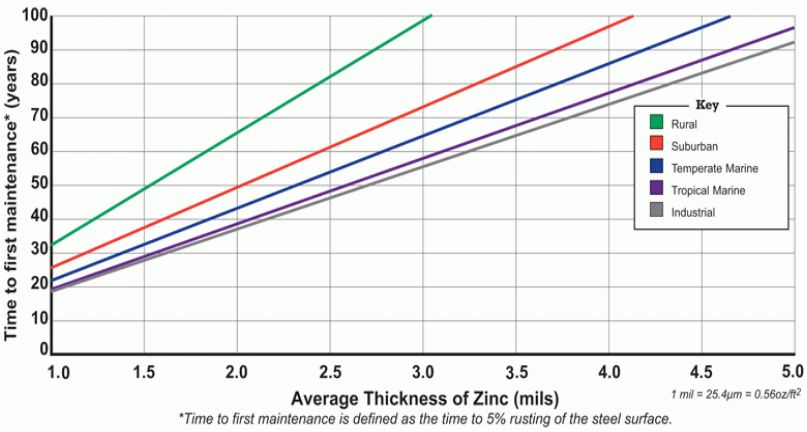

Figure 6. Time to First Maintenance (American Galvanization Association 2011)

- Temperate Marine environments are less corrosive than tropical marine environments due to the lower temperature and humidity levels in the temperate region. However in any marine air, chlorides from sea spray can react with the normally protective corrosion products to form soluble zinc chlorides. When these chlorides are washed away, fresh zinc is exposed to corrosion. Chlorides, wind speed, wind direction, and distance from the sea also affect the corrosion rate of zinc coatings in temperate marine atmospheres. Such environments are: Seattle, WA; San Francisco, CA; Milwaukee, WI; Norfolk, VA; Atlantic City, NJ; and Boston, MA.
- Suburban atmospheres are generally less corrosive than moderately industrial areas. As the term suggests, they are found in the largely residential perimeter communities of urban or city areas with little or no heavy industry. Such environments are: Vallejo, CA; Tucson, AZ; Cedar Rapids, IA; Jackson, MS; Harrisburg, PA; and Columbia, SC.
- Rural atmospheres are the least aggressive of the five types. This is due to the relatively low level of sulfur and other emissions found in such environments, for

instance: Boise, ID; Las Cruces, NM; Fargo, ND; Little Rock, AK; and Macon, GA.

3.3.2.2. Geographic Map Method

In this method, corrosion rates of materials in a geographic area are determined and classified within a grid of sites to map the corrosivity (King 1995). It recognizes the difficulty of using general corrosion rate prediction and attempts to estimate product service life based directly on field data from the service site in question. However, its usefulness is limited to the areas where such mapping is available and there are relatively few regions of the world that have been suitably mapped for this purpose. Figure 7 below shows one such corrosion map of the United States according to a specific company (Fort Pierce Air Conditioning 2016). This map can be used as a high-level approximation, and not to determine the exact corrosivity because the characteristics of the local areas within each region may vary significantly. Therefore, it is used here for illustration purposes but will not be part of the corrosion modeling approach presented later in the study.

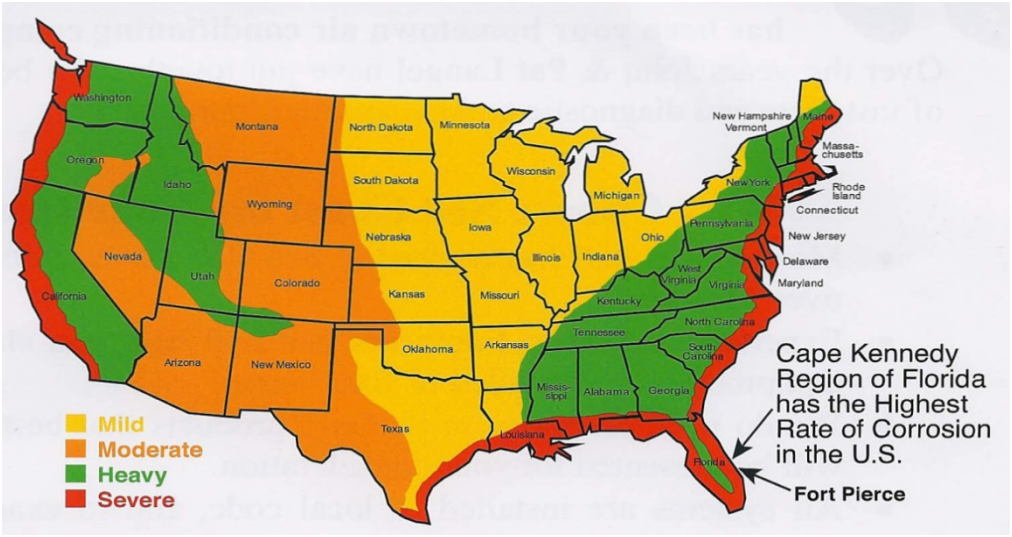

Figure 7. A Corrosion Map of the U.S. (Seacostair 2017)

3.3.2.3.ISO-9223 Method

The ISO-9223 (ISO Standard 9223-92 1992) standard classifies the corrosivity of an atmosphere based on measurements of TOW, and pollution categories, i.e. airborne chlorides and sulfur dioxide. This standard was not intended to be used in extreme service atmospheres such as those within chemical or metallurgical processing facilities or where there is direct contact with salt spray. The ISO-9223 distinguishes the following five environments for the atmospheric corrosivity:

3.3.2.3.1. C1 (Very Low)

The wetting of surfaces is caused by many factors, for example, dew, rainfall, and high humidity levels. The length of time during which the relative humidity is greater than 80 percent at a temperature above 32° F (0° C) is used to calculate the TOW for corroding surfaces. Environments usually classified C1 are the dry or cold zones with very low pollutants contamination and TOW (e.g., desert, Antarctic zone). Moreover, interior heated spaces with low relative humidity and unpolluted atmosphere, such as offices, shops, schools, and hotels are considered within the C1 environment. For a C1 environment:

- The time of wetness is defined as TOW $\leq$ 10 hours per year (h/yr)
- The airborne chloride content or salinity is defined as $S_d \leq 3$ $\mu g/m^3$
- The airborne sulfur dioxide content $P_c \leq 2$ $\mu g/m^3$

Numerical values for initial corrosion rates (CR_i) for the first year of exposure are provided in ISO 9223, Corrosion of metals and alloys – Corrosivity of atmospheres – Classification, determination and estimation. Moreover, numerical values for the average corrosion rate (CR_{avg}) over the first 10 years of exposure are provided in ISO 9224,

Corrosion of Metals and Alloys – Corrosivity of Atmospheres – Guiding Values for the Corrosivity Categories. For a C1 environment, the initial and average corrosion rates of zinc are shown in Table 2.

Table 2. C1 Category (Very Low Corrosive) - Initial and Average Zinc Corrosion Rates [Adapted from (ISO Standard 9223-92 1992)]

Unit	Initial Corrosion	Average Corrosion
$g/(m^2/yr)$	$CR_i \leq 0.70$	$CR_{avg} \leq 0.50$
μm/yr	$CR_i \leq 0.10$	$CR_{avg} \leq 0.07$

3.3.2.3.2. C2 (Low)

Outdoor environments that are classified as C2 include arid and urban inland environments with low pollution. Interior C2 environments represent unheated spaces, which may condense, such as warehouses and gyms. For a C2 environment:

- The time of wetness is defined as $10 < TOW \leq 250$ hours per year (h/yr)
- The airborne chloride content or salinity is defined as $S_d \leq 3$ $\mu g/m^3$
- The airborne sulfur dioxide content $P_c \leq 2$ $\mu g/m^3$

For a C2 environment, the initial and average corrosion rates of zinc are shown in Table 3.

Table 3. C2 Category (Low Corrosive) - Initial and Average Zinc Corrosion Rates [Adapted from (ISO Standard 9223-92 1992)]

Unit	Initial Corrosion	Average Corrosion
$g/(m^2/yr)$	$0.70 < CR_i \leq 5.00$	$0.50 < CR_{avg} \leq 3.50$
μm/yr	$0.10 < CR_i \leq 0.70$	$0.07 < CR_{avg} \leq 0.50$

3.3.2.3.3. C3 (Medium)

Outdoor environments that are classified as C3 include dry, rural areas as well as other regions remote from the coast or sources of pollution. "Remote from the coast" is typically defined as more than 50 kilometers from a body of salt water. C3

environments, however, can extend as close as 1 kilometer from a body of salt water that is relatively sheltered and quiet. Wind velocity and prevailing direction are important factors in classifying C3 environments relative to distance from a body of salt water. Typical areas include arid and rural inland regions and towns. Interior C3 environments are usually classified as the manufacturing spaces with high humidity and low air pollution, such as swimming pools and chemical plants. For a C3 environment:

- The time of wetness is defined as $250 < TOW \leq 2{,}500$ hours per year (h/yr)
- The airborne chloride content or salinity is defined as $3 < S_d \leq 60$ µg/m^3
- The airborne sulfur dioxide content $2 < P_c \leq 5$ µg/m^3

The initial and average corrosion rates of zinc are shown in Table 4.

Table 4. C3 Category (Medium Corrosive) - Initial and Average Zinc Corrosion Rates [Adapted from (ISO Standard 9223-92 1992)]

Unit	Initial Corrosion	Average Corrosion
g/(m^2/yr)	$5.00 < CR_i \leq 15.00$	$3.50 < CR_{avg} \leq 10.00$
µm/yr	$0.70 < CR_i \leq 2.10$	$0.50 < CR_{avg} \leq 1.40$

3.3.2.3.4. C4 (High)

Outdoor environments that are classified as C4 include those with low salinity. C4 environments can extend a distance of about 4 kilometers to 50 kilometers from a body of salt water, depending on the strength of prevailing winds and topography. Such regions are also found in urban and industrial areas with low pollution levels, such as manufacturing facilities and natural gas fired power generation stations, and exist for several kilometers around major industries, such as smelters and steelworks, chemical plants, refineries, and coal fired power generation stations. Interior C4 environments include manufacturing spaces with high humidity and high air pollution.

For a C4 environment:

- The time of wetness is defined as $2{,}500 < TOW \leq 5{,}500$ hours per year (h/yr)
- The airborne chloride content or salinity is defined as $60 < S_d \leq 300$ μg/m^3
- The airborne sulfur dioxide content $5 < P_c \leq 30$ μg/m^3

The initial and average corrosion rates of zinc are shown in Table 5.

Table 5. C4 Category (High Corrosive) - Initial and Average Zinc Corrosion Rates [Adapted from (ISO Standard 9223-92 1992)]

Unit	Initial Corrosion	Average Corrosion
g/(m^2/yr)	$15.00 < CR_i \leq 30.00$	$10.00 < CR_{avg} \leq 19.00$
μm/yr	$2.10 < CR_i \leq 4.20$	$1.40 < CR_{avg} \leq 2.70$

3.3.2.3.5. C5 (Very High)

Outdoor environments that are classified as C5 include those with high salinity and are typically areas within 4 kilometers of a body of salt water. As with Categories C3 and C4, the extent depends on winds, wave action, and topography. Industrial regions and areas found within 1.5 kilometers of the plant are included in this category. This category extends inside the industrial facilities, where it is best considered a microenvironment. For a C5 environment:

- The time of wetness is defined as $TOW > 5{,}500$ hours per year (h/yr)
- The airborne chloride content or salinity is defined as $S_d > 300$ μg/m^3
- The airborne sulfur dioxide content $P_c > 30$ μg/m^3

The initial and average corrosion rates of zinc are shown in Table 6.

Table 6. C5 Category (Very High Corrosive) - Initial and Average Zinc Corrosion Rates [Adapted from (ISO Standard 9223-92 1992)]

Unit	Initial Corrosion	Average Corrosion
g/(m^2/yr)	$30.00 < CR_i \leq 60.00$	$19.00 < CR_{avg} \leq 39.00$
μm/yr	$4.20 < CR_i \leq 8.40$	$2.70 < CR_{avg} \leq 5.50$

3.3.2.4.Regression Models

In the following methods, mathematical functions are empirically formulated based on the statistical analysis of historical data with respect to the relevant factors. The following are the predictive models of such corrosion rates found in the literature.

3.3.2.4.1. Haagenrud et al. (1985)

The corrosion in urban Sarpsborg/Fredrikstad area (Norway) was modelled and mapped in a four year exposure program at 13 sites with specimen withdrawal monthly, quarterly, yearly and after two and four years. Dose response function for yearly zinc corrosion in mils per year (mpy) developed by linear regression analysis is:

$$\text{Corrosion Rate (mpy)} = 0.00195[SO_2] + 5.57E\text{-}05TOW - 0.12145 \qquad (R^2=0.94)$$

Where:

- TOW (h/year) is the time of wetness (hours per year with T > 32°F, RH ≥ 80 %)
- $[SO_2]$ = SO_2 concentration, $\mu g/m^3$

3.3.2.4.2. Kucera et al. (1987)

The study consisted of eight-year exposure of galvanized steel at 32 test sites in rural, urban and marine environments. Dose response function for yearly zinc corrosion developed by linear regression analysis is:

$$\text{Corrosion Rate (mpy)} = 9.055*10^{-4}[SO_2] + 4.331*10^{-4}[Cl^-] + 2.087*10^{-4} \qquad (R^2=0.89)$$

Where:

- SO_2 = SO_2 concentration, $\mu g/m^3$
- $[Cl^-]$ = deposition rate of chloride, $mg/m^2.day$

3.3.2.4.3. Feliu and Morcillo (1993)

Data from 28 countries comprising 250 test fields in various parts of the world. Dose response function for yearly zinc corrosion developed by linear regression analysis is:

Corrosion depth (mils) = $A.t^n$ (R^2=0.73)

Where:

- $A = 3.091*10^{-2} + 1.972*10^{-1}[Cl^-] + 8.898*10^{-2}[SO_2]$
- $n = 0.0855 + 1.2148[SO_2] + 0.0138T - 0.0207[SO_2]T$
- C is the corrosion depth (mils)
- t the time (years)
- $[Cl^-]$ and $[SO_2]$ are the yearly average deposition rates ($mg/m^2.d$)
- T the yearly average temperature (ºF)

3.3.2.4.4. Wallinder et al. (1998)

The study investigated the zinc corrosion rate in different locations in Sweden and Belgium. The following relationship was established:

Corrosion Rate (mpy) = $2.087*10^{-2} + 1.260*10^{-3}[SO_2]$ (R^2=0.98)

Where:

- $[SO_2]$ is in $\mu g/m^3$

3.3.2.4.5. Veleva et al. (2010)

Flat sheet specimens of commercial galvanized steel were exposed in open air for two years in rural (Cunduacan, 50 km from the coast) and urban (Villahermosa, 68 km from the coast) environments located in the humid tropical climate of the Gulf of Mexico.

The corrosion rates were found to be:

- Corrosion Rate in humid tropical urban area (mpy) = $1.783*10^{-3} + 1.181*10^{-2}$ TOW + $7.494*10^{-2}[SO_2] + 4.274*10^{-3}$ $[Cl^-]$ ($R^2 = 0.99$)

  Corrosion Rate in humid tropical rural area (mpy) = $3.900*10^{-4} + 1.226*10^{-2}$ TOW + $8.059*10^{-2}[SO_2] + 4.579*10^{-4}$ $[Cl^-]$ ($R^2 = 0.99$)

  Where:

  - $[SO_2]$, and $[Cl^-]$ are in $mg/m^2.day$
  - TOW in hours

3.3.2.4.6. Del Angel et al. (2015)

The behavior of the atmospheric corrosion of galvanized steel is evaluated in three cities in Chile and Mexico. The results obtained indicate a clear trend of decreased corrosion on the galvanized steel with the increase in mean temperature, irrespective of the level of pollution present at all testing stations. This trend suggests that the corrosion of galvanized steel should decrease with the increased effects of climate change, which will bring higher mean temperatures. The corrosion was found to be:

Corrosion depth (mils) = $5.859*10^{-2} + 3.714*10^{-4}t - 1.857*10^{-3}T + 1.114*10^{-3}RH$ (R^2=091)

Where:

- t the time (years)
- T the yearly average temperature (ºF)
- RH is the yearly average relative humidity (%)

Numerous investigations have indicated that corrosion rates are strongly affected by certain factors, such as time of wetness, sulfur dioxide and chloride concentrations in the air. These findings form the basis for corrosion rate and lifetime prediction.

Historically, there have been four main approaches to predict the life of galvanized steels in atmospheric environments: the traditional method, the geographic map method, the ISO-9223 method, and regression modeling method. Each of these aforementioned approaches was described in this section with respect to its range of operation and constraints. Combining the different methods and selecting the most appropriate for each site, depending on its characteristics and the range of operation of each existing method, establishes the proposed approach to assess the above-ground corrosion rate. Next section elaborates more on the development of the *First Solar* – ASU research approach and applies the proposed decision framework on a site in Phoenix, AZ.

3.3.3. First Solar – ASU Proposed Method

To account for the above-ground corrosion of the zinc coating, the *First Solar* – ASU proposed method consists of developing a meta-model based on the existing approaches in the literature and the industry. In addition, the approach involves two independent analyses for the above-ground corrosion of the galvanized substructure (driven post) and the galvanized structure. To complete the atmospheric corrosion analysis, the meta-model requires the following inputs:

- **Design life:** is the estimated design life of the system. The default value is 25 years.
- **Zinc coating thickness:** is the initial zinc coating thickness of the galvanized structure and substructure (posts) in mils.
- **Site environment:** is essential to assess the corrosivity of the site. Such environments are defined by the AGA, as discussed earlier in section 3.2.1, and

are classified between rural, suburban, temperate marine, tropical marine, and industrial.

- **Latitude and longitude:** helps in determining the corrosivity level based on the geographic map method.
- **Average yearly temperature:** plays a major role in the corrosion process.
- **Average yearly humidity:** highly affects the corrosivity of the atmosphere.
- **TOW:** is the number of hours per year that the relative humidity is above 80 percent for temperatures above 32° F (0° C). *First Solar* has developed a tool to quantify the TOW (in hours/years) for a specific environment. The tool's output can be integrated in this approach to provide an accurate estimation of the above-ground corrosion.
- **Sulfur dioxide:** the ISO-9223 classification of airborne sulfur dioxide suggests three ranges based on the typical environment. A rural environment has SO_2 less than 12 $\mu g/m^3$, an urban or industrial environment has a SO_2 level between 12 and 90 $\mu g/m^3$, and a heavily polluted local environment has between 90 and 250 $\mu g/m^3$ of SO_2.
- **Airborne chloride:** the ISO-9223 classification of airborne chloride suggests three ranges based on the distance between the site and the shoreline. A non-coastal environment has less than 3 mg/m^2.day of airborne chloride, a coastal environment has between 3 and 300 mg/m^2.day, and a site within 650 ft. from the shoreline has between 300 and 1500 mg/m^2.day of airborne chloride.

Once the above inputs are provided for a specific location, the research approach consists of selecting the desirable models, which have similar conditions and

environments. Table 7 below summarizes the different atmospheric corrosion models of zinc. For each model, the method displays the estimated corrosion rate in mpy, the expected degradation and remaining thickness in mils at the end of the design life in mils, and the ESL for the zinc coating of both the structure and the substructure (post). Additionally, the minimum, average and maximum of the above-ground corrosion ESL are computed and will be compared to those of the underground corrosion in order to define the overall system ESL. A demonstration of the above-ground corrosion tool is presented in the following subsections.

Table 7. Above-Ground Zinc Corrosion Models

Corrosion Loss Model	Source	R^2 value
Corrosion Rate (mpy) = 0.00195*[SO2] + 5.57E-05*TOW - 0.12145	Haagenrud et al. (1985)	0.94
Corrosion Rate (mpy) =9.055E-04*[SO2] + 4.331E-04*[Cl] + 2.087E-02	Kucera et al. (1987)	0.89
Traditional method	American Galvanizers Association (1990)	-
Corrosion depth (mils) = A*t^n, where A =3.091E-02 +1.972E-01*[Cl−] +8.898E-02*[SO2] and n = 0.0855 + 1.2148*[SO2] + 0.0138*T - 0.0207*[SO2]*T	Feliu and Morcillo (1993)	0.73
Corrosion Rate (mpy) = 2.087E-02 +1.260E-03*[SO2]	Wallinder et al. (1998)	0.98
Corrosion Rate (mpy) = 1.783E-03 + 1.181E-02*TOW + 7.494E-02*[SO2] + 4.274E-03*[Cl-]	Veleva et al. (2010)	0.99
Corrosion Rate (mpy) = 3.900E-04 +1.226E-02*TOW +8.059E-02*[SO2] + 4.579E-04*[Cl-]	Veleva et al. (2010)	0.99
ISO method	ISO 9223 (2012)	-
Corrosion (mils) = 5.859E-02 +3.714E-04*t – 1.857E-03*T + 1.114E-03*RH	Del Angel et al. (2015)	0.91

3.3.3.1.Above-Ground Tool Demonstration – Case of Phoenix, AZ

The following is an example to illustrate the prediction of the above-ground zinc corrosion rate for a site located in Phoenix, AZ. The above-ground corrosion tool is part of the comprehensive **πCAT** tool developed as part of this study, which combines both underground and above-ground corrosion assessments. Table 8 summarizes the inputs corresponding to Phoenix environment and that are needed in the "Inputs" tab to complete the above-ground corrosion analysis. Moreover, for demonstration purposes, all the nine models, as illustrated in Figure 8, are initially selected to estimate the above-ground zinc corrosion rates and ESL of both structure and substructure. In order to select the most convenient models, a description of the models and their locations is provided.

Table 8. Inputs for Above-Ground Corrosion for Phoenix, Arizona

Inputs	Values for Phoenix, AZ
Design life	25 years
Environment	Rural
Average yearly temperature	24 °C
Average yearly humidity	37%
Time of wetness	500 hours/year
Airborne sulfur dioxide	3 mg/m².day
Airborne chloride	2 mg/m².day
Galvanized structure zinc coating	4 mils
Galvanized substructure (post) zinc coating	3 mils

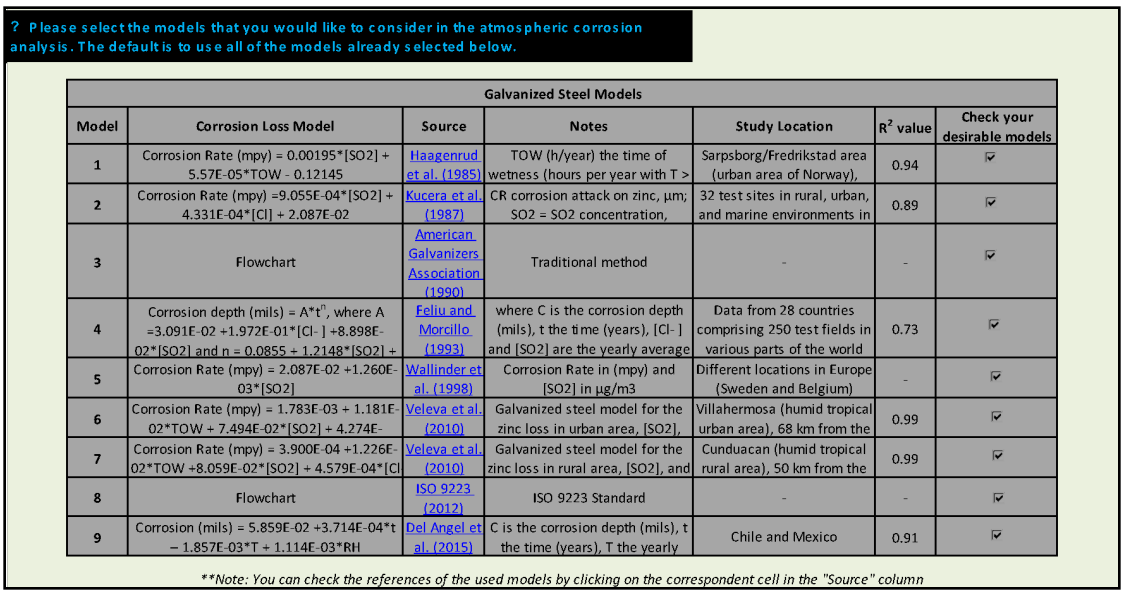

? Please select the models that you would like to consider in the atmospheric corrosion analysis. The default is to use all of the models already selected below.

Galvanized Steel Models						
Model	Corrosion Loss Model	Source	Notes	Study Location	R^2 value	Check your desirable models
1	Corrosion Rate (mpy) = 0.00195*[SO2] + 5.57E-05*TOW - 0.12145	Haagenrud et al. (1985)	TOW (h/year) the time of wetness (hours per year with T >	Sarpsborg/Fredrikstad area (urban area of Norway),	0.94	☑
2	Corrosion Rate (mpy) =9.055E-04*[SO2] + 4.331E-04*[Cl] + 2.087E-02	Kucera et al. (1987)	CR corrosion attack on zinc, µm; SO2 = SO2 concentration,	32 test sites in rural, urban, and marine environments in	0.89	☑
3	Flowchart	American Galvanizers Association (1990)	Traditional method	-	-	☑
4	Corrosion depth (mils) = $A*t^n$, where A =3.091E-02 +1.972E-01*[Cl-] +8.898E-02*[SO2] and n = 0.0855 + 1.2148*[SO2] +	Feliu and Morcillo (1993)	where C is the corrosion depth (mils), t the time (years), [Cl-] and [SO2] are the yearly average	Data from 28 countries comprising 250 test fields in various parts of the world	0.73	☑
5	Corrosion Rate (mpy) = 2.087E-02 +1.260E-03*[SO2]	Wallinder et al. (1998)	Corrosion Rate in (mpy) and [SO2] in µg/m3	Different locations in Europe (Sweden and Belgium)	-	☑
6	Corrosion Rate (mpy) = 1.783E-03 + 1.181E-02*TOW + 7.494E-02*[SO2] + 4.274E-	Veleva et al. (2010)	Galvanized steel model for the zinc loss in urban area, [SO2],	Villahermosa (humid tropical urban area), 68 km from the	0.99	☑
7	Corrosion Rate (mpy) = 3.900E-04 +1.226E-02*TOW +8.059E-02*[SO2] + 4.579E-04*[Cl	Veleva et al. (2010)	Galvanized steel model for the zinc loss in rural area, [SO2], and	Cunduacan (humid tropical rural area), 50 km from the	0.99	☑
8	Flowchart	ISO 9223 (2012)	ISO 9223 Standard	-	-	☑
9	Corrosion (mils) = 5.859E-02 +3.714E-04*t – 1.857E-03*T + 1.114E-03*RH	Del Angel et al. (2015)	C is the corrosion depth (mils), t the time (years), T the yearly	Chile and Mexico	0.91	☑

***Note: You can check the references of the used models by clicking on the correspondent cell in the "Source" column*

Figure 8. Models Selection for the Above-Ground Corrosion Estimation (Phoenix, AZ)

While some models are developed for cold (models 1 and 2) or tropical (models 6, 7 and 9) locations, other models cover several environments and atmospheres (models 3, 4, and 8). The estimations of the above-ground corrosion rates for the system structure and substructure are displayed in the "Above-Ground Corrosion" tab. For each selected model, the tool provides the corrosion rate (mpy), the expected degradation and remaining thickness at the end of the design life (mils), and the expected service life (years). Additionally, the minimums, averages, and maximums values are computed for the considered models. Figures 9 and 10 show the predicted zinc corrosion rates for the structure and the substructure (post), respectively. After selecting the suitable models for Phoenix, AZ, the average predicted zinc atmospheric corrosion rate is 0.041 mpy, varying between a minimum of 0.025 and a maximum of 0.083 mpy.

Initial Zinc coating thickness of the structure (mils) =	4

Galvanized Steel Models							
Model	Corrosion Loss Model	Source	Corrosion Rate (mpy)	Expected degradation at the end of design life (mils)	Expected remaining thickness at the end of design life (mils)	Expected service life (years)	To consider?
1	Corrosion Rate (mpy) = 0.00195*[SO2] + 5.57E-05*TOW - 0.12145	Haagenrud et al. (1985)	N/A	N/A	N/A	N/A	☐
2	Corrosion Rate (mpy) =9.055E-04*[SO2] + 4.331E-04*[Cl] + 2.087E 02	Kucera et al. (1987)	0.025	0.625	3.375	160.026	☑
3	Flowchart	American Galvanizers Association (1990)	0.031	0.772	3.229	129.618	☑
4	Corrosion depth (mils) = A*t^n, where A =3.091E-02 +1.972E-01*[Cl-] +8.898E-02*[SO2] and n = 0.0855 + 1.2148*[SO2] + 0.0138*T - 0.0207*[SO2]*T	Feliu and Morcillo (1993)	1.75E-03	4.37E-02	3.96E+00	2.29E+03	☐
5	Corrosion Rate (mpy) = 2.087E-02 +1.260E-03*[SO2]	Wallinder et al. (1998)	0.025	0.635	3.365	157.443	☑
6	Corrosion Rate (mpy) = 1.783E-03 + 1.181E-02*TOW + 7.494E-02*[SO2] + 4.274E-03*[Cl-]	Veleva et al. (2010)	6.140	4.000	0.000	0.651	☐
7	Corrosion Rate (mpy) = 3.900E-04 +1.226E-02*TOW +8.059E-02*[SO2] + 4.579E-04*[Cl-]	Veleva et al. (2010)	6.373	4.000	0.000	0.628	☐
8	Flowchart, CLASS 3	ISO 9223 (2012)	0.083	2.067	1.933	48.381	☑
9	Corrosion (mils) = 5.859E-02 +3.714E-04*t − 1.857E-03*T + 1.114E-03*RH	Del Angel et al. (2015)	N/A	N/A	N/A	N/A	☐

Figure 9. The Above-Ground Corrosion Results of the Structure

Initial Zinc coating thickness of the susbtructure (pile) (mils) =	3

Galvanized Steel Models							
Model	Corrosion Loss Model	Source	Corrosion Rate (mpy)	Expected degradation at the end of design life (mils)	Expected remaining thickness at the end of design life (mils)	Expected service life (years)	To consider?
1	Corrosion Rate (mpy) = 0.00195*[SO2] + 5.57E-05*TOW - 0.12145	Haagenrud et al. (1985)	N/A	N/A	N/A	N/A	☐
2	Corrosion Rate (mpy) =9.055E-04*[SO2] + 4.331E-04*[Cl] + 2.087E 02	Kucera et al. (1987)	0.025	0.625	2.375	120.019	☑
3	Flowchart	American Galvanizers Association (1990)	0.031	0.772	2.229	97.213	☑
4	Corrosion depth (mils) = A*t^n, where A =3.091E-02 +1.972E-01*[Cl-] +8.898E-02*[SO2] and n = 0.0855 + 1.2148*[SO2] + 0.0138*T - 0.0207*[SO2]*T	Feliu and Morcillo (1993)	1.75E-03	4.37E-02	2.96E+00	1.72E+03	☐
5	Corrosion Rate (mpy) = 2.087E-02 +1.260E-03*[SO2]	Wallinder et al. (1998)	0.025	0.635	2.365	118.082	☑
6	Corrosion Rate (mpy) = 1.783E-03 + 1.181E-02*TOW + 7.494E-02*[SO2] + 4.274E-03*[Cl-]	Veleva et al. (2010)	6.140	3.000	0.000	0.489	☐
7	Corrosion Rate (mpy) = 3.900E-04 +1.226E-02*TOW +8.059E-02*[SO2] + 4.579E-04*[Cl-]	Veleva et al. (2010)	6.373	3.000	0.000	0.471	☐
8	Flowchart, CLASS 3	ISO 9223 (2012)	0.083	2.067	0.933	36.286	☑
9	Corrosion (mils) = 5.859E-02 +3.714E-04*t − 1.857E-03*T + 1.114E-03*RH	Del Angel et al. (2015)	N/A	N/A	N/A	N/A	☐

Figure 10. The Above-Ground Corrosion Results for the Substructure (Post)

This section focused on the above-ground soil corrosion of driven posts. The following section describes the underground corrosion factors, details the predictive models for zinc and steel, including a newly-developed model based on *First Solar* data, and applies the proposed framework on *First Solar* sites.

3.4. UNDERGROUND CORROSION

Degradation of driven posts due to corrosion is a major concern for many industries, including PV solar plants. When it is easier to examine above-ground corrosion, driven

posts are exposed to complex and infinitely variable external environment and usually not readily accessible for inspection. Being less predictable than atmospheric corrosion, underground corrosion depends on the soil characteristics that can vary within a single site.

Soil corrosion, a complex phenomenon with a multitude of involved variables (Galvanizeit 2016), is a geologic hazard that affects buried metals and concrete that is in direct contact with soil or bedrock. Corrosive soils contain chemical constituents that can react with construction materials, which may damage foundations and buried structures. The electrochemical corrosion processes that take place on metal surfaces in soils occur in the groundwater that is in contact with the corroding structure (Wan et al. 2013). While the effects of corrosive soil can cause structural failure and financial burden, mitigating measures taken into account during design and construction, as well as an understanding of the corrosive potential in a particular soil can minimize these issues.

This section describes the underground soil corrosion of driven posts. First, it discusses the factors contributing to the underground corrosion. Second, it presents the potential methods used for the assessment and prediction of zinc and steel underground corrosion. Then, it proposes an alternative meta-model.

3.4.1. Underground Corrosion Factors

The *National Association of Corrosion Engineers* (*NACE) - Recommend Standard Practice 0502-2002, External Corrosion Direct Assessment (ECDA)* (NACE 2002) delineates the main factors affecting the underground corrosion for structures that are buried in soil by: soil resistivity, pH level, chloride contents, sulfate contents, redox

potentials, along with other factors. The following is a more detailed description of the manner in which each of the above factors influences soil corrosivity.

3.4.1.1.Soil Resistivity

Soil resistivity, a common parameter for evaluating the corrosiveness of soil, is a function of soil moisture and the concentrations of ionic soluble salts. This parameter follows the chloride ion concentration in that higher resistivity means lower chloride ion content and a lower corrosion rate. Soil resistivity, measured in ohm-cm, is computed using several methods. Out of these methods, Wenner method is the most widely used method for measuring soil resistivity for electrical grounding purposes (IEEE 2012). Soil resistivity generally relate to the salinity or purity of the water or moisture, which historically has permeated the soil and remains there to one degree or another. When the geotechnical data is not available, the following broad guidelines, presented in Table 9, are used to relate USA areas and soil type conditions with its resistivity (Roberge 2006).

As water is one of the three components necessary for electrochemical corrosion (the other two being oxygen and metal), corrosion will not occur if the soil is completely dry. Experimental evidence dictates that an increase in moisture content decreases resistivity of soils, in turn increasing their corrosive potential (Guma et al. 2015). However, when the saturation point of the soil is reached, additional moisture has little or no effect on resistivity. For instance, sandy soils are high up on the resistivity scale and therefore considered the least corrosive. Clay soils, especially those contaminated with saline water are on the opposite end of the spectrum. The relationship between the resistivity of the soil and the corrosion resistance for steel is summarized in the following Table 10 below (Roberge 2012).

Table 9. Soil Type Conditions and their Related Resistivity [Adapted from (Roberge 2006)]

Area and/or Soil Type	Resistivity Range (ohm-cm)
Brackish water lowlands, poor or slow drainage, coastal areas	150 -1,200
Coastal plains, low elevation	600 - 1,500
Central coastal areas, satisfactory to good drainage	1,200 - 5,000
South central, Midwest and central, farm and range lands	3,500 - 10,000
West central desert plains, mountains	5,000 - 25,000
Eastern and northeast high country, excellent drainage, dry and arid	10,000 - 25,000

Table 10. Relation between Soil Corrosivity and Resistivity [Adapted from (Roberge 2012)]

Soil resistivity (ohm-cm)	Corrosivity Rating
> 20,000	Essentially non-corrosive
10,000 to 20,000	Mildly corrosive
5,000 to 10,000	Moderately corrosive
3,000 to 5,000	Corrosive
1,000 to 3,000	Highly corrosive
< 1,000	Extremely corrosive

3.4.1.2.pH Level

Soils can have a wide range of acidity, reaching anywhere from 3.5 to 10. As pH levels of 5 or below can lead to extreme corrosion rates of metallic objects, a neutral pH of about 7 is most desirable to minimize this potential for damage. The intrinsic pH level of a soil can also be affected by rainfall. Table 11 details the corrosivity rating for different values of pH levels (Caltrans 2003).

Table 11. Relation between Soil Corrosivity and PH [Adapted from (Caltrans 2003)]

pH	Corrosivity Rating
≥ 7	Essentially non-corrosive
5.5 to 7	Mildly corrosive
≤ 5.5	Corrosive

3.4.1.3.Chloride Content

Laboratory measurements of the chloride ions concentration are analyzed in conjunction with soil resistivity to determine the corrosivity of a soil with respect to metals. As the chloride concentration increases, the resistivity tends to decrease and the corrosivity increases. Soils with higher chloride concentrations usually represent areas that have been contaminated with salts from a marine environment or from road deicing salts. Chloride ions attack the surfaces of metallic structures and promote accelerated corrosion. Generally, chloride concentrations that are over 150 parts per million (ppm) indicate heavily contaminated areas that will promote corrosion. Table 12 shows the common classification of soil corrosivity per chloride contents (FHWA 2009).

Table 12. Relation between Soil Corrosivity and Chloride Contents [Adapted from (FHWA 2009)]

Chloride Content (ppm)	Corrosivity Rating
≤ 100	Essentially non-corrosive
100 to 200	Mildly corrosive
≥ 200	Corrosive

3.4.1.4.Sulfate Content

The sulfates of sodium, magnesium calcium and potassium are often found in soils or dissolved in groundwater. Compared to the corrosive effect of chloride ion levels, sulfates are considered more benign in their corrosive action toward buried structures. The presence of sulfates does pose a risk for the materials in the sense that sulfates can be converted to highly corrosive sulfides by anaerobic sulfate-reducing bacteria. Table 13 shows sulfate concentrations and their relationship to the soil corrosivity (FHWA 2009).

Table 13. Relation between Soil Corrosivity and Sulfate Contents [Adapted from (FHWA 2009)]

Sulfate Content (ppm)	Corrosivity Rating
≤ 150	Essentially non-corrosive
150 to 1,500	Mildly corrosive
1,500 to 10,000	Corrosive
≥ 10,000	Highly Corrosive

3.4.1.5.Redox Potentials

The reduction–oxidation (redox) potential provides an indication of a possible presence of anaerobic bacterial corrosion. A redox potential greater than +100 millivolts (mV) demonstrates that the soil is sufficiently aerated, preventing sulfate reducers from forming. Although no national standard exists, the common classification for redox potentials is shown in Table 14 below.

Table 14. Relation between Soil Corrosivity and Redox Potential [Adapted from (Roberge 2000)]

Redox Potential (mV)	Corrosivity Rating
≤ 100	Very Corrosive
100 to 200	Moderately Corrosive
200 to 400	Slightly Corrosive
≥ 400	Essentially non-corrosive

3.4.1.6.Other Factors and Considerations

While the above factors are the driving ones to determine the corrosiveness of the soil, other factors can affect the underground corrosion rate. The following subsections elaborate on the effect of such factors and considerations on the underground corrosion.

3.4.1.6.1. Soil texture

Soil texture refers to the size distribution of mineral particles in a soil (Soil Survey Division 1993). Table 15 shows the US Department of Agriculture (USDA) separation

limits of the soil based on specific ranges of particle sizes (Soil Conservation Service 1975).

Table 15. Soil Classification [Adapted from (Soil Conservation Service 1975)]

Name of soil separate	Diameter limits (mm)
Clay	less than 0.002
Silt	0.002 to 0.05
Very fine sand	0.05 to 0.10
Fine sand	0.10 to 0.25
Medium sand	0.25 to 0.50
Coarse sand	0.50 to 1.00
Very coarse sand	1.00 to 2.00

Soil textures are classified by the fractions of each soil separate (sand, silt, and clay) present in a soil. Classifications are typically named for the primary constituent particle size or a combination of the most abundant particles sizes, e.g. "sandy clay" or "silty clay". A fourth term, loam, is used to describe a roughly equal concentration of sand, silt, and clay, and lends to the naming of even more classifications, e.g. "clay loam" or "silt loam". Undisturbed natural soils have been found to be noncorrosive relative to disturbed soil and manmade products. In general, the process of drilled/augured piling installation disturbs the soil, increasing the oxygen content, compared to that of driven piling. In the United States, the USDA defines twelve major soil texture classifications, as shown in Figure 11.

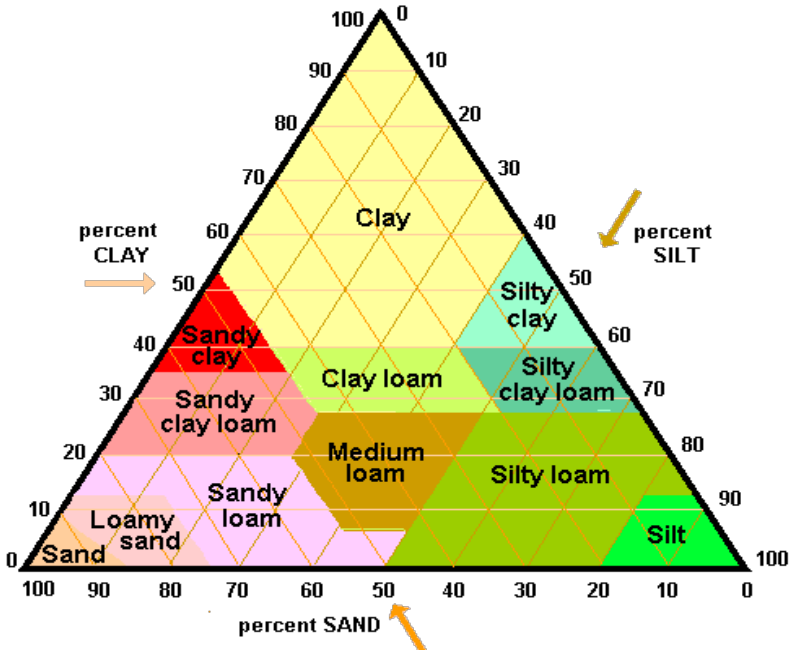

Figure 11. USDA Soil Texture Triangle (U.S. Department of Agriculture 1975)

3.4.1.6.2. Aeration

This is defined as the amount of oxygen (or air) trapped within the soil. Aeration is an important factor in corrosion as it is a factor in water retention and evaporation rates. Well-aerated soil is more favorable from a (low) corrosivity standpoint because this generally leads to lower water retention and higher evaporation rates. The particle size and gradation within the soil plays a major role in determining the amount of aeration. Sandy soils are generally desirable, as the relatively large particles allow for better aeration, and facilitate faster evaporation rates after water has been introduced into the soil. A quick way to classify soils in terms of their aeration is by examining their color. Reddish, brown, or yellow soils indicate good aeration, while gray soil is indicative of poor aeration (Levlin 1996).

Moreover, the difference in the concentration of dissolved oxygen at two points on a metal surface enhances the corrosivity of the soil. For instance, the surface in contact

with the higher concentration of dissolved oxygen will become cathodic to the surface in contact with a lower concentration of dissolved oxygen, which will be suffering from corrosion due to differential aeration.

3.4.1.6.3. Sulfide Content

Sulfides are a reduced form of sulfur and can be created by sulfur-reducing bacteria under anaerobic conditions. Sulfides can chemically react with metals and degrade their strength. They can also be involved in the generation of sulfuric acid that will attack metal and oxidize to sulfate by microbes in the presence of oxygen concrete. Hydrogen sulfide is one form of sulfide that can be present in soil.

3.4.1.6.4. Galvanic Corrosion

Galvanic corrosion occurs when two or more dissimilar metals and alloys, with different electrode potentials, come into contact in an electrolyte. Then, the anode metal dissolves into the electrolyte and the deposit collects on the cathodic metal. Usually, solar PV facilities have both a copper grounding system and galvanized steel PV driven posts in the ground. Theoretically, the differential voltage between copper (cathode) and carbon steel (anode) is 0.30 v and between copper (cathode) and zinc (anode) is 0.65 v. In this galvanic corrosion cell, the surface area ratio of anode to the cathode will affect the severity of corrosion. The larger the anodic-to-cathodic area ratio, the less severe the corrosion will be since there is more anodic surface area over which to distribute the galvanic corrosion. Knowing that the galvanic corrosion rate is proportional to the diffusion rate of oxygen (Stern and Geary 1957), the net effect of galvanic corrosion for driven posts into undisturbed soils will be minimal. The galvanic corrosion current between steel and copper may be calculated using Ohm's Law as follows:

$$Icorr = \frac{Ecopper - Esteel}{Rsteel - Rcopper}$$

Where:

- I_{corr} = Total galvanic corrosion current (ampere)
- E_{copper} = Free corrosion potential of copper in soil (volts versus copper sulfate electrode)
- E_{steel} = Free corrosion potential of steel in soil (volts versus copper sulfate electrode)
- R_{steel} = Calculated resistance to earth of steel anode (ohms)
- R_{copper} = Calculated resistance to earth of copper cathode (ohms)

The main factors that dictate the corrosivity of the soil include soil resistivity, pH level, chloride contents, sulfate contents, redox potential, and others. This section described the manner in which each of the above factors influences soil corrosivity and outlined the needed inputs for the underground corrosion potential methods. The next section presents the common approaches that use some of these input factors to assess the underground corrosion of galvanized driven posts.

3.4.2. Potential Methods for Underground Corrosion Assessment

Researchers and organizations have developed several methods and standards for the assessment of the underground corrosion rate. This section describes some of the most common methods and their applications for driven posts.

3.4.2.1.Weight Loss Method

This method measures the corrosivity toward steel of both aqueous and non-aqueous liquid wastes. It exposes coupons of SAE Type 1020 steel to the liquid waste to be evaluated and, by measuring the degree to which the coupon has been dissolved,

determines the corrosivity of the waste (Rodriguez et al. 1999). The difference between the weight of the exposed coupon and its original weight (before exposure) corresponds to the weight loss as a result of corrosion. Weight loss is measured in grams, and the corrosion rate is calculated in mpy. The typical corrosion rate calculation is as follows:

$$Corrosion\ Rate\ (mpy) = \frac{weight\ loss\ (g)\ \text{x}\ 393.7}{Density\left(\frac{g}{cm^3}\right)\ \text{x}\ Area\ (cm^2)\ \text{x}\ Time\ (years)}$$

However, this test was criticized for the associated uncertainties with the assessment of the corrosion rate from a coupon weight loss measurement. Measurement uncertainties considered for the test include: statistical errors for the balance used to weigh the coupons, possible loss of base metal (in addition to corrosion material) to the wash/brush process, and possible loss of base metal (in addition to corrosion material) to the chemical treatment.

3.4.2.2.AWWA Numerical Corrosivity Scale

The AWWA developed a numerical soil corrosivity scale, applicable to cast iron alloys. AWWA C-105 Standard (American Water Works Association 1993) evaluates the likelihood of corrosion deterioration by assigning points for different variables in order to predict the severity of the soil corrosivity. Table 16 describes the AWWA point system. When the points total of a soil in the AWWA scale equals ten (or higher), corrosion protective measures (such as cathodic protection) have been recommended for cast iron alloys.

Table 16. The AWWA C-105 Point System for Predicting Soil Corrosivity [Adapted from (American Water Works Association 1993)]

Factor	Soil Parameter	Assigned Points
Resistivity (ohm-cm)	<700	10
	700 - 1000	8
	1000 - 1200	5
	1200 - 1500	2
	1500 - 2000	1
	> 2000	0
pH Levels	0-2	5
	2-4	3
	4-6.5	0
	6.5-7.5	0
	7.5-8.5	0
	>8.5	3
Redox Potential (Millivolts)	>100	0
	50-100	3.5
	0-50	4
	<0	5
Sulfides	Positive	3.5
	Trace	2
	Negative	0
Moisture	Poor drainage continuously wet	2
	Fair drainage generally moist	1
	Good drainage generally dry	0

3.4.2.3.Electrochemical In-Situ Methods

Linear Polarization methods are faster experimental techniques compared to the classical weight loss estimation. For an electrochemical reaction under activation control, polarization curves exhibit linear behavior in the E versus log (i) plots called Tafel behavior. Typical polarization behavior of metals in acid solution in the presence and absence of oxygen is illustrated in Figure 12 (Abdallah 2002) below.

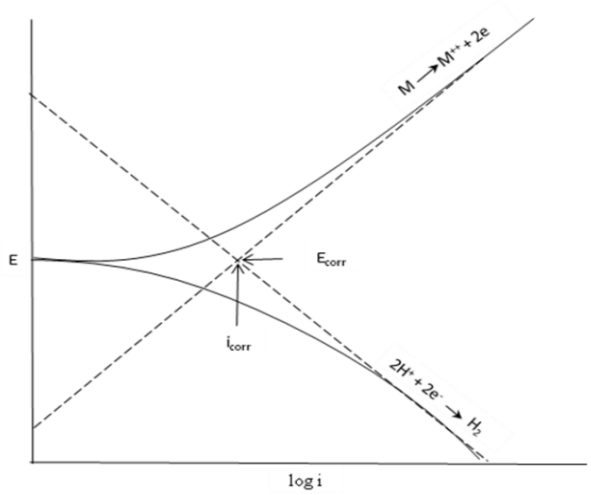

Figure 12. Polarization Typical Behavior of a Metal in Acid Solution in the Presence and Absence of Oxygen (Abdallah 2002)

Extrapolation of cathodic and anodic Tafel slopes' intersection point corresponds to corrosion current (I_{corr}) density and corrosion potential (E_{corr}). Faraday's method is usually used to assess the soil corrosivity rate. This method converts the corrosion current (amps) that is resulted from the E-Log I testing to the corrosion rate (mpy) using the following formula:

$$CR = \frac{K1 \text{ x } Icorr \text{ x } Ew}{d \text{ x } A}$$

Where:

- CR = Corrosion Rate in mpy
- K1 = A constant= 128800 (units for corrosion rate)
- I_{corr} = Corrosion current (A/cm^2)
- Ew = Equivalent weight in grams/equivalent (27.92 for steel and 32.68 for Zinc)
- d = Density (g/cm^3)
- A = Surface Area (cm^3)

3.4.2.4.Romanoff - NBS Method

Since the last century, the NBS initiated a research to investigate the primary processes of corrosion (Logan and Grodsky 1931). Based on these studies, Romanoff (1957) postulated the following exponential equation to predict the amount of general corrosion at some time (t) after burial:

$$y(t) = k\ t^n$$

Where:

- y(t) is the loss of thickness or pit depth in the metal at time (t)
- k and n (less than unity) are regression parameters that are soil and site dependent

The results of extensive filed testing on metal pipes and sheet steel buried by the NBS programs originating as early as 1910 constitute the most comprehensive quantitative data available in the field of underground corrosion. For low alloy and carbon steels in a number of soil burial conditions, Romanoff determined “n” and “k” constants varying from 0.5 to 0.6 and 150 to 180 μm, respectively at the end of the first year.

The Romanoff - NBS method is one of the most popular methods that are currently applied in the industry. However, using this method to predict corrosion rates is still a controversial issue. From one hand, practitioners refer to the NBS database as a foundation to predict the corrosion rate, by mapping the characteristics of a new site to the characteristics of one or more sites out of the existing 47 projects in their database. From the other hand, this method is criticized for the uncertainty and the large scatter in the data that couldn’t be explained, when using data from several sites to predict

corrosion rates. Moreover, the limitation of this method appears in the accuracy of finding an existing site having the same characteristics of another new site. Appendix A provides a further analysis on this method and its application.

3.4.2.5.NACE Corrosion Reference

NACE has developed the *Corrosion Engineer*'s reference book and its own standards (NACE 2007) for the assessment of corrosion. Moreover, the NACE identifies materials manifestly unsuitable for use in corrosive environments and locates materials that have satisfactory performance and are candidates for consideration in the *Corrosion Data Survey—Metals Section, 6th edition* (Graver 1985). However, the NACE data is criticized for the wide range of corrosion rates classification:

- Less than 2 mpy
- Between 2 and 20 mpy
- Between 20 and 50 mpy
- More than 50 mpy

3.4.2.6.NYSDOT Method

A corrosion study (Picozzi et al. 1993) by New York State Department of Transportation (NYSDOT) for steel H-posts specifies the following alternative corrosion prediction relationships, which explain 75% and 73%, respectively, of the variability of the corrosion rates:

$$Section\ loss\ (mils)\ =\ 1.2964\,pH\ +\ 0.0025\,[Cl^{-}]\ (ppm)$$

$$Section\ loss\ (mils)\ =\ 1.5616\,pH$$

Those relationships above were obtained from weight loss measurements of H-posts exposed to miscellaneous fill and natural soil in the Buffalo Skyway Bridge site, New

York. The averaged corrosion rates measured for the different environment conditions were 0.34 mm (13.2 mils) for an exposure time over 35 years, regardless of the soil type. However, the above models do not account for the effect of the resistivity, sulfates and redox potentials on the corrosion rate establishing a major limitation for their applicability.

3.4.2.7.FHWA Method

The Federal Highway Administration (FHWA), an agency within the U.S. Department of Transportation, recommended several designs to evaluate the corrosion loss in metals. FHWA-SA-96-072 report (FHWA 2009) analyzed the NBS data and proposed the following equations for the loss determinations using Romanoff's uniform model concept: $y(t) = 25\,t^{0.65}$ for galvanized steel and $y(t) = 40\,t^{0.80}$ for carbon steel. The FHWA Manual on Design and Construction of Driven Post Foundations (Hannigan et al. 1997) proposes the following corrosion rate estimates:

- Posts buried in fill or disturbed natural soils: 3.2 mpy
- Posts immersed in fresh water: 2 mpy; however, corrosion rates at the waterline can be as high as 13.6 mpy
- Posts in marine environments, where the numbers in brackets represent 95% maximum probable rates are:
    - Splash zone: 3.6 mpy (7.2 mpy)
    - Inter-tidal zone: 1.6 mpy (4.4 mpy)
    - Low-water zone: 3.6 mpy (7.2 mpy); abrasion damage can increase losses to 16.4 mpy
    - Immersion zone: 2 mpy (5.6 mpy)

- Buried zone: 0.8 mpy (2 mpy)

Figure 13 determines the corrosion rates based on the environmental classification according to FHWA (2009).

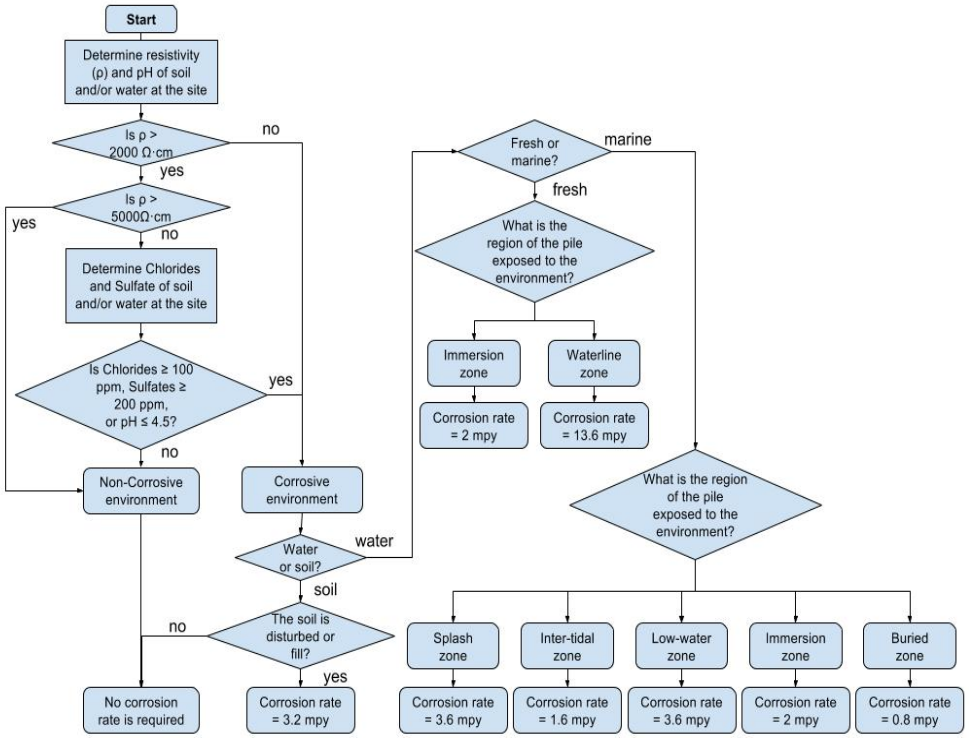

Figure 13. FHWA Corrosion Classification Flowchart [Adapted from (FHWA 2009)]

3.4.2.8.Caltrans Method

California Department of Transportation (Caltrans) uses the following corrosion rates estimates for steel piling exposed to corrosive soil and/or water:

- Soil Embedded Zone: 1 mpy
- Immersed Zone: 4 mpy
- Scour Zone: 5 mpy
- Undisturbed soil:
    - Within the region of the post down to 3 ft. below the water table: 1 mpy

- Outside the region of the post down to 3 ft. below the water table: no corrosion rate is required.

If a site is characterized as non-corrosive, then no corrosion allowance (sacrificial metal loss) is necessary. A flowchart to determine the environmental classification and the corresponding corrosion rates is shown in Figure 14.

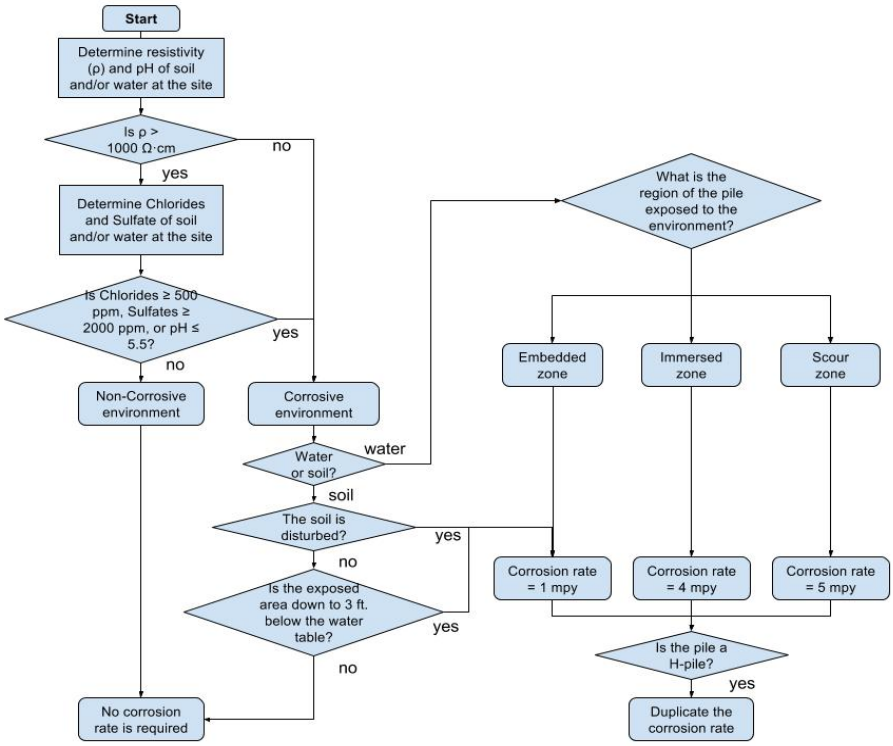

Figure 14. Caltrans Corrosion Classification Flowchart [Adapted from (Caltrans 2003)]

Caltrans (2003) has also proposed design guidance for the zinc loss. These metal loss rates are based on limited data collected from California sites. The guidance proposes four different models for the different fill types:

- For neutral and alkaline fills, which have minimum resistivity > 1000 Ω.cm and pH > 7:
  - X (μm) = (t -10 yrs)*28

- For acidic fills, which have minimum resistivity > 1000 Ω.cm and pH < 7:
  - X (μm) = (t -10 yrs)*33
- For corrosive fills, which have minimum resistivity < 1000 Ω.cm:
  - X (μm) = (t - 6 yrs)*71
- For select granular fills, which are clean, free draining gravels with less than 5% fines and have minimum resistivity < 1000 Ω.cm:
  - X (μm) = (t -30 yrs)*13

However, the limitation of the Caltrans models is highlighted by the small sample size. Moreover, these models assume that the corrosion initiates after a specific number of years such as 6, 10 or 30 years.

3.4.2.9.NCHRP Report 408

In this National Cooperative Highway Research Program (NCHRP) study (Beavers and Durr 1998), a statistical model was developed to explain the variation in piling corrosion rates at eight different sites:

$$Weight\ loss\ (mpy) = -17.2 + 0.000761\ [Cl^-]\ (ppm) + 2.52\ pH$$

From the Pearson correlation matrix for measured soil parameters, chloride concentration was highly correlated with both weight loss observed in steel posts (r=0.96) and with pH (r=0.84). Although the high correlation factors that were obtained, the study recommends to not use the above model for predictive purposes.

3.4.2.10. AASHTO Model

The American Association of State Highway and Transportation Officials (AASHTO) (2010) defines the zinc corrosion loss model to be:

- X (μm) = (t -10.5 yrs)*12

However, this model is considered valid when the backfill conforms to the following electrochemical limits:

- Resistivity ≥ 3,000 ohm-cm
- pH = 5 to 10
- Chlorides ≤ 100 ppm
- Sulfates ≤ 200 ppm
- Organic content ≤ 1%.

3.4.2.11. UK Model

The UK Design Manual for Roads and Bridges provides a zinc loss model (Highways England 2012). The manual classified the soil between aggressive and non-aggressive according to the soil electrochemical characteristics. A soil is classified as aggressive if:

- Resistivity = 667 to 2,000 ohm-cm
- pH = 5 to 6
- Chlorides = 50 to 250 ppm
- Sulfates = 240 to 600 ppm

Moreover, a soil is considered non-aggressive if:

- Resistivity = 2,000 to 8,000 ohm-cm
- pH = 6 to 9
- Chlorides ≤ 50 ppm
- Sulfates ≤ 240 ppm

Hence, the recommended corrosion models are:

  - For aggressive soil: $X\ (\mu m) = 40*(t - 4.6yrs)^{0.80}$
  - For non-aggressive soil: $X\ (\mu m) = 22.5*(t - 16yrs)^{0.67}$

3.4.2.12. First Solar Regression Model

The *First Solar* regression model is a new predictive model, based on the available *First Solar* data, which estimates the underground corrosion rates and ESL of galvanized driven posts. The development of zinc and steel corrosion models consists of three steps: 1) data collection; 2) outliers detection; and 3) multivariate linear regression modeling.

3.4.2.12.1. Data Collection

First Solar provided the geotechnical studies of 62 projects. For each project, data related to location (county, state, and country), study's date, and geotechnical consultant was collected. Out of the 62 projects, 59 sites (95.2 %) are in the U.S. and the remaining 3 projects are in Australia (3.2 %) and South Africa (1.6%), as shown in Figure 15.

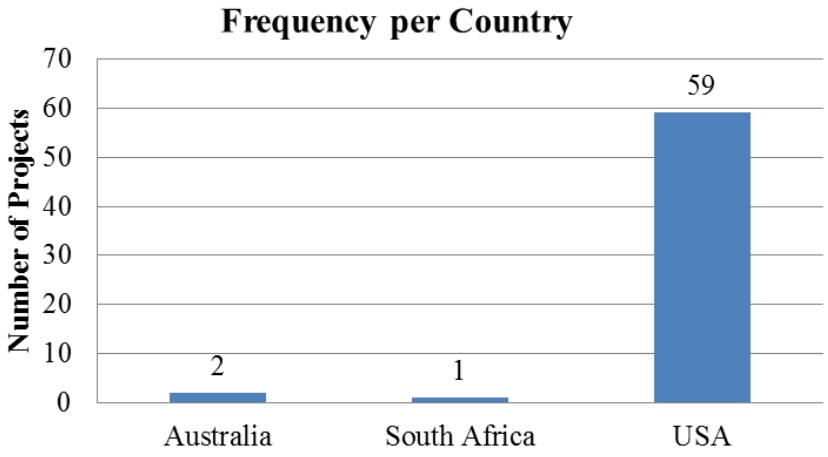

Figure 15. The Distribution of First Solar Projects per Country (N=62)

After collecting the data and analyzing the available data within each report, 21 projects out of the 62 (33.8%) include corrosion studies for zinc and steel. For each study, consultants have estimated the maximum corrosion rates (in mpy) for zinc and steel as well as the ESL (in years). By taking into account the underground corrosion factors, data on resistivity, pH level, chlorides, sulfates and redox were extracted from the reports. Furthermore, in order to predict the maximum expected corrosion rates, the

electrochemical soil characteristics corresponding to the most corrosive conditions were considered, i.e. minimum resistivity, pH, and redox as well as maximum chlorides and sulfates. Only 14 projects out of 62 (22.6%) have complete data while the remaining 7 projects have some missing electrochemical data. Hence, outliers' detection analysis will be applied on the sites with complete data (14 projects) before generating the corrosion models, as discussed in the following sections.

3.4.2.12.2. Outliers' Detection

To detect outliers in the dataset, Grubbs' test, also known as the maximum normed residual test, is used at a significance level α of 0.05. Knowing that 95% of a normal distrusted data is within two standard deviations, a z-score value is computed according to the following formula:

$$z = \frac{x - \mu}{\sigma}$$

Where:

- μ is the mean of the population
- σ is the standard deviation of the population

Z-score values were computed independently for each variable and outliers with z scores +/- 2 were excluded. Five out 14 projects are highlighted as outliers by having z-score values that are higher than 2 or lower than -2. The remaining nine projects are selected to generate the predictive models as discussed in the next section.

3.4.2.12.3. Multivariate Linear Regression Modeling

Multivariate linear regression intends to model the relationship between two or more variables by fitting a linear equation to observed data. One variable is considered to be an explanatory variable, and the others are considered to be dependent variables. The

multivariate linear regression modeling consists of analyzing the relationship and directionality of the data, estimating the model, i.e., fitting the line, and evaluating the validity and usefulness of the model.

An analysis of variability ranges of dependent variables was completed, i.e., zinc and steel corrosion rates, and independent variables, i.e., minimum resistivity, pH, and redox as well as maximum chlorides and sulfates. It is important to emphasize that the available corrosion rates are measured by *First Solar* consultants and represent the maximum corrosion rates at a depth of 6ft. Therefore, the newly-developed models are designed to predict the most-conservative corrosion rates at a depth of 6ft. Table 17 shows the coefficients of determination (R^2) percentages between the different variables.

Table 17. The Coefficients of Determination R^2 (%) between the Independent and Dependent Variables

Variables	Min. Resistivity	Min. pH	Max. Chlorides	Max. Sulfates	Min. Redox	Corrosion Rate Zinc	Corrosion Rate Steel
Min. Resistivity	100%	9%	1%	1%	42%	70%	71%
Min. pH	9%	100%	26%	17%	0%	7%	8%
Max. Chlorides	1%	26%	100%	7%	3%	4%	1%
Max. Sulfates	1%	17%	7%	100%	12%	0%	4%
Min. Redox	42%	0%	3%	12%	100%	23%	15%
Corrosion Rate Zinc	70%	7%	4%	0%	23%	100%	94%
Corrosion Rate Steel	71%	8%	1%	4%	15%	94%	100%

An R^2 value gives the proportion of the variance (fluctuation) of one variable that is predictable from the other variable and is the ratio of the explained variation to the total variation. In other words, R^2 represents the percent of the data that is the closest to the line of best fit. For instance, the R^2 value of 71% between the minimum resistivity and

the steel corrosion rate means that 71% of the total variation in steel corrosion rate can be explained by the linear relationship between the two variables. The other 29% of the total variation in steel corrosion rate remains unexplained. The results show a strong relationship between the resistivity from one side and the zinc corrosion rate (70%) and steel corrosion rate (71%) from the other side. Yet, the effects of other independent variables on the corrosion rates are minimal varying between a minimum of 0% (sulfates for zinc corrosion rate) and a maximum of 23% (redox for zinc corrosion rate).

Fitting the zinc corrosion rate data into a multivariate linear regression model yields to the following equation:

$$Predicted\ Corrosion\ Rate\ of\ Zinc\ (mpy)$$

$$= \begin{cases} 5.64 - 1.51\times10^{-3}\ Min.Resistivity\ (\Omega.cm) - \\ 0.41\ Min.pH + 6.83\times10^{-4}\ Max.Chlorides\ (ppm) + \\ 2.95\times10^{-5} Max.Sulfates\ (ppm) + \\ 6.73\times10^{-3}\ Minimum\ Redox(mV) \\ \textbf{if Predicted corrosion rate} \geq \textbf{0} \\ \\ 0 \\ \textbf{otherwise} \end{cases}$$

The above model is based on 9 observations and has 3 degrees of freedom. The R^2 value of 73.4% between the soil electrochemical variables and the zinc corrosion rate indicates that 73.4% of the total variation in zinc corrosion rate can be explained by the above linear relationship. Table 18 summarizes the standardized coefficients of the above model. The p-value for each term tests the null hypothesis that the coefficient is equal to zero (no effect). A low p-value indicates that the null hypothesis can be rejected. In other words, a predictor that has a low p-value is likely to be a meaningful addition to the model because changes in the predictor's value are related to changes in the response variable. Conversely, a larger (insignificant) p-value suggests that changes in the

predictor are not associated with changes in the response. The results of the zinc corrosion model show the resistivity to be relatively significant with a low p-value (p=0.120), when compared to other predictor variables.

Table 18. The Standardized Coefficients of the Zinc Corrosion Model

Source	Value	Standard error	t	P-value	Lower bound (95%)	Upper bound (95%)
Minimum Resistivity	-0.972	0.450	-2.161	0.120	-2.404	0.460
Minimum pH	-0.131	0.482	-0.271	0.804	-1.664	1.403
Maximum Chlorides	0.191	0.440	0.434	0.694	-1.209	1.590
Maximum Sulfates	0.009	0.463	0.019	0.986	-1.465	1.483
Minimum Redox	0.178	0.468	0.379	0.730	-1.313	1.668

Similarly, fitting the steel corrosion rate data into a multivariate linear regression model yields to:

$$Predicted\ Corrosion\ Rate\ of\ Steel\ (mpy) = \begin{cases} 6.54 - 2.06\times10^{-3}\ Min.Resistivity\ (\Omega.cm) - \\ 0.56\ Min.pH + 6.50\times10^{-4}\ Max.Chlorides\ (ppm) + \\ 3.96\times10^{-4} Max.Sulfates\ (ppm) + \\ 1.31\times10^{-2}\ Minimum\ Redox(mV) \\ \textbf{if Predicted corrosion rate} \geq \textbf{0} \\ \\ 0 \\ \textbf{otherwise} \end{cases}$$

The steel corrosion model is also based on 9 observations and has 3 degrees of freedom. The R^2 value between the soil electrochemical variables and the steel corrosion rate is 76.6%. Table 19 summarizes the standardized coefficients of the steel corrosion model. Similar to zinc, the results of the steel corrosion model show the resistivity to be relatively significant with a low p-value (p=0.092), when compared to other predictor variables.

Table 19. The Standardized Coefficients of the Steel Corrosion Model

Source	Value	Standard error	t	P-value	Lower bound (95%)	Upper bound (95%)
Minimum Resistivity	-1.035	0.423	-2.450	0.092	-2.380	0.309
Minimum pH	-0.138	0.452	-0.304	0.781	-1.577	1.302
Maximum Chlorides	0.141	0.413	0.342	0.755	-1.173	1.455
Maximum Sulfates	0.093	0.435	0.214	0.845	-1.291	1.477
Minimum Redox	0.269	0.440	0.612	0.584	-1.131	1.669

As described in this section, there exist several approaches to predict the underground corrosion of zinc and steel structures. Because of the usefulness of such methods, the developed approach implements all of the applicable existing methods in the decision framework. The methods that are excluded from the modeling approach are the following:

- Weight loss method: this method consists of experimentally measuring the difference in weight and thus the degradation loss due to corrosion. Using this method to predict the corrosion rate is not feasible without experimental testing.
- AWWA numerical corrosivity scale: this method provides a qualitative assessment of the soil corrosivity and therefore does not provide a quantitative assessment of corrosion rates.
- Electrochemical in-situ method: this method is a faster experimental technique compared to the classical weight loss estimation to quantify the corrosion rate. Similar to the weight loss method, it consists of an experimental testing of the corrosion current and therefore could not serve for prediction purposes.

- Romanoff-NBS method: this method is limited by a data from 47 projects. Although practitioners frequently refer to this method as a foundation to predict corrosion rates on one given site, many studies investigate the limitations of such method (Ricker 2007), especially when used for statistical modeling.
- NACE corrosion reference: this method classifies corrosion rates into four main categories, lacking an accurate quantitative assessment of soil corrosivity.
- NYSDOT method: this method does not account for the effect of the resistivity, sulfates and redox potential on the corrosion rate, establishing a major limitation for its applicability.

In summary, all potential methods for underground corrosion assessment were reviewed qualitatively. Since, no single method was found to be superior and the logical approach was to leverage all relevant methods selecting based on site characteristics and range of operation of each method to assess the underground corrosion rate. The next section elaborates on this approach which is henceforth referred to as the *First Solar* – ASU approach.

3.4.3. First Solar – ASU Proposed Method

To account for the underground corrosion of the zinc and steel components of driven posts, the *First Solar* – ASU proposed method consists of designing a meta-model that leverages all of the relevant existing approaches on the existing approaches in the literature as well as two newly-developed models from *First Solar* data. The approach consists of predicting the underground corrosion rates followed by a quantification of the ESL of zinc and steel for a specific site. As a result, the ESL of the underground system is achieved, as discussed in the following subsections.

To complete the underground corrosion analysis, the meta-model requires the following inputs:

- **Design life:** the estimated design life of the system. The default value is 25 years.
- **Soil electrochemical data:** the minimum, average, and maximum values of resistivity (ohm-cm), pH, chlorides (ppm), sulfates (ppm), and redox (mV) for three depth layers (0 to 2 ft., 2 to 4 ft., and 4 to 6 ft.).
- **Steel beam design:** the steel beam design of the underground system in order to determine its critical dimension in mils (typically the web thickness). In addition to the seven default designs that are provided (W 6x7, W 6x8.5, W 6x9, W 6x12, W 6x16, IPE140, and IPE 160), custom values can be entered manually.
- **Zinc coating thickness:** the initial zinc coating thickness of the underground system in mils.
- **Steel corrosion allowance:** the allowable steel corrosion either in mils per side or percentage.

Once the above inputs are provided for a specific location, the method consists of selecting the desirable models, which have similar conditions and ranges of operation. Table 20 and 21 summarize the different underground corrosion models for zinc and steel, respectively.

For each model, the method displays the estimated corrosion rate in mpy, the expected degradation and remaining thickness in mils at the end of the design life in mils, and the ESL for both zinc and steel at different depth layers. Additionally, the minimum, average and maximum of the underground corrosion ESL are computed and will be

compared to those of the above-ground corrosion in order to define the overall system ESL.

Table 20. Underground Zinc Corrosion Models

Corrosion Loss Model	Source	Description	Resistivity (Ω-cm)	pH	Chlorides (ppm)	Sulfates (ppm)	Redox (mV)
$X\ (\mu m) = 25*t(yrs)^{0.65}$	FHWA	Average loss based on NBS-Romanoff	> 2,000	-	-	-	-
X (µm) = (t -10 yrs)*28	Caltrans	Caltrans guidance for "Neutral & Alkaline" fills	> 1,000	> 7	-	-	-
X (µm) = (t -10 yrs)*33	Caltrans	Caltrans guidance for "Acidic" fills	> 1,000	< 7	-	-	-
X (µm) = (t - 6 yrs)*71	Caltrans	Caltrans guidance for "Corrosive" fills	< 1,000	-	-	-	-
X (µm) = (t - 10.5 yrs)*12	AASHTO	AASHTO model	> 3,000	5 to 10	≤ 100	≤ 200	-
$X\ (\mu m) = 22.5*(t\text{-}16\ yrs)^{0.67}$	UK Model	UK guidance for Non-Aggressive soils	2,000 to 8,000	6 to 9	≤ 50	≤ 240	-
$X\ (\mu m) = 40*(t\text{-}4.6\ yrs)^{0.80}$	UK Model	UK guidance for Aggressive soils	667 to 2,000	5 to 6	50 to 250	240 to 600	-
$Corrosion\ Rate\ Zinc = 5.64 - 1.51\times10^{-3}\ Min.Resistivity - 0.41\ Min.pH + 6.83\times10^{-4}\ Max.Chlorides + 2.95\times10^{-5}\ Max.Sulfates + 6.73\times10^{-3}\ Minimum\ Redox$	First Solar	Fitting First Solar data in a regression model (R^2 value = 0.734), for most-conservative scenario at a depth of 6ft.	172 to 3,525	6.7 to 8.0	14 to 1,345	190 to 1,800	164 to 301

Table 21. Underground Steel Corrosion Models

Corrosion Loss Model	Source	Description	Resistivity (Ω-cm)	pH	Chlorides (ppm)	Sulfates (ppm)	Redox (mV)
X (µm) = $40*t(yrs)^{0.80}$	FHWA	Average loss based on NBS-Romanoff	> 2,000	-	-	-	-
Flowchart	FHWA	Corrosion guidance	-	-	-	-	-
Flowchart	Caltrans	Corrosion guidance	-	-	-	-	-
$Weight\ loss\ (mpy) = -17.2 + 0.000761\ [Cl-]\ (ppm) + 2.52\ pH$	NCHRP	Report 408	-	-	-	-	-
$Corrosion\ Rate\ Steel = 6.54 - 2.06\times10^{-3}\ Min.Resistivity - 0.56\ Min.pH + 6.50\times10^{-4}\ Max.Chlorides + 3.96\times10^{-4} Max.Sulfates + 1.31\times10^{-2}\ Minimum\ Redox$	First Solar	Fitting First Solar data in a regression model (R^2 value = 0.766), for most-conservative scenario at a depth of 6ft.	172 to 3,525	6.70 to 8.00	14 to 1,345	190 to 1,800	164 to 301

A demonstration of the underground corrosion tool is presented next, followed by a comparison of the underground corrosion models performance on *First Solar* sites.

3.4.3.1. Underground Tool Demonstration

The following is an example to illustrate the prediction of the underground zinc corrosion rate for a project located in California. The underground corrosion tool is part of the comprehensive **πCAT** tool, which combines both underground and above-ground corrosion assessments. Table 22 summarizes the inputs corresponding to the site and that

are required in the "Inputs" tab to complete the underground corrosion analysis, as shown in Figure 16.

Table 22. Inputs for Underground Corrosion

<table>
<tr><th>Inputs</th><th>Values of the project</th></tr>
<tr><td>Design life</td><td>25 years</td></tr>
<tr><td>Soil electrochemical data</td><td>
<table>
<tr><th>Depth</th><th>Variables</th><th>Resistivity (ohm-cm)</th><th>pH</th><th>Chlorides (ppm)</th><th>Sulfates (ppm)</th><th>Redox (mV)</th></tr>
<tr><td rowspan="3">0-2 ft.</td><td>Minimum</td><td>2,000</td><td>7.50</td><td>45</td><td>10</td><td>164</td></tr>
<tr><td>Average</td><td>11,183</td><td>8.10</td><td>134</td><td>132</td><td>230</td></tr>
<tr><td>Maximum</td><td>20,925</td><td>8.50</td><td>450</td><td>285</td><td>285</td></tr>
<tr><td rowspan="3">2-4 ft.</td><td>Minimum</td><td>1,600</td><td>7.50</td><td>45</td><td>10</td><td>164</td></tr>
<tr><td>Average</td><td>10,261</td><td>8.10</td><td>134</td><td>132</td><td>230</td></tr>
<tr><td>Maximum</td><td>20,525</td><td>8.50</td><td>450</td><td>285</td><td>285</td></tr>
<tr><td rowspan="3">4-6 ft.</td><td>Minimum</td><td>900</td><td>7.50</td><td>45</td><td>10</td><td>164</td></tr>
<tr><td>Average</td><td>8,580</td><td>8.10</td><td>134</td><td>132</td><td>230</td></tr>
<tr><td>Maximum</td><td>17,425</td><td>8.50</td><td>450</td><td>285</td><td>285</td></tr>
</table>
</td></tr>
<tr><td>Steel beam design</td><td>W6X7 beam</td></tr>
<tr><td>Zinc coating thickness</td><td>3 mils</td></tr>
<tr><td>Steel corrosion allowance</td><td>100%</td></tr>
</table>

Moreover, for demonstration purposes, all the models, as illustrated in Figure 17, are selected to estimate the underground corrosion rates and ESL of both zinc and steel. The estimations of the underground corrosion rates among the three different depth layers (0 to 2 ft., 2 to 4 ft., and 4 to 6 ft.) are displayed in the "Underground Corrosion" tab.

To help the end-user in the models selection, the tool is designed to highlight in "green" and "red" the applicable and non-applicable models, respectively. For three different layers, the tool provides the corrosion rate (mpy), the expected degradation and remaining thickness at the end of the design life (mils), and the expected service life (years) per model.

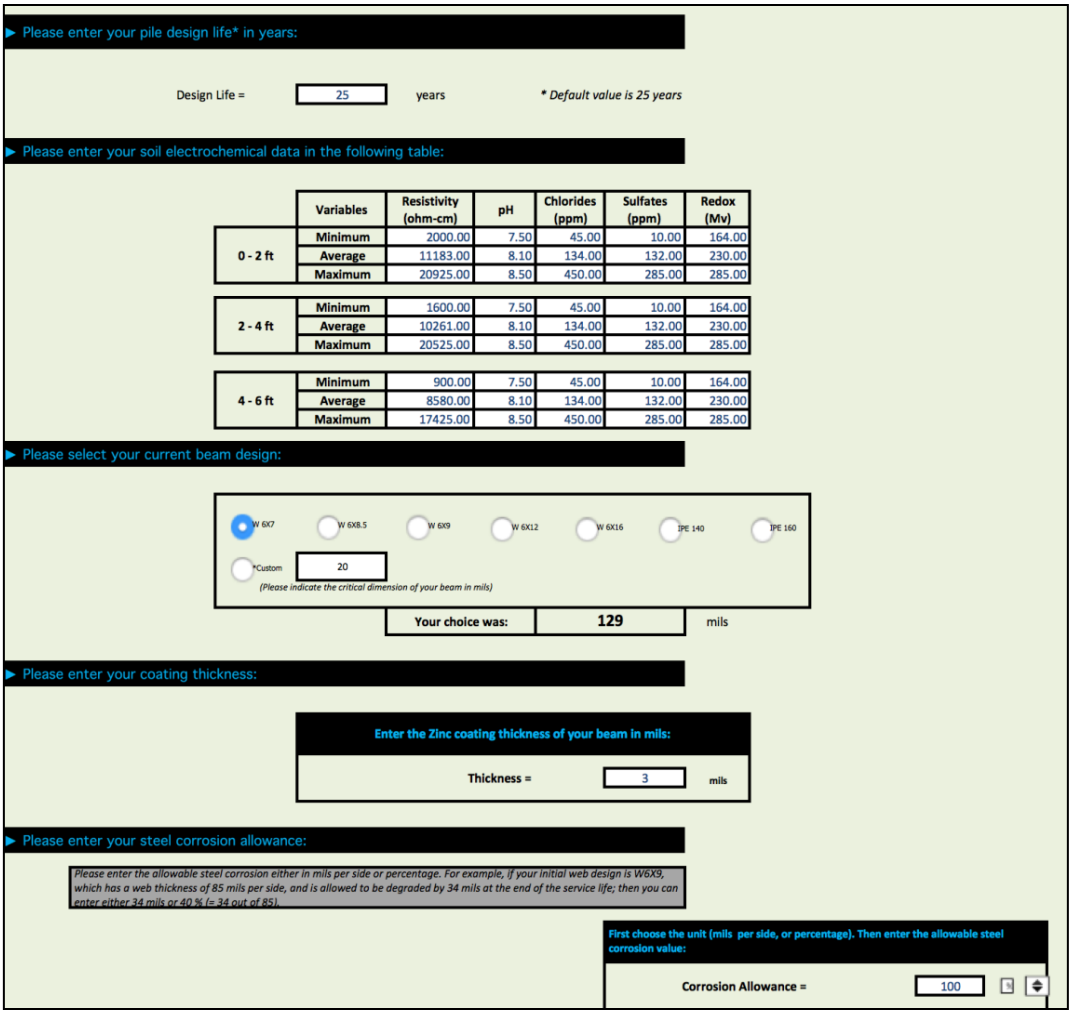

Figure 16. πCAT's Inputs for the Underground Corrosion Rate Estimation

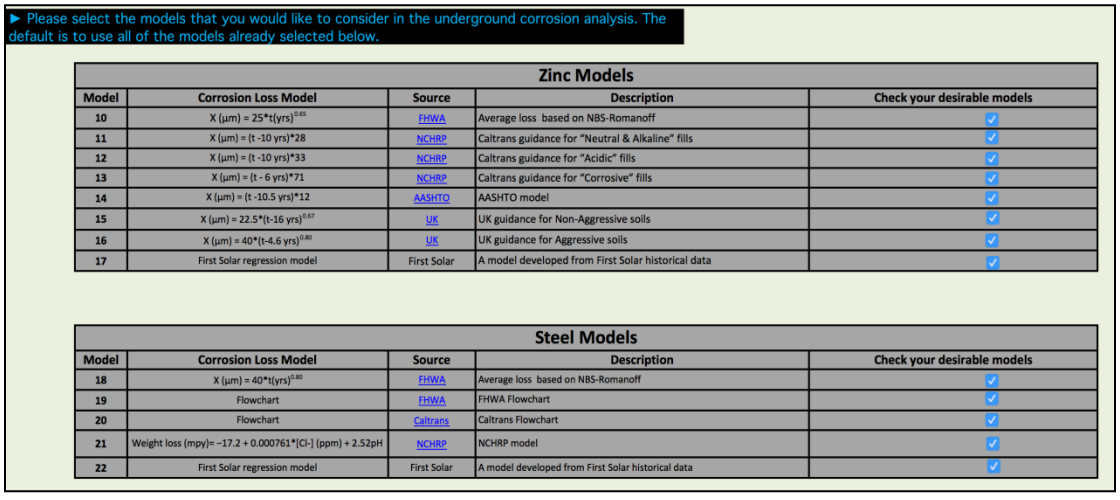

Figure 17. Models Selection for the Underground Corrosion Rate Estimation

Additionally, the minimums, averages, and maximums values are computed for the considered models. Figures 18 and 19 show the selected models to predict the corrosion rate of zinc and steel, respectively. Then, the underground system ESL is computed by adding the ESL of both zinc and steel subsystems. For each depth layer, a summary of the results for zinc and steel is presented. Finally, corrosion rates from both underground and above-ground corrosion analyses are summarized in the "Combined Model" tab.

Zinc Models										
Go to model	Corrosion Loss Model	Source	Description	Resistivity (Ω-cm)	pH	Chlorides (ppm)	Sulfates (ppm)	Least Conservative	Moderate	Most Conservative
10	X (μm) = 25*t(yrs)$^{0.65}$	FHWA	Average loss based on NBS-Romanoff	> 2,000	-	-	-	☐	☑	☑
11	X (μm) = (t -10 yrs)*28	NCHRP	Caltrans guidance for "Neutral & Alkaline" fills	> 1,000	> 7	-	-	☑	☑	☑
12	X (μm) = (t -10 yrs)*33	NCHRP	Caltrans guidance for "Acidic" fills	> 1,000	< 7	-	-	☐	☐	☐
13	X (μm) = (t - 6 yrs)*71	NCHRP	Caltrans guidance for "Corrosive" fills	< 1,000	-	-	-	☐	☐	☐
14	X (μm) = (t -10.5 yrs)*12	AASHTO	AASHTO model	> 3,000	5 - 10	≤ 100	≤ 200	☐	☐	☐
15	X (μm) = 22.5*(t-16 yrs)$^{0.67}$	UK	UK guidance for Non-Aggressive soils	2,000 - 8,000	6 - 9	≤ 50	≤ 240	☑	☐	☐
16	X (μm) = 40*(t-4.6 yrs)$^{0.80}$	UK	UK guidance for Aggressive soils	667 - 2000	5 - 6	50 - 250	240 - 600	☐	☐	☐

Figure 18. The Underground Corrosion Models of Zinc

Steel Models										
Go to model	Corrosion Loss Model	Source	Description	Resistivity (Ω-cm)	pH	Chlorides (ppm)	Sulfates (ppm)	Least Conservative	Moderate	Most Conservative
18	X (μm) = 40*t(yrs)$^{0.80}$	FHWA	Average loss based on NBS-Romanoff	> 2,000	-	-	-	☐	☑	☑
19	Flowchart	FHWA	FHWA Flowchart	-	-	-	-	☐	☐	☐
20	Flowchart	Caltrans	Caltrans Flowchart	-	-	-	-	☐	☐	☐
21	Weight loss (mpy)= −17.2 + 0.000761*[Cl-] + 2.52pH	NCHRP	NCHRP model	-	-	-	-	☑	☑	☑

Figure 19. The Underground Corrosion Models of Steel

3.4.3.2.Model Validation Approach

This aim of this section is to validate the developed research approach on *First Solar* sites to test the model's value for decision makers. Moreover, a comparison between the different models, for the same site, can lead to the assessment of models performance under different conditions. Knowing the importance of both underground and above-ground corrosion on the ESL of the overall system, the validation is limited by the availability of real measurements data. Due to the availability of underground corrosion studies and measurements at *First Solar* sites, this scope of this section entails a comparison of the tool's predicted values to the measured below ground corrosion rate provided by the site geotechnical analysis and physical measurements.

Three different scenarios or possibilities can be made when applying the developed model on *First Solar* sites. Corrosion rate is negatively correlated with resistivity, pH, and redox and positively correlated with chlorides and sulfates. Thus, a higher corrosion rate involves a low resistivity, low pH, low redox, high chlorides or high sulfates. Hence the three scenarios are defined as:

- Least conservative scenario: maximum resistivity, maximum pH, maximum redox, minimum chlorides, and minimum sulfates.
- Moderate conservative scenario: average resistivity, average pH, average redox, average chlorides, and average sulfates.
- Most conservative scenario: minimum resistivity, minimum pH, minimum redox, maximum chlorides, and maximum sulfates.

However, *First Solar* consultants use the measured minimum resistivity to estimate the maximum corrosion rate. While other scenarios were taken into account, the developed approach mainly compares the tool's predicted values assuming the most conservative scenario, to the measured corrosion rate provided by *First Solar* consultants. The following subsections detail the model validation for both zinc and steel corrosion rates.

3.4.3.2.1. Zinc Models Validation on First Solar Sites

After applying the zinc corrosion models on *First Solar* sites with complete data (N=9 projects), only four out of the eight other models are applicable, as shown in Figure 20. Additionally, the absolute error percentages between the predicted values and the measured zinc corrosion rate highlight the superiority of the *First Solar* developed model when compared to the literature models, as shown in Figure 21. The results feature a

noticeable discrepancy between literature models prediction and the real measured values of corrosion rate.

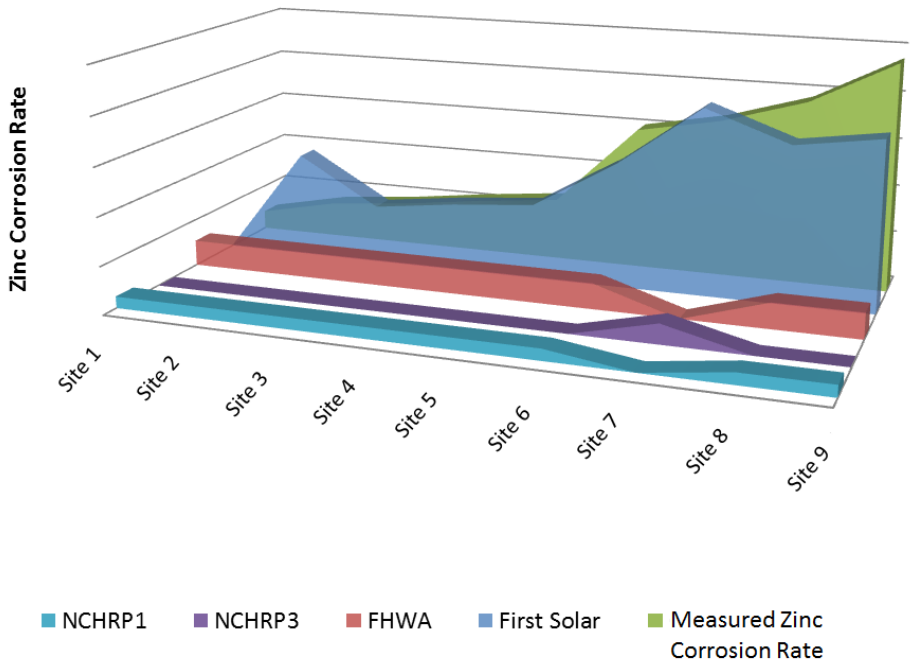

Figure 20. Zinc Model Validation on First Solar Sites (N=9)

Consequently, the remaining analysis focuses on the *First Solar* model performance, as one of the most promising model out of the existing ones. Also, additional sites that are tagged as outliers (N=5), have missing data (N=7), or have site measured data (N=3) are taken into consideration in order to validate the developed *First Solar* model on the maximum number of soil conditions.

Figure 22 compares the actual zinc corrosion rates to the predicted values from *First Solar* developed model (using the five independent variables) for a total of 24 projects. The sites are arranged from least to most corrosive on chart and tagged (# for outliers; * for sites with missing data; and ** for sites with actual rate measurements). In other words, the *First Solar* newly developed model performs better when the corrosion

rate in higher than 1 mpy. Overall, after applying the underground corrosion models on *First Solar* sites, the results show a superiority of the newly developed model in comparison with the existing methods.

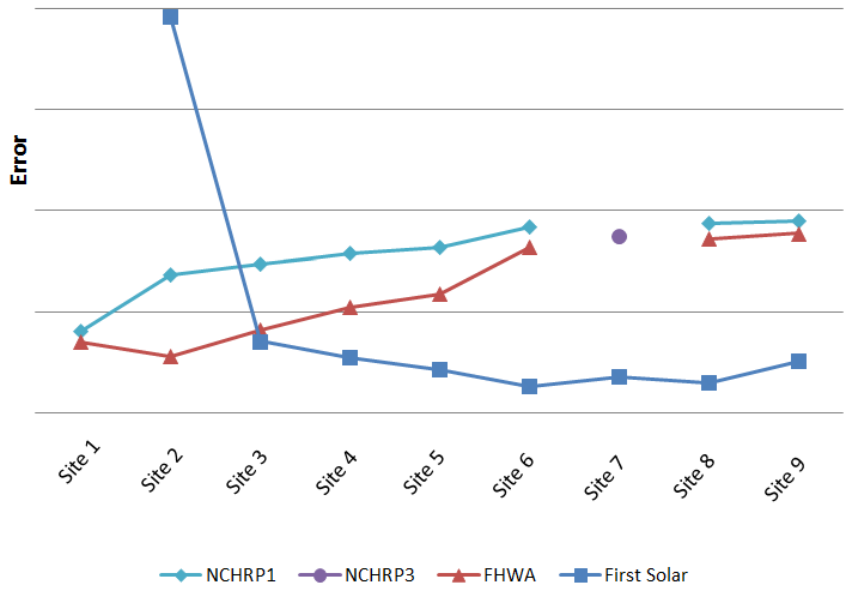

Figure 21. Validation Error of Zinc Corrosion Models (N=9)

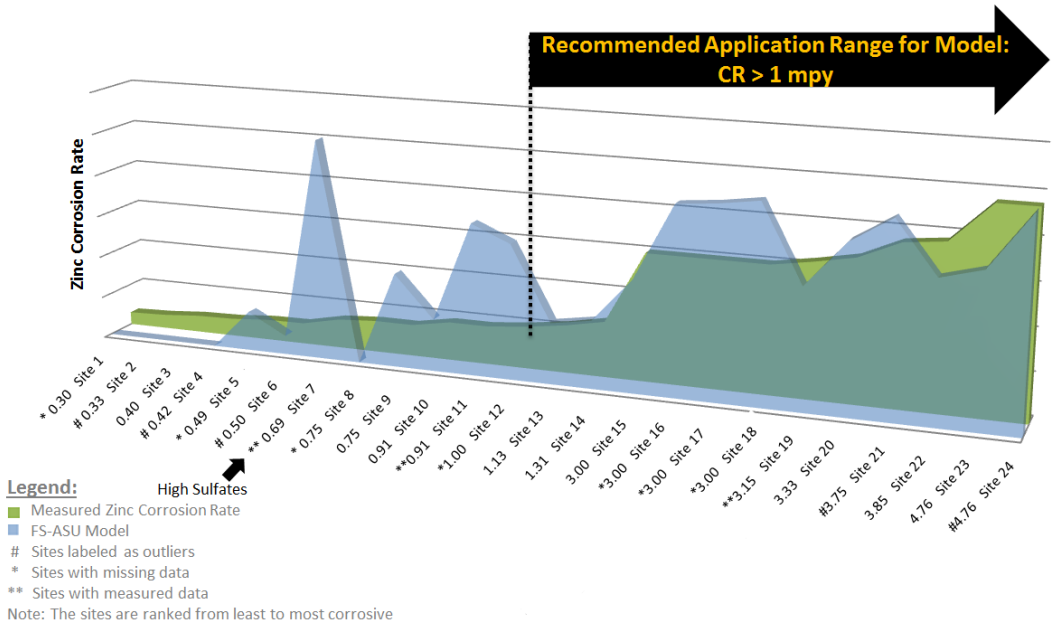

Figure 22. A Comparison of the Measured Zinc Corrosion Rate and the Newly-Developed Model Predicted Values (N=24)

Based on the approach validation on *First Solar* sites, if First Solar's model is applicable for a specific site, i.e. the site characteristics fall within the operation range, it is proven that its predicted value is closer to the measured one as compared to other existing models. Thus, the recommended zinc corrosion rate is defined as:

$$Predicted\ Corrosion\ Rate\ of\ Zinc\ (mpy)$$

$$= \begin{cases} 5.64 - 1.51\times10^{-3}\ Min.Resistivity\ (\Omega.cm) - \\ 0.41\ Min.pH\ +\ 6.83\times10^{-4}\ Max.Chlorides\ (ppm) + \\ 2.95\times10^{-5} Max.Sulfates\ (ppm) + \\ 6.73\times10^{-3}\ Minimum\ Redox(mV) \\ \textbf{if Predicted corrosion rate} \geq \textbf{0} \\ \\ 0 \\ \textbf{otherwise} \end{cases}$$

Subject to:

- Minimum resistivity: 172 to 3,525 ohm-cm
- Minimum pH: 6.7 to 8.0
- Minimum redox: 164 to 301 mV
- Maximum chlorides: 14 to 1,345 ppm
- Maximum sulfates: 190 to 1,800 ppm

3.4.3.2.2. Steel Models Validation on First Solar Sites

Similar to zinc models validation, steel corrosion models are applied on *First Solar* sites with complete data (N=9 projects), as shown in Figure 23. Although the NCHRP model is performing better than its existing counterparts, the performance of the *First Solar* developed model remains superior to the literatures methods (see Figure 24).

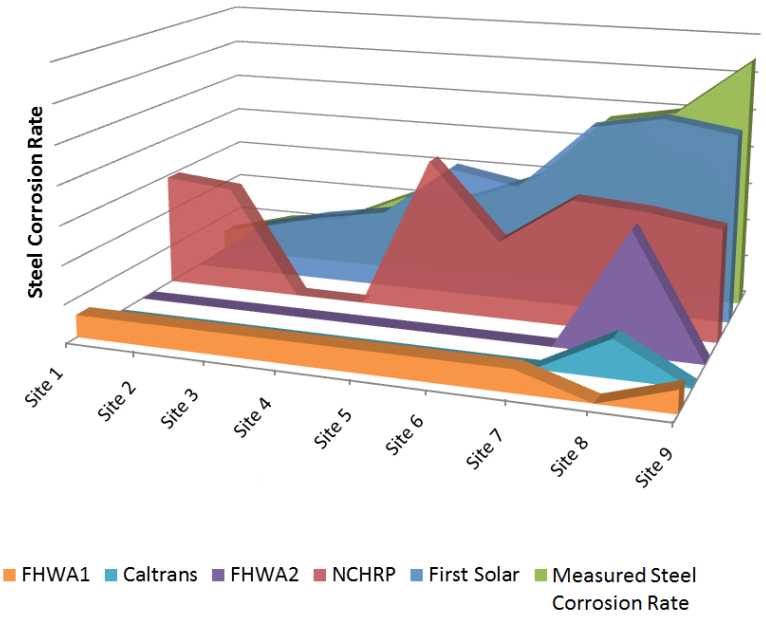

Figure 23. Steel Model Validation on First Solar Sites (N=9)

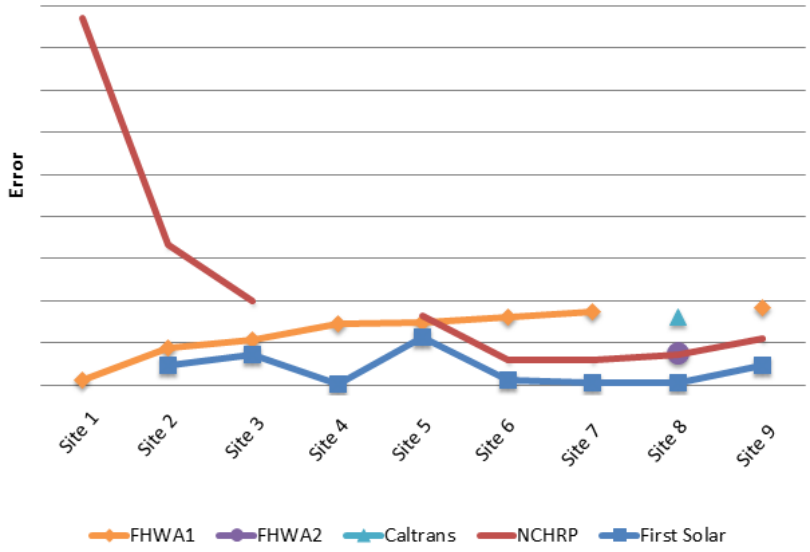

Figure 24. Validation Error (%) of Steel Corrosion Models (N=9)

Based on the approach validation on *First Solar* sites, if First Solar's model is applicable for a specific site, i.e. the site characteristics fall within the operation range, it is proven that its predicted value is closer to the measured one as compared to other existing models. Moreover, the NCHRP model is the second best model to be considered

while evaluating the ranges of existing models. Figure 25 compares the actual steel corrosion rates to the predicted values from a *First Solar* developed model (using the five independent variables) for the available 20 projects, from the least to the most corrosive.

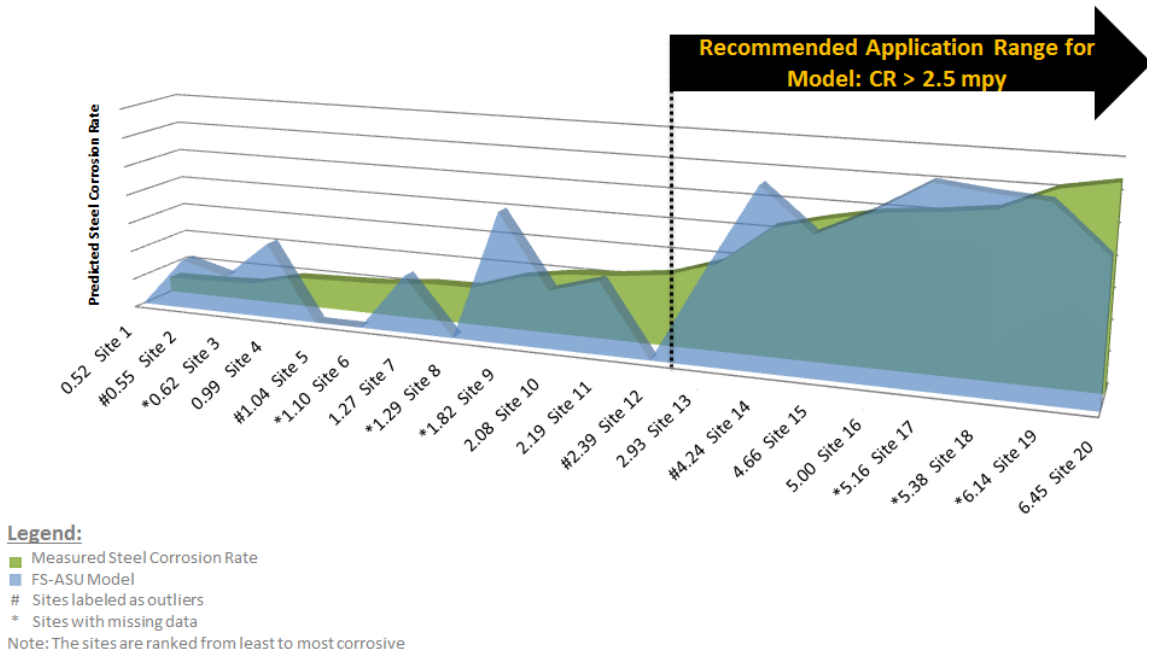

Figure 25. A Comparison of the Measured Steel Corrosion Rate and the Newly-Developed Model Predicted Values (N=20)

In conclusion, the newly developed model is recommended over the existing ones and mainly applies for sites with high corrosivity. The recommended steel corrosion rate is defined as:

$$Predicted\ Corrosion\ Rate\ of\ Steel\ (mpy)$$

$$= \begin{cases} 6.54 - 2.06\times10^{-3}\ Min.Resistivity\ (\Omega.cm) - \\ 0.56\ Min.pH + 6.50\times10^{-4}\ Max.Chlorides\ (ppm) + \\ 3.96\times10^{-4} Max.Sulfates\ (ppm) + \\ 1.31\times10^{-2}\ Minimum\ Redox(mV) \\ \textbf{if Predicted corrosion rate} \geq \textbf{0} \\ \\ 0 \\ \textbf{otherwise} \end{cases}$$

Subject to:

- Minimum resistivity: 172 to 3,525 ohm-cm
- Minimum pH: 6.7 to 8.0
- Minimum redox: 164 to 301 mV
- Maximum chlorides: 14 to 1,345 ppm
- Maximum sulfates: 190 to 1,800 ppm

This section concentrated on the underground soil corrosion of driven posts. First, a discussion of the factors contributing to the underground corrosion underlined the key variables to consider in the research modeling. Second, a presentation of the potential methods used for the assessment and prediction of corrosion, including a newly-developed model based on *First Solar* sites data, led to the development of the underground corrosion research framework. Third, the research approach was outlined and applied on a case study from a project in California along with other *First Solar* sites. The next section summarizes the conclusions of both underground and above-ground corrosion analyses, recommendations, and opportunities for future studies.

3.5. CONCLUSIONS AND RECOMMENDATIONS

Corrosion can lead to failures in solar PV plant infrastructure. Decisions regarding the future integrity of a structure or its components depend in large part on an accurate assessment of the site environment and conditions affecting its corrosion and rate of degradation. The objective of this research project is to curate the available approaches and identify the optimal approach to assess the corrosion of driven posts that are used in tracker and fixed tilt systems. As a result, this chapter develops a framework to inform and support decision-makers in design and reliability applications.

First, this chapter details the factors affecting the corrosivity rate of a site. Second, a complete meta-analysis of corrosion modeling, as it applies to PV solar support structures, highlights the current methods and practices used in industry to predict underground and above-ground corrosion rates. The research approach consists of developing a framework that integrates all the existing and applicable corrosion models in addition to newly-developed models based on the collected data to evaluate corrosion rates and estimated service lives of assets (structures).

Applying the underground corrosion models on current sites shows a noticeable discrepancy between the prediction of existing models and the real measured values of corrosion rates. The results demonstrate the superiority of the newly developed approach, compared to existing methods, in predicting zinc and steel underground corrosion rates. However, the application of the developed models is limited to the range of data found on the available *First Solar* sites. Moreover, the proposed approach is found to work best in highly corrosive environments.

To bolster the proposed decision making framework, the research team provides the following four recommendations:

1. A solar company is recommended to request (and consultants are recommended to include) the critical soil electrochemical data in the commissioned geotechnical studies, in order to help predicting corrosion rates. Specifically, minimum, average, and maximum values of resistivity, pH, redox, chlorides, and sulfates need to be provided to the solar company. To improve the accuracy (and predictive power) of the newly-developed model, site data for a range of 41 to 78

projects are needed. The new data, originating from *First Solar* sites or other sites, should be used to strengthen the model and widen its range of application.

2. A solar company is recommended to continue its internal quality assurance testing and inspection of the 3 mils zinc coating thickness requirement, in compliance with ASTM A123.
3. In addition to corrosion predictive models, accelerated testing is recommended to simulate underground and above-ground conditions to experimentally quantify the impact of corrosion. Further analysis of the air composition is recommended in specific microenvironments, where industrial emissions can include different types of contaminants boosting the atmospheric corrosivity of the site.
4. To plan for future studies and site monitoring, the study recommends including 5 to 10 additional benchmark/reference posts on each new site. One of these posts will be unearthed every few years to reliably quantify the losses due to underground corrosion, without impacting operations

CHAPTER 4

PROBABILISTIC RISK/FAILURE RATE ASSESSMENT OF POLYMERIC MATERIALS USED IN PV SYSTEMS

4.1. ABSTRACT

The solar energy sector has been growing rapidly over the past decade. As global energy demands increase, the photovoltaic industry is expected to continue to grow along with the technological advancements in large scale manufacturing. Such growth in renewable electricity generation using photovoltaic systems is accompanied by an increased awareness of the different faults in polymeric materials supporting solar plants during the operational lifetime. This awareness is translated as a growing need to reduce costs through an optimized material selection that will ensure an increase in service lifetimes and a reduction in product liability, repair and maintenance. To address this problem, this research develops, implements and delivers a decision framework to support the polymeric materials selection for cables, connectors, and module clips rubber insulation, used in tracker and fixed tilt systems. Starting with an understanding of the current practices and designs, the research method starts with three steps: a) fault tree analysis; b) qualitative assessment; and c) an investigation of existing decision frameworks. Next, the research builds on these steps and develops a tool that integrates all the findings to inform and support design and reliability decision-makers in the selection of polymeric materials for the studied components. Then, the research validates the developed framework and showcases its advantages in materials selection, design, and logistical support of fielded and future photovoltaic systems.

4.2. INTRODUCTION

Polymeric materials are increasingly being used in a wide range of applications where long-term service in hostile environments is required (Maxwell et al. 2005), such as renewable energy aerospace, automotive, marine, infrastructure, military etc. This increase in usage was accompanied with a growing need to reduce costs through an optimized material selection to increase service lifetimes and reduce product liability, repair and maintenance.

To support their PV power plants, *First Solar*, Inc., a leading global provider of solar energy solutions, uses different types of polymeric materials that are used in tracker and fixed tilt systems, as shown in Figure 26 below.

Figure 26. First Solar Site (First Solar Procurement and Construction Management, 2017)

As further evidence of *First Solar*'s foresight and leadership in the industry, *First Solar* partnered with ASU to study the failure of polymeric materials used in solar projects and to develop a decision-making framework dedicated to this topic.

Performance during use is a key feature of any polymeric material, which decides the suitability of a product for outdoor applications. As there is an increase concern regarding the durability of polymeric materials in solar projects, the objectives of this study involve mitigating the risk associated with the failure of these materials by providing a decision-making framework. This research focuses on three specific components:

A. Cables;

B. Connectors; and

C. Rubber insulation in module clips

The scope of the study consists of:

- Understanding current practices, designs, concerns and limitations;
- Studying the factors leading to the failure of polymeric materials;
- Developing a research method to assess the probabilistic risk of polymeric materials failures based on the literature assessment methods as it applies to PV systems;
- Applying the developed model on *First Solar* materials and components; and
- Establishing a tool to inform and support design and reliability decision-makers in materials selection.

The optimal design of stationary photovoltaic in a solar field, taking into account shading and masking effects, is based on several criteria: maximum incident energy on collector plane from a given field, minimum field area for given incident energy, minimum cost per unit energy, minimum plant cost, maximum energy per unit collector area as well as the reliability of these systems over the estimated service life of the

project (Weinstock and Appelbaum 2004). Such design involves the selection of different solar PV components and materials according to the system type, site location and applications. The long-term reliability of a PV panel is highly affected by the degradation behavior of the polymeric materials within the module (Schlothauer et al. 2012), such as the encapsulant and back-sheet, as well as the supporting structures and systems components, such as clips, cables, and connectors (Plaček et al. 2003).

Figure 27 summarizes the research method, which is thoroughly discussed in this chapter.

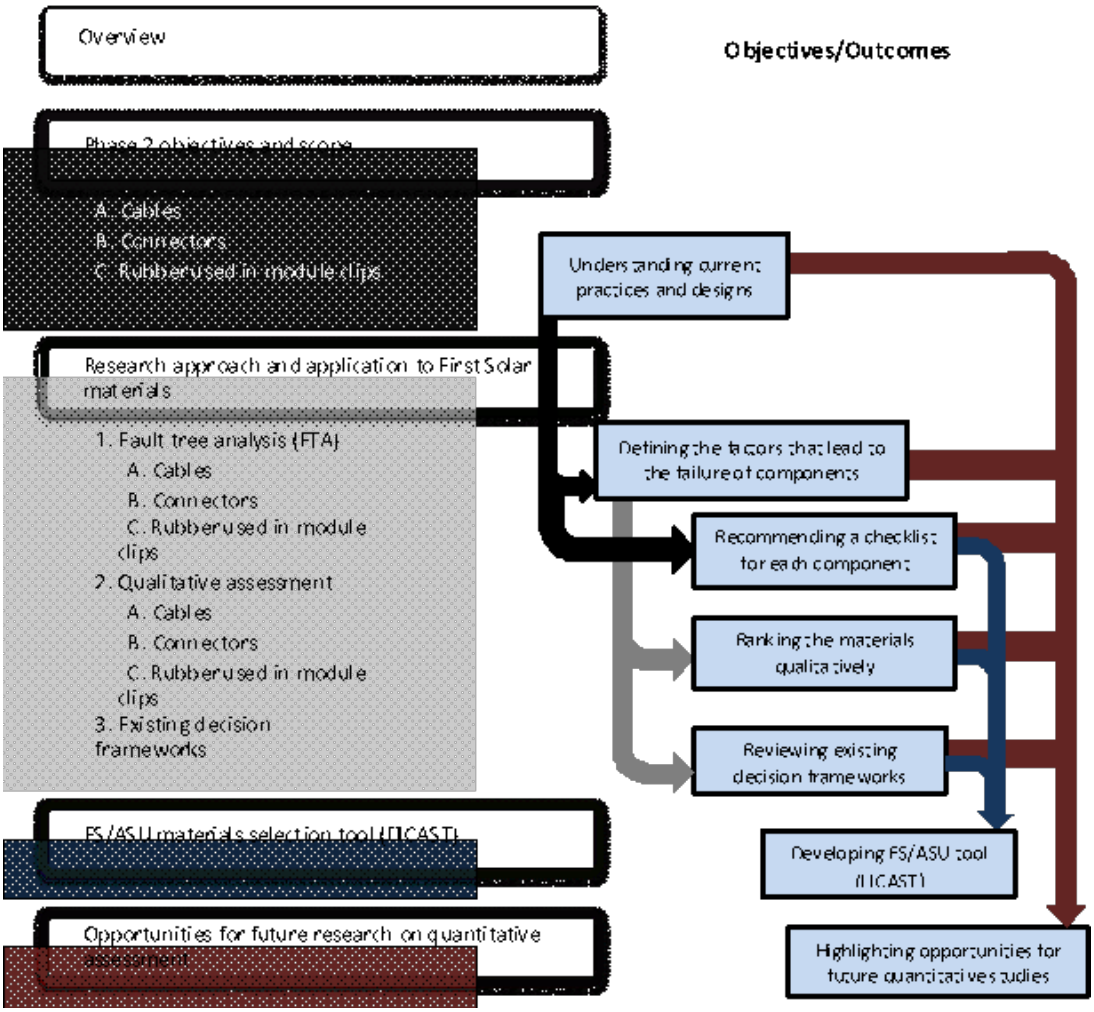

Figure 27. Research Scope

The developed approach consists of studying the performance of polymeric materials deployed in cable insulation, connectors, and module clips rubber. After understanding the current practices and designs, the research method entails three steps:

1. Fault tree analysis: building fault trees for components paves the way to define the root factors causing their failures. The research method builds on these factors to recommend inspection checklists for each component.
2. Qualitative assessment: collecting performance data from polymeric materials suppliers leads to rank them qualitatively.
3. Existing decision frameworks: analyzing the existing decision frameworks highlights the different considerations for an optimal selection of polymers.

Next, the outcomes of these above three steps are integrated into a supportive tool to inform and support design and reliability decision-makers in selection polymeric materials for their components. In addition, the study highlights the challenges and opportunities for future quantitative assessment studies.

This chapter establishes the probabilistic risk/failure rate assessment methods with respect to First Solar polymeric materials used in PV systems. Section 4.3 classifies the different types of polymers, outlines the main degradation factors, and describes current practices and designs of *First Solar* polymeric materials. Section 4.4 details the research plan, presents the different assessment approaches, and applies the comprehensive research method on *First Solar* materials. Section 4.5 describes the materials selection tool development. Section 4.6 summarizes the learned lessons and recommendations to select polymeric materials for electrical components.

4.3. RESEARCH BACKGROUND AND SCOPE

This section describes the current practices, designs, and concerns related to polymeric materials used in PV systems. First, it explains the structure of polymers and distinguishes their different types and classifications based on their characteristics. Second, it outlines the main factors affecting their degradation. Then, it describes the features and types of polymeric materials deployed in cables, connectors, and module clips rubber insulation to meet the objectives of this study.

4.3.1. Polymers Classification

Synthetic and natural polymers play an essential and ubiquitous role in everyday life. Polymers already have a range of applications that far exceeds that of any other class of material available to man. Current applications extend from adhesives, coatings, foams, and packaging materials to textile and industrial fibers, composites, electronic devices, biomedical devices, optical devices, and precursors for many newly developed high-tech ceramics. Polymers are defined as macromolecules composed of one or more monomers that are repeated throughout a chain (McCrum et al. 1997). The process by which these monomers are linked together is known as polymerization. For example, polymerization of ethylene yields polyethylene, a typical sample of which may contain molecules with 50,000 carbon atoms linked together in a chain. Their consequently large molecular mass relative to small molecule compounds produces unique physical properties, including toughness and viscoelasticity (Young and Lovell 2011).

Depending on how polymers are linked or joined (chemical bonds or intermolecular forces) and on the arrangement of the different chains, the resulting polymeric materials can be first separated into two groups: elastomers (rubber) and

plastics. Table 23 highlights the differences between the characteristics and features of both classes (Massey 2003).

Table 23. Comparison between Rubbers and Plastics [Adapted from (Massey 2003)]

Basis	Rubbers	Plastics
Definition	A tough elastic polymeric substance made from the latex of a tropical plant or synthetically.	A synthetic material made from a wide range of the organic polymers that can be molded into the shape while soft, and then into rigid or slightly elastic form.
Components	They mainly consist of: • Iso-propene • Other organic compounds • Water	They mainly consist of: • Plasticizer • Stabilizer • Filler • Pigments, etc.
Deformable	They are deformable.	They are non-deformable.
Elasticity	They are naturally more elastic.	They are less elastic in nature.
Toxicity	They have high toxicity because of their water content.	They have low toxicity because of their insolubility in water.
Synthetic materials	Synthetic rubbers are made from crude oil.	Synthetic plastics are made from natural gas or petroleum.
Advantages/ Benefits	• They are flexible and can be turned into any shape.	• Plastics are cheap to produce. • Plastics are unbreakable. • They possess good shock absorption capacity.
Disadvantages	• They expand when they are heated.	• Plastics are non-renewable resource.

Moreover, polymers are classified based on their response to heat between thermoset and thermoplastic. From one side, thermoset polymers are cross-linked together during the curing process to form an irreversible chemical bond. This process eliminates the risk of the product re-melting when heat is applied, making thermosets ideal for high-heat applications such as electronics and appliances. From the other side, thermoplastic polymers soften when heated and become more fluid as additional heat is applied.

The curing process is completely reversible as no chemical bonding takes place. This characteristic allows thermoplastics to be remolded and recycled without negatively affecting the material's physical properties. Table 24 compares the features, pros, and cons of both groups (Hocheng and Puw 1992).

Polymers are encountered in everyday life and are used for many purposes. Table 25 shows the eight most common types of synthetic organic polymers, which are commonly consumed in our daily life (Andrew and Allison 2006). The following section describes the main degradation factors and modes that could affect polymeric materials.

4.3.2. Degradation Factors and Modes

Despite advances in polymers manufacturing and continuous attempts to make durable and long-lasting components, the material can still experience failure. When a part or product fails, the consequences can be severe. Therefore, to control the stability of PV polymeric materials, an understanding of different degradation mechanisms is a primary requisite. As there is an increase concern regarding the durability of polymeric materials in solar projects, the following subsections discuss the various types of polymeric materials degradation.

Table 24. Comparison between Thermosets and Thermoplastics [Adapted from (Hocheng and Puw 1992)]

Basis	Thermosets	Thermoplastics
Features	Thermosets significantly improve the material's mechanical properties, providing enhances chemical resistance, heat resistance and structural integrity. Thermosets are often used for sealed products due to their resistance to deformation.	There are multiple thermoplastic resins that offer various performance benefits, but most materials commonly offer high strength, shrink-resistance and easy bendability. Depending on the resin, thermoplastics can serve low-stress applications such as plastic bags or high-stress mechanical parts.
Pros	• More resistant to high temperatures than thermoplastics • Highly flexible design • Thick to thin wall capabilities • Excellent aesthetic appearance • High levels of dimensional stability • Cost-effective	• Highly recyclable • Aesthetically-superior finishes • High-impact resistance • Remolding/reshaping capabilities • Chemical resistant • Hard rubbery surface options • Eco-friendly manufacturing
Cons	• Cannot be recycled • More difficult to surface finish • Cannot be remolded or reshaped	• Generally more expensive than thermosets • Can melt if heated

Table 25. Common Types of Polymers [Adapted from (Andrew and Allison 2006)]

Polymer	Properties	Uses
Low-density polyethylene (LDPE)	• Chemically inert • Flexible • Insulator	Squeeze bottles, toys, flexible pipes, insulation cover (electric wires), six pack rings, etc.
High-density polyethylene (HDPE)	• Inert • Thermally stable • Tough and high tensile strength	Bottles, pipes, inner insulation of coax cable, plastic bags, etc.
Polypropylene (PP)	• Resistant to acids and alkalies • High tensile strength	Auto parts, industrial fibers, food containers, liner in bags, dishware and as a wrapping material for textiles and food
Polystyrene (thermocole) (PS)	• Thermal insulator • Properties vary	Petri dishes, CD case, plastic cutlery
Polytetrafluoroethylene (PTFE)	• Very low coefficient of friction • Excellent dielectric properties • Chemically inert	Low friction bearings, non-stick pans, coating against chemical attack etc.
Polyvinyl Chloride (PVC)	• Insulator • Flame retardant • Chemical inert	Pipe, lawn chairs, hand-bags, curtain clothes, non-food bottles, toys, electrical installation insulations, etc.
Polychlorotri Fluoroethylene (PCTFE)	• Stable to heat and thermal attacks • High tensile strength and non-wetting	valves, seals, gaskets etc.

4.3.2.1. Thermal degradation

Thermal degradation refers to the chemical and physical processes in polymers that occur at elevated temperatures. Increased temperature accelerates most of the degradation processes that occur in polymers such as oxidation, chemical attack and mechanical

creep. It is a typical degradation condition for commercial polymer products as well as industrial products including electrical components in PV systems. At high temperatures, the components of the long chain backbone of the polymer can begin to separate (molecular scission) and react with one another to change the properties of the polymer. It is part of a larger group of degradation mechanisms for polymers that can occur from a variety of causes such as:

- Heat (thermal degradation and thermal oxidative degradation when in the presence of oxygen).
- Light (Photodegradation).
- Oxygen (oxidative degradation).
- Weathering (generally UV degradation).

Thermal degradation is mostly classified into two categories: (a) thermal oxidation (the thermal degradation in the presence of oxygen); and (b) thermal decomposition (the thermal degradation in the absence of oxygen).

a. Thermal oxidation

Thermal oxidation is generally considered to be the most serious problem when using polymers at elevated temperatures (Wright 2001). The influence of temperature on the oxidation processes will depend on the chemical structure of the polymer. Thermal oxidation is initiated by the reaction of free radicals $P\cdot$ with oxygen to form peroxide radicals:

$$P\cdot + O_2 \rightarrow POO\cdot$$

All polymers contain these free radicals due to their polymerization and processing history. However, the concentration of free radicals can be significantly

increased by interaction with light, ionizing radiation or the presence of transition metals. Once formed the peroxide radicals undergo slower propagation reactions that breakdown the polymer chains. The overall degradation process will normally involve a relatively long induction period during which little degradation is observed (Wright 2001). At the end of this period there is a rapid increase in degradation leading to a significant reduction in the mechanical properties of the polymer. This induction period is temperature sensitive and is reduced significantly at elevated temperatures. The induction period of the degradation process can normally be regarded as the serviceable lifetime of the polymer.

The thermal oxidation is subdivided into two categories, non-flaming and flaming modes (Einhorn et al. 1977). The thermal oxidation at non-flaming mode is close to the standard circumstance. On one hand, thermal oxidation of organic compound was studied in different studies (Yur'Ev et al. 1961; Girard et al. 1965). The reaction rate of the thermal oxidation is promoted by higher temperature (George 1979; Celina et al. 1997; Celina et al. 2005; Ito and Nagai 2008) and its activation energy can be calculated by an Arrhenius plot (George 1979) (Celina et al. 2005; Ito and Nagai 2008). On the other hand, thermal oxidation at a flaming mode was also performed (Nakatani et al. 2005; Fayolle et al. 2007). In some cases, characteristic conditions of thermal oxidation were studied such as the cycle test of UV irradiation and thermal oxidation (Karlsson et al. 1997), Thermogravimetric Analysis/Differential Thermal Analysis (TG/DTA) under air condition (Horrocks et al. 1994), the thermal aging under humidity control (Chiellini et al. 2006) and the exposure to ozone atmosphere. For instance, in the case of plasticized polyvinyl chloride (PVC), the contents of plasticizer were decreased by the thermal

oxidation condition when the temperature is less than 120 °C (Ito and Nagai 2007).Through the thermal oxidation condition, the plasticizer is migrated in the bulk and volatilized from the surface. Accordingly, the mechanical properties, in particular the elongation, are closely related to the loss of plasticizer.

b. Thermal decomposition

The thermal decomposition and the thermal oxidation are closely related to each other, because the initiation reaction is the generation of the radicals. Thermal decomposition affects polymeric materials at high temperature without atmosphere condition in particular oxygen and moisture. TG and DTA were applied as the traditional methods to study this mechanism. The combination method of TG – Fourier transform infrared spectroscopy (FTIR) was also performed to identify the decomposition product (Xue et al. 1997). Thermal volatilization analysis (TVA) was a characteristic method to distinguish the thermal decomposition products between condensable and non-condensable at -190 °C (McNeill et al. 1995).

In polymer composites the mismatch between the thermal expansion of the polymer matrix and the fibers may cause thermo-mechanical degradation during thermal cycling. Similar mechanisms may also occur in adhesive joints. A sudden brief exposure to high temperatures can result in a phenomenon known as thermal spiking.

Polymers can be protected from thermal degradation by incorporating stabilizers into them. Stabilizers are used to keep the polymer chains and the original molecular structure intact and therefore properties such as strength, stiffness and toughness can be retained over a longer period. Stabilizers can work in a variety of ways but in most cases they work by interrupting the thermal degradation cycle to slow down or prevent the

cycle from completing. Some stabilizers work by 'mopping up' the available free radicals (radical scavengers). In this case the stabilizer reacts rapidly with the available free radicals to produce another much less active free radical and thus slow the process down.

Thermal degradation of polymers at elevated temperatures is an inevitable event and for many polymers it can be a significant limitation to the application service life of a product. Even at moderate service temperatures long-term thermal degradation can represent a limitation to the service life. Despite this, the use of a base polymer that is naturally highly resistant to thermal degradation will enable PV products to be used at elevated temperatures with confidence that they will work as designed. If the use of a naturally resistant polymer is not possible then the correct selection and use of a relevant stabilizer package can also considerably extend the service life of a component part.

4.3.2.2.Photodegradation

Weathering or more specifically photo-oxidation of polymers refers to the chemical and physical changes that occur when radiation is absorbed by a polymer (White and Turnbull 1994; Brown et al. 1995; Brown et al. 2002). Photodegradation is initiated by solar radiation, which results in the absorption of UV radiation by chromophores and in the activation of excited states in macromolecules. However, other climatic quantities such as heat, moisture and airborne pollution all influence the mechanisms of degradation and the subsequent results of ageing (White and Turnbull 1994).

When a polymer is exposed to solar radiation the energy absorbed by the polymer results in the formation of free radicals within the polymer by the dissociation of the C-H bonds in the polymer chains.

$$PH \rightarrow P\cdot + H\cdot$$

The extent of this chemical reaction depends on the radiation exposure that is the quantity of ultraviolet light (<350nm) to which it is exposed. Once free radicals have been produced, reaction with oxygen generates hydroperoxides (POOH).

$$P\cdot + O2 \rightarrow POO\cdot \qquad\qquad POO\cdot + PH \rightarrow POOH + P\cdot$$

These hydroperoxides can dissociate further to produce a series of decomposition products including aldehydes and ketones. The presence of these carbonyl groups in a degraded polymer can be used as a chemical index for degradation. Once formed, these free radicals can continue to react via propagation reactions long after the initial UV exposure has ended. Termination of these free radical reactions is normally achieved through the reaction of pairs of free radicals.

$$P\cdot + P\cdot \rightarrow P\text{-}P$$

The formation and propagation of free radicals in itself does not serious affect the mechanical properties of the polymer, as they do not significantly alter the long-chain nature of the polymer molecules. Degradation of the mechanical properties occurs because the free radicals produced are highly unstable and readily undergo chain scission reactions.

The intensity of the UV radiation decreases with increasing depth in the material, so that the reaction tends to be a near surface process. Since oxygen is involved in the reaction process, there is an important balance between UV radiation and oxygen diffusion, and of course temperature since that will also determine the kinetics of reaction and the transport of reactive species. Under natural exposure conditions there will be wetting and drying cycles and dark periods. The significance of the latter is that some recovery of the oxygen concentration in the material can occur, which otherwise is

confined to the very near surface due to consumption by reaction with the polymer radicals. Since the concentration of these radicals diminishes by termination reaction during the dark period, oxygen ingress can extend to greater depth.

4.3.2.3.Biological Degradation

Biodegradation is a biochemical transformation of compounds in mineralization by microorganisms. Mineralization of organic compounds yields carbon dioxide and water under aerobic conditions, and methane and carbon dioxide under anaerobic conditions. Abiotic hydrolysis, photo-oxidation and physical disintegration of polymers may enhance biodegradation of polymers by increasing their surface area for microbial colonization or by reducing molecular weight (Palmisano and Pettigrew 1992). Biodegradation has been defined as change in surface properties or loss of mechanical strength, assimilation by microorganisms, degradation by enzymes (Swift 1994) backbone chain breakage and subsequent reduction in the average molecular weight of the polymers (Ratner et al. 1988; Hergenrother et al. 1992).

Biodegradability is also defined as the propensity of a material to get breakdown into its constituent molecules by natural processes. The metabolites released by degradation are also expected to be non-toxic to the environment and redistributed through the carbon, nitrogen and sulfur cycles. Biological degradation is chemical in nature but the source of the attacking chemicals is from microorganisms. These chemicals are of catalytic nature e.g. enzymes. The susceptibility of the polymers to microbial attack generally depends on enzyme availability, availability of a site in the polymers for enzyme attack, enzyme specificity for that polymer and the presence of coenzyme if required (Reich and Stivala 1971).

Degradation may begin by hydrolysis, but as the polymer breaks and surface area and accessibility increases, enzymatic degradation may dominate. Thereby biodegradation includes all types of degradation occurring in vivo whether the degradation is due to hydrolysis or metabolic processes. Therefore, biodegradation is also defined as the conversion of materials into less complex intermediates or end products by solubilization, simple hydrolysis or the action of biologically formed entities such as enzymes and other products of the organism. Polymer molecules may, but not necessarily breakdown to produce fragments in this process, but the integrity of the material decreases in this type of process.

4.3.2.4.Ozone-induced degradation

Atmospheric ozone usually causes the degradation of polymers under conditions that may be considered as normal; when other oxidative aging processes are very slow and the polymer retains its properties for a rather longer time (Cataldo et al. 2000). The presence of ozone in the air, even in very small concentrations, markedly accelerates the aging of polymeric materials (Kefeli et al. 1971). This process in saturated polymers is accompanied by the intensive formation of oxygen-containing compounds, by a change in the molecular weight and by impairment of the mechanical and electrical properties of the specimens (Andrady et al. 1998). Exposure of polymers to ozone results in the rapid and consistent formation of a variety of carbonyl and unsaturated carbonyl products based on aliphatic esters, ketones, and lactones as well as aromatic carbonyl associated with the styrene phase. This follows by a more gradual formation of ether, hydroxyl and terminal vinyl groups with time and concentration (Allen et al. 2003). Ozen et al. (2002) have studied the effect on structural and mechanical properties of packaging films by

ozone exposure and have reported that ozone treatment has affected the polyethylene (PE) and polyamide films differently. It is responsible for formation of oxygen-containing functional groups and degradation of polymeric chains in PE films. Clough and Gillen (1989) have observed that the ozone generated by the action of the ionizing radiation in the air present in the atmosphere surrounding the samples affect the surface of the polymer (Clough and Gillen 1989). This observation has been made during gamma-radiation degradation studies of poly(butadiene-co-styrene) and poly(butadiene-co-acrylonitrile) in the presence of air. The oxides of nitrogen, sulfur, and ozone promote UV-induced oxidative damage of common plastics, particularly in rubber products (Andrady et al. 2003) .Ozone mainly affects vulcanized rubbers with unsaturation in the main polymer chain and causes cracking in stretched form in rubber. Exposure to ozone gas causes change in the mechanical properties of linear Low-Density Polyethylene (LDPE), oriented polypropylene (PP) and biaxial oriented nylon. Gatenholm et al. (1997) have studied the effect of ozone on the microporous structure of PP. Exposure of isotactic PP to ozone results in surface oxidation which further increases when a microporous membrane has large surface area (Gatenholm et al. 1997)

4.3.2.5. Mechanochemical degradation

Mechanochemical degradation of polymers involves the degradation of polymer under mechanical stress and by strong ultrasonic irradiations (Li et al. 2005). Breakdown of molecular chains under shear or mechanical force is often aided by a chemical reaction and is known as mechanochemical degradation.

Polymers suffer from mechanical failure when they are exposed to cyclic loads at stresses well below those they can sustain under static load. This phenomenon is known

as fatigue and is responsible for approximately 1 in 5 of all polymer failures (Maxwell et al. 2005). This is due to increases in the temperature of the plastic caused by mechanical hysteresis that results in thermal softening. This means that failure under cyclic loading can be either ductile or brittle. Fatigue failures are particularly serious as there is often little visual warning that failure is imminent (Brown and Greenwood 2002). Another effect of mechanical stress is creep. Creep is a gradual increase in strain that occurs in a material when it is subjected to a constant load over an extended period of time. Viscoelastic materials, such as polymers can undergo creep at relatively low stress levels and often at temperatures below room temperature (Brown and Greenwood 2002). Dimensional stability under stress is essential in many applications so creep can be a significant problem. Creep will ultimately lead to rupture either by ductile or brittle failure. At low temperatures and high loads creep rupture will be brittle; at intermediate loads and temperatures failure will be ductile; and after long lifetimes slow low energy brittle failures will occur. It is these slow low energy brittle failures that are more problematic in the prediction of life expectancy (Maxwell et al. 2005).

The polymer product used in outdoor circumstances has a great concern about the chemical degradation; because the product for outdoor use is exposed to rain, sunlight, temperature, and environmental bacteria. These factors have sufficient effects in proceeding with the oxidation and the hydrolysis of the polymer materials; moreover, acidic and/or basic conditions have effect in promoting the reaction (Bellenger et al. 1995). Chemical degradation involves specific chemical reaction of the polymer with the fluid with the most common mode of failure being hydrolysis by water, acids and alkalis (Brown et al. 1995). Esters, amides, imides, and carbonate groups are particularly

susceptible. Where these groups are located in the backbone chain rather than the side chain, chain scission ensues.

For example, mastication of rubber can lead to chain breakage and development of plasticity under shear. In the atmosphere of nitrogen at ordinary temperature mastication of rubber does not change the plasticity and molecular weight appreciably, but in the presence of oxygen, degradation occurs rapidly. This is due to the reason that the rubber molecule breaks into radicals, and oxygen as radical scavenger readily reacts with them, leading to permanent chain breakage, whereas nitrogen is not a radical scavenger and thereby led to radical recombination. The degradation of high molecular weight polystyrene (PS) occurs under the turbulent flow and the drag reduction efficiency decreases with time due to the mechanical degradation of the polymer molecules (Brostow 1983; Kim et al. 2000).

Polymers are subjected to degradation and failure due to different factors and mechanisms. An understanding of degradation mechanisms can go a long way in helping the researchers and the technologists to induce the different types of degradation in polymers. These degradations can further be enhanced by the addition of the additives in polymers and by understanding the various factors responsible for these degradations. The following section delineates the scope of this study and describes the studied First Solar materials and components.

4.3.3. Polymer Materials in PV

The solar PV industry deploys different types of polymers into their components. Figure 28 below shows the classification of different materials used for cables, connectors, and rubber insulation. This section provided an overview about polymeric

materials. It described the different classification frameworks and their main degradation factors and modes. Outlining the different polymeric materials establishes the scope of the study to develop materials selection framework and tool. The next section elaborates on the research approach, including fault tree analysis, qualitative assessment, and existing decision frameworks examination.

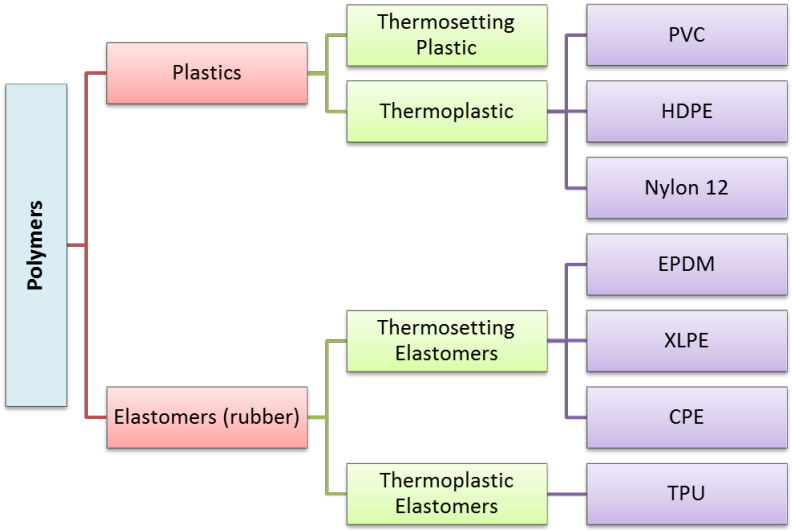

Figure 28. Deployed Polymeric Materials for Cables, Connectors, and Rubber

4.4. RESEARCH APPROACH AND APPLICATION TO PV POLYMERIC COMPONENTS

As PV systems age under relatively harsh and changing environmental conditions, several potential fault conditions can be developed during the operational lifetime including polymeric materials failures. To account for the failure of polymeric materials that are used in tracker and fixed tilt systems, the *First Solar* – ASU proposed method aims to advance analytical tools and decision frameworks capable of providing crucial data to explain the degradation mechanisms and failure modes of PV polymeric components. The ability to select an appropriate material for a specific environment is

critical for solar plants designers and engineers. The study method consists of optimizing the selection of polymeric materials after applying a three-step analysis: 1) fault tree analysis; 2) qualitative assessment; and 3) existing decision frameworks examination, as discussed in the following subsections and shown in Figure 29.

4.4.1. Fault Tree Analysis

This section develops fault trees for the different studied components in order to define the root factors causing their failures. Following an overview description of this analysis, the following subsections present the developed trees as they apply to *First Solar*.

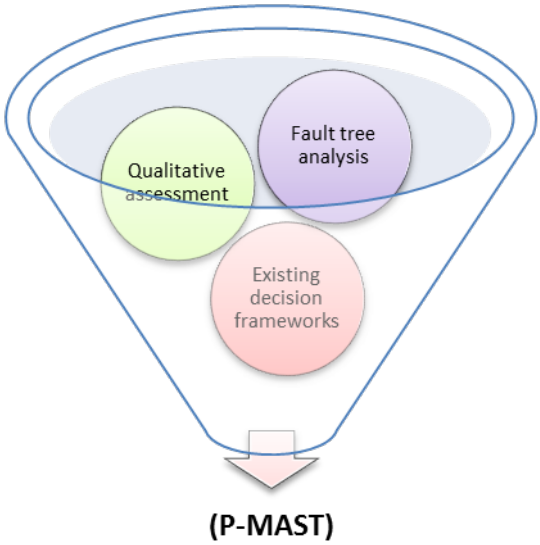

Figure 29. Polymeric Materials Selection Support Tool (P-MAST) Development

4.4.1.1.Overview

Fault-tree analysis, also known as Fault Tree Analysis (FTA), is a logical and diagrammatic method to evaluate the likelihood of an accident resulting from sequences and combinations of faults and failure events (Tanaka et al. 1983). A fault tree describes an accident-model and interprets the relations between malfunctions of the components and observed symptoms. Thus, the fault tree is useful for understanding logically the mode of occurrence of an accident. FTA is a top down failure analysis can be used to

understand the logic leading to the top undesired event (failure), show compliance with the system reliability requirements, prioritize the contributors leading to the top event, minimize and optimize resources, and help with the creation of diagnostic manuals (Javadi et al. 2011). Table 26 below shows some of the starting questions for risk and failure modes discovery (Carlson 2014). The information in the trees below came from several sources (Brostow 1983; Tanaka et al. 1983; Brown et al. 1995; Bellenger et al. 1995; Kim et al. 2000; Densley 2001; Whitlock 2004; Maxwell et al. 2005; Javadi et al. 2011; Carlson 2014) and was organized in the FTA in the following subsections.

Table 26. Starting Questions for Risk and Failure Modes Discovery [Adapted from (Carlson 2014)]

Category	Question
a. New Technology	Does the design involve new technology?
b. New Application	Does the design apply existing technology in a new way?
c. Historical Problems	Have there been historical problems with this item?
d. Safety Issues	Is there a potential for safety-related issues?
e. Mission-Critical	Is this a mission-critical item?
f. Regulatory	Changes or concerns related to the regulatory requirements?
g. Specifications	Changes or concerns related to the specifications?
h. Functions	Changes or concerns related to the expected functions?
i. Performance	Changes or concerns related to the performance requirements?
j. Environmental Loads	Changes or concerns related to environmental loads?
k. Use Loads/Stresses	Changes or concerns related to use loads/stresses?
l. Temperature	Changes or concerns related to high/low temperature limit?
m. Humidity	Changes or concerns related to the expected humidity?

4.4.1.2.FTA Applied to Cables

The applied FTA to cables considers the potential risks of failures due to application variability or inadequate choice of materials, which is the result of inadequate design, operational robustness, and application information, as shown in Figure 30 below.

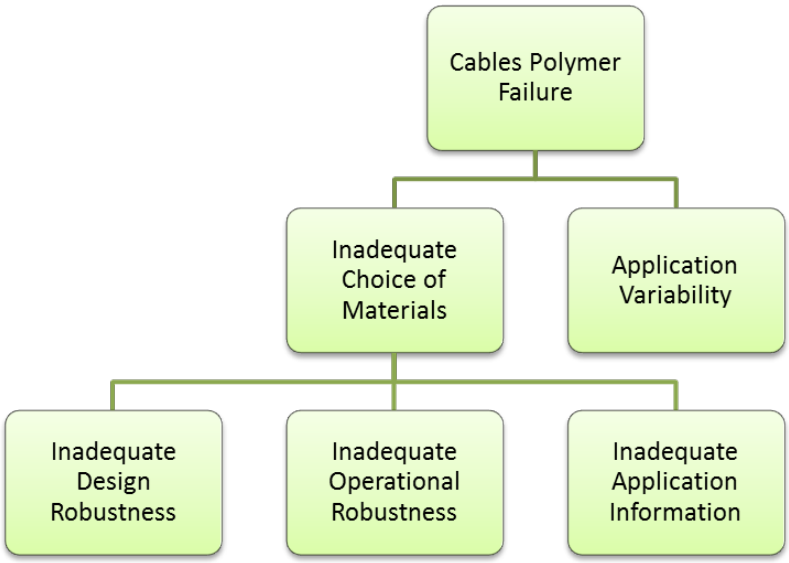

Figure 30. Causes of Cables Failure Risks

Several cause events can lead to the failure of cables polymer due to application variability, as shown in Figure 31:

- Part quality: By not meeting the requirement specifications or end-user expectations, a quality malfunction might cause the application variability of polymeric materials deployed in PV cables. Such malfunction can be the result of manufacturers' defects due to a lack in the QA/QC process at the supplier and/or on site; inappropriate assembly strength and compatibility during bonding, welding, fastening and inserting, or staking; inadequate finishing in terms of color or printing; poor packaging; and unsuitable storage.

- Customer requested changes: When a customer requests changes from what is documented in the project initial agreement, the new cable applications may not be suitable with the design requirements.
- Project site to project site: A change from a project site to another is accompanied with a variation in the application and design constraints.
- Operator to operator: Different operators might use the cables for different applications. A cable that is suitable for one application can be unsuitable for another one.

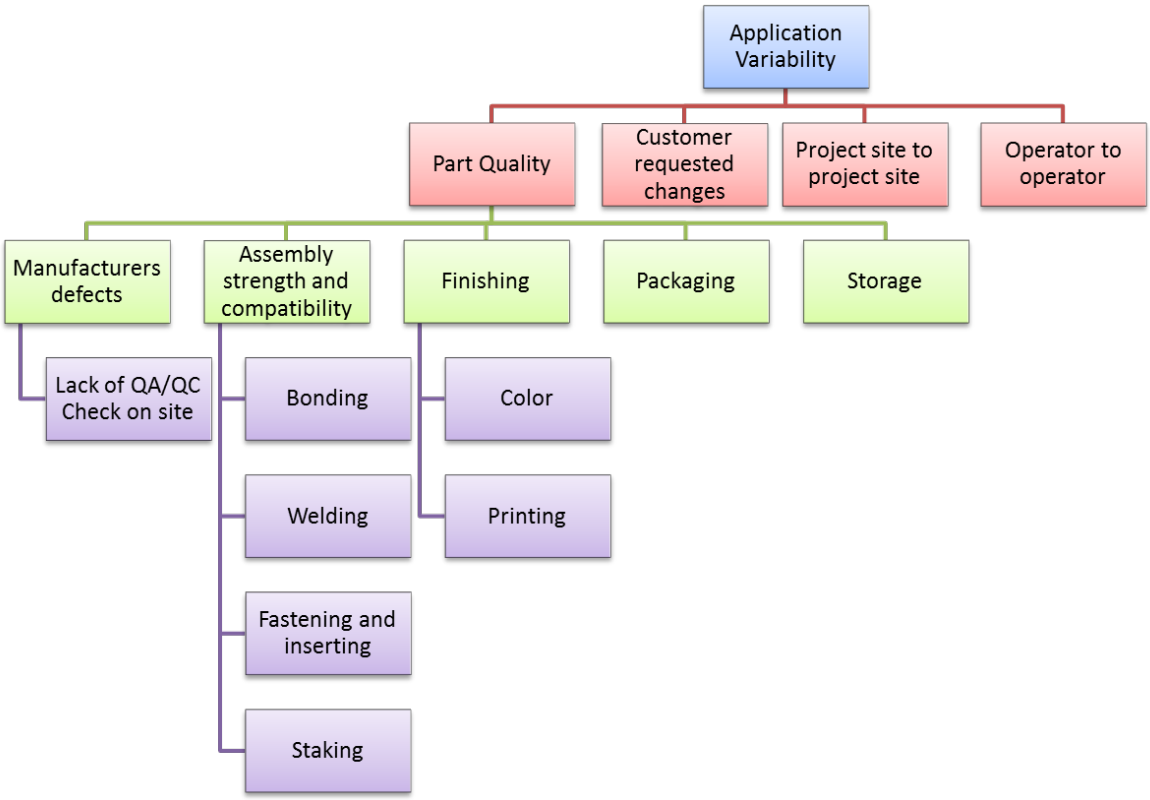

Figure 31. FTA for Cables' Application Variability

Inadequate design robustness plays a major role during the failure of cables polymer. Figure 32 illustrates the different events leading to cables failure, including:

- General information: A cable is inadequate for its intended uses if its design does not meet the acceptance codes or specifications, has wrong means for location or objective, expects to serve less than the projected life, and exceeds the space or weight limitations.
- Operating versus design load: A discrepancy between the operating and design load, in terms of thermal, chemical, mechanical, or electrical stresses, can lead to the cable failure.
- Degradation: A cable design is inadequate if it does not account for the effect of polymers degradation over time, due to: operating temperature, chemical environment, humidity, permeability, or exposure to sunlight and weathering.
- Economic considerations: Exceeding the budget or cost limitations affects cables' design robustness, as a result of expensive materials or unavailability of materials or skilled labors.

Figure 33 shows the FTA for cables' inadequate application information. Accessing adequate information about the application minimizes the possibility of cables failure. Some of the key information entails:

- Clear guidance
- Adequate guidance (proper estimation of operating load and knowledge edges sharpness)
- Appropriate cables weight, aligned with the deployed wires
- Suitable length of cables
- Compatible cables with the available connectors and joints

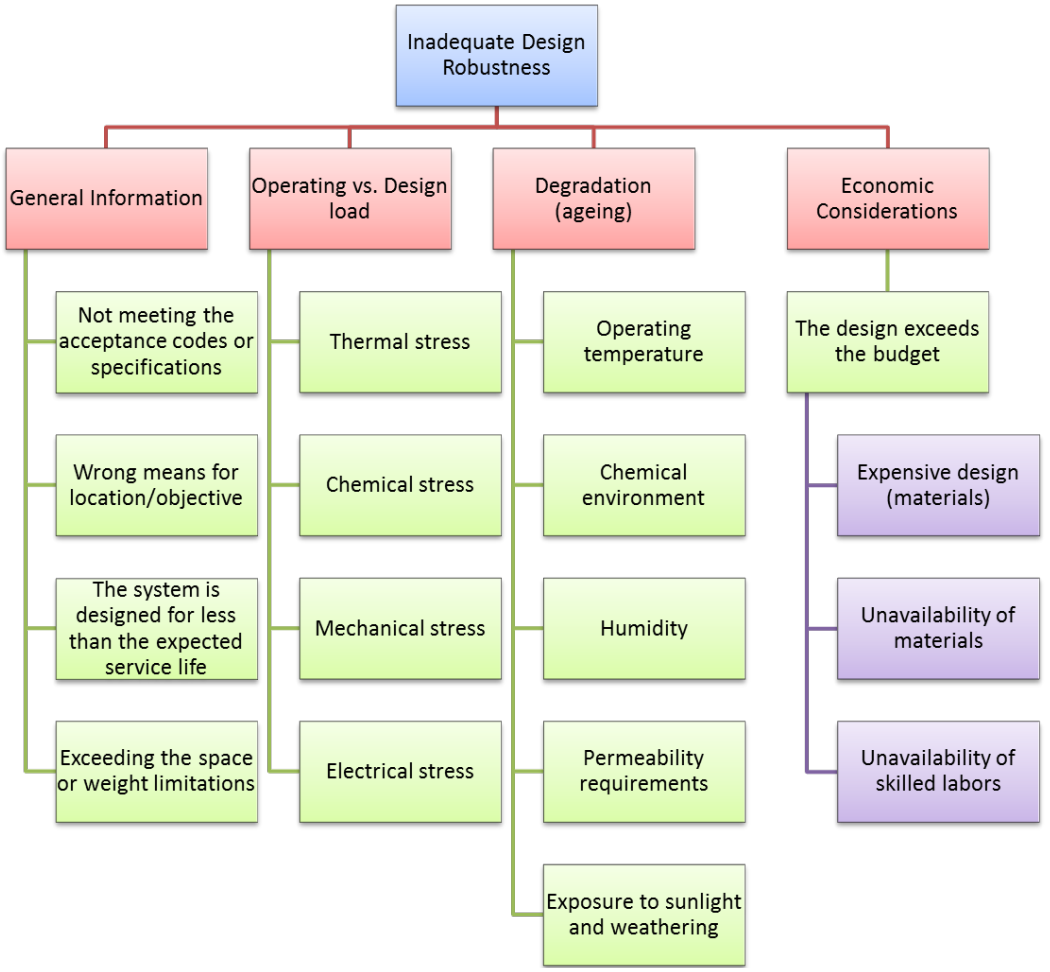

Figure 32. FTA for Cables' Inadequate Design Robustness

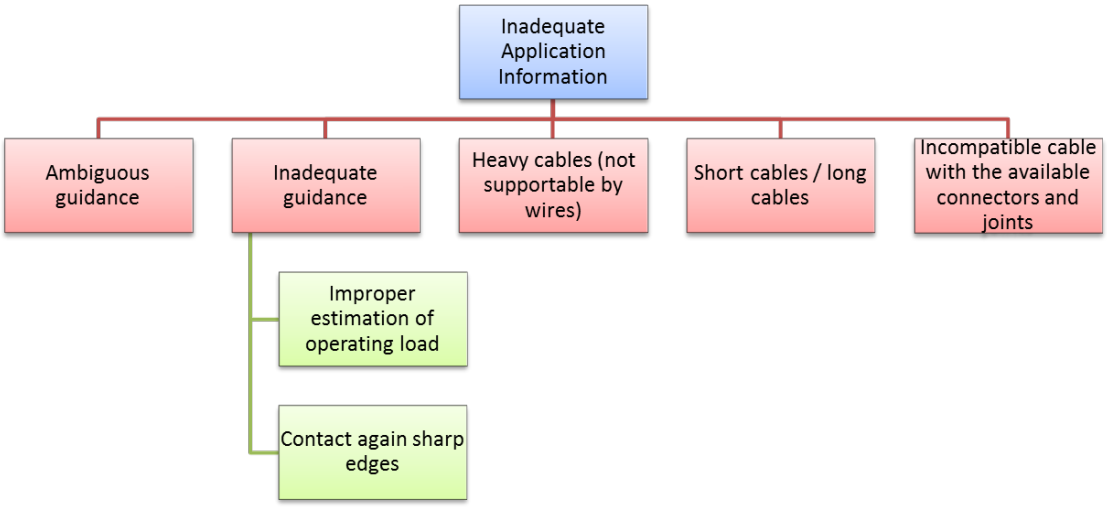

Figure 33. FTA for Cables' Inadequate Application Information

Operational robustness is a key factor towards the reliability of cables. The following factors, shown in Figure 34, cause an operational robustness inadequacy and therefore lead to cables failure:

- Thermal effects: Thermal cycling, including continuous expansion and contraction, affects the mechanical and electrical properties of cables and therefore lead to their embrittlement, creep, warpage, and softening.
- Chemical stresses: Several factors impose chemical stresses on cables, including: oxygen and/or ozone, water and moisture, UV radiation, reaction with the galvanization coating, and dust.
- Biological effects: Bacterial and fungus growth impacts cables operational robustness.
- Mechanical effects: Applied static and dynamic load creates shear, tensile, and flexural stresses on cables.
- Electrical effects: Electrical breakdown of insulators as a function of applied voltage, water treeing of the insulation, and electrochemical treeing affects the operational robustness of cables.
- Piercing: A buried cable is subject to piercing and thus to failure.

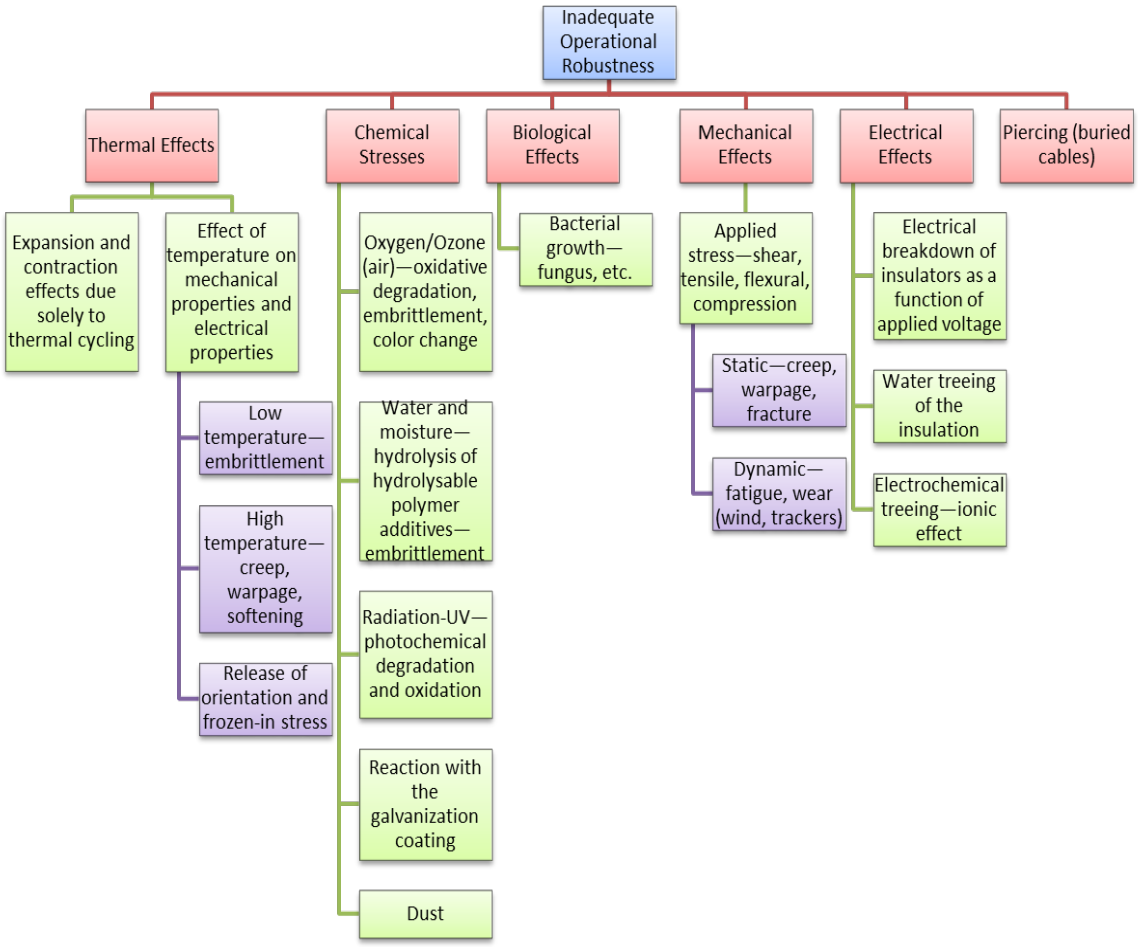

Figure 34. FTA for Cables' Inadequate Operational Robustness

FTA is an effective method in revealing the true cause(s) of polymer failures and in proposing the corrective actions needed to avoid future failures. An investigation of polymeric materials failure in cables uncovers a wide range of factors that need to be avoided on any solar site. Table 27 illustrates in an alternative way these factors by associating them to the potential failure mechanisms and their effects (Densley 2001).

After analyzing the causes, mechanisms, and effects of polymeric materials failures in electrical cables on solar sites, developing inspection checklists can ensure an integrated mitigation of the associated risks.

Table 27. Causes, Mechanisms, and Effects of Polymers Failure in Cables [Adapted from (Densley 2001)]

Type	Cause	Mechanism	Effect
Thermal	• High temperature • Temperature cycling	• Chemical reaction • Incompatibility of materials • Thermal expansion • Diffusion • Melting/Flow of insulation	• Hardening, softening, loss of mechanical strength, embrittlement • Shrinkage, loss of adhesion, separation, delamination at interfaces • Loss/ingress of liquids and gases • Movement of cables • Formation of soft spots and wrinkles
	• Low temperature	• Cracking • Thermal Contraction	• Shrinkage, loss of adhesion, separation, delamination at interfaces • Loss/ingress of liquids and gases • Movement of joints and terminations
Electrical	• Voltage, AC, DC, Impulse	• Partial discharges • Electrical treeing • Water treeing	• Erosion of insulation • Increased losses • Immediate failure
	• Current	• Overheating	• Increased temperature and thermal ageing
Mechanical	• Tensile, compressive, shear stresses, fatigue, cycling bending, vibration	• Yielding of materials • Cracking • Rupture	• Mechanical rupture • Loss of adhesion, separation, delamination at interfaces • Loss/ingress of liquids and gases
Environmental	• Water/ humidity • Liquids/gases • Contamination	• Dielectric losses and capacitance • Electrical tracking • Water treeing • Corrosion	• Increased temperature and thermal ageing • Increased losses • Flashover
	• Radiation	• Increase chemical reaction rate	• Hardening, softening, loss of mechanical strength, embrittlement

These checklists are then recommended for future inspection during design, installation, and maintenance phases of studied components. Hence, the design checklist for PV cables includes the following item:

- The guidance is adequate and clear.
- The cables meet the acceptance codes or specifications.
- The cables meet the applied stress (shear, tensile, flexural, and compression) requirements.
- The cables do not exceed the space or weight limitations (supportable by wires).
- The cables are within the allowed budget (materials choice and availability, skilled labors, etc.).

Moreover, the checklist items during cables installation are as follows:

- The cables are deployed for the appropriate objective/location.
- The cables are checked for manufacturer defects, i.e. dimensions, cross section, sharpness of edges, etc.
- The cables are bonded, packaged, and stored appropriately.
- The cables are connected with smooth angles (bending diameter larger than 80 mm).
- The cables are not long or short.
- The cables are compatible with the connectors.

In addition, the items included in the maintenance checklist entail the following:

- The cables are robust to low, high, and cycle of temperatures.
- The cables are resistant to oxidative degradation.
- The cables are resistant to the effect of water and moisture.

- The cables are UV resistant.
- The cables are not reacting with the galvanization coating.
- The cables are not affected by the dust.
- The cables are no longer buried when they are buried underground.

4.4.1.3.FTA Applied to Connectors

Similar to cables, the aim of this subsection is to develop fault trees for the designed and deployed connectors. The applied FTA considers the potential risks of failures due to application variability as a result of inadequate workmanship or inadequate manufacturing and due to an inadequate choice of materials as a result of inadequate design, operational robustness, or application information, as shown in Figure 35 below.

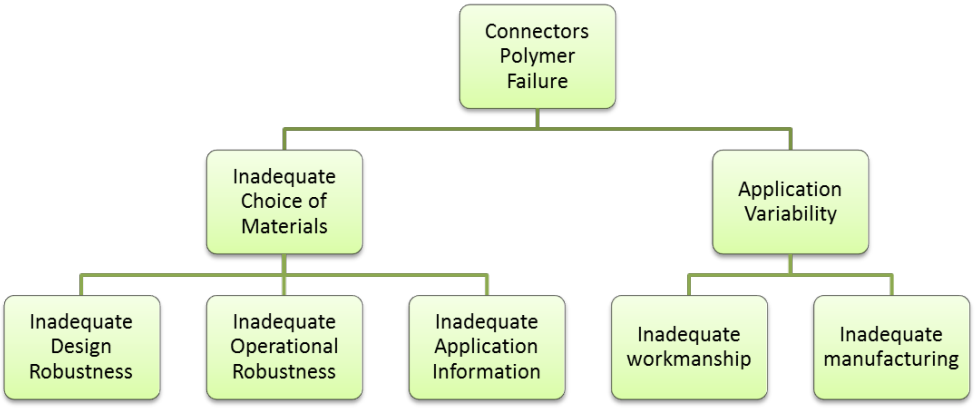

Figure 35. Causes of Connectors Failure Risks

Inadequate design robustness plays a major role in the failure of connectors. Figure 36 illustrates the different events leading to connectors' failure, including:

- General information: A connector is inadequate for its intended uses if its design does not meet the account for an appropriate seal between the male and female subparts, contains misaligned pins, has an inadequate size and/or profile of glans,

involves high impedance due to dissimilar metals or pin profile, and is contaminated using bare copper.

- Operating versus design load: A discrepancy between the operating and design load, in terms of thermal, chemical, mechanical, or electrical stresses, can lead to the connector failure.

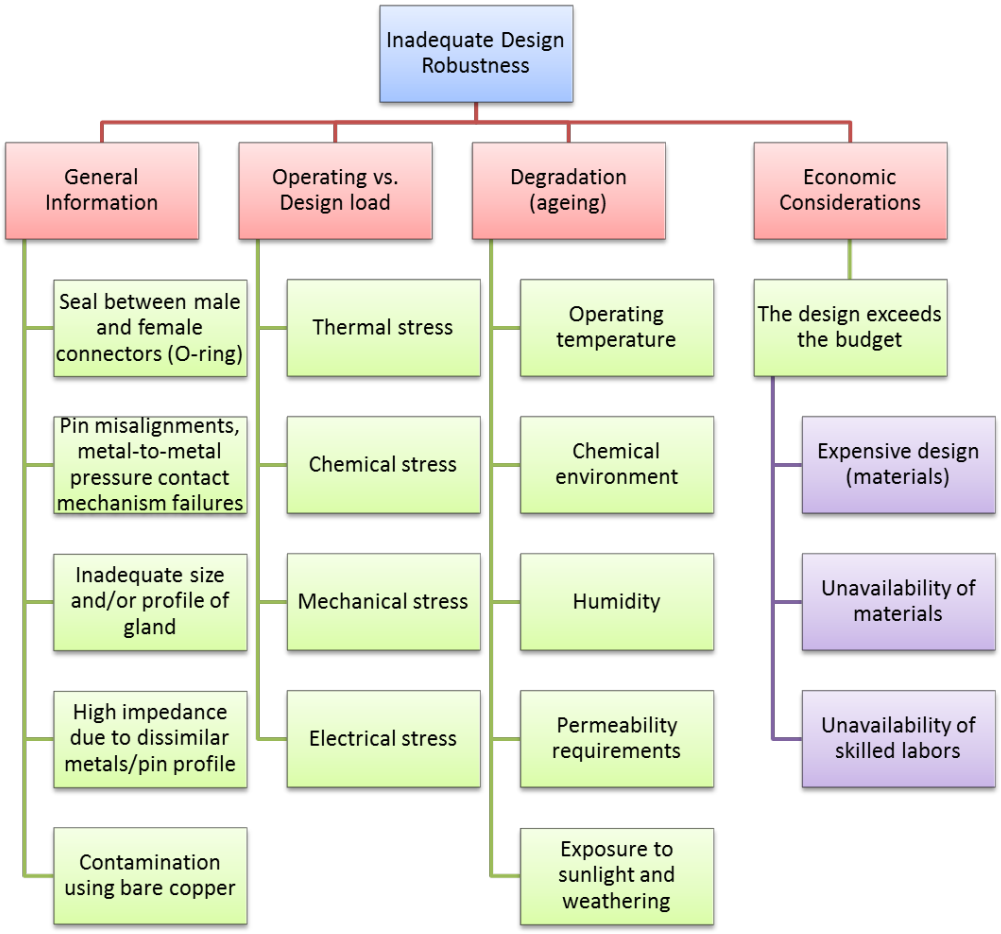

Figure 36. FTA for Connectors' Inadequate Design Robustness

- Degradation: A connector design is inadequate if it does not account for the effect of polymers degradation over time, due to: operating temperature, chemical environment, humidity, permeability, or exposure to sunlight and weathering.

- Economic considerations: Exceeding the budget or cost limitations affects connectors' design robustness, as a result of expensive materials or unavailability of materials or skilled labors.

Operational robustness is also a key factor towards the reliability of connectors. The following factors, shown in Figure 37, cause an operational robustness inadequacy and therefore lead to connectors' failure:

- Inadequate environmental conditions: High humidity, chemical exposure, UV exposure, thermal cycling, wind stress, and high brine content environments affect the operational robustness of connectors.
- Risk due to weather conditions during installation
- Scheduled inspection not conducted
- Electrical or metallurgical changes due to operation
- Ice/snow mechanical stress and moisture ingress
- Rodents or animals

Figure 38 shows the FTA for connectors' inadequate application information. Accessing adequate information about the application minimizes the possibility of connectors' failure. Some of the key information entails:

- Clear guidance;
- Adequate guidance (proper estimation of operating load and knowledge edges sharpness);
- Appropriate cables weight, aligned with the deployed connectors;
- Compatible connectors with the available cables.

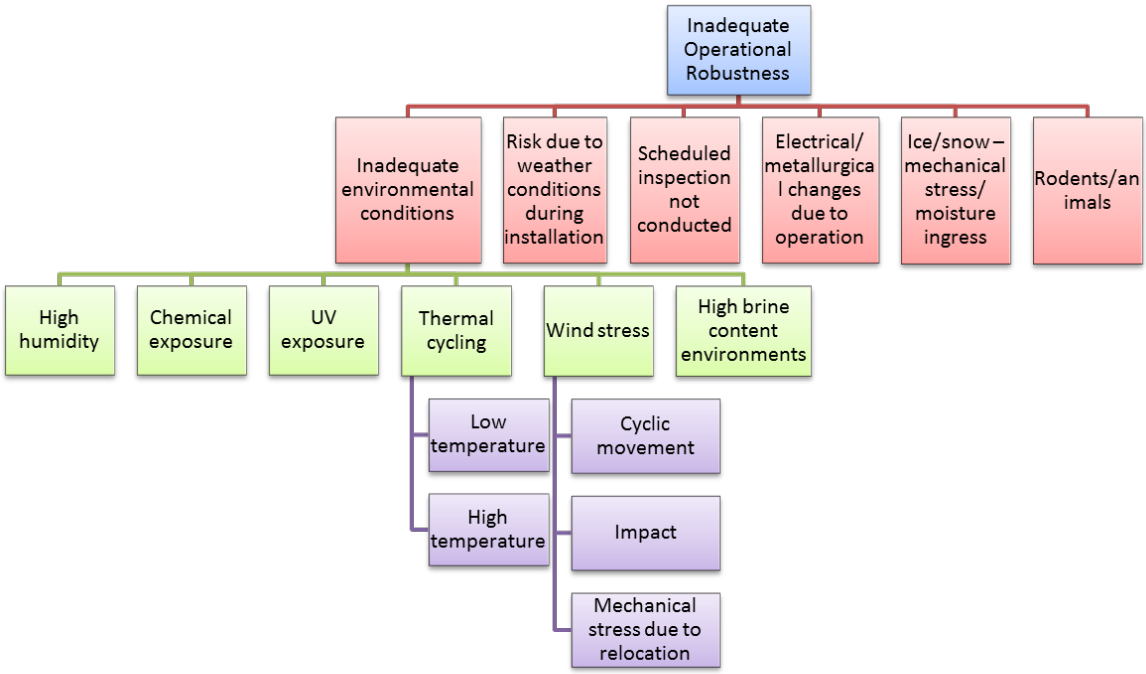

Figure 37. FTA for Connectors' Inadequate Operational Robustness

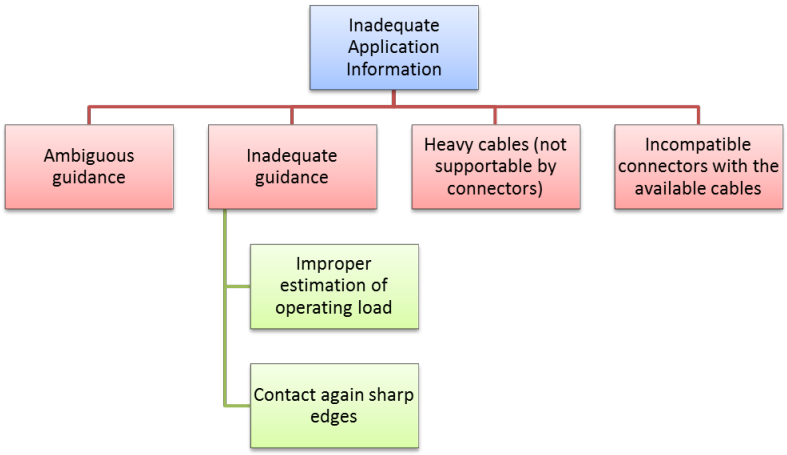

Figure 38. FTA for Connectors' Inadequate Application Information

Figure 39 shows the FTA for cables' inadequate or poor workmanship. Some of the key mistakes are as follows:

- Combining visually compatible connector parts from different manufacturers
- Shield connectors are placed above the panel so water fall on the connection

- Cables and connectors are overtighten or hang loose and are moved around by wind
- Not fully mating connectors
- Applying sharp bends radius
- Improper strip length
- Conductor not fully inserted into crimp
- Applying incorrect torque on cap nut
- Installing safety lock incorrectly
- Twisting cables
- Installed at correct height from roof
- Improper wire management

Several cause events can lead to the failure of connectors' polymer due to inadequate manufacturing, as shown in Figure 40. By not meeting the requirement specifications or end-user expectations, a quality malfunction might cause the application variability of polymeric materials deployed in PV connectors. Such malfunction can be the result of the following items:

- Manufacturers' defects due to a lack in the QA/QC process at the supplier or on site and dirt or dust ingress in connector joint areas
- Inappropriate assembly strength and compatibility during bonding, welding, fastening and inserting, or staking
- Inadequate finishing of connectors color and printing
- Poor packaging
- Unsuitable storage

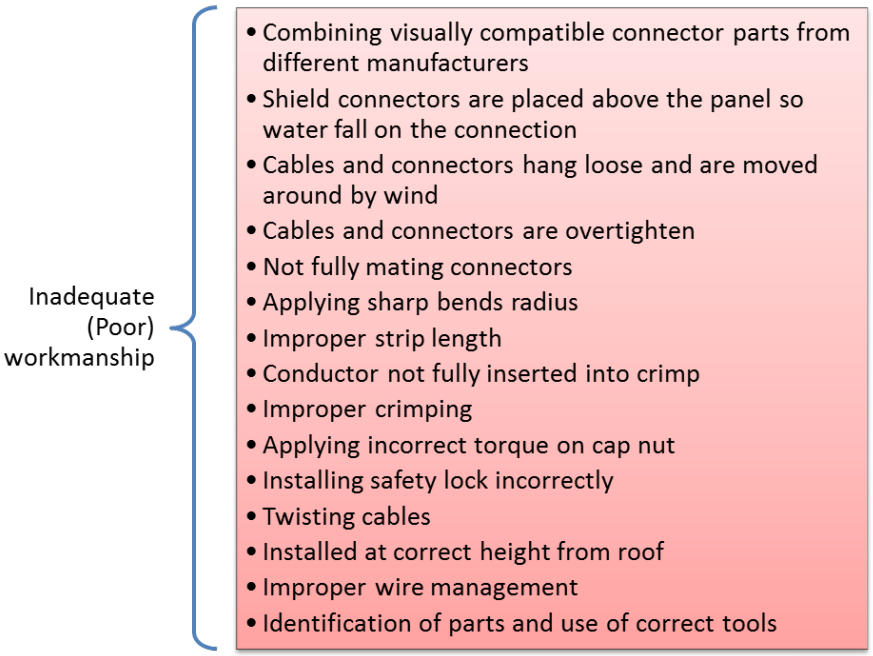

Figure 39. FTA for Connectors' Inadequate (Poor) Workmanship

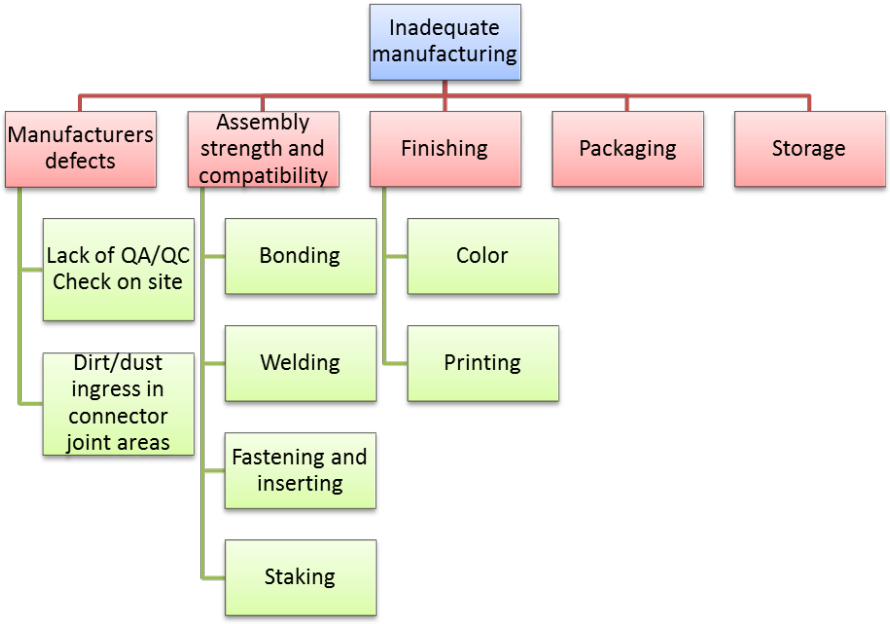

Figure 40. FTA for Connectors' Inadequate Manufacturing

After analyzing the causes, mechanisms, and effects of polymeric materials failures in connectors on solar sites, developing an inspection checklist can ensure an

integrated mitigation of such associated risks. To mitigate the risk of connector's failure, the following checklist is recommended during the design stage:

- The guidance is adequate and clear.
- The connectors meet the acceptance codes or specifications.
- The connectors are compatible with the cables.
- The connectors meet the applied stress (shear, tensile, flexural, and compression) requirements.

Below are the items included in the installation checklist:

- The connectors are checked for manufacturer defects, i.e. dimensions (adequate size and/or profile of gland, proper strip length, proper crimping), cross section, sharpness of edges, and for dirt/dust ingress in the joint areas.
- Safety locks are installed correctly.
- Applying incorrect torque on cap nut.
- Shield connectors are placed under the panel to avoid direct contact with the rain.
- Combining compatible connector parts from same manufacturers.
- The connectors are well fixed at a certain elevation so animal and rodents cannot reach them.
- The connectors are bonded, packaged, and stored appropriately.
- Pins are aligned to avoid metal-to-metal pressure contact mechanism failures.
- The conductors are fully inserted into crimp.

Additionally, the maintenance checklist for connectors includes the following items:

- The connectors are robust to low, high, and cycle of temperatures.
- The connectors are resistant to oxidative degradation.

- The connectors are resistant to the wind stress, e.g. cyclic movement, mechanical stress, etc.
- The connectors are resistant to the effect of water/ice/snow and moisture.
- The connectors are UV resistant.
- The connectors are not contaminated using bare copper.
- Proper wire management.

4.4.1.4.FTA Applied to Rubber Insulation

This subsection develops fault trees for the rubber insulation, which is deployed in module clips. The applied FTA considers the potential risks of failures due to application variability as well as the inadequacy in choosing the materials as a result of inadequate design or operational robustness, as shown in Figure 41 below.

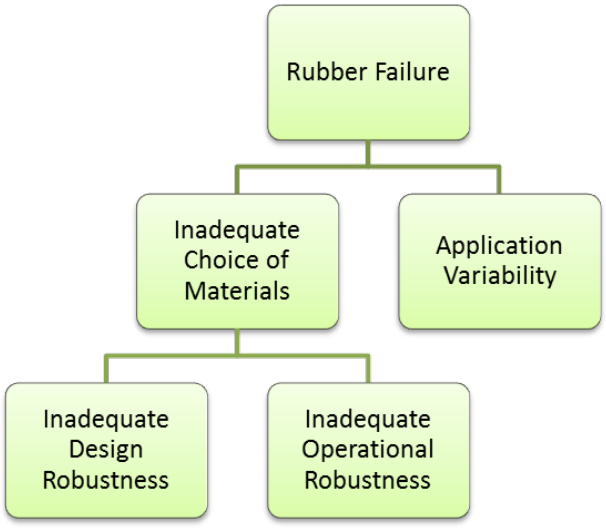

Figure 41. Causes of Rubber Insulation Failure Risks

Several cause events can lead to the failure of rubber insulation due to application variability, as shown in Figure 42:

- Manufacturers' defects due to a lack in the QA/QC process at the supplier and/or on site
- Inappropriate installation resulting in damage due to sharp edges, improper sizing, and surface contamination
- Inadequate location of the clamps on the module
- Improper fastening or tightening torque on the screw
- Rubber is not inserted properly in the clamps

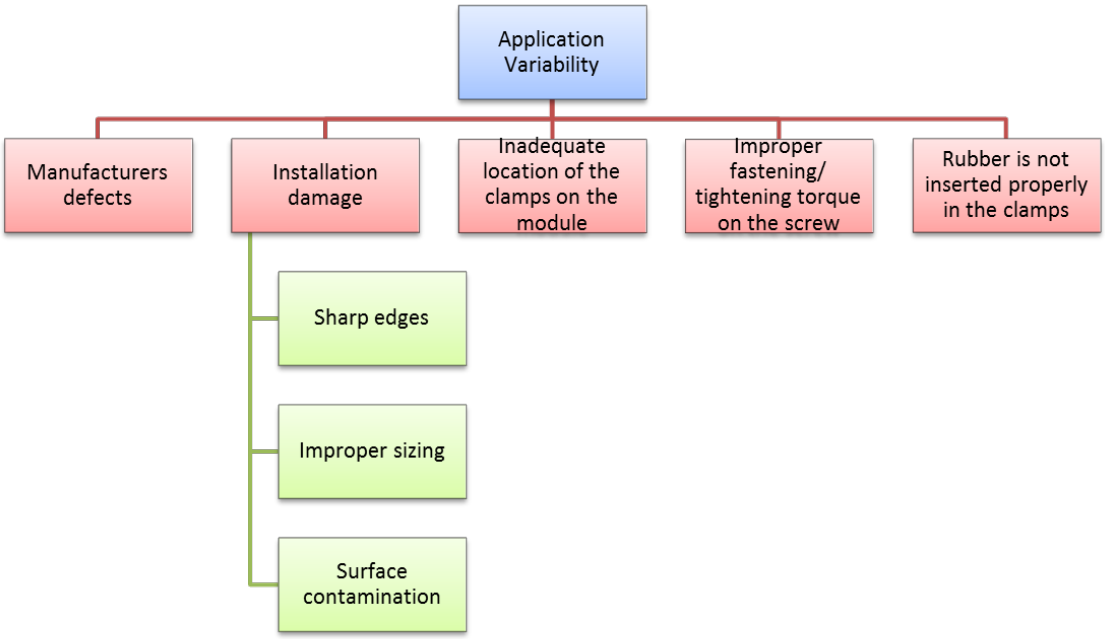

Figure 42. FTA for Rubber Insulation's Inadequate Application Variability

Inadequate design robustness plays a major role in the failure of rubber insulation. The following events summarize the main factors behind rubbers' failure, as illustrated in Figure 43:

- Squeeze compression due to inadequate depth, length, and thickness
- Installed stretch because of excessive stretch that is overstressing material
- Excessive clearance and or pressure against the clearance gap can result in failure

- Tolerance is not taken into consideration
- Too rough of a surface can result in abrasion or spiraling
- Sharp Corners
- Too much squeeze on one side and not enough on the other or none at all

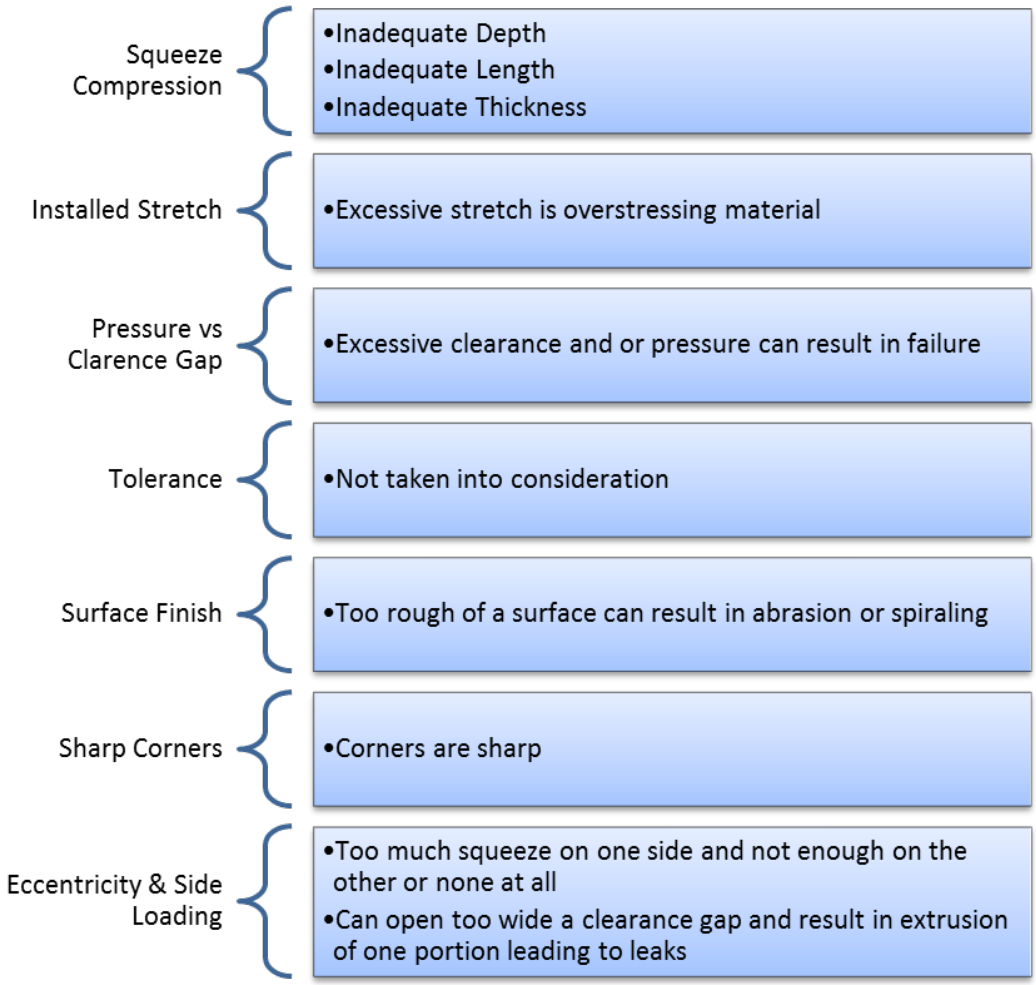

Figure 43. FTA for Rubber Insulation's Inadequate Design Robustness

Moreover, Table 28 illustrates the underlying cause events for rubber insulation's inadequate operational robustness (Whitlock 2004). Several failure modes can occur to operational environment, such as: compression set, over compression, outgassing extraction, extrusion, thermal degradation, and chemical degradation.

Table 28. FTA for Rubber Insulation's Inadequate Operational Robustness [Adapted from (Whitlock 2004)]

Failure Mode	Description	Factors	Solutions
Compression Set	The seal exhibits a flat-sided cross-section, the flat sides corresponding to the mating seal surfaces	• Excessive compression • Excessive temperature • Incompletely cured rubber • Rubber with high compression set	• Low compression set rubber • Proper design for the specific elastomer • Confirm material compatibility
Over Compression	The seal exhibits parallel flat surfaces (corresponding to the contact areas)	• Improper design—failure to account for thermal or chemical volume changes, or excessive compression	• Design should take into account material responses to chemical and thermal environments
Outgassing Extraction	The seal may exhibit a decrease in cross-sectional size	• Improper or improperly cured rubber • High vacuum levels • Low hardness/ plasticized rubber	• Avoid plasticized rubber • Ensure all rubber are properly post-cured to minimize outgassing
Extrusion	The seal develops ragged edges (generally on the low-pressure side) which appear tattered	• Excessive clearances • Excessive pressure • Low-modulus/hardness rubber • Irregular clearance gaps • Sharp gland edges • Improper sizing	• Decrease clearances • Higher-modulus/hard-ness rubber • Proper design
Thermal Degradation	The seal exhibits cracks located on the highest temperature surfaces	• Elastomer thermal properties • Excessive temperature excursions or cycling	• Selection of a rubber with improved thermal stability • Evaluation of the possibility of cooling sealing surfaces
Chemical Degradation	The seal may exhibit many signs of degradation including blisters, cracks, or voids	• Incompatibility with the chemical and/or thermal environment	• Selection of more chemically resistant rubber

After analyzing the causes, mechanisms, and effects of polymeric materials failures in rubber insulation on solar sites, the subsection develops an inspection checklist to ensure an integrated mitigation of the accompanied failure risks. Similar to cables and connectors, three checklists are developed to inspect the rubber insulation during design, installation, and maintenance phases. The design checklist for rubber insulation included the following:

- The guidance is adequate and clear.
- The rubber insulations meet the acceptance codes or specifications.
- The rubber insulations are not squeezed or compressed (adequate depth, length and thickness).
- The rubber insulations meet the applied stress (shear, tensile, flexural, and compression) requirements.

During installation of rubber insulation, the following items are inspected:

- The rubber insulations are packaged and stored appropriately.
- The rubber insulations are compatible with the clips.
- The rubber insulations are adequately located in the center of the clips.
- The clips are adequately located on the module.
- The torque on screw is properly fastened or tightened.

The inspection checklist for rubber insulation during maintenance includes:

- The rubber insulations are robust to the low, high, and cycle of temperatures.
- The rubber insulations are resistant to oxidative degradation.
- The rubber insulations are resistant to the effect of water and moisture.
- The rubber insulations are UV resistant.

- The rubber insulations are not affected by the dust.
- The rubber insulations are not contaminated and do not have sharp edges.

4.4.2. Qualitative Assessment

Polymeric materials need be selected and used such that the product does not present an unacceptable risk or danger to life or property when used in its intended manner. They are also selected so that they are suitable for the operating environment condition, including fire performance in solar projects, robustness against high temperature and humidity, protection against attack by rodents, etc. Hence, suppliers and manufacturers have developed qualitative charts and tables to rank the performance of these polymers on a 5-point Likert scale (1 being poor, 5 being outstanding).

This section builds on the root factors, which are defined in the previous subsection, in order to qualitatively assess the resistance of a polymer material vis-à-vis different criteria, such as: abrasion, acid, alcohol, electrical, flame resistance, oil underground burial, etc. Thus, the research method consists of collecting the qualitative performance data from common suppliers. For instance, Figure 44 illustrates an example of polymeric materials comparison sheet from one of the suppliers. Similar to this comparison sheet, this study collects data from 5 additional resources and integrates them together to reduce any possible variation between the six different suppliers, as shown in Figure 45. After collecting the qualitative data from six suppliers (see Appendix D), their averages are computed and summarized in Table 29 below.

	Thermoplastic					Thermosetting				
	TPU Polyurethane	**LDPE** Low density Polyethylene	**HDPE** High density Polyethylene	**PP** Poly-propylene	**PVC** Polyvinyl Chloride	**CR** Neoprene (Poly-chloroprene)	**CPE** Chlorinated Polyethylene	**XLPE** Cross-linked Polyethylene	**Hypalon** Chloro-Sulfonated Polyethylene	**EPR** Ethylene Propylene Rubber
Water resistance	Poor - Good	Very good	Very good	Very good	Fair - Good	Very good	Good - Very good	Good - Very good	Very good	Good - Very good
Oil resistance	Very good	Good - Very good	Good - Very good	Fair	Fair	Good	Good - Very good	Good	Very good	Poor
Abrasion resistance	Excellent	Good	Very good	Fair - Good	Fair - Good	Good - Very good	Good - Very good	Fair - Good	Good	Good - Very good
Flame resistance	Poor	Poor	Poor	Poor	Very good	Good	Good	Poor	Good	Poor
Heat resistance	Good	Good	Very good	Very good	Good - Very good	Good	Excellent	Good	Very good	Very good
Weather resistance	Good	Very good	Very good	Very good	Good - Very good	Good	Very good	Good	Very good	Very good
Sunlight resistance	Good	Very good	Very good	Very good	Good - Very good	Good	Very good	Good	Very good	Very good
Ozone resistance	Very good	Very good	Very good	Very good	Very good	Good	Good - Very good	Good	Very good	Very good
Low temp flexibility	Good	Very good	Very good	Poor	Poor - Good	Fair-Good	Fair	Excellent	Fair	Good - Very good
Oxidation resistance	Very good	Very good	Very good	Very good	Very good	Good	Very good	Very good	Very good	Very good
Acid resistance	Fair	Good - Very good	Very good	Very good	Good - Very good	Good	Very good	Good -Very good	Very good	Good - Very good
Alcohol resistance	Poor - Good	Very good	Very good	Very good	Good - Very good	Fair	Good - Very good	Very good	Good	Poor
Gasoline resistance	Poor - Good	Good - Very good	Good - Very good	Poor - Fair	Poor	Good	Fair	Fair	Fair	Poor
Electrical properties	Poor	Very good	Very good	Very good	Fair - Good	Poor	Fair - Good	Very good	Good	Very good

Figure 44. An Example of Polymeric Materials Comparison Sheet from a Supplier

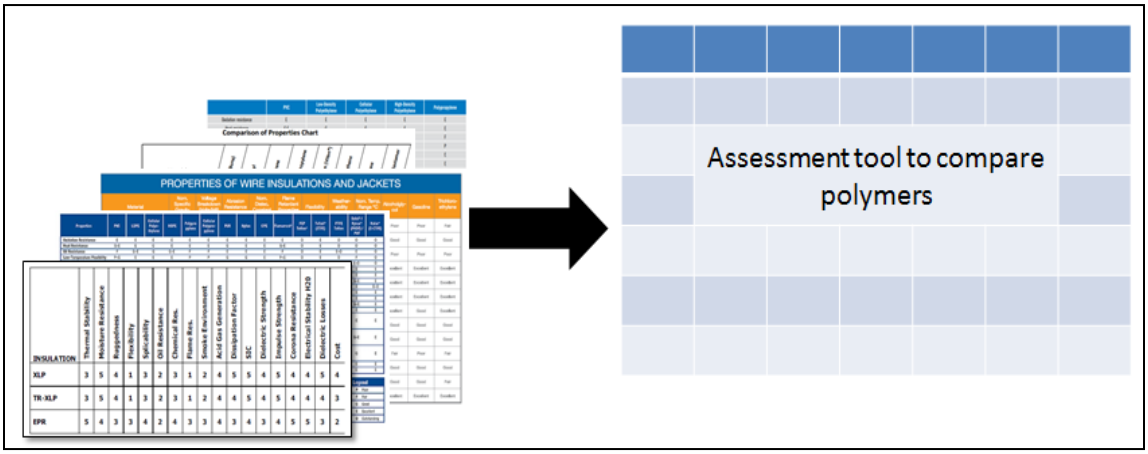

Figure 45. Qualitative Assessment Method

Table 29. Suppliers' Data (N=6)

Criteria	PVC	LDPE	PE	HDPE	PP	PUR	Nylon	EPDM	XLPE	CPE	TPE-E	TPE-O	Teflon	Silicon Rubber	Natural Rubber
Abrasion resistance	2.5	3.0	2.0	4.0	3.0	4.8	4.0	3.3	2.5	4.0	4.3	3.7	3.8	1.5	4.0
Acid resistance	3.5	3.5	3.5	4.0	4.0	2.0	1.8	3.4	3.5	3.8	2.0	2.5	4.0	2.5	2.5
Alcohol resistance	2.0	4.0	4.0	4.0	4.0	2.1	1.8	1.0	4.0	3.9	2.8	2.8	4.0	3.0	3.0
Alkali resistance	3.5	3.5	3.5	4.0	4.0	2.0	4.0	3.5	3.5	3.7	2.0	3.0	4.0	2.5	2.5
Benzol resistance	1.5	1.0	1.0	1.0	1.5	2.0	3.0	2.0	2.0	2.8	-	-	4.0	1.0	-
Degreaser solvents	1.5	3.0	3.0	3.0	1.0	2.0	3.0	1.0	2.0	2.5	-	-	4.0	2.0	-
Electrical properties	2.5	4.0	4.0	4.0	4.0	1.0	1.0	3.7	4.0	3.0	1.0	1.0	4.0	3.0	-
Flame resistance	4.0	1.0	1.0	1.0	1.0	1.0	1.0	1.0	1.5	3.5	1.5	1.8	5.0	2.3	1.0
Gasoline resistance	1.0	3.5	3.0	3.5	2.0	2.3	3.0	1.0	2.0	2.7	1.5	1.5	4.0	2.3	-
Heat resistance	3.5	3.0	3.0	4.0	4.0	3.0	4.0	4.0	3.0	4.3	3.5	3.5	5.0	4.7	2.0
Low temperature flexibility	2.0	4.0	4.0	4.0	1.0	3.0	3.0	3.5	5.0	3.0	3.5	3.5	5.0	4.7	3.0
Nuclear radiation resistance	2.0	3.5	3.0	3.5	2.0	2.5	2.8	3.0	4.0	4.0	-	-	2.0	4.0	-
Oil resistance	2.0	3.5	3.0	3.5	2.0	4.0	4.0	1.3	3.0	3.8	4.0	3.0	5.0	2.5	1.0
Oxidation resistance	4.0	4.0	3.3	4.0	3.5	3.3	3.3	3.7	4.0	4.0	3.7	3.7	4.7	3.3	2.0
Ozone resistance	4.0	4.0	4.0	4.0	4.0	4.0	4.0	3.3	3.3	3.8	4.0	4.0	4.0	4.7	1.0
Underground burial	2.0	3.0	2.5	4.0	3.5	3.0	1.0	4.0	4.0	4.3	-	-	4.0	3.0	-
Water resistance	2.5	4.0	4.0	4.0	4.0	2.2	1.5	3.6	3.5	4.0	3.0	3.0	4.0	3.2	3.5
Weather, sun resistance	3.5	4.0	4.0	4.0	4.0	3.3	4.0	4.0	3.0	4.0	3.7	3.7	4.7	4.5	2.0

Legend: *1: Poor 2: Fair 3: Good 4: Excellent 5: Outstanding*

Figure 46 illustrates the qualitative assessment as it applies to cables used in PV systems. Four main polymeric materials are used in cables (ranked from most to least expensive): HDPE, XLPE, CPE, and EPDM. This plot compares the performance of different polymers for different criteria, such as: abrasion, acid, alcohol, electrical, flame resistance, oil underground burial, etc. For instance, for low-temperature flexible

conditions, XLPE is the most suitable (outstanding), followed by HDPE (excellent), EPDM (good-excellent) and CPE (good).

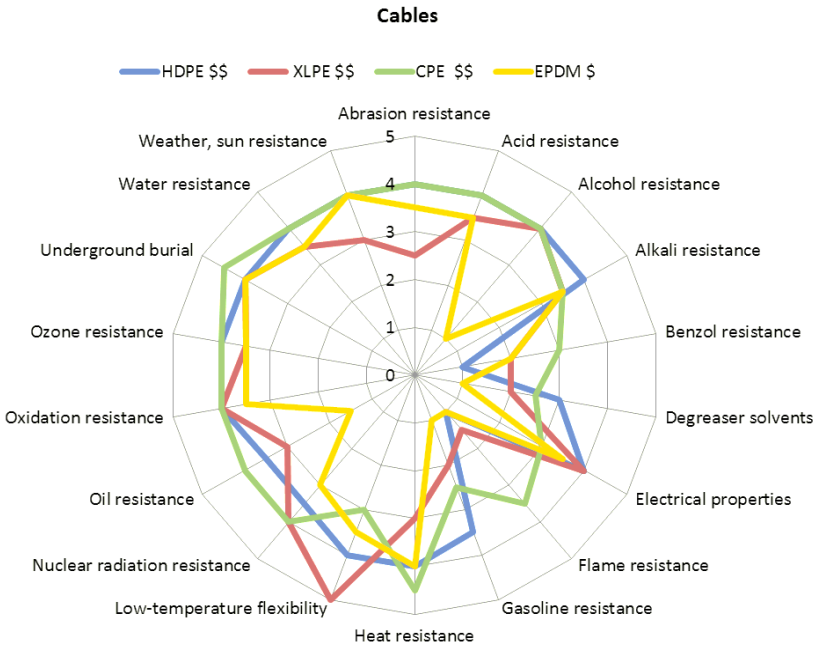

Figure 46. Qualitative Assessment for Cables

Figure 47 shows the qualitative assessment as it applies to connectors used in PV systems. Three main polymeric materials are used in connectors (ranked from most to least expensive): Nylon, TPU, and PVC. As shown in this figure, the TPU line is disconnected due to some missing data in suppliers' data sheets. Depending on the actual design criteria, some materials are preferred over others. For instance, the PVC is an excellent polymer for flame resistance while Nylon and TPU perform poorly. However, Nylon performs better than Nylon and TPU against heat.

Similarly, Figure 48 illustrates the qualitative assessment as it applies to rubber insulation used in PV systems. However, as shown in this plot, only TPU is being deployed for that application. Moreover, the missing data from suppliers' performance

sheets is the reason behind the unavailability of data for all metrics. TPU appears to be a good-excellent polymer for heat, ozone, oxidation, and low-temperature flexibility resistance.

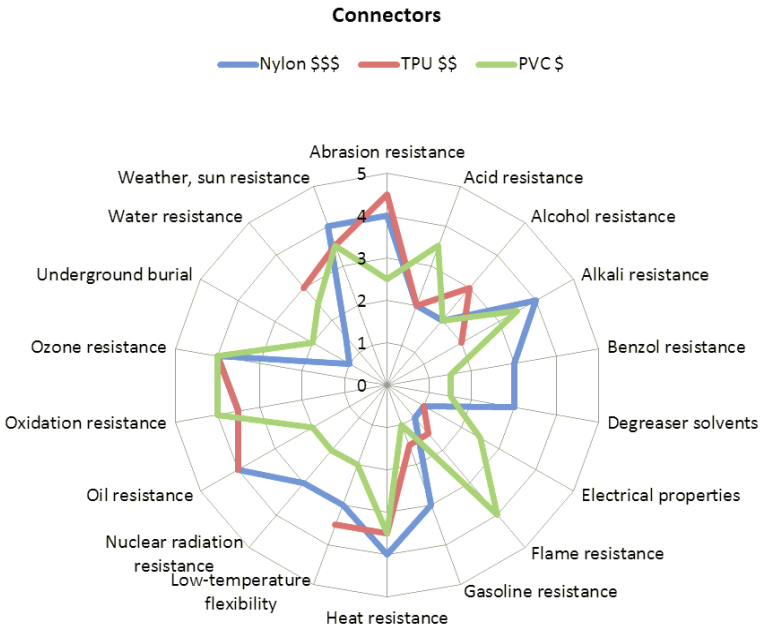

Figure 47. Qualitative Assessment for Connectors

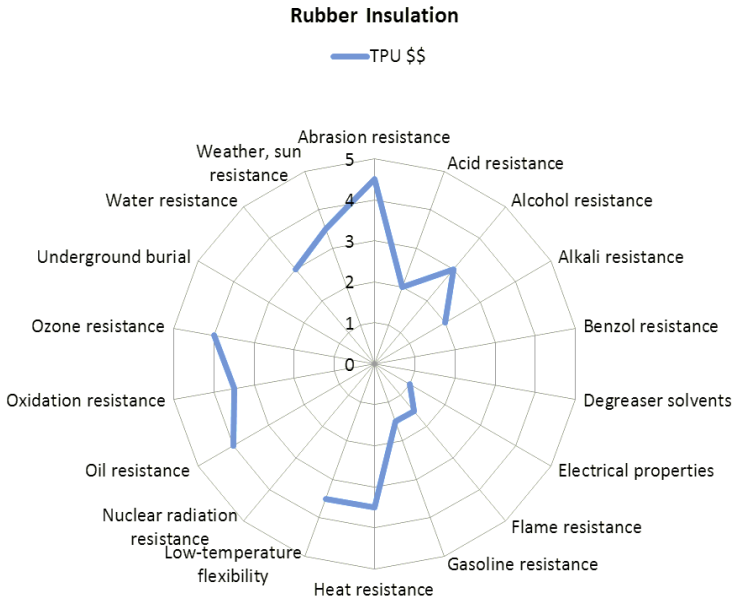

Figure 48. Qualitative Assessment for Rubber Insulation

4.4.3. Existing Decision Frameworks

An ever increasing variety of materials is available today, with each having its own characteristics, applications, advantages, and limitations. When selecting polymeric materials for solar systems, a clear understanding of the functional requirements for each individual component is required and various important criteria or attributes need to be considered. Although polymeric material selection is a difficult and subtle task, in choosing the right material, there is not always a single definite criterion of selection and the designers and engineers have to take into account a large number of material selection criteria. Therefore, researchers and scholars have developed different types of decision-frameworks. Some of these decision frameworks are based on some questions or design topics that are useful and should be considered before deciding on the material selection, such as the following recommendations (Peacock 1980):

When selecting elastomers, the following criteria need to be considered:

1. ***Static or dynamic:*** *If there is movement, is it rotary, linear, due to thermal expansion or pressure cycling?*
2. ***Temperature:*** *Continuous, minimum, maximum, thermal cycling, glass transition temperature shift.*
3. ***Application:*** *Clearance gaps, surface finish.*
4. ***Media:*** *Chemical compatibility, solubility parameter (e.g. physical interaction, such as swelling, and chemical interaction)*
5. ***Pressure:*** *Continuous, maximum, fluctuations, rate of decompression.*
6. ***Aesthetics:*** *Colour, surface finish, avoidance of split lines, etc.*
7. ***Cost:*** *Primary consideration, trade off in performance, cost of failure, and Total Cost of Ownership (TCO).*
8. ***Approvals and specifications:*** *International standards, such as ISO, industry standards or customer specific.*

Another type of frameworks is proposed as a decision tree for the selection of polymeric material. Figure 49 illustrates an example of elastomer selection diagram (Parco 2013) based on different criteria, such as: type (hydrocarbon fluids), temperature, and load type (static or dynamic).

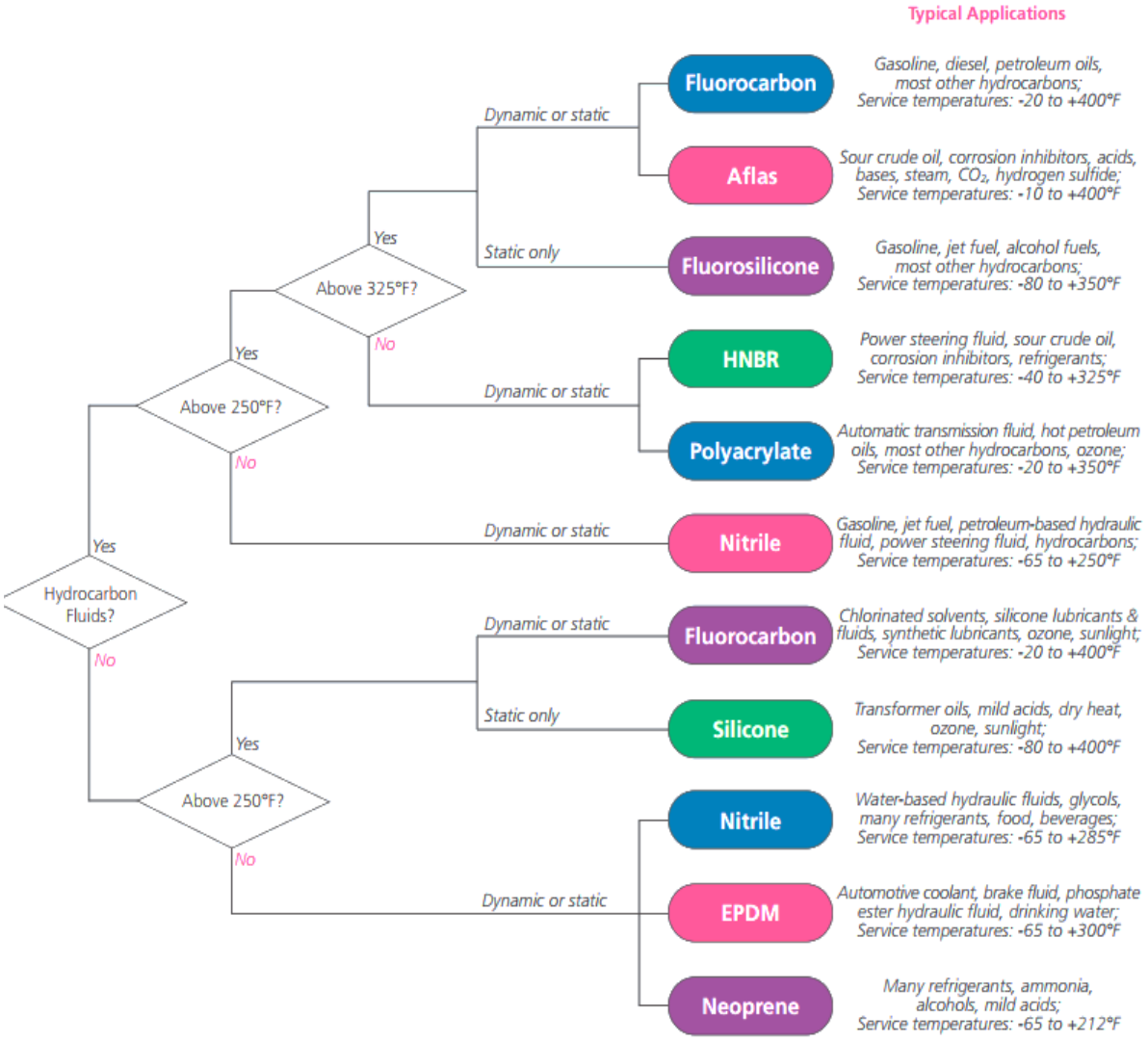

The six elastomers with superior oil resistance are found in the top half of the diagram. Elastomers used mainly in non-hydrocarbon applications are found in the bottom half of the diagram. Fluorocarbon and nitrile are repeated because they are also widely used with nonhydrocarbons.

Figure 49. Polymers Selection Decision Tree (Parco 2013)

Other forms of decision frameworks are based on a series of different steps, where some of the materials are eliminated progressively if they do not comply with the design requirements. Below is an example of 6-step framework (Curbell 2013) that considers the group characteristics of polymers, cost and temperature resistance, tensile strength, flexural modulus, IZOD impact, and dielectrical strength.

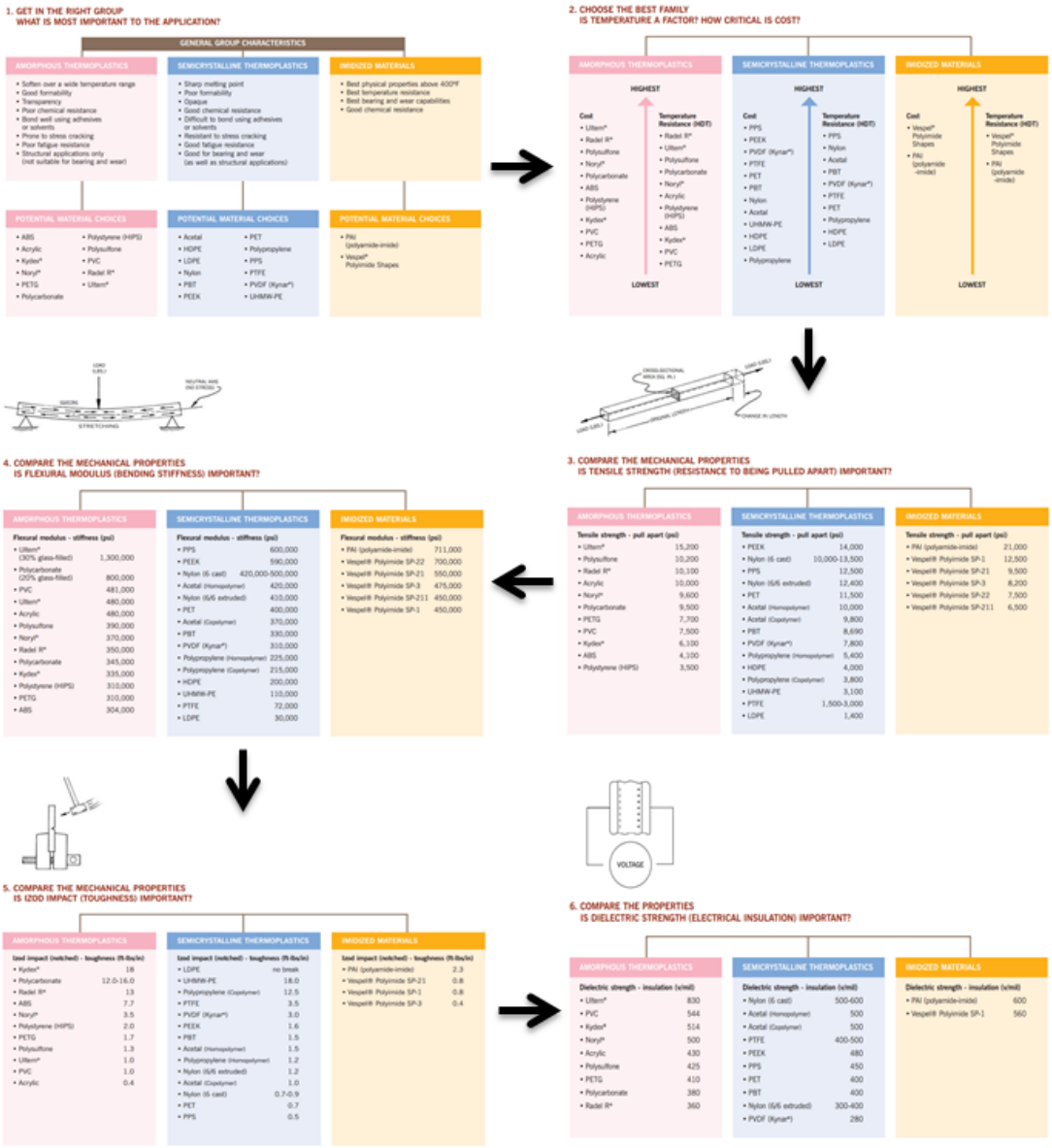

Figure 50. Material Selection Process [Adapted from (Curbell 2013)]

This section described the potential methods to appropriately choose a polymeric material for electrical components. Combining the different methods and building on their outcomes, depending on the site characteristics, establishes the proposed approach to optimize the selection of polymers. Developing fault trees for each component leads to the definition of the root factors behind polymeric materials degradation and also paves the way to develop inspection checklists for different components. Moreover, assessing qualitatively the performance of different polymers and investigating existing decision frameworks introduce the development of *First Solar* – ASU tool. The next section elaborates on the development of this tool and applies the proposed decision framework to optimize the selection of the materials.

4.5. MATERIALS SELECTION TOOL

To account for the degradation of polymeric materials, the *First Solar* – ASU proposed method consists of designing a decision-framework based on the existing approaches in the literature. The approach consists of computing the percentage of compatibility of different polymers with different conditions. To complete the analysis, the tool considers the following criteria:

- Commercial availability: plays a major role in the budget of the project. Using locally available polymeric materials reduces the transportation cost, labor cost, probability of any damage to the materials etc., which may result in reducing the cost of the developing a project. Additionally, the availability of a polymeric material highly depends on the current standards and designs, which can limit or allow the use of limited number of polymers.

- Commodity prices: is related to the previous criterion and plays a major role during the material selection process. Therefore, the developed tool offers the user the possibility of eliminating any undesirable material at the beginning of the analysis either to commercial unavailability, applicable standards, or high prices.
- Properties of the materials: is a crucial part in selecting materials. Polymers behave differently for the same conditions and environments; therefore, selecting the materials with the highest compatibility percentage with the site conditions is a necessary part towards the optimization of material selection.
- Inspection Checklists: are needed to monitor the health of the different polymeric materials and mitigate the failure possibilities due to different factors. The tool displays a list of recommendations within different stages of the project for a selected component.

A demonstration of the **P**olymer**ic** **Ma**terials **S**election Support **T**ool (**P-MAST**) developed by *First Solar* and ASU is presented next.

4.5.1. Tool Demonstration and Testing

The following is an example to illustrate the comparison and selection of polymeric materials that are used in tracker and fixed tilt systems. To help the end-user in the materials selection, the tool is designed to highlight in "green" and "red" the recommended and non-recommended polymeric materials for a specific environment, respectively.

For demonstration purposes, an investigation of the polymeric materials selection for connectors is presented below.

First, the user has to choose a component between cables, connectors, and rubber insulation, as shown in Figure 51. Three plots comparing the different polymeric materials over the studied criteria are also presented to offer a general overview of the pros and cons of each polymer for each component.

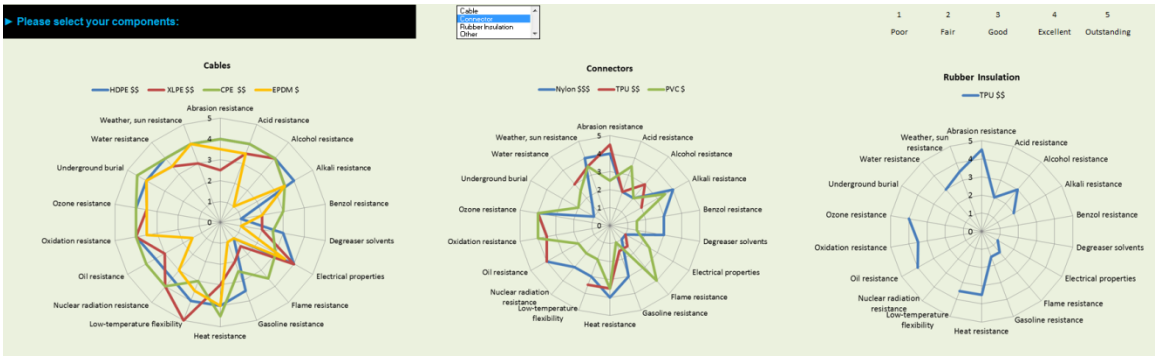

Figure 51. Tool Demonstration - Choosing Connectors

Second, the tool shows the ranking of different polymers in terms of cost: cheap ($), medium ($$), and expensive ($$$). At this step, the user has the ability to not consider any polymer for the remaining analysis, as shown in Figure 52. By deselecting the unsuitable polymer(s) due to cost, or commercial availability, or applicable standards and codes, the user is narrowing down the comparison.

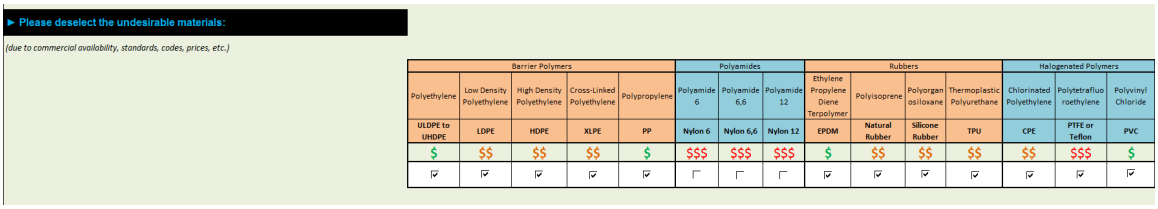

Figure 52. Tool Demonstration – Deselecting Expensive Polymers

Third, the user enters the requirements for both qualitative and quantitative scales according the site design, as shown in Figure 53. Such inputs include the resistance to heat, oxidation, dielectric strength, tensile strength, etc. Then, the tool highlights in green and red the suitable and unsuitable polymers, respectively, and in purple when data is

missing. At the end, a percentage of compatibility is computed, ranging between 0% and 100%, in order to rank the polymers from the least to the most compatible with the design requirements.

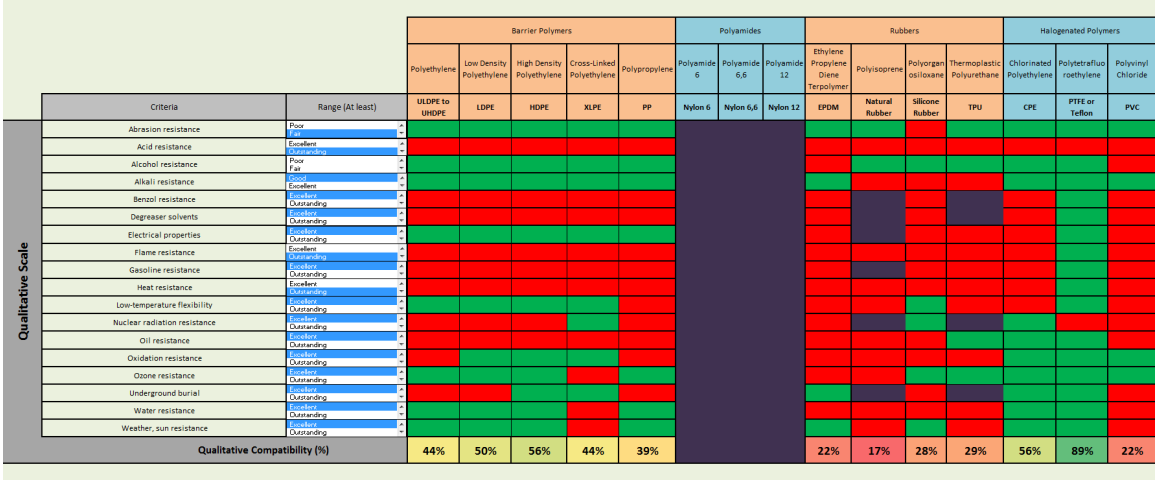

			Barrier Polymers					Polyamides			Rubbers				Halogenated Polymers		
			Polyethylene	Low Density Polyethylene	High Density Polyethylene	Cross-Linked Polyethylene	Polypropylene	Polyamide 6	Polyamide 6,6	Polyamide 12	Ethylene Propylene Diene Terpolymer	Polyisoprene	Polyorganosiloxane	Thermoplastic Polyurethane	Chlorinated Polyethylene	Polytetrafluoroethylene	Polyvinyl Chloride
	Criteria	Range (At least)	ULDPE to UHDPE	LDPE	HDPE	XLPE	PP	Nylon 6	Nylon 6,6	Nylon 12	EPDM	Natural Rubber	Silicone Rubber	TPU	CPE	PTFE or Teflon	PVC
Qualitative Scale	Abrasion resistance	Poor															
	Acid resistance	Excellent															
	Alcohol resistance	Poor															
	Alkali resistance	Good															
	Benzol resistance	Excellent															
	Degreaser solvents	Excellent															
	Electrical properties	Excellent															
	Flame resistance	Excellent															
	Gasoline resistance	Excellent															
	Heat resistance	Excellent															
	Low-temperature flexibility	Excellent															
	Nuclear radiation resistance	Excellent															
	Oil resistance	Excellent															
	Oxidation resistance	Excellent															
	Ozone resistance	Excellent															
	Underground burial	Excellent															
	Water resistance	Excellent															
	Weather, sun resistance	Excellent															
	Qualitative Compatibility (%)		44%	50%	56%	44%	39%				22%	17%	28%	29%	56%	89%	22%

Figure 53. Tool Demonstration – Computing the Compatibility Percentages

Fourth, the tool displays a set of inspection checklists for the selected component, as shown in Figure 54. These checklists are organized in three different sets based on the project stage from design, to installation, and O&M.

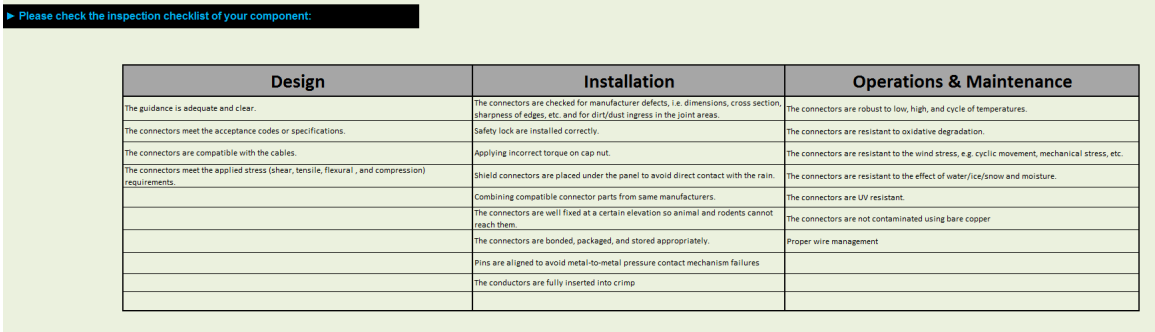

▶ Please check the inspection checklist of your component:

Design	Installation	Operations & Maintenance
The guidance is adequate and clear.	The connectors are checked for manufacturer defects, i.e. dimensions, cross section, sharpness of edges, etc. and for dirt/dust ingress in the joint areas.	The connectors are robust to low, high, and cycle of temperatures.
The connectors meet the acceptance codes or specifications.	Safety lock are installed correctly.	The connectors are resistant to oxidative degradation.
The connectors are compatible with the cables.	Applying incorrect torque on cap nut.	The connectors are resistant to the wind stress, e.g. cyclic movement, mechanical stress, etc.
The connectors meet the applied stress (shear, tensile, flexural , and compression) requirements.	Shield connectors are placed under the panel to avoid direct contact with the rain.	The connectors are resistant to the effect of water/ice/snow and moisture.
	Combining compatible connector parts from same manufacturers.	The connectors are UV resistant.
	The connectors are well fixed at a certain elevation so animal and rodents cannot reach them.	The connectors are not contaminated using bare copper
	The connectors are bonded, packaged, and stored appropriately.	Proper wire management
	Pins are aligned to avoid metal-to-metal pressure contact mechanism failures	
	The conductors are fully inserted into crimp	

Figure 54. Tool Demonstration – Reviewing the Inspection Checklists

4.6. CONCLUSIONS AND RECOMMENDATIONS

Polymeric materials degradation can lead to failures in solar PV plant infrastructure. Decisions regarding the long-term integrity of a structure or its components depend in

large part on choosing an optimal material to resist the conditions affecting its degradation. This research develops, implements, and delivers a decision framework to support the polymeric materials selection for cables, connectors, and module clips rubber insulation, used in tracker and fixed tilt systems.

First, this study classifies the different types of polymers, outlines the main degradation factors, and describes current practices and designs of PV polymeric materials. Then, it presents the different assessment approaches, combines them, develops a materials selection tool and validates the comprehensive research method on *First Solar* materials. Lastly, the research summarizes the learned lessons and recommendations to select polymeric materials for PV components.

This research developed a decision-support tool that integrates different decision frameworks to select polymeric materials for different PV components. The framework is flexible to incorporate new needs and data. In addition to developing new decision frameworks, accelerated testing is recommended for future studies to simulate different conditions and experimentally quantify the degradation rate of different polymeric materials. By selecting the applicable materials, the failure risks are decreased. Effective polymeric material failure mitigation strategies start with a correct selection of such materials.

CHAPTER 5

CONCLUSIONS AND CONTRIBUTIONS

The solar energy sector has been growing rapidly over the past decade. As the global energy demand and technological advancements in large scale manufacturing increase, the photovoltaic industry is expected to continue growing. Such growth in renewable electricity generation using photovoltaic systems is accompanied by an increased awareness of the fault conditions developing during the operational lifetime of these systems. This dissertation contributes to the body of knowledge of photovoltaic systems reliability by providing decision-making tools for utility scale PV systems that outperform the existing models and frameworks. This chapter summarizes the results and contributions, and discusses the research limitations and opportunities for future work.

5.1. SUMMARY OF THE RESULTS AND CONTRIBUTIONS

In this dissertation, the state of the art and practice of prognostics and health management for the DC side of photovoltaic systems was reviewed. Using a data-driven method, the corrosion of the driven posts supporting photovoltaic structures was assessed. The probabilistic risk associated with the failure of polymeric materials, which are used in tracker and fixed tilt systems, was investigated. The results of this dissertation led to distinct contributions to the body of knowledge; the next section will provide a summary of these contributions along with the key results of this research.

PHM applications are essential for the reliability of PV systems by facilitating condition-based maintenance and minimization of cascading failures. This study provided an overview of the different types of failure modes in the DC side of PV systems. Next, it summarized the PV fault detection, diagnostics and prognostics approaches. The

presented methods showed the different approaches documented in the literature to address the faults in the DC side of PV systems. However, depending on the monitoring technology, communication infrastructure, availability of physical models, and measured data, some solution approaches may perform better than the others. Through the integration of fault detection, diagnostics, and prognostics, future PV systems will possess the ability to sustain power generation while increasing the reliability and resiliency of the system itself. A review of the PHM applications for PV systems paved the way to emphasize the key research gaps and challenges in the current practice as well as the available opportunities. One such opportunity was investigating the structure supporting PV modules, specifically the impact of corrosion on the structure.

Corrosion can lead to failures in solar PV plant infrastructure. Decisions regarding the long-term integrity of a structure or its components depend in large part on an accurate assessment of the conditions affecting its corrosion and rate of degradation. The objective of this research phase was to assess the corrosion of driven posts used in tracker and fixed tilt systems. As a result, a framework was developed to inform and support decision-makers in design and reliability applications.

The phase starts with detailing the factors affecting the corrosivity rate of a site. Second, a complete meta-analysis of corrosion modeling, as it applies to PV structures, highlights the current methods and practices used in industry to predict underground and above-ground corrosion rates. The research approach consists of running two independent analyses for underground and above-ground corrosion. By selecting the applicable models out of the existing available models, the corrosion rate and estimated

service life are quantified. Moreover, the method entails developing new predictive models for zinc and steel corrosion based on the available data from *First Solar* sites.

The results demonstrate the superiority of the newly developed approach, compared to existing methods, in predicting zinc and steel corrosion rates. The application of the developed models is limited to the range of data found on the available *First Solar* sites. Moreover, the proposed framework is found to work best in highly corrosive environments. This framework is geared to support decision-makers in design and reliability studies, and is flexible to incorporate new data and needs.

PV power plants and components, by virtue of their application, are exposed to some of the harshest outdoor environments. Most equipment is subject directly to the environment and all the myriad stresses possible. Other aspects also influence the likelihood of such hazards, including local site conditions, micro and macro environment, construction variability and quality, and maintenance practices. Poor choices of wire management means can expose the operator of the PV power plant to increased risks of power loss, shock, fire and other hazards and affect overall cost of ownership. The choice of polymeric materials should be informed by such factors to assure a level of robustness and minimize costs both initial, and over the plant design lifetime.

5.2. RESEARCH LIMITATIONS AND FUTURE WORK

By investigating the root causes leading to the failure of supporting posts and polymeric materials that are used in tracker and fixed tilt systems, this study contributes to the body of knowledge on the reliability of solar systems. The focused scope of this study on specific types of polymers and posts reduces variation and adds value to the findings, but at the same time it presents a limitation of not being generalizable to the whole

population of mounting structures and polymers. However, the new assessment methods and predictive models introduced in this study can certainly be replicated for other types of steel posts and polymeric materials, and in other environments. Additional types of components and materials affecting the reliability of solar systems are currently being investigated in ongoing studies on the topic. Future work also will consist of continuing to collect actual data from an increasing number of sites and expanding the analysis to include several environments and designs. Future studies will aim to fill the identified gaps by: (1) determining the parameters, location, resolution and precision of required sensors in the PV systems; (2) developing and testing new data-driven models; (3) generating new prognostics models for the different parts and materials of PV systems; (4) verifying and validating the developed models using experimental data; (5) designing online frameworks and algorithms to implement the PHM models; and (6) assisting the decision-makers in their investigation of the ROI for PHM activities.

BIBLIOGRAPHY

AASHTO. "LRFD Bridge Construction Specifications, 3rd Edition." Washington, DC: The American Association of State Highway and Transportation Officials, 2010.

Abdallah, M. "Rhodanine azosulpha drugs as corrosion inhibitors for corrosion of 304 stainless steel in hydrochloric acid solution." *Corrosion science*, 2002: 44(4), 717-728.

Adinoyi, M., and Said, S. (2013). "Effect of dust accumulation on the power outputs of solar photovoltaic modules." *Renewable Energy*, 60, 633-636.

Alam, M., Khan, F., Johnson, J., and Flicker, J. (2015). "A Comprehensive Review of Catastrophic Faults in PV Arrays: Types, Detection, and Mitigation Techniques." *IEEE Journal of Photovoltaics*, 5 (3), 982-997.

Alam, M., Khan, F., Johnson, J., and Flicker, J. (2013). "PV faults: Overview, modeling, prevention and detection techniques." *IEEE 14th Workshop on Control and Modeling for Power Electronics (COMPEL)*.

American Galvanizaton Association. (2011). "Performance of Hot-Dip Galvanized Steel Products."

American Water Works Association. "American National Standard for Polyethylene Encasement of Ductile-Iron Pipe Systems." AWWA C105, 1993.

Ancuta, F., and Cepisca, C. (2011). "Fault analysis possibilities for PV panels." *Proceedings of the 2011 3rd International Youth Conference on Energetics (IYCE)*.

Andrew, J. P., and Allison, R. C. (2006). "Polymer chemistry: Properties and Applications".

Arnold, J. C. (1996). "Environmental stress crack initiation in glassy polymers." Trends in polymer science, 4(12), 403-408.

Beavers, J. A. "Corrosion of steel piling in nonmarine applications (No. 408)." Transportation Research Board, 1998.

Bower, W., and Wiles, J. (1994). "Analysis of grounded and ungrounded photovoltaic systems." *IEEE Photovoltaic Specialists Conference*.

Bradford, S. A., and Bringas, J. E. "Corrosion control." New York: Van Nostrand Reinhold, 1993.

Braun, H., Banavar, M., and Spanias, A. (2012). "Signal Processing for Solar Array Monitoring, Fault Detection, and Optimization." *Morgan & Claypool Publishers*.

Braun, H., Buddha, S., Krishnan, V., Spanias, A., Tepedelenlioglu, C., Yeider, T., and al. (2012). "Signal processing for fault detection in photovoltaic arrays." *IEEE International Conference on Acoustics, Speech and Signal Processing (ICASSP)*.

Brown, R. P., and Greenwood, J. H. (2002). "Practical guide to the assessment of the useful life of plastics." iSmithers Rapra Publishing.

Brown, R. P., Kockott, D., Trubiroha, P., Ketola, W., and Shorthouse, J. (1995). "A Review of Accelerated Durability Tests."Versailles Project on Advanced Materials and Standards (VAMAS Report no. 18).

Caltrans. "Corrosion Guidelines." Sacramento, CA: California Department of Transportation, Corrosion Technology Branch, 2003.

Carfagno, S. P., and Gibson, R. J. (1980). "Review of equipment aging theory and technology."Final report (No. EPRI-NP-1558). Franklin Research Center, Philadelphia, PA (USA).

Carlson, C. S. (2014). "Understanding and applying the fundamentals of FMEAs." In Annual Reliability and Maintainability Symposium.

Chao, K. (2010). "A novel fault diagnosis method based-on modified neural networks for photovoltaic systems." In *Advances in Swarm Intelligence*, pp. 531-539. Springer Berlin Heidelberg.

Chao, K., Ho, S., and Wang, M. (2008). "Modeling and fault diagnosis of a photovoltaic system." *Electric Power Systems Research*, 78 (1), 97-105.

Charki, A., Laronde, R., and Bigaud, D. (2013). "Accelerated degradation testing of a photovoltaic module." *Journal of Photonics for Energy*, 3 (1).

Cheng, Z., Zhong, D., Li, B., and Liu, Y. (2011). "Research on fault detection of PV array based on data fusion and fuzzy mathematics." *Power and Energy Engineering Conference*.

Chokor, A., El Asmar, M., and Lokanath, S. "A Review of Photovoltaic DC Systems Prognostics and Health Management: Challenges and Opportunities." *The 8th Annual Conference of the Prognostics and Health Management*, Denver, October 1 – 6, 2016.

Chouder, A., and Silvestre, S. (2010). "Automatic supervision and fault detection of PV systems based on power losses analysis." *Energy Conversion and Management*, 51 (10), 1929-1937.

Chuang, S., Ishibashi, A., Kijima, S., Nakayama, N., Ukita, M., and Taniguchi, S. (1997). "Kinetic model for degradation of light emitting diodes." *IEEE Journal of Quantum electronics*, 33, pp 970–979.

Cocca, M., D'Arienzo, L., and D'Orazio, L. (2011). "Effects of Different Artificial Agings on Structure and Properties of Whatman Paper Samples." *Materials Science*, 863083.

Cohen, J. "Statistical Power Analysis for the Behavioral Sciences." Routledge, 1988.

Coleman, A., and Zalewski, J. (2011). "Intelligent fault detection and diagnostics in solar plants." *Intelligent Data Acquisition and Advanced Computing Systems (IDAACS)*.

Collier, D., and Key, T. (1988). "Electrical fault protection for a large photovoltaic power plant inverter." *IEEE Photovoltaic Specialists Conference*.

Cristaldi, L., Faifer, M., Lazzaroni, M., Khalil, A., Catelani, M., and Ciani, L. (2014). "Failure modes analysis and diagnostic architecture for photovoltaic plants." *Proceedings of the 13 the IMEKO TC10 Workshop on Technical Diagnostics Advanced measurement tools in technical diagnostics for systems' reliability and safety*.

Cristaldi, L., Faifer, M., Lazzaroni, M., Khalil, A., Catelani, M., and Ciani, L. (2014). "Failure modes analysis and diagnostic architecture for photovoltaic plants." *IMEKO TC10 Workshop on Technical Diagnostics Advanced measurement tools in technical diagnostics for systems' reliability and safety*.

Curbell (2013). "Material selection guide."

Del Angel, E., Vera, R. and Corvo, F. (2015) "Atmospheric Corrosion of Galvanised Steel in Different Environments in Chile and Mexico." *Int. J. Electrochem. Sc*,: 10, 7985-8004.

Densley, J. (2001). "Ageing mechanisms and diagnostics for power cables-an overview". IEEE Electrical Insulation Magazine, 17(1), 14-22.

Dini, D., Brazis, P., and Yen, K. (2011). "Development of arc-fault circuit-interrupter requirements for photovoltaic systems." *IEEE Photovoltaic Specialists Conference (PVSC)*.

Drews, A., De Keizer, A., Beyer, H., Lorenz, E., Betcke, J., Van Sark, W., et al. (2007). "Monitoring and remote failure detection of grid-connected PV systems based on satellite observations." *Solar Energy*, 81 (4), 548-564.

Ducange, P., Fazzolari, M., Lazzerini, B., and Marcelloni, F. (2011). "An intelligent system for detecting faults in photovoltaic fields." *Intelligent systems design and applications (ISDA)*.

Dumas, L., and Shumka, A. (1982). "Photovoltaic module reliability improvement through application testing and failure analysis." *IEEE Transactions on Reliability*, 31 (3), 228-234.

Ellis, P. D. "The essential guide to effect sizes: Statistical power, meta-analysis, and the interpretation of research results." Cambridge University Press, 2010.

Emanuel, N. and Buchachenko, A. (1987). "Chemical physics of polymer degradation and stabilization". New York.

Escobar, L. and Meeker, W. (2006). "A review of accelerated test models." *Statistical Science*, 21 (4), 552–577.

Faul, F., Erdfelder, E., Lang, A. G. and Buchner, A. (2007). "G* Power 3: A flexible statistical power analysis program for the social, behavioral, and biomedical sciences." *Behavior research methods*: 39(2), 175-191.

Feliu, S., and Morcillo, M. (1993). "The prediction of atmospheric corrosion from meteorological and pollution parameters—I. Annual corrosion." *Corrosion Science*: 34(3), 403-414.

FHWA. (2009). "Corrosion/degradation of soil reinforcements for mechanically stabilized earth walls and reinforced soil slopes."

First Solar (2015). "Annual Report."

First Solar Procurement and Construction Management. (2017). Retrieved from: http://www.firstsolar.com/en/Technologies-and-Capabilities/Procurement-and-Construction-Management.

Firth, S., Lomas, K., and Rees, S. (2010). "A simple model of PV system performance and its use in fault detection." *Solar Energy*, 84 (4), 624-635.

Flicker, J., and Johnson, J. (2013). "Electrical simulations of series and parallel." *39th IEEE Photovoltaic Specialist Conference*.

Fort Pierce Air Conditioning. (2016) "Corrosion Protection." Retrieved from: http://www.fortpierceairconditioning.com/html/corrosion_protection.html.

Galvanizeit. "Performance of Galvanized Steel Products." Retrieved from: http://www.galvanizeit.org/uploads/publications/Performance_of_Galvanized_Steel_Products.pdf.

Gokmen, N., Karatepe, E., Celik, B., and Silvestre, S. (2012). "Simple diagnostic approach for determining of faulted PV modules in string based PV arrays." *Solar Energy*, 86 (11), 3364-3377.

Gokmen, N., Karatepe, E., Silvestre, S., Celik, B., and Ortega, P. (2013). "An efficient fault diagnosis method for PV systems based on operating voltage-window." *Energy Conversion and Management*, 73, 350-360.

Graver, D. "Corrosion Data Survey - Metals Section." Houston, TX: NACE, 1985.

Greewnood, J.H. (1997). "Life prediction in polymers." ERA Technology Report No. 97-0782.

Gueguen, V., Audouin, L., Pinel, B., and Verdu, J. (1994). "Lifetime prediction in the case of radiooxidative ageing of an ethylenepropylene rubber used for electrical insulation."Polymer degradation and stability, 46(1), 113-122.

Guma, T., Mohammed, S. and Tanimu, A. (2015). "A Field Survey of Soil Corrosivity Level of Kaduna Metropolitan Area through Electrical Resistivity Method." *International journal of scientific engineering and research*: 3 (12).

Haagenrud, S. E., Henriksen, J. F. and Gram, F. (1985). "Dose-response functions and corrosion mapping for a small geographical area." The fall 1985 meeting of the Electrochemical Society.

Hammond, R., Srinivasan, D., Harris, A., Whitfield, K., and Wohlgemuth, J. (1997). "Effects of soiling on PV module and radiometer performance." *Photovoltaic Specialists Conference*.

Hannigan, P. J., Goble, G. G., Thendean, G., Likins, G. E. and Rausche, F. "Design and Construction of Driven Post Foundations." Report No. FHWA HI-97-013, Washington, DC: Federal Highway Administration, 1997.

Hare, J., Shi, X., Gupta, S., and Bazzi, A. (2016). "Fault diagnostics in smart micro-grids: A survey." *Renewable and Sustainable Energy Reviews*, 60, 1114-1124.

Hastings, J., Juds, M., Luebke, C., and Pahl, B. (2011). "A study of ignition time for materials exposed to DC arcing in PV systems." *37th IEEE Photovoltaic Specialists Conference*.

Heng, A., Zhang, S., Tan, A., and Mathew, J. (2009). "Rotating machinery prognostics: State of the art, challenges and opportunities." *Mechanical Systems and Signal Processing*, 23(3), 724-739.

Highways England. "The United Kingdom Design Manual for Roads and Bridges BD 12/01 Design of Corrugated Steel Buried Structures with Spans Greater than 0.9 Meters and up to 8.0 Meters." 2012.

Hocheng, H., and Puw, H. Y. (1992). "On drilling characteristics of fiber-reinforced thermoset and thermoplastics." International Journal of Machine Tools and Manufacture, 32(4), 583-592.

Houssein, A., Heraud, N., Souleiman, I., and Pellet, G. (2010). "Monitoring and fault diagnosis of photovoltaic panels." *IEEE Energy Conference and Exhibition*.

Hu, Y., Gao, B., Song, X., Tian, G., Li, K., and He, X. (2013). "Photovoltaic fault detection using a parameter based model." *Solar Energy*, 96, 96-102.

IEEE. "IEEE Guide for Measuring Earth Resistivity, Ground Impedance and Earth Surface Potentials of a Ground System." Standard 81, 2012.

ISO Standard 9223-92. "Corrosion of metals and alloys - Corrosivity of atmospheres Classification." 1992.

Jackura, J. A., Garofalo, G. and Beddard, D. "Investigation of Corrosion at 14 Mechanically Stabilized Embankment Sites." Report no. CA/TL-87/12, Sacramento, CA: California Department of Transportation, 1987.

Javadi, M. S., Nobakht, A., and Meskarbashee, A. (2011). "Fault tree analysis approach in reliability assessment of power system." International Journal of Multidisciplinary Sciences and Engineering, 2(6), 46-50.

Jeong, J., and Park, N. (2013). "Field discoloration analysis and UV/temperature accelerated degradation test of EVA for PV." *Photovoltaic Specialists Conference (PVSC)*.

Jiang, H., Lu, L., and Sun, K. (2011). "Experimental investigation of the impact of airborne dust deposition on the performance of solar photovoltaic (PV) modules." *Atmospheric Environment*, 45 (25), 4299-4304.

Jiang, L., and Maskell, D. (2015). "Automatic fault detection and diagnosis for photovoltaic systems using combined artificial neural network and analytical based methods." *International Joint Conference on Neural Networks (IJCNN)*.

Johnson, J., Kuszmaul, S., Bower, W., and Schoenwald, D. (2011). "Using PV module and line frequency response data to create robust arc fault detectors." *Proceedings of the 26th European Photovoltaic Solar Energy Conference and Exhibition*.

Johnson, J., Schoenwald, D., Kuszmaul, S., Strauch, J., and Bower, W. (2011). "Creating dynamic equivalent PV circuit models with impedance spectroscopy for arc fault modeling." *Photovoltaic Specialists Conference (PVSC)*.

Kalogirou, S., and Tripanagnostopoulos, Y. (2007). "Industrial application of PV/T solar energy systems." *Applied Thermal Engineering*, 27 (8), 1259-1270.

Kaplani, E. (2012). "Detection of degradation effects in field-aged c-Si solar cells through IR thermography and digital image processing." *International Journal of Photoenergy*.

Katiraei, F., and Agüero, J. (2011). "Solar PV integration challenges." *Power and Energy Magazine*, 9 (3), 62-71.

Kaushik, A., and Golnas, A. (2011). "PV system reliability: lessons learned from a fleet of 333 systems." *SPIE Solar Energy and Technology. International Society for Optics and Photonics*.

King, G. A. (1995). "Corrosivity mapping-A novel tool for materials selection and asset management." *Materials Performance*: 34(1).

Kempe, M. (2005). "Control of moisture ingress into photovoltaic modules." *Photovoltaic Specialists Conference*.

Kojima, T., and Yanagisawa, T. (2004). "The evaluation of accelerated test for degradation a stacked a-Si solar cell and EVA films." *Solar Energy Materials & Solar Cells*, 81 (1), 119–123.

Kucera, V., Mattsson, E. and Mansfeld, F. (1987). "Atmospheric Corrosion." *Corrosion mechanisms*: 211-284.

Laidler, K. (1984). "The development of the Arrhenius equation." *Journal of Chemical Education*, 61 (6), 494-498.

Levlin, E. (1996). "Aeration cell corrosion of carbon steel in soil: In situ monitoring cell current and potential." *Corrosion science*: 38(12), 2083-2090.

Leygraf, C., Wallinder, I. O., Tidblad, J. and Graedel, T. "Atmospheric corrosion." John Wiley & Sons, 2016.

Li, Z., Wang, Y., Zhou, D., and Wu, C. (2012). "An intelligent method for fault diagnosis in photovoltaic array." *System Simulation and Scientific Computing*.

Lin, X., Wang, Y., Zhu, D., Chang, N., and Pedram, M. (2012). "Online fault detection and tolerance for photovoltaic energy harvesting systems." *Proceedings of the International Conference on Computer-Aided Design*.

Logan, K., and Grodsky, V. "Soil-corrosion Studies - Rates of Corrosion and Pitting of Bare Ferrous Specimens." US Department of Commerce, Bureau of Standards, 1931.

Manganiello, P., Balato, M., and Vitelli, M. (2015). "A survey on mismatching and aging of PV modules: The closed loop." *IEEE Transactions on Industrial Electronics*, 62 (11), 7276-7286.

Marion, B., and Adelstein, J. (2003). "Long-term performance of the SERF PV systems." *NCPV and Solar Program Review Meeting*.

Massey, L. K. (2003). "Permeability properties of plastics and elastomers: a guide to packaging and barrier materials."William Andrew.

Maxwell, A. S., Broughton, W. R., Dean, G., and Sims, G. D. (2005). "Review of accelerated ageing methods and lifetime prediction techniques for polymeric materials." NPL Report DEPC MPR, 16, 22.

McCrum, N. G., Buckley, C. P., and Bucknall, C. B. (1997). "Principles of polymer engineering". Oxford University Press, USA

Molenbroek, E., Waddington, D., and Emery, K. (1991). "Hot spot susceptibility and testing of PV modules." *Photovoltaic Specialists Conference*.

Montgomery, D. C., and Runger, G. C. "Applied statistics and probability for engineers." John Wiley & Sons, 2010.

NACE. "Pipeline external corrosion direct assessment methodology." Houston, Texas, USA.: NACE International, 2002.

NACE. "Standard Practice-Control of External Corrosion on Underground or Submerged Metallic Piping Systems." Houston, Texas, USA: NACE International, 2007.

Ndiaye, A., Charki, A., Kobi, A., Kébé, C., Ndiaye, P., and Sambou, V. (2013). "Degradations of silicon photovoltaic modules: A literature review." *Solar Energy*, 96, 140-151.

Nguyen, D., and Lehman, B. (2006). "Modeling and simulation of solar PV arrays under changing illumination conditions." *IEEE Workshops on Computers in Power Electronics*.

Nilsson, D. (2014). “Fault detection in photovoltaic systems.” KTH Royal Institute of Technology, Master's Thesis.

Obi, M., and Bass, R. (2016). “Trends and challenges of grid-connected photovoltaic systems–A review.” *Renewable and Sustainable Energy Reviews*, 58, 1082-1094.

Oreski, G., and Wallner, G. (2005). “Aging mechanisms of polymeric films for PV encapsulation.” *Solar Energy*, 79, 612–617.

Oreski, G., and Wallner, G. (2010). “Damp heat induced physical aging of PV encapsulation materials.” *12th IEEE Intersociety Conference on Thermal and Thermo-Mechanical Phenomena in Electronic Systems*.

Osterwald, C., Benner, J., Pruett, J., Anderberg, A., Rummeland, S., and Ottoson, L. (2003). “Degradation in weathered crystalline-silicon PV modules apparently caused by UV radiation.” *The 3rd World Conference on Photovoltaic Energy Conversion*, Osaka, Japan, pp. 2911– 2915.

Pan, R., Kuitche, J., and Tamizhmani, G. (2011). “Degradation analysis of solar photovoltaic modules: Influence of environmental factor.” *Annual Reliability and Maintainability Symposium*.

Parco (2013). “Elastomer selection guide.”

Patel, H., and Agarwal, V. (2008). “MATLAB-Based modeling to study the effects of partial shading on PV array characteristics.” *IEEE Transactions on Energy Conversion*, 23 (1), 302-310.

Peacock, R. N. (1980). “Practical selection of elastomer materials for vacuum seals.” Journal of Vacuum Science and Technology, 17(1), 330-336.

Phinikarides, A., Kindyni, N., Makrides, G., and Georghiou, G. (2014). “Review of photovoltaic degradation rate methodologies.” *Renewable and Sustainable Energy Reviews*, 40, 143-152.

Picozzi, O. E., Lamb, S. E. and Frank, A. C. “Evaluation of prediction methods for post corrosion at the Buffalo Skyway.” Technical Services Division, 30, 41-46, New York State Department of Transportation, 1993.

Pierre, R. “Corrosion Engineering-Principles and Practice.” Editorial McGraw-Hill, 2008.

Plaček, V., Bartoníček, B., Hnát, V., and Otáhal, B. (2003). “Dose rate effects in radiation degradation of polymer-based cable materials”. Nuclear Instruments and Methods in Physics Research Section B: Beam Interactions with Materials and Atoms, 208, 448-453.

Polo, F., Del Rosario, J., and García, G. (2010). "Supervisory control and automatic failure detection in grid-connected photovoltaic systems." *Trends in Applied Intelligent Systems*.

Quaschning, V., and Hanitsch, R. (1996). "Numerical simulation of current-voltage characteristics of photovoltaic systems with shaded solar cells." *Solar Energy*, 56 (6).

Quintana, M., King, D., McMahon, T., and Osterwald, C. (2002). "Commonly observed degradation in field-aged photovoltaic modules." *Photovoltaic Specialists Conference*.

Raghuraman, B., Laksman, V., Kuitche, J., Shisler, W., Tamizhani, G., and Kapoor, H. (2006). "An overview of SMUDs outdoor photovoltaic test program at Arizona State University." *IEEE World Conference on Photovoltaic Energy Conversion*, Hawaii, USA.

Rauschenbach, H., and Maiden, E. (1972). "Breakdown phenomena in reverse biased silicon solar cells." *IEEE Photovoltaic Specialists Conference*.

Ricker, R. (2010). "Analysis of Pipeline Steel Corrosion Data From NBS (NIST) Studies Conducted Between 1922–1940 and Relevance to Pipeline Management." *Journal of research of the National Institute of Standards and Technology*: 115(5), 373.

Ricker, R.E. "Analysis of Pipeline Steel Corrosion Data from NBS (NIST) Studies Conducted Between 1922-1940 and Relevance to Pipeline Management." Internal Report 7415, National Institute of Standards and Technology, 2007.

Roberge, P. "Corrosion Basics: An Introduction." NACE International, 2006.

Roberge, P. "Handbook of Corrosion Engineering." McGraw Hill Professional, 2012.

Rodriguez, R., Basta, N., Casteel, S. and Pace, L. (1999). "An in vitro gastrointestinal method to estimate bioavailable arsenic in contaminated soils and solid media." *Environmental Science & Technology*: 33(4), 642-649.

Romanoff, M. "Underground Corrosion - NBS Circular 579." Washington, D.C.: National Bureau of Standard, 1957.

Schlothauer, J., Jungwirth, S., Köhl, M., and Röder, B. (2012). "Degradation of the encapsulant polymer in outdoor weathered photovoltaic modules: spatially resolved inspection of EVA ageing by fluorescence and correlation to electroluminescence". Solar Energy Materials and Solar Cells, 102, 75-85.

Syafaruddin, S. and Karatepe, E. (2011). "Controlling of artificial neural network." *Intelligent System Application to Power Systems (ISAP)*.

Saly, V., Ruzinsky, M., Packa, J., and Redi, P. (2002). "Examination of solar cells and encapsulations of small experimental photovoltaic modules." *2nd International IEEE Conference on Polymers and Adhesives in Microelectronics and Photonics*.

Schimpf, F., and Norum, L. (2009). "Recognition of electric arcing in the DC-wiring of photovoltaic systems." *International Telecommunications Energy Conference*.

Schirone, L., Califano, F., Moschella, U., and Rocca, U. (1994). "Fault finding in a 1 MW photovoltaic plant by reflectometry." *Photovoltaic Energy Conversion, IEEE Photovoltaic Specialists Conference*.

Schwerdtfeger, W. J. (1971) "Polarization measurements as related to corrosion of underground steel piling." *J Research Eng & Instrumentation*.

Schwerdtfeger, W. J. (1966). "Soil resistivity as related to underground corrosion and cathodic protection." *Highway Research Record*: 110.

Seacostair. (2017). "Anti-corrosion coatings used by treasure coast air conditioning experts."

Sharma, N., and Dalal, D. (2015). "Efficiency and Result Analysis of 50Kw Grid Connected PV System Using MATLAB/SIMULINK." *International Journal of Advanced Research in Electrical, Electronics and Instrumentation Engineering*, 4 (10), 8200-8206.

Silvestre, S., Chouder, A., and Karatepe, E. (2013). "Automatic fault detection in grid connected PV systems." *Solar Energy*, 94, 119-127.

Skoczek, A., Sample, T., and Dunlop, E. (2009). "The results of performance measurements of field-aged crystalline silicon photovoltaic modules." *Progress in Photovoltaics: Research and Applications*, 17 (4), 227-240.

Soil Conservation Service. "Soil Taxonomy: A basic system of soil classification for making and interpreting soil surveys." US Department of Agriculture, Soil Conservation Service, 1975.

Soil Survey Division. "Soil survey manual." United States Department of Agriculture, 1993.

Solórzano, J., and Egido, M. (2013). "Automatic fault diagnosis in PV systems with distributed MPPT." *Energy Conversion and Management*, 76, 925-934.

Spagnuolo, G., Xiao, W., and Cecati, C. (2015). "Monitoring, Diagnosis, Prognosis, and Techniques for Increasing the Lifetime/Reliability of Photovoltaic Systems." *IEEE Transactions Industrial Electronics*, 62 (11), 7226-7227.

Spertino, F., and Akilimali, J. (2009). "Are Manufacturing–Mismatch and Reverse Currents Key Factors in Large Photovoltaic Arrays?" *IEEE Transactions on Industrial Electronics*, 56 (11), 4520-4531.

Stellbogen, D. (1993). "Use of PV circuit simulation for fault detection in PV array fields." *IEEE Photovoltaic Specialists Conference*.

Stern, M., and Geary, A. (1957). "A theoretical analysis of the shape of polarization curves." *Journal of the electrochemical society*: 104(1), 56-63.

Takashima, T., Yamaguchi, J., and Ishida, M. (2008a). "Disconnection detection using earth capacitance measurement in photovoltaic module string." *Progress in Photovoltaics: Research and Applications*, 16 (8), 669-677.

Takashima, T., Yamaguchi, J., and Ishida, M. (2008b). "Fault detection by signal response in PV module strings." *IEEE Photovoltaic Specialists Conference*.

Takashima, T., Yamaguchi, J., Otani, K., Kato, K., and Ishida, M. (2006). "Experimental studies of failure detection methods in PV module strings." *IEEE 4th World Conference on Photovoltaic Energy Conversion*.

Tanaka, H., Fan, L. T., Lai, F. S., and Toguchi, K. (1983). "Fault-tree analysis by fuzzy probability." IEEE Transactions on Reliability, 32(5), 453-457.

U.S. Department of Agriculture. (1975). "Soil Taxonomy: A Basic System of Soil Classification for Making and Interpreting Soil Surveys-Soil Survey Staff."

Vazquez, M., Ignacio, R.S. (2008). "Photovoltaic module reliability model based on field degradation studies." *Progress in Photovoltaics: Research and Applications*, 16, 419–433.

Veleva, L., Meraz, E. and Acosta, M. (2010). "Zinc precipitation runoff from galvanised steel in humid tropical climate." *Corrosion Engineering, Science and Technology*: 76-83.

Vergura, S., Acciani, G., Amoruso, V., and Patrono, G. (2008). "Inferential statistics for monitoring and fault forecasting of PV plants." *IEEE International Symposium on Industrial Electronics*.

Wallinder, I. O., Verbiest, P., He, W. and Leygraf. C. (1998). "The influence of patina age and pollutant levels on the runoff rate of zinc from roofing materials." *Corrosion Science*: 40(11), 1977-1982.

Wan, Y., Ding, L., Wang, X., Li, Y., Sun, H. and Wang, Q. (2013). "Corrosion Behaviors of Q235 Steel in Indoor Soil." *International Journal of Electrochemical Science*, 8: 12531-12542.

Weinstock, D., and Appelbaum, J. (2004). "Optimal solar field design of stationary collectors". Transactions-American Society of Mechanical Engineers Journal of Solar Energy Engineering, 126(3), 898-905.

White, J. R., and Turnbull, A. (1994). "Weathering of polymers: mechanisms of degradation and stabilization, testing strategies and modeling." Journal of materials science, 29(3), 584-613.

Whitlock, J. (2004)."The Seal Man's O-Ring Handbook."

Wohlgemuth, J., and Kurtz, S. (2011). "Reliability testing beyond Qualification as a key component in photovoltaic progress toward grid parity." *IEEE International Reliability Physics Symposium (IRPS)*.

Xie, J., and Pecht, M. (2003). "Reliability prediction modelling of semiconductor light emitting device." *IEEE Transactions on Device and Materials Reliability*, 3, 218–222.

Xu, X., Wang, H., and Zuo, Y. (2011). "Method for diagnosing photovoltaic array fault in solar photovoltaic system." *Power and Energy Engineering Conference (APPEEC)*.

Wright, D. (2001). "Failure of Plastics and Rubber Products – Causes, Effects and Case Studies involving Degradation."Rapra Technology Report.

Wright, D. (1996). "Environmental Stress Cracking of Plastics."Rapra Technology Ltd.

Young, R. J., and Lovell, P. A. (2011). "Introduction to polymers". CRC press.

Zhao, Y., Ball, R., Mosesian, J., De Palma, J., and Lehman, B. (2015). "Graph-based semi-supervised learning for fault detection and classification in solar photovoltaic arrays." *IEEE Transactions on Power Electronics*, 30 (5), 2848-2858.

Zhao, Y., De Palma, J., Mosesian, J., Lyons, R., and Lehman, B. (2013). "Line–line fault analysis and protection challenges in solar photovoltaic arrays." *IEEE Transactions on Industrial Electronics*, 60 (9), 3784-3795.

Zhao, Y., Lehman, B., De Palma, J., Mosesian, J., and Lyons, R. (2011). "Fault analysis in solar PV arrays under: Low irradiance conditions and reverse connections." *Photovoltaic Specialists Conference (PVSC)*.

Zhao, Y., Lehman, B., De Palma, J., Mosesian, J., and Lyons, R. (2011). "Fault analysis in solar PV arrays under: Low irradiance conditions and reverse connections." *Photovoltaic Specialists Conference (PVSC)*.

Zhao, Y., Yang, L., Lehman, B., De Palma, J., Mosesian, J., and Lyons, R. (2012). "Decision tree-based fault detection and classification in solar photovoltaic arrays." *Applied Power Electronics Conference and Exposition (APEC)*.

Zhiqiang, H., and Li, G. (2009). "Research and implementation of microcomputer online fault detection of solar array." *International Conference on Computer Science & Education*.

Zhou, E. (2015). "US Renewable Energy Policy and Industry." *National Renewable Energy Laboratory (NREL)*.

Zimmerman, C. (2008). "Time dependent degradation of photovoltaic modules by ultraviolet light." *Applied Physics Letter*.

APPENDIX A

NBS DATA ANALYSIS

A.1. INTRODUCTION

The results of extensive filed testing on metal pipes and sheet steel buried by the NBS programs originating as early as 1910 constitute the most comprehensive quantitative data available in the field of underground corrosion (Logan and Grodsky 1931). For low alloy and carbon steels in a number of soil burial conditions, Romanoff (1957) determined "n" and "k" constants varying from 0.5 to 0.6 and 150 to 180 μm, respectively at the end of the first year. However, this method was criticized for the uncertainty and the large scatter in the data that couldn't be explained. More recently in 2010, the National Institute of Standards and Technology (NIST), formerly known as NBS, released the most comprehensive reanalysis study of the NBS data (Ricker 2010). The study carried out statistical analysis and confirmed a lack of crisp correlation between corrosion rate and other parameters. The report explains the absence of the correlation to the fact that the parameters related to the soil environment and chemistry during the study did not represent real condition in the vicinity of samples. This document presents a comprehensive analysis of the NBS steel data.

Since the last century, researchers and scholars (Ricker 2007; Ricker 2010) tried to correlate the NBS data with numerous variables, such as the soil texture and contents. However, a conclusive correlation between the corrosion rate and these variables was not established. Meanwhile, other studies (Romanoff 1957) were conducting studies on the variation of corrosion rate with the exposure time. Knowing that the corrosion process in the first few years is quite large and decreases over time, several studies (Schwerdtfeger 1964; Schwerdtfeger 1971) recommended accounting for the long-term corrosion current density after five years of exposure. This study builds on previous studies and will

consider the data after five years of exposure in the prediction of corrosion rate. The study database will be used as a benchmark for future studies to estimate the probability distribution of underground corrosion rates in different environments and different soil textures.

Romanoff investigated the results of field studies by the NBS from 1922 to 1939 and postulated a non-linear law of the corrosion loss at some time (t) after burial:

$$y(t) = k\, t^n$$

Where:

- y(t) is the loss of thickness or pit depth in the metal at time (t)
- k and n (less than unity) are regression parameters that are soil and site dependent

Figure 55 below shows the variation of the maximum penetration depth in the steel over time for all the collected data from NBS studies. Moreover, the variation of the corrosion rate is shown in Figure 56.

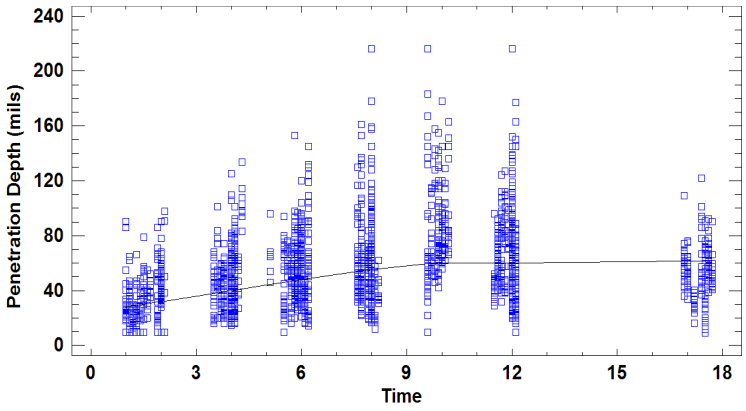

Figure 55. The Variation of the Maximum Penetration Depth of the Steel Collected Data over Time

Romanoff's model is well illustrated in the non-linear nature of the corrosion loss and rate over time in the figures below. Although Romanoff's model can explain the variation of the results over time, the sparsity of the data confines the efficiency of this

method. A further investigation to model the corrosion rate (mpy) and the penetration depth (mils) over time is presented next.

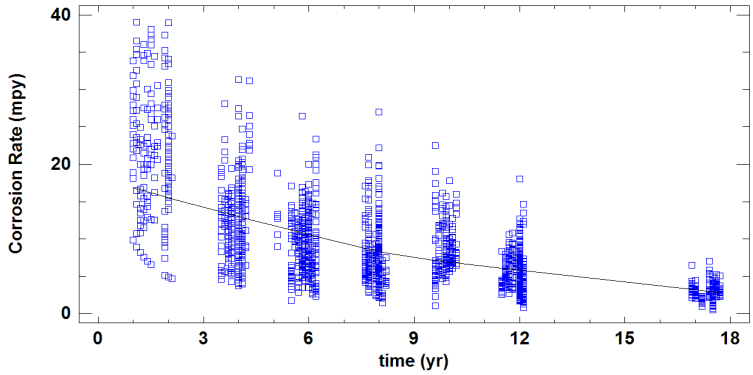

Figure 56. The Variation of the Corrosion Rate of the Collected Data over Time

A.2. MODEL DEVELOPMENT

This study involves two different formulations that have been considered from the literature to model uncertainty in changes. This section details the model development for the corrosion assessment of the Carbon steel pipes filtered from the First Solar-ASU database. The corrosion rates and penetration rate models are also presented based on soil classifications per texture, internal drainage, aeration, and chemical groups.

The first approach involves a deterministic approach where the corrosion rate is assumed to be linear in time at a fixed rate. Therefore, the RUL at some value, t, is:

$$RUL(t) = \frac{y_{cri} - y_t}{r}$$

Where:

- y_{cri} is the allowable penetration depth, it is considered to be 50% of the design web thickness in this study
- y_t is the corrosion penetration depth at some value t
- r is the rate of corrosion

This approach will be implemented through a regression model to estimate a long-term underground corrosion rate. The regression model assumes the degradation of the posts over time is given by a known equation. Therefore, future evolution of a sample path presents no uncertainty.

The second approach involves a probabilistic stochastic model where the penetration depth at any given time is the result of accumulation of degradation that took place in the previous intervals. Therefore, the probability distribution of posts lifetime, T, is related to the corrosion rate, R so that the probability of T to be less than or equal to some value, t, is:

$$P(T \leq t) = P(\, y_t > y_{cri}\,)$$

Where:

- y_{cri} is the allowable penetration depth, it is considered to be 50% of the design web thickness in this study
- y_t is the corrosion penetration depth at some value t

This approach will be implemented through a stochastic cumulative model to estimate the penetration depth at any given time t. Unlike the deterministic method, the stochastic model retains the temporal uncertainty associated with the evolution of the penetration.

A.2.1. Corrosion Rate Assessment

Regression attempts to model the relationship between two or more features and a response variable. Every value of the independent variable x is associated with a value of the dependent variable y. Several methods were used to model the corrosion process as detailed in this section.

A.2.1.1. ***Long-Term Corrosion Model***

Using the data collected by the NBS between 1922 and 1939, Romanoff investigated the correlation between the corrosion rate and the soil parameters, including soil resistivity, pH, moisture, etc. By fitting the corrosion rate data into the log-normal regression model,

$$\ln\big(y(t)\big) = \ln(k) + n\ln\,(t)$$

a clear correlation between the soil properties and the underground corrosion rate was not established. However, the study showed the corrosion rate reaching a stable value after five years of exposure. This model builds on Romanoff's non-linear logarithmic regression model of corrosion penetration and ignores the corrosion penetration variation during the first five years. In order to assess the long-term corrosion performance, the following steps are followed:

- The penetration depth versus time data in the above log-normal regression model are used to estimate the model parameters as shown in Figure 57 below. A 95% confidence interval (between dashed lines) was used to detect and remove the outliers
- The generated logarithmic model is used to estimate:
    - $Y_{initial}$, the estimated penetration depth at 5 years
    - Y_{final}, the estimated penetration depth at t_{final}, the last available year in the data (NBS collected data in different exposure durations between 1 year and 17 years)
- The long-term corrosion rate is the slope of the line joining $Y_{initial}$ and Y_{final}, such as:

$$Longterm\ Corrosion\ Rate\ (mpy) = \frac{Y_{final} - Y_{initial}}{t_{final} - 5}$$

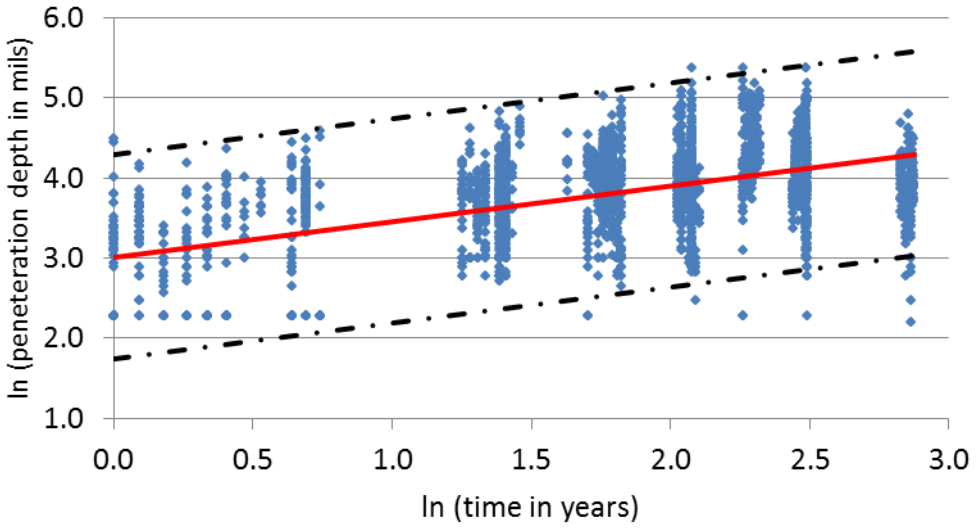

Figure 57. Romanoff Logarithmic Regression Model for NBS Steel Pipes Data

The long-term corrosion rate for NBS carbon steel posts, shown in Figure 58, is equal to 1.743 mpy. This method can be used to estimate the penetration depth in mils within time. Table 30 presents the results of long-term corrosion rate results according to the considered soil classifications. The correspondent Logarithmic regression models are included in Tables 31-34 below.

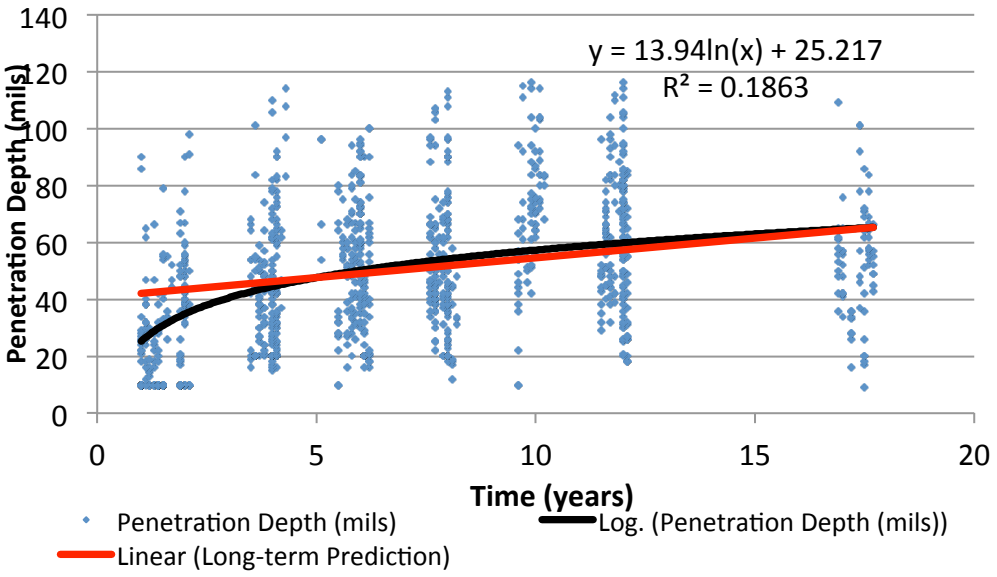

Figure 58. Long-term Penetration Depth Prediction

Table 30. Long-term Corrosion Rate (mpy) Results

Classification System	Class	Logarithmic Regression Model Penetration Depth = a.ln(t) + b				Long-term Corrosion Rate (mpy)
		Data Sample after Outliers Removal	R^2	a	b	
Soil Texture	Clay	155	0.297	19.795	19.692	1.977
	Loam/Clay Loam	184	0.217	12.896	24.520	1.292
	Other	138	0.323	24.093	22.297	2.398
	Sandy Loam	191	0.057	7.161	28.104	0.713
	Silt Loam	368	0.213	13.688	24.962	1.377
Internal Drainage	Very Poor	69	0.558	34.314	14.113	4.292
	Poor	359	0.198	14.072	24.121	1.406
	Good	344	0.087	7.805	30.371	0.777
	Fair	257	0.309	18.786	19.723	1.883
Aeration	Very Poor	84	0.544	36.838	13.435	4.607
	Poor	374	0.343	16.180	14.412	1.616
	Good	333	0.076	7.806	30.642	0.777
	Fair	246	0.229	16.634	32.380	1.673
Chemical Groups	Inorganic Reducing Acid	283	0.201	13.975	25.486	1.396
	Inorganic Oxidizing Acid	453	0.126	10.412	28.183	1.036
	Inorganic Reducing Alkaline	132	0.172	16.014	23.521	1.599
	Inorganic Oxidizing Alkaline	12	0.138	11.280	44.670	2.075
	Organic Reducing Acid	69	0.558	34.314	14.113	4.292
Overall Data		1032	0.186	13.940	25.217	1.388

Table 31. Long-term Corrosion Rate Logarithmic Regression Models per Soil Texture Classification

Class	Model
Clay	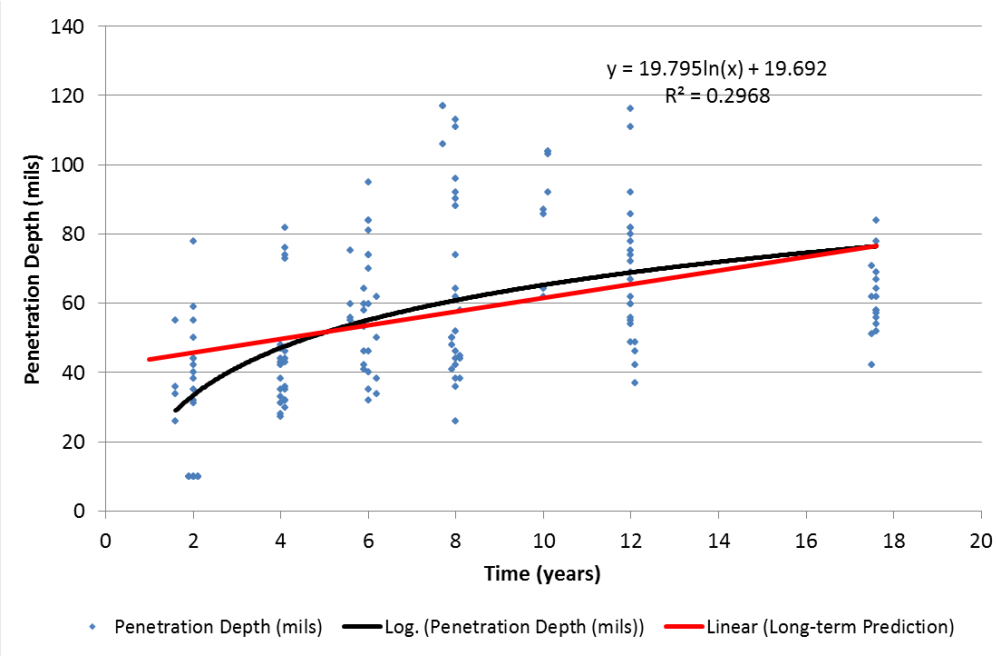
Loam/Clay Loam	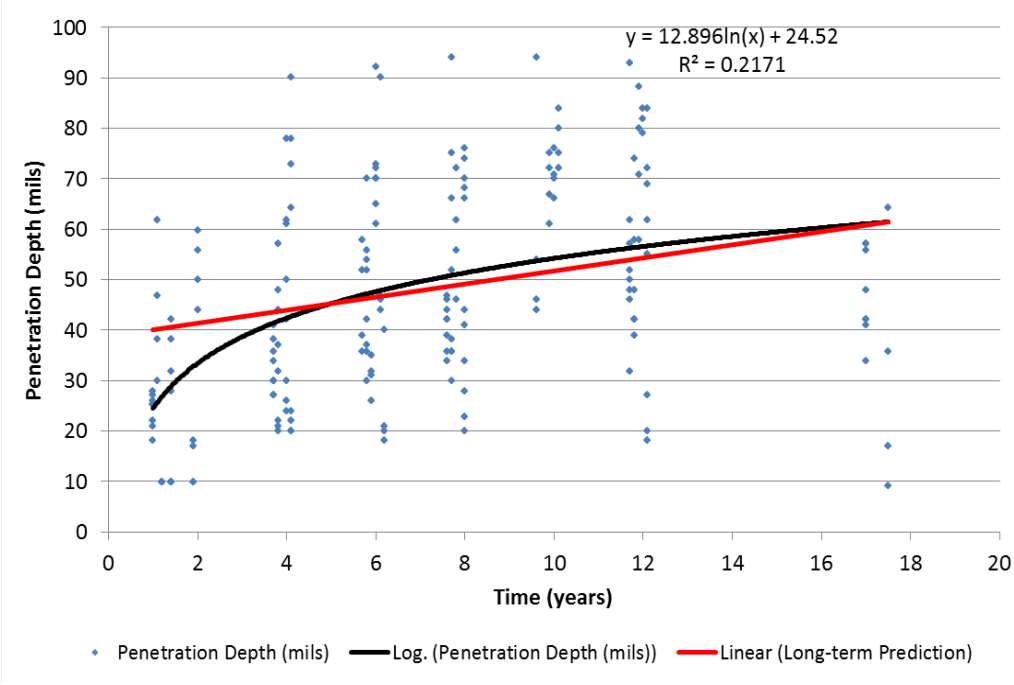

Class	Model
Other	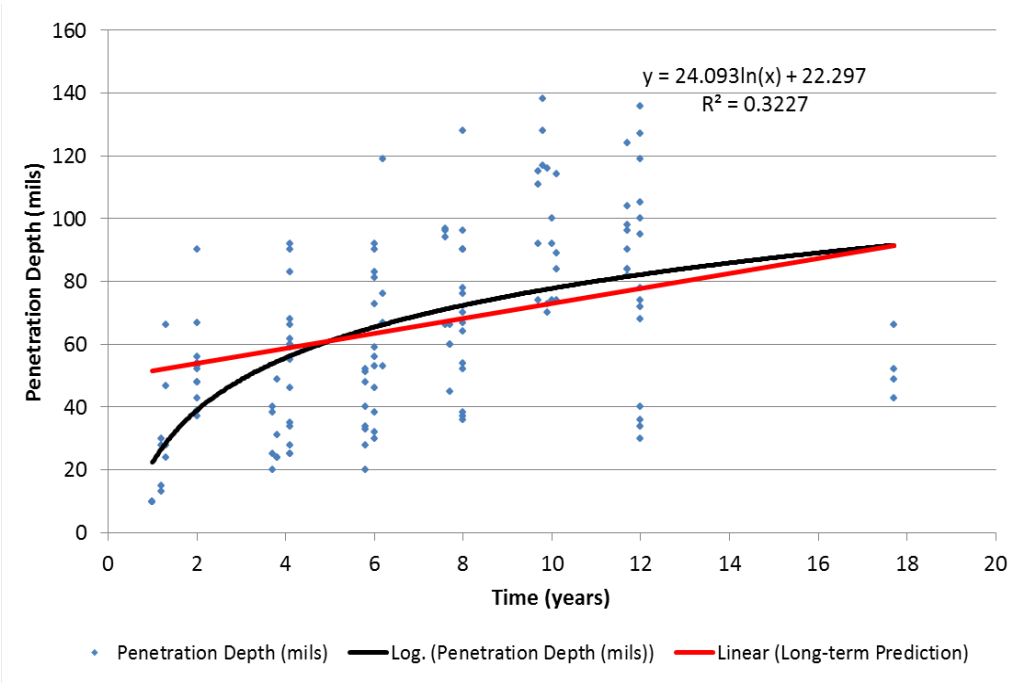
Sandy Loam	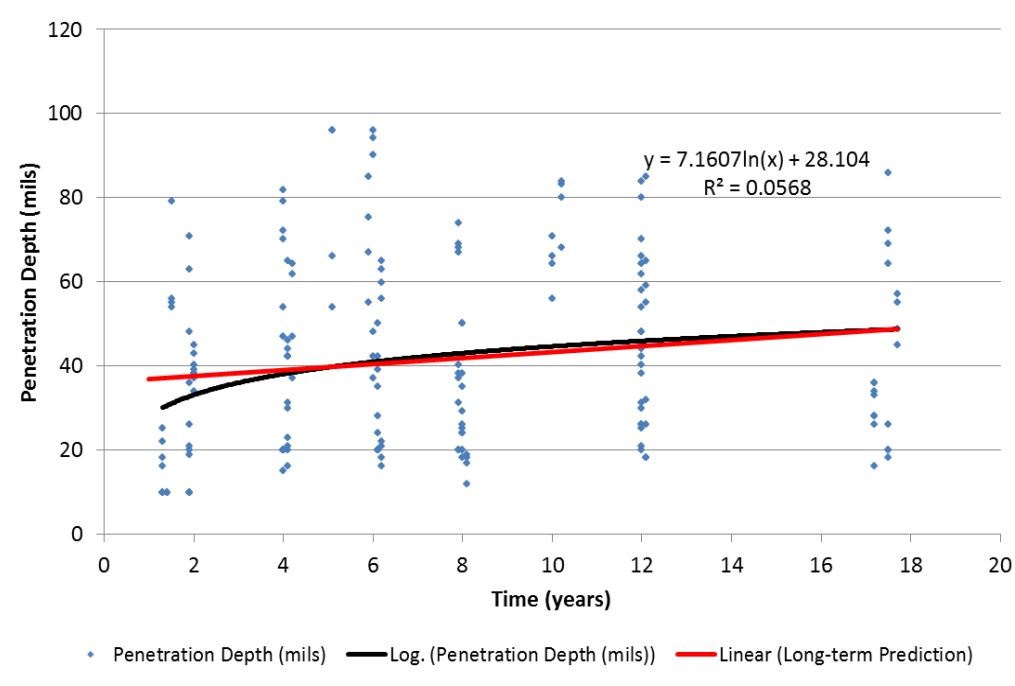

Class	Model
Silt Loam	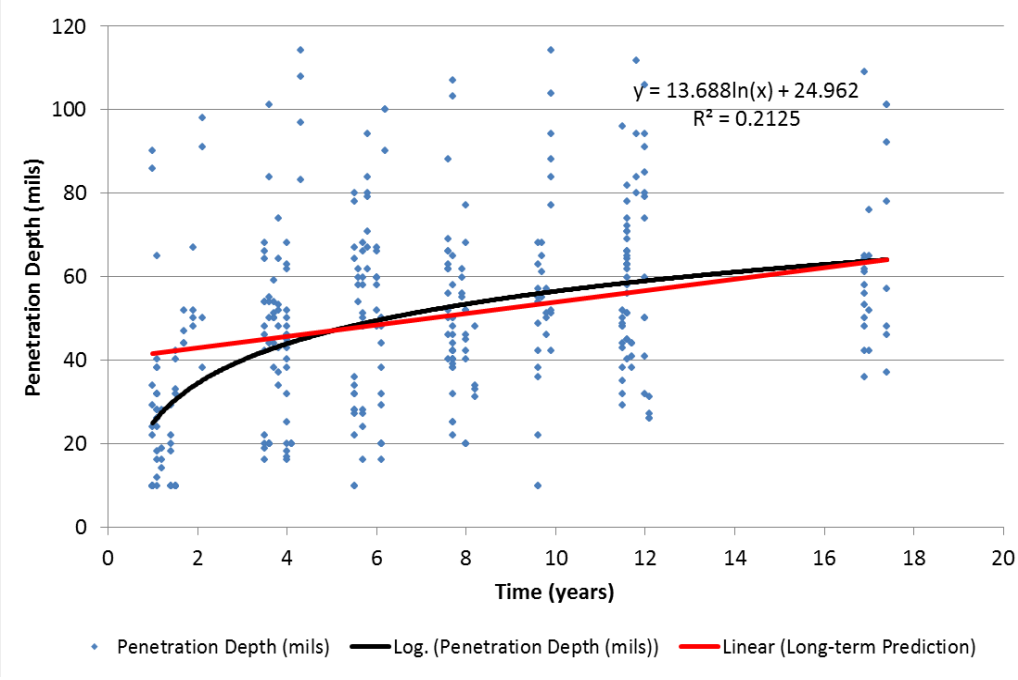

Table 32. Long-term Corrosion Rate Logarithmic Regression Models per Internal Drainage

Class	Model
Very Poor	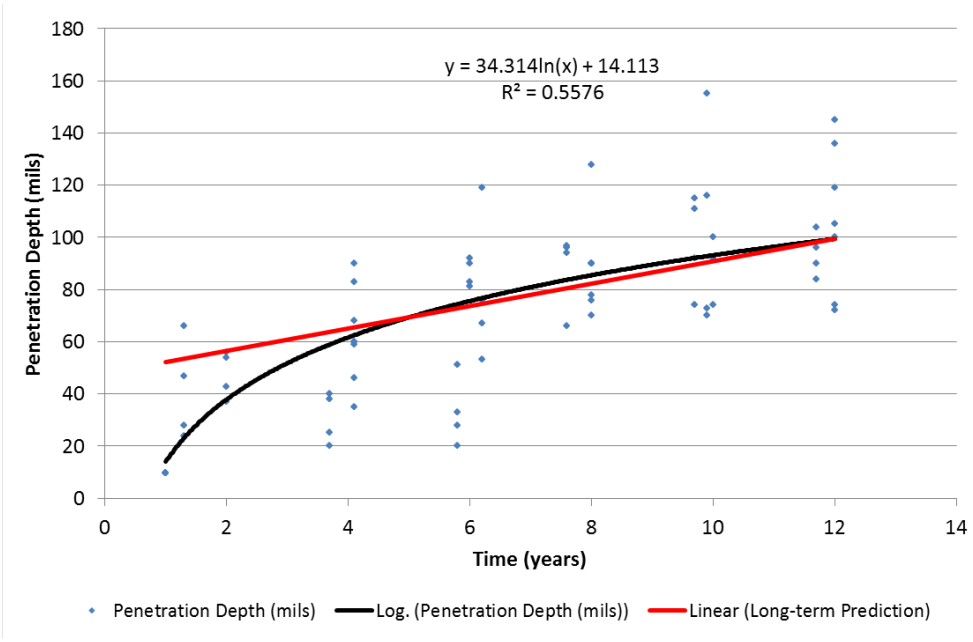
Poor	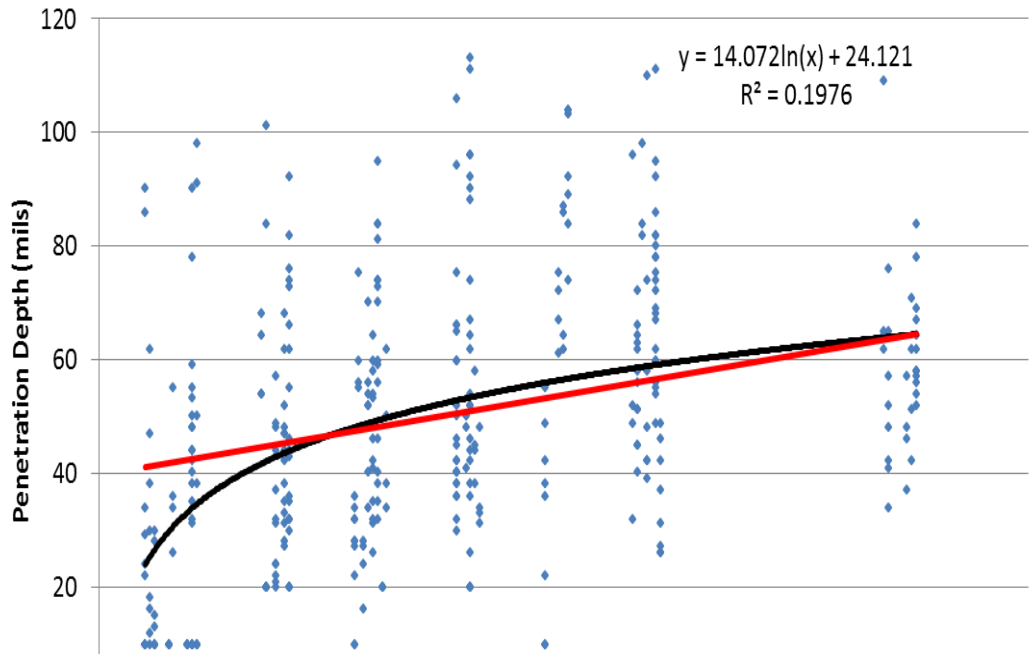

Class	Model
Good	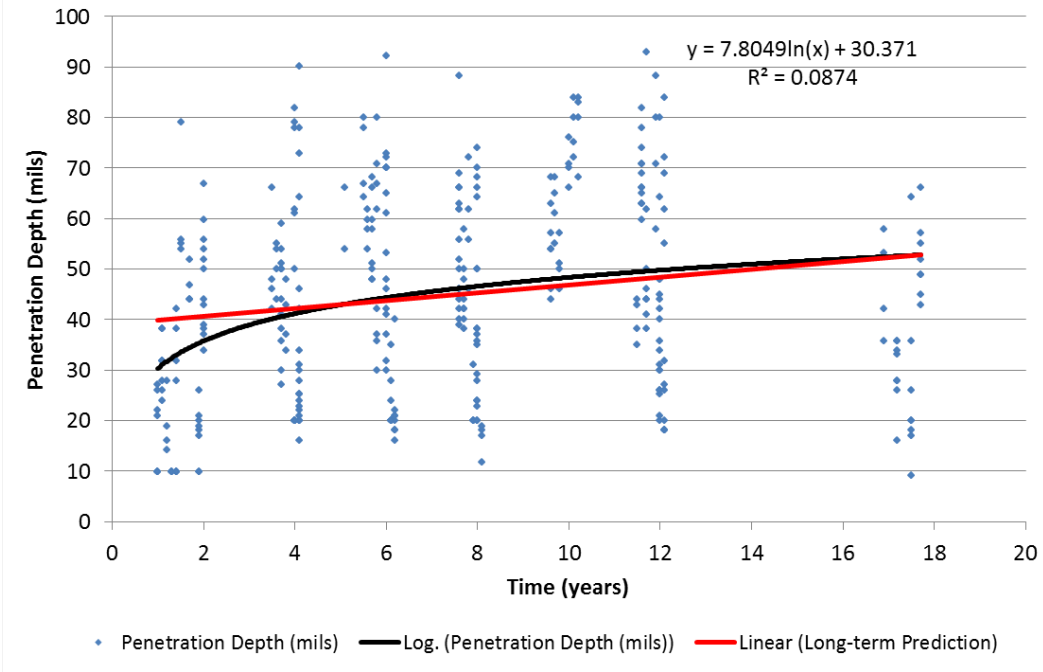
Fair	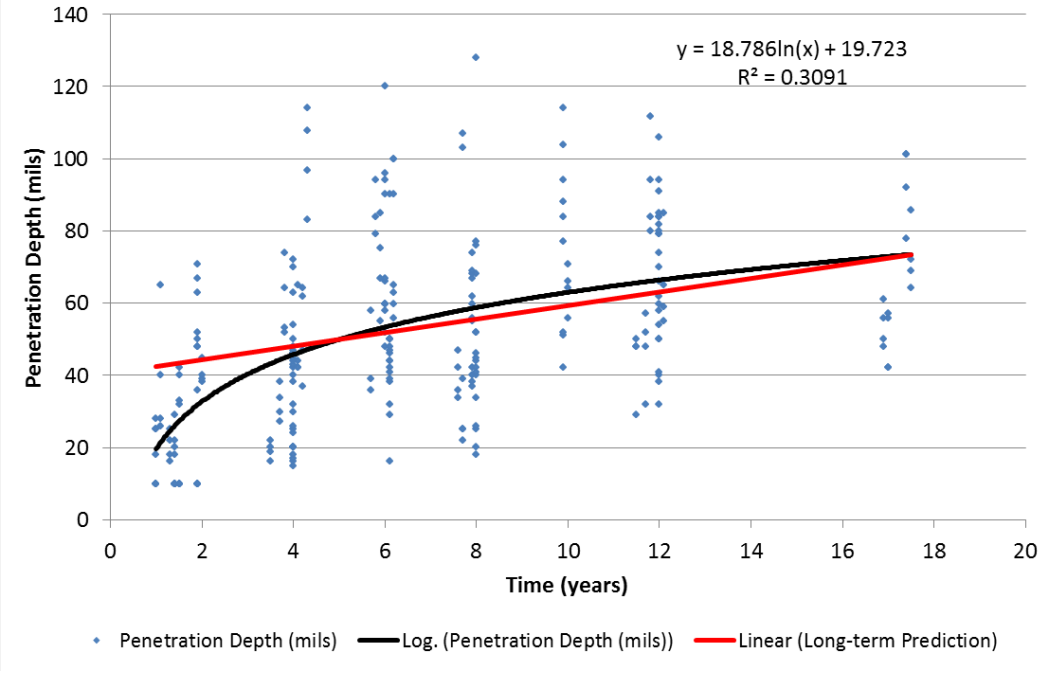

Table 33. Long-term Corrosion Rate Logarithmic Regression Models per Soil Aeration

Class	Model
Very Poor	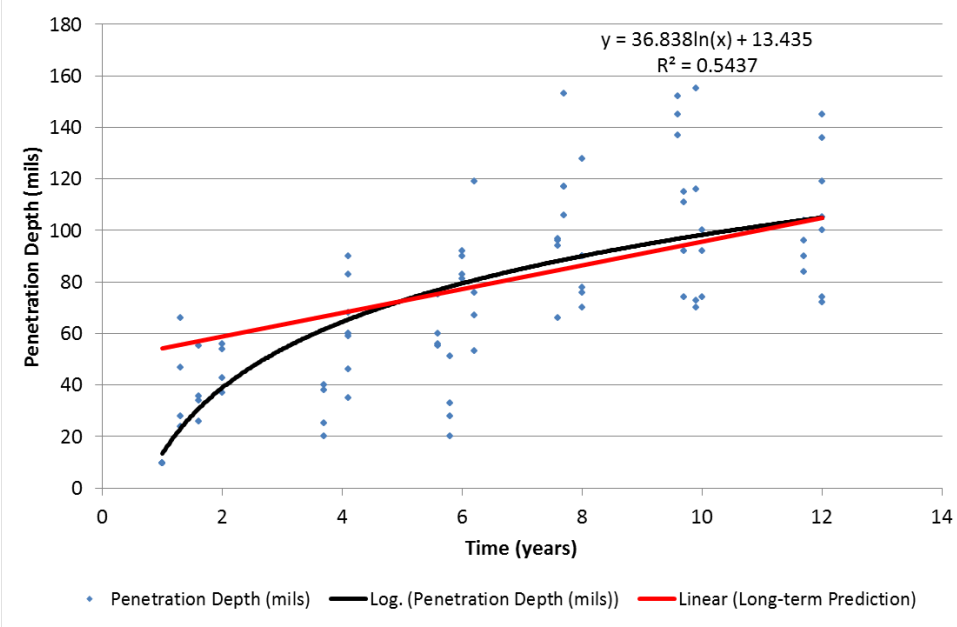
Poor	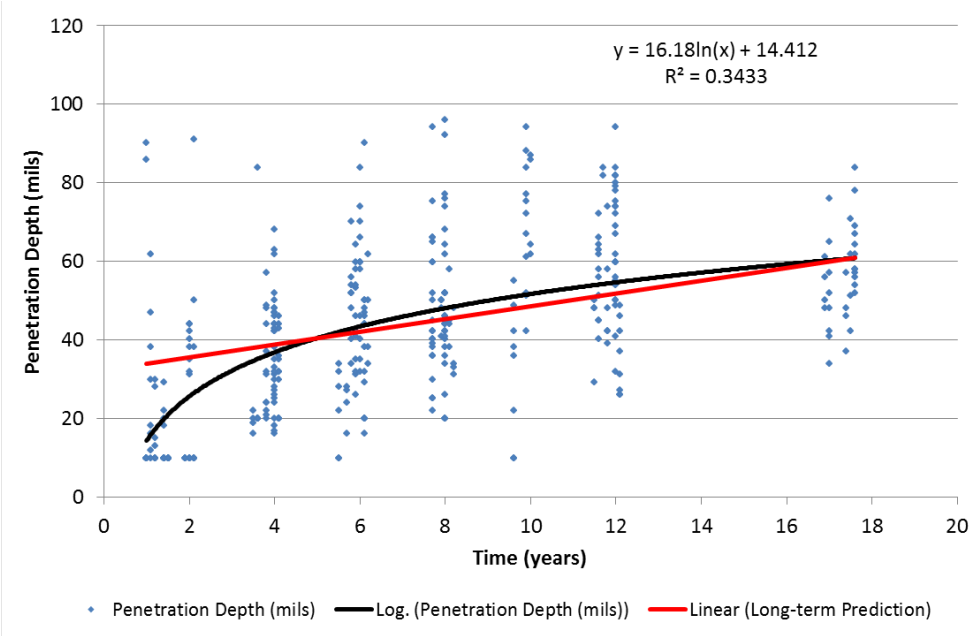

Class	Model
Good	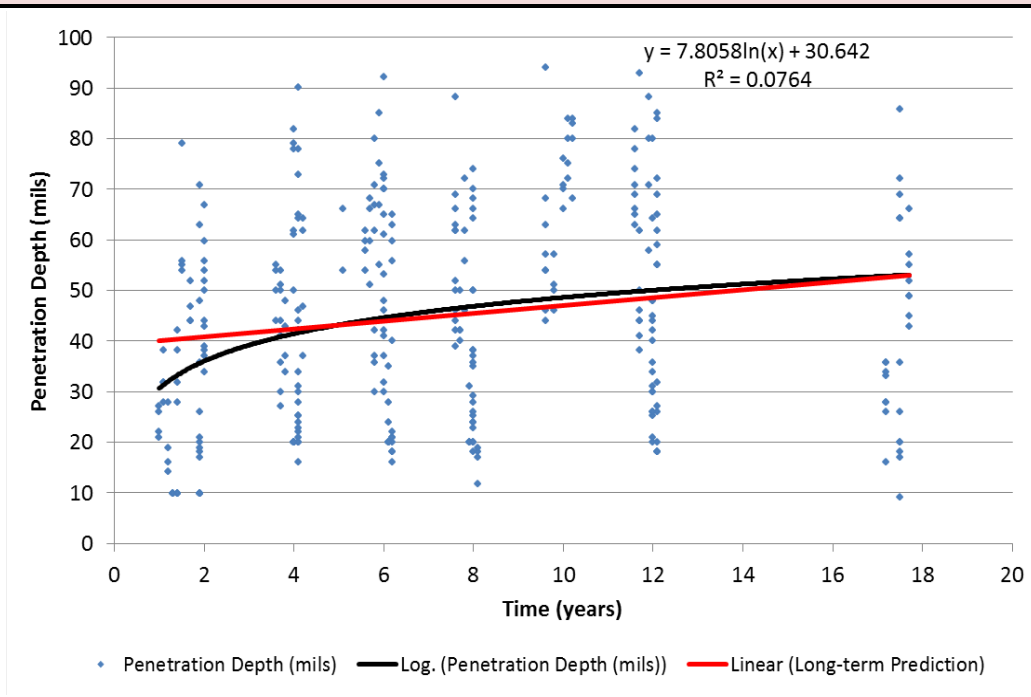
Fair	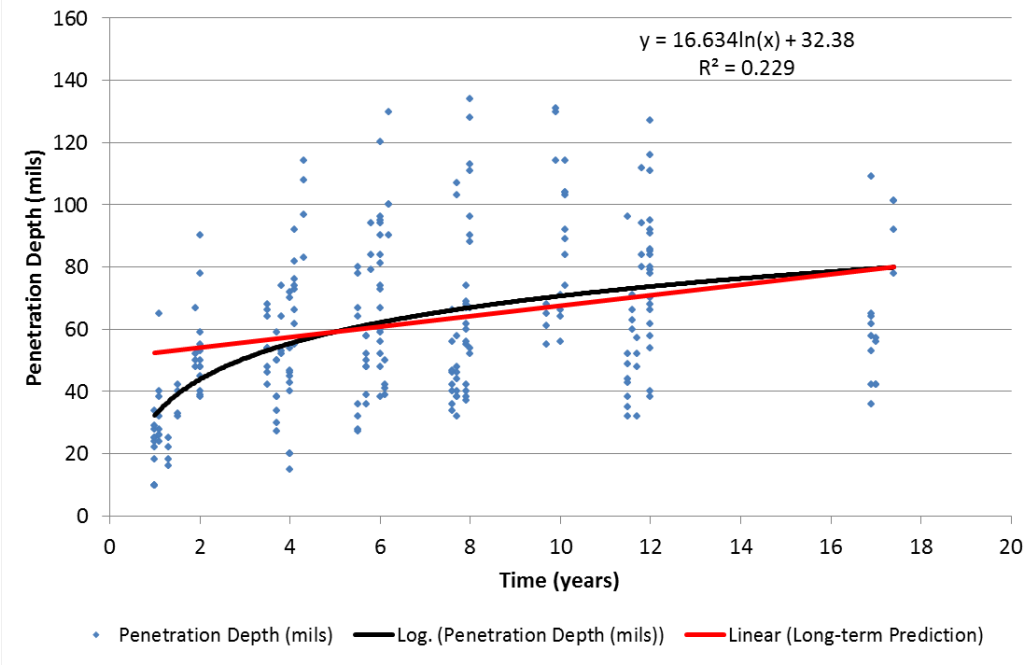

Table 34. Long-term Corrosion Rate Logarithmic Regression Models per Soil Chemical Groups

Class	Model
Inorganic Reducing Acid	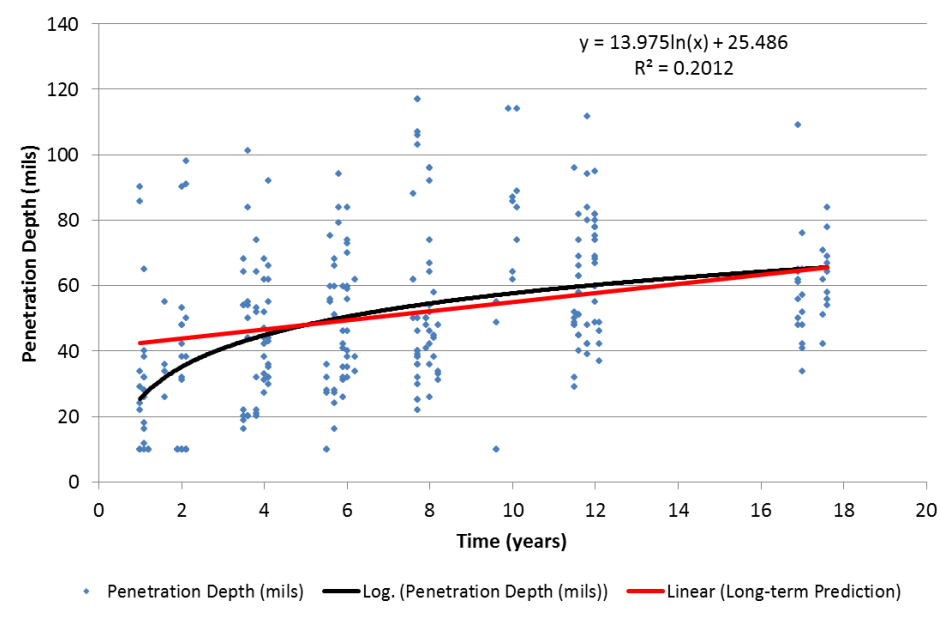
Inorganic Oxidizing Acid	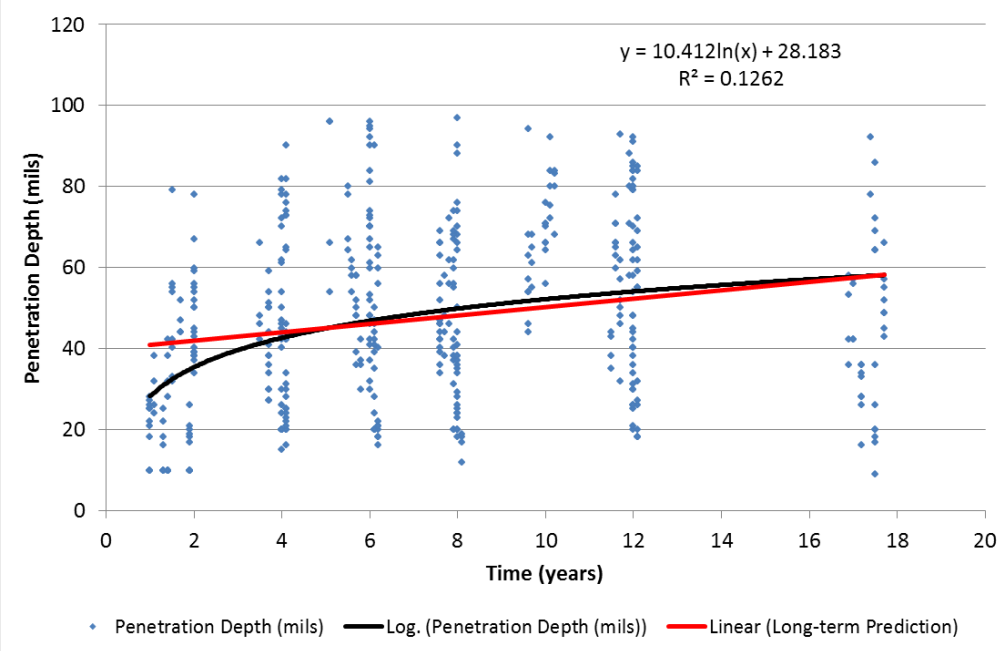

Class	Model
Inorganic Reducing Alkaline	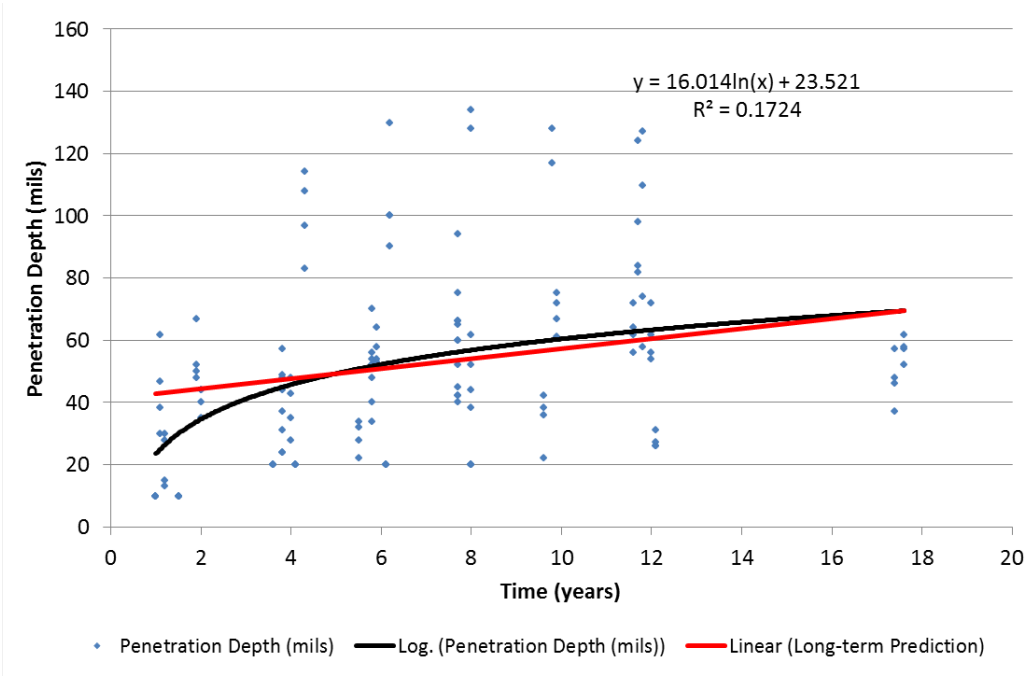
Inorganic Oxidizing Alkaline	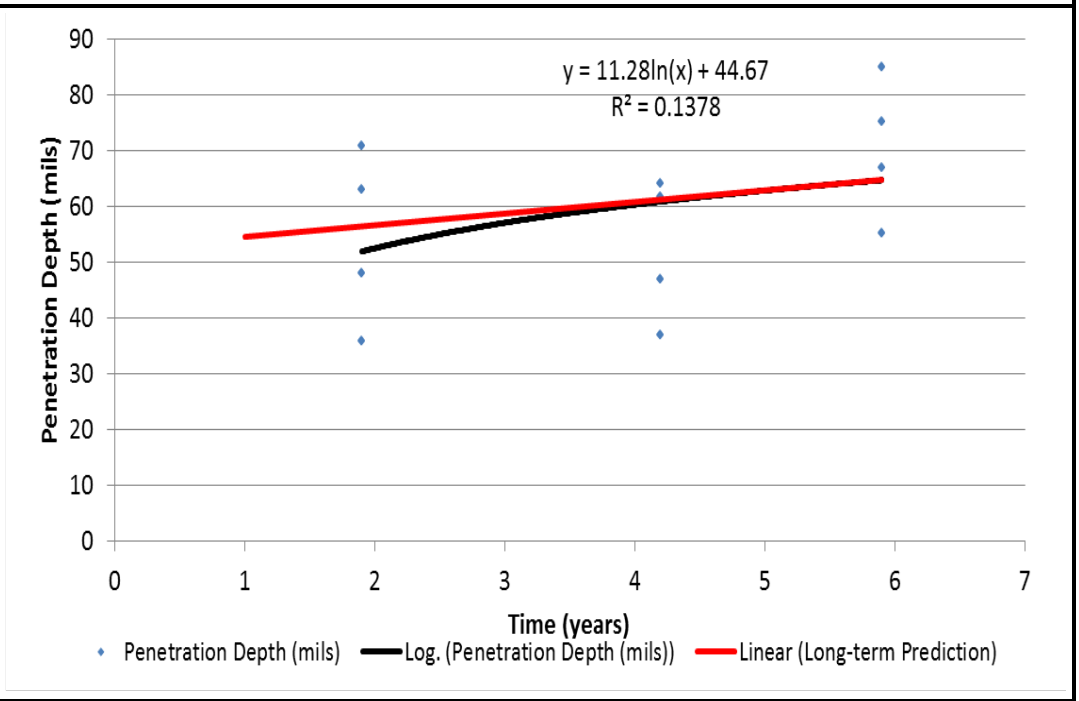

Class	Model
Organic Reducing Acid	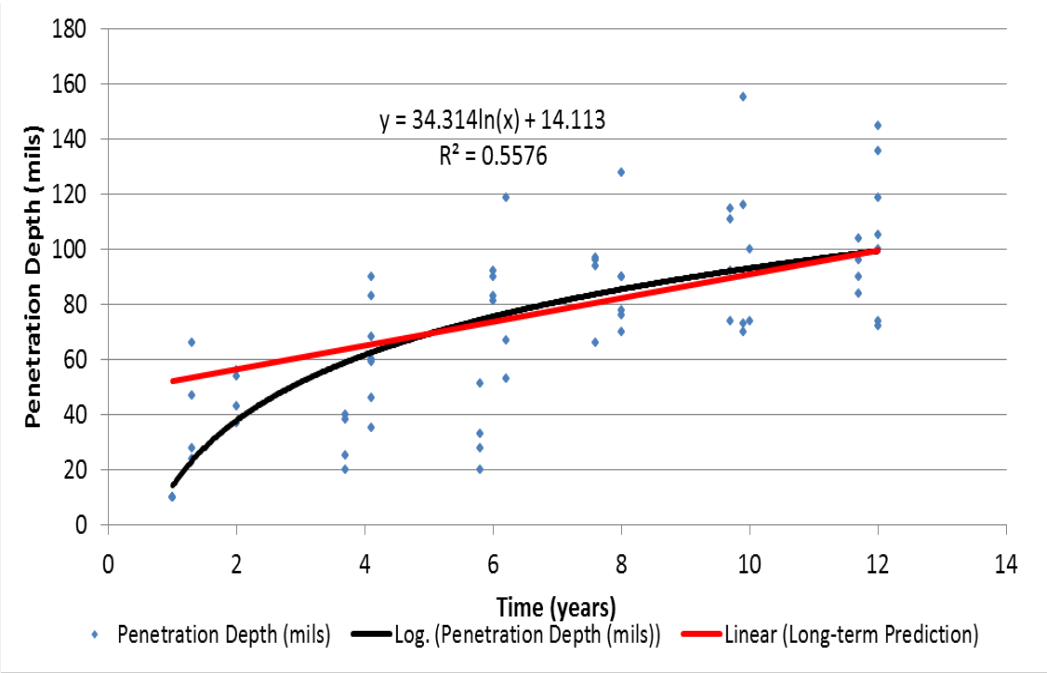

A.2.1.2. ***Multivariate Regression Models***

Despite the different types of regression that were used to correlate the penetration depth and the corrosion rate from one side and the soil characteristics from the other side, no clear correlation were found. After applying principal component analysis (PCA) and factor analysis (FA) on the NBS data, several methods were applied such as, the principal components regression, the correlated components regression, and nonparametric regression. However, these models didn't reach a high accuracy due to the sparsity of the data. Figure 59 and Table 35 below illustrate the correlation between the different variables.

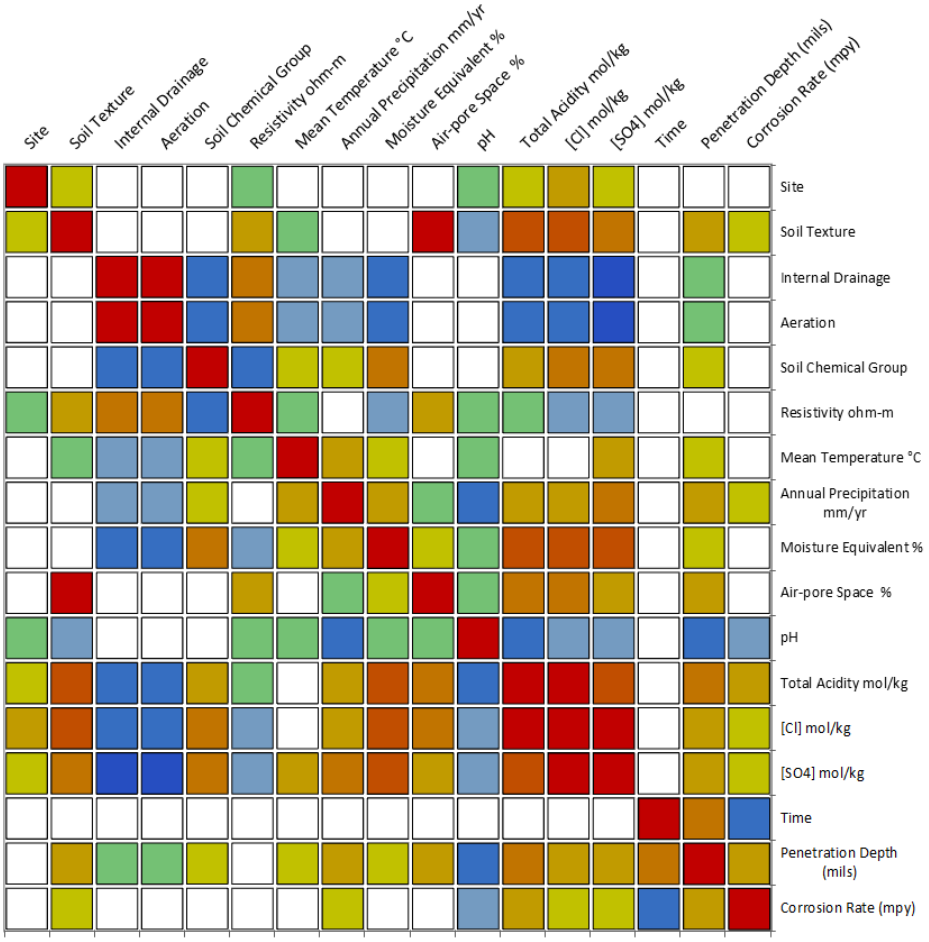

Figure 59. Correlation Map

Table 35. Multivariate Analysis Correlation Matrix

Variables	Soil Texture	Internal Drainage	Aeration	Soil Chemical Group	Resistivity ohm-m	Mean Temperature °C	Annual Precipitation mm/yr	Moisture Equivalent %	Air-pore Space %	pH	Total Acidity mol/kg	[Cl] mol/kg	[SO4] mol/kg	Time	Penetration Depth (mils)	Corrosion Rate (mpy)
Soil Texture	**1.00**	-0.08	0.02	0.03	**0.25**	**-0.19**	-0.07	**0.10**	**0.84**	**-0.28**	**0.64**	**0.68**	**0.49**	-0.04	**0.24**	**0.10**
Internal Drainage	-0.08	**1.00**	**0.93**	**-0.60**	**0.49**	**-0.30**	**-0.29**	**-0.57**	0.00	-0.03	**-0.46**	**-0.48**	**-0.60**	-0.03	**-0.15**	0.00
Aeration	0.02	**0.93**	**1.00**	**-0.57**	**0.52**	**-0.22**	**-0.39**	**-0.60**	**0.10**	0.06	**-0.50**	**-0.49**	**-0.62**	-0.01	**-0.15**	-0.02
Soil Chemical Group	0.03	**-0.60**	**-0.57**	**1.00**	**-0.45**	**0.10**	**0.14**	**0.52**	0.07	**0.10**	**0.33**	**0.49**	**0.51**	-0.04	**0.11**	0.02
Resistivity ohm-m	**0.25**	**0.49**	**0.52**	**-0.45**	**1.00**	**-0.19**	0.03	**-0.31**	**0.20**	**-0.16**	**-0.11**	**-0.22**	**-0.34**	-0.04	0.03	0.05
Mean Temperature °C	**-0.19**	**-0.30**	**-0.22**	**0.10**	**-0.19**	**1.00**	**0.39**	**0.11**	-0.04	**-0.18**	0.02	-0.02	**0.22**	0.09	**0.19**	-0.04
Annual Precipitation mm/yr	-0.07	**-0.29**	**-0.39**	**0.14**	0.03	**0.39**	**1.00**	**0.26**	**-0.10**	**-0.55**	**0.30**	**0.20**	**0.40**	-0.04	**0.38**	**0.19**
Moisture Equivalent %	**0.10**	**-0.57**	**-0.60**	**0.52**	**-0.31**	**0.11**	**0.26**	**1.00**	**0.12**	**-0.14**	**0.67**	**0.66**	**0.65**	-0.02	**0.20**	0.06
Air-pore Space %	**0.84**	0.00	**0.10**	0.07	**0.20**	-0.04	**-0.10**	**0.12**	**1.00**	**-0.12**	**0.50**	**0.59**	**0.37**	-0.01	**0.21**	0.03
pH	**-0.28**	-0.03	0.06	**0.10**	**-0.16**	**-0.18**	**-0.55**	**-0.14**	**-0.12**	**1.00**	**-0.55**	**-0.34**	**-0.36**	0.06	**-0.45**	**-0.27**
Total Acidity mol/kg	**0.64**	**-0.46**	**-0.50**	**0.33**	**-0.11**	0.02	**0.30**	**0.67**	**0.50**	**-0.55**	**1.00**	**0.91**	**0.79**	-0.06	**0.40**	**0.21**
[Cl] mol/kg	**0.68**	**-0.48**	**-0.49**	**0.49**	**-0.22**	-0.02	**0.20**	**0.66**	**0.59**	**-0.34**	**0.91**	**1.00**	**0.83**	-0.06	**0.33**	**0.14**
[SO4] mol/kg	**0.49**	**-0.60**	**-0.62**	**0.51**	**-0.34**	**0.22**	**0.40**	**0.65**	**0.37**	**-0.36**	**0.79**	**0.83**	**1.00**	-0.03	**0.33**	**0.14**
Time	-0.04	-0.03	-0.01	-0.04	-0.04	0.09	-0.04	-0.02	-0.01	0.06	-0.06	-0.06	-0.03	**1.00**	**0.42**	**-0.49**
Penetration Depth (mils)	**0.24**	**-0.15**	**-0.15**	**0.11**	0.03	**0.19**	**0.38**	**0.20**	**0.21**	**-0.45**	**0.40**	**0.33**	**0.33**	**0.42**	**1.00**	**0.22**
Corrosion Rate (mpy)	**0.10**	0.00	-0.02	0.02	0.05	-0.04	**0.19**	0.06	0.03	**-0.27**	**0.21**	**0.14**	**0.14**	**-0.49**	**0.22**	**1.00**

Values in bold are different from 0 with a significance level alpha=0.05

A.2.2. Penetration Depth Assessment

A stochastic cumulative analysis illustrates the random changes in variables with certain probabilities. Based on a set of random values, a stochastic model simulates the

distribution of the data based on a degradation analysis that involves measurements for multiple samples at different points in time. The sum of the random degradation increments after k intervals, X_k, is equivalent to the overall degradation at time t, Y(t):

$$Y(t) = X_1 + X_2 + \ldots + X_n$$

In order to represent the variability in the measurement at a given time, this approach presumes the degradation value to be a random variable that follows a certain distribution at a given time. The Weibull distribution, one of the most widely used lifetime distributions in reliability engineering, is considered to model the corrosion degradation in this sutdy. Afterward, the scale parameter (η) will decrease with time as the post corrodes over time and the shape parameter (β) will stay constant since the process of corroding will not change. Based on Romanoff's study model, the degradation of the posts over time is assumed to be logarithmic, such that:

$$\ln(\eta(t)) = a.\ln(t) + b$$

After defining the Weibull distribution parameters (a, b and β) using maximum likelihood estimation (MLE), a critical level of the corrosion penetration depth is considered to be the 50% of the web thickness design value. While the three main types of beams used in *First Solar* sites are W6X7, W6X9, and W6X12, the critical depth are 64.5, 85, and 115 mils respectively. Hence, the reliability at time t, R(t), can be derived as:

$$R(t) = 1 - F(t) = P(D_t < D_{cri}) = e^{-\left(\frac{D_{cri}}{\eta(t)}\right)^{\beta}}$$

Where:

- D_t is the random penetration depth value at time t

- D_{cri} is the critical penetration depth value:
    - 64.5 mils for W6X7 beam
    - 85 mils for W6X9 beam
    - 115 mils for W6X12 beam
- β is the shape parameter for the Weibull distribution
- $\eta(t)$ is the scale parameter at time t

At a confidence level of 90%, the distribution models for the penetration depth over time were established for the carbon steel collected data. The following figures illustrate the relationship between the distribution of the penetration depth measurement and the distribution of failure times for W6X7, W6X9, and W6X12 beams. Moreover, the reliability plots show the probability of having an acceptable penetration depth (less than the critical value) at different times of inspection. After 25 years of posts installation, the probabilities of not exceeding the critical penetration depth were found to be 0.444, 0.663, and 0.881 for W6X7, W6X9, and W6X12 respectively. An analysis of the corrosion data based on soil texture, internal drainage, aeration, and chemical groups, is presented for the three different types of beams in tables 36 through 40.

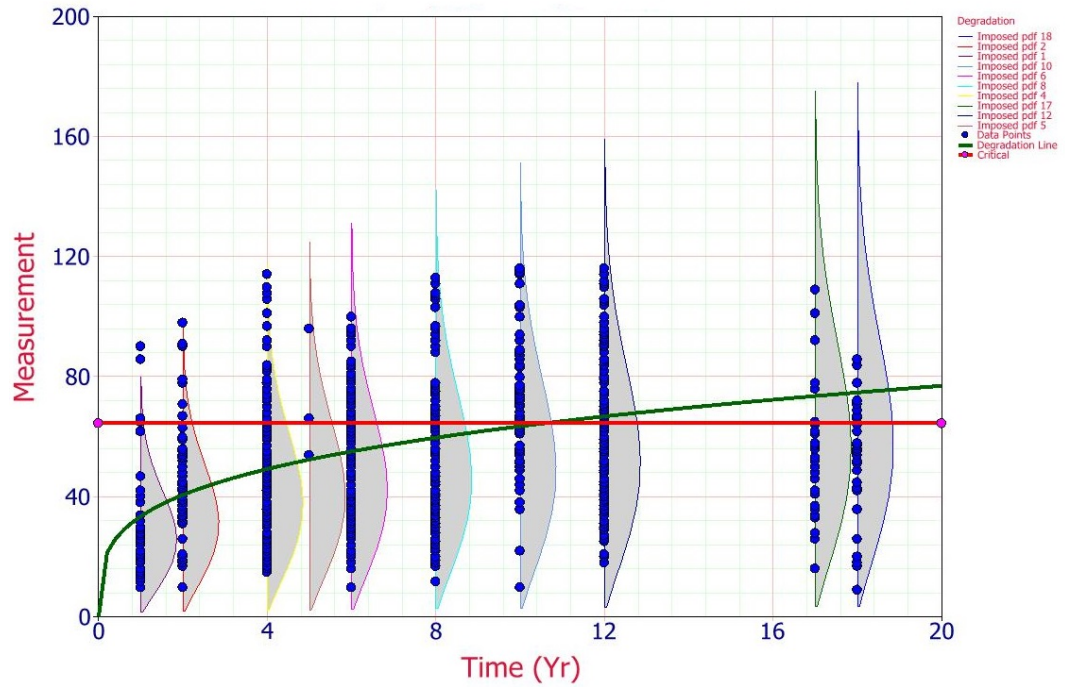

Figure 60. Penetration Depth (mils) Distribution Model versus Time (Years) for W6X7 Beam

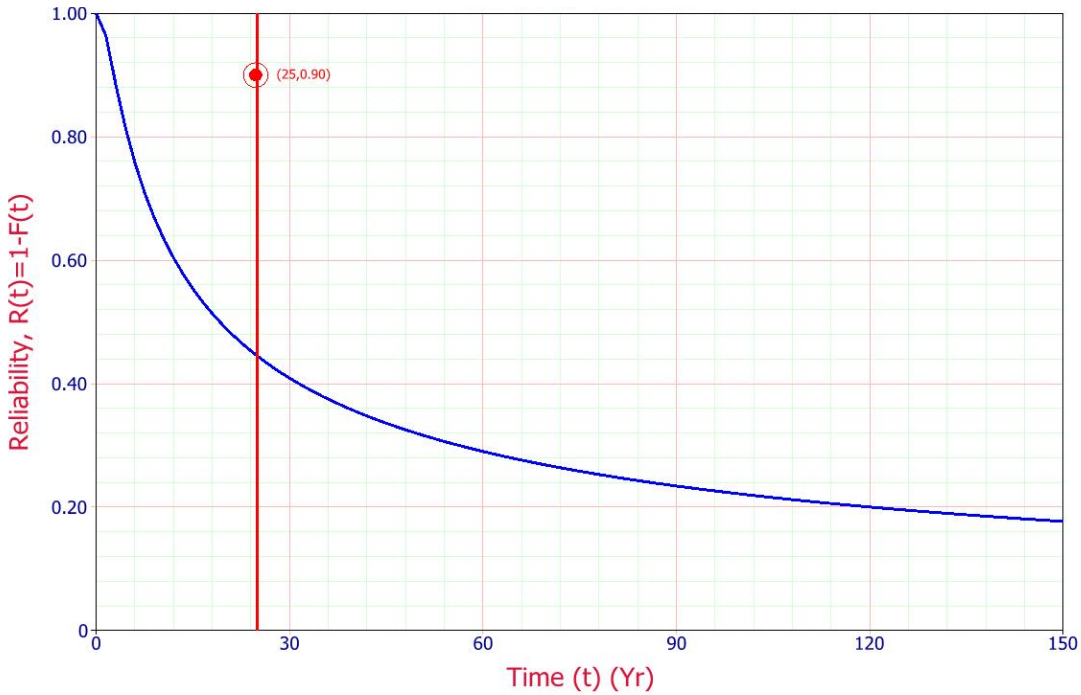

Figure 61. Reliability versus Time (Years) for W6X7 Beam

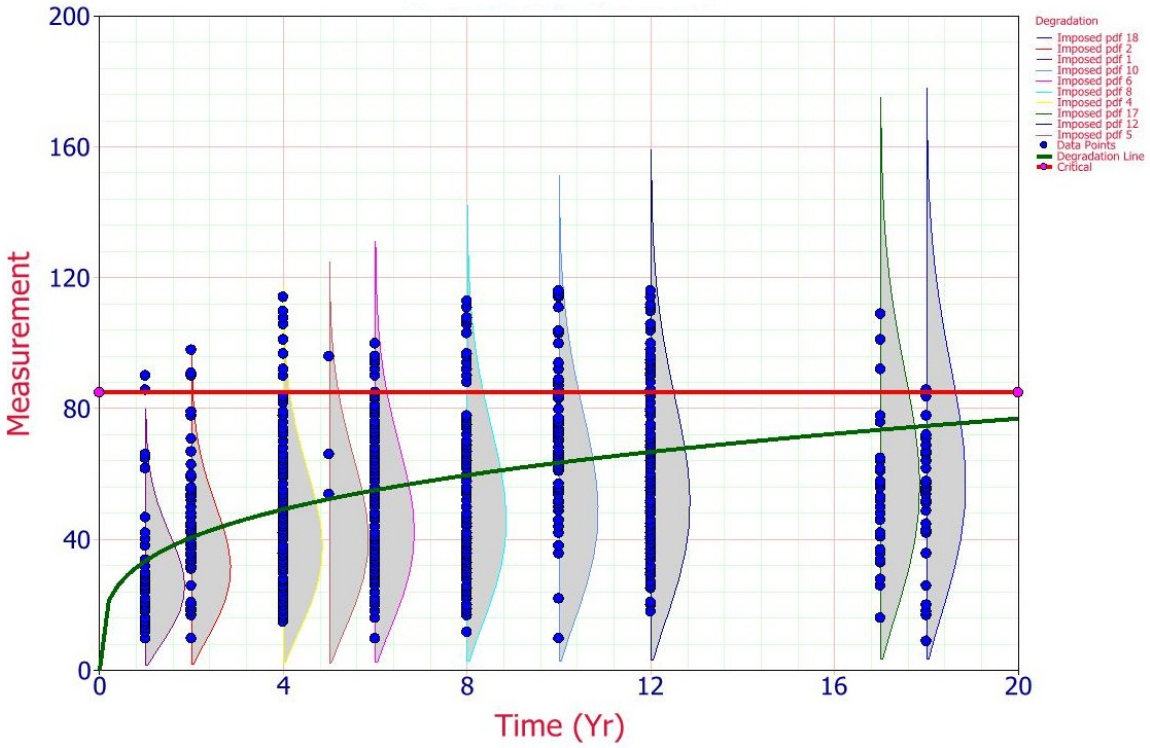

Figure 62. Penetration Depth (mils) Distribution Model versus Time (Years) for W6X9 Beam

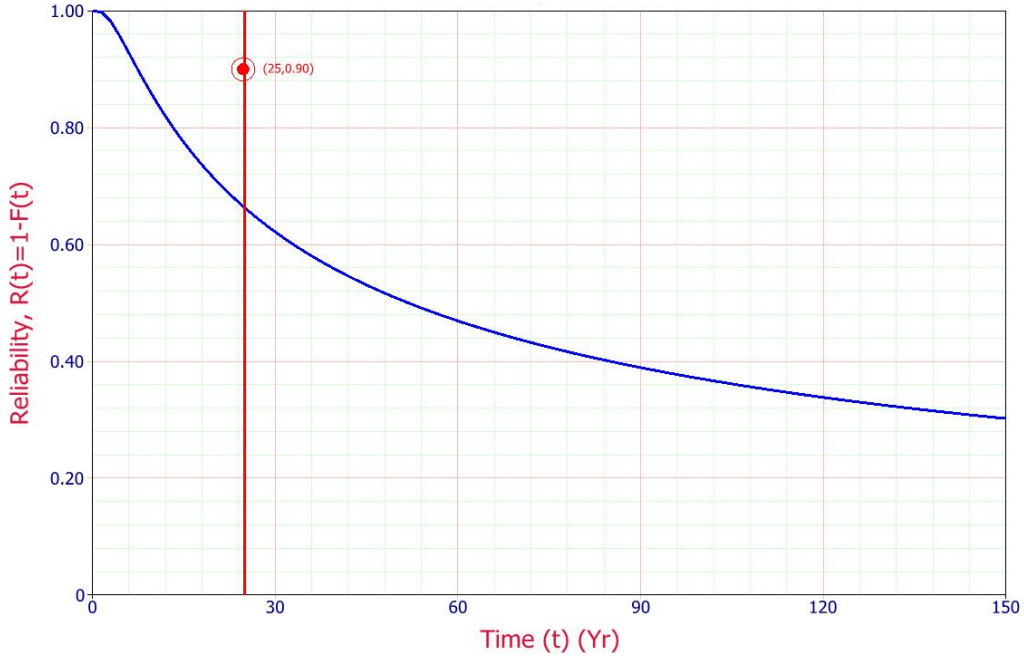

Figure 63. Reliability versus Time (Years) for W6X9 Beam

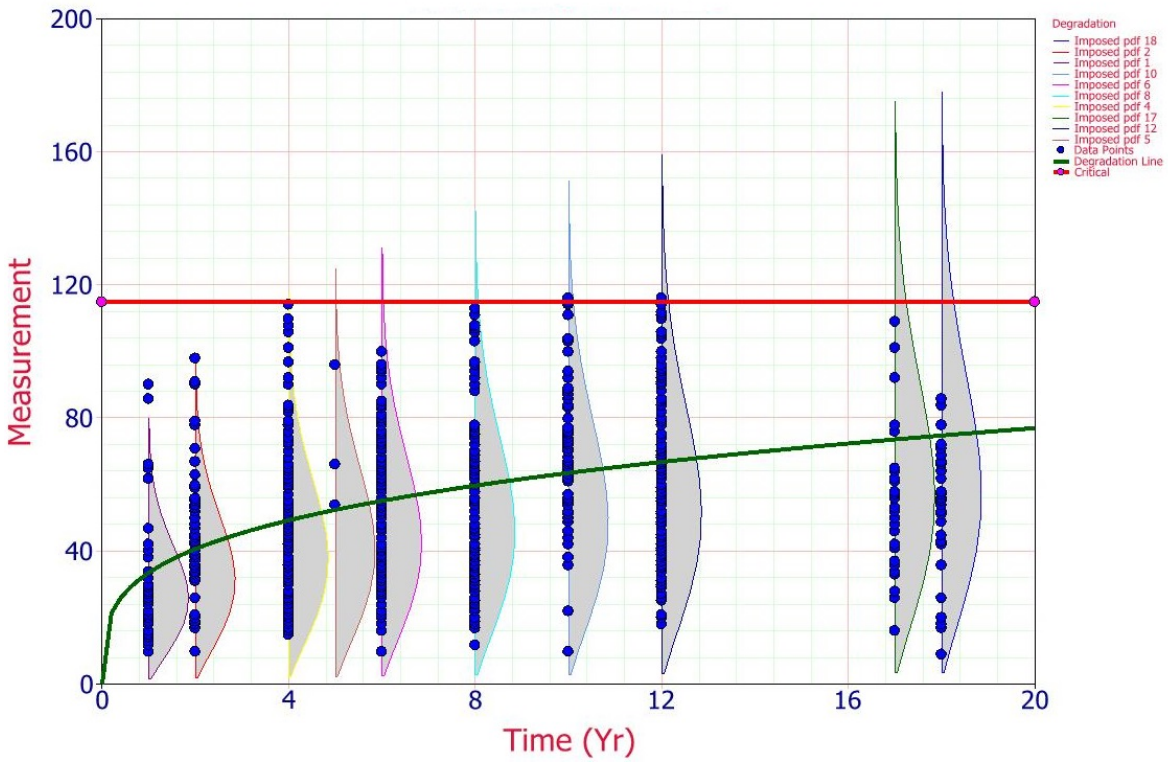

Figure 64. Penetration Depth (mils) Distribution Model versus Time (Years) for W6X12 Beam

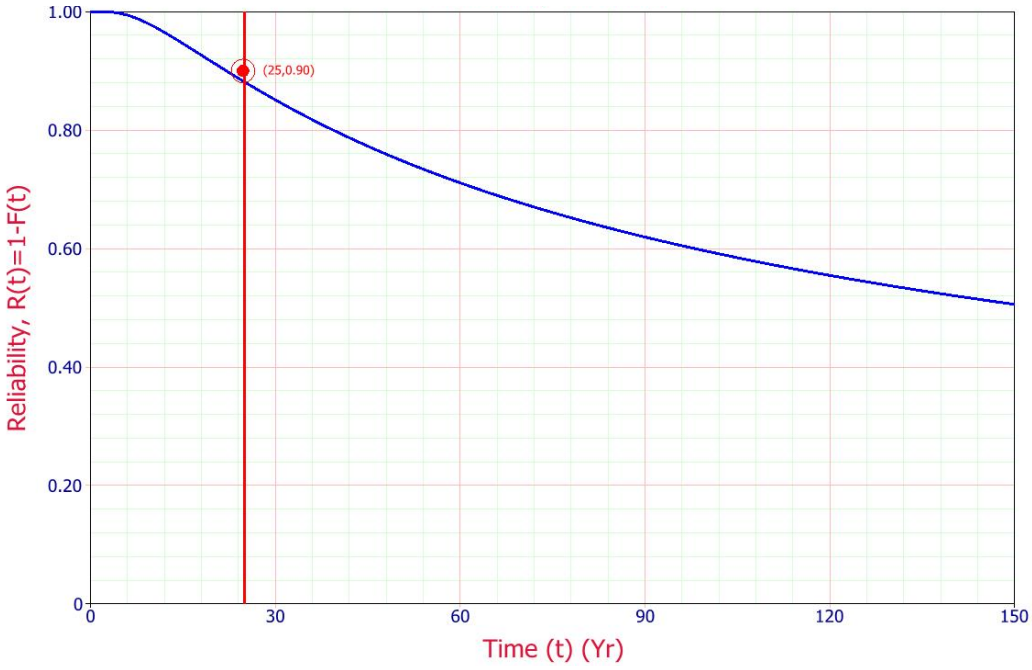

Figure 65. Reliability versus Time (Years) for W6X12 Beam

Table 36. Penetration Depth Assessment Results

Level	Class	Weibull Distribution Parameters			Beam type	Reliable Life t (R) in years			Reliability at t=25 years
		β	a	b		R=0.90	R=0.80	R=0.50	
Soil Texture	Clay	2.595	0.360	3.445	W6X7	3.042	4.464	10.998	0.275
					W6X9	6.550	9.610	23.677	0.483
					W6X12	15.169	22.256	54.831	0.764
	Loam/ Clay Loam	2.522	0.275	3.464	W6X7	3.866	6.474	21.767	0.467
					W6X9	10.532	17.635	59.292	0.717
					W6X12	31.560	52.848	177.680	0.933
	Silt Loam	2.169	0.251	3.534	W6X7	2.683	5.176	24.279	0.494
					W6X9	8.048	15.526	72.827	0.711
					W6X12	26.804	51.710	242.550	0.909
	Sandy Loam	1.961	0.194	3.480	W6X7	3.843	9.838	89.768	0.676
					W6X9	15.909	40.727	371.628	0.856
					W6X12	75.406	193.042	1761.481	0.970
	Other	2.659	0.377	3.584	W6X7	2.044	2.922	6.777	0.171
					W6X9	4.252	6.081	14.103	0.323
					W6X12	9.488	13.568	31.466	0.582
Internal Drainage	Very Poor	2.940	0.442	3.573	W6X7	2.019	2.660	5.087	0.084
					W6X9	3.771	4.967	9.501	0.179
					W6X12	7.474	9.847	18.831	0.381
	Poor	2.174	0.226	3.585	W6X7	2.399	4.972	27.615	0.517
					W6X9	8.133	16.859	93.641	0.734
					W6X12	30.981	64.221	356.703	0.922
	Good	2.435	0.206	3.532	W6X7	4.129	8.436	45.277	0.607
					W6X9	15.781	32.238	173.022	0.840
					W6X12	68.521	139.981	751.271	0.978
	Fair	2.280	0.383	3.367	W6X7	3.100	4.670	12.239	0.310
					W6X9	6.368	9.592	25.137	0.502
					W6X12	14.007	21.098	55.293	0.750
Aeration	Very Poor	2.912	0.492	3.522	W6X7	2.071	2.659	4.789	0.063
					W6X9	3.631	4.662	8.396	0.135
					W6X12	6.714	8.621	15.525	0.296
	Poor	2.164	0.298	3.304	W6X7	4.943	8.609	31.748	0.555
					W6X9	12.469	21.716	80.083	0.770
					W6X12	34.352	59.828	220.624	0.941
	Good	2.338	0.196	3.559	W6X7	3.597	7.852	49.265	0.612
					W6X9	14.687	32.063	201.153	0.835
					W6X12	68.570	149.693	939.135	0.974
	Fair	2.677	0.315	3.656	W6X7	1.881	2.876	7.813	0.228
					W6X9	4.519	6.911	18.770	0.420
					W6X12	11.801	18.048	49.018	0.706

Level	Class	Weibull Distribution Parameters			Beam type	Reliable Life t (R) in years			Reliability at t=25 years
		β	a	b		R=0.90	R=0.80	R=0.50	
Chemical Groups	Inorganic Oxidizing Acid	2.362	0.250	3.503	W6X7	3.469	6.366	26.543	0.512
					W6X9	10.474	19.221	80.143	0.748
					W6X12	35.138	64.478	268.843	0.940
	Inorganic Oxidizing Alkaline	5.140	0.168	3.945	W6X7	1.425	2.157	5.716	0.176
					W6X9	7.356	11.133	29.507	0.550
					W6X12	44.401	67.199	178.100	0.977
	Inorganic Reducing Acid	2.158	0.227	3.604	W6X7	2.173	4.510	25.121	0.501
					W6X9	7.319	15.189	84.602	0.716
					W6X12	27.671	57.429	319.868	0.911
	Inorganic Reducing Alkaline	1.937	0.322	3.466	W6X7	2.310	4.101	15.803	0.406
					W6X9	5.439	9.651	37.195	0.589
					W6X12	13.890	24.648	94.987	0.797
	Organic Reducing Acid	2.940	0.442	3.573	W6X7	2.019	2.659	5.087	0.083
					W6X9	3.771	4.967	9.501	0.178
					W6X12	7.473	9.846	18.831	0.381
All Data		2.224	0.278	3.511	W6X7	2.745	4.904	19.190	0.444
					W6X9	7.421	13.255	51.867	0.663
					W6X12	22.051	39.386	154.120	0.881

Table 37. Stochastic Models per Soil Texture

Clay	W 6X7	
	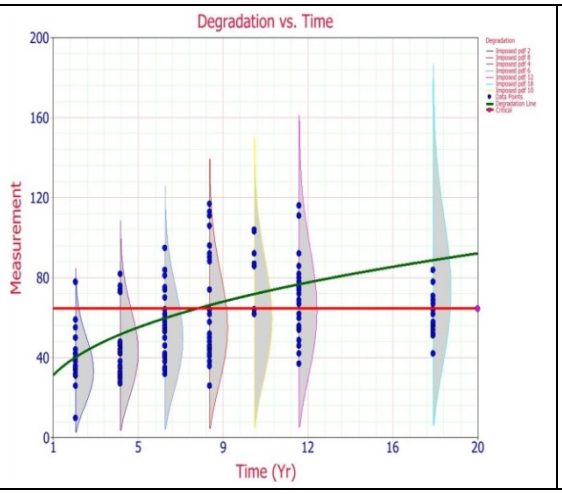	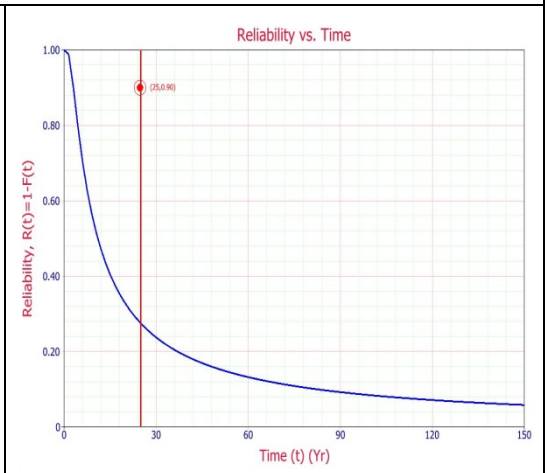
Clay	W 6X9	
	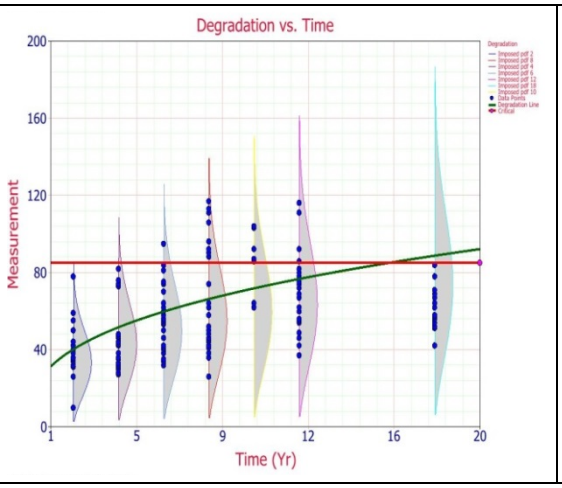	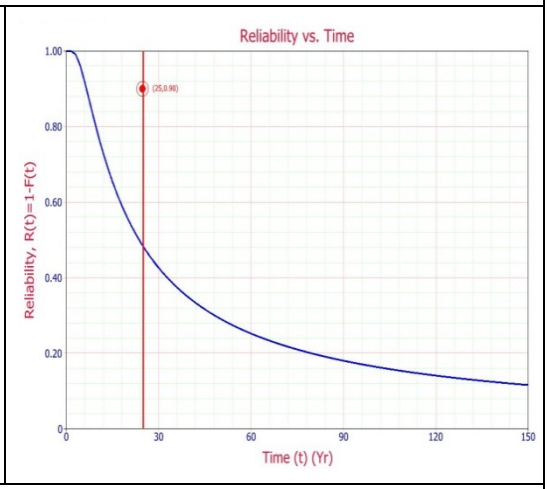
Clay	W 6X12	
	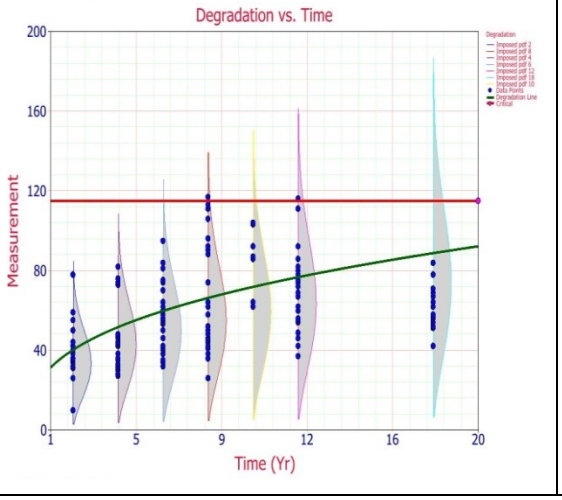	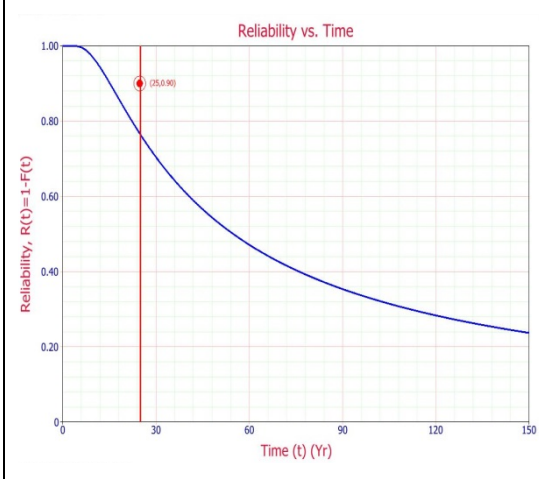

Loam/ Clay Loam	W 6X7	
	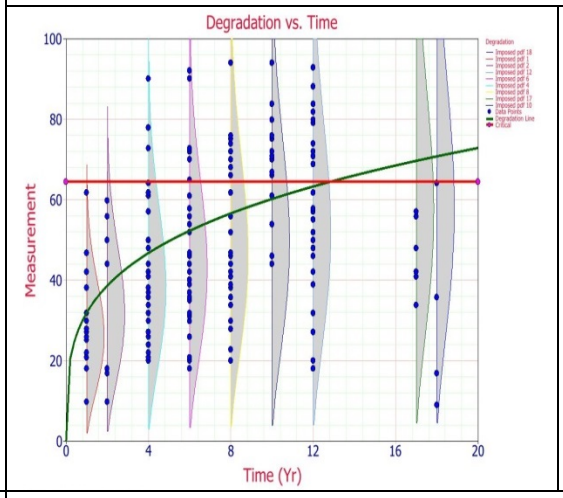	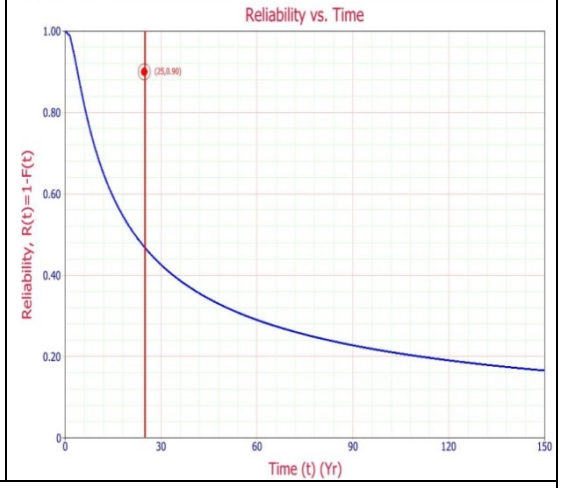
Loam/ Clay Loam	W 6X9	
	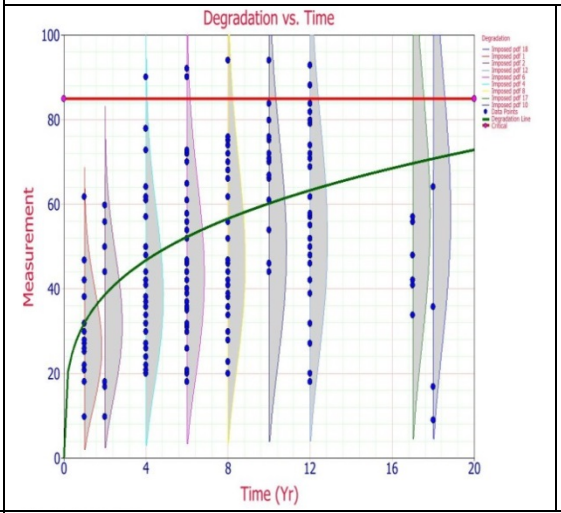	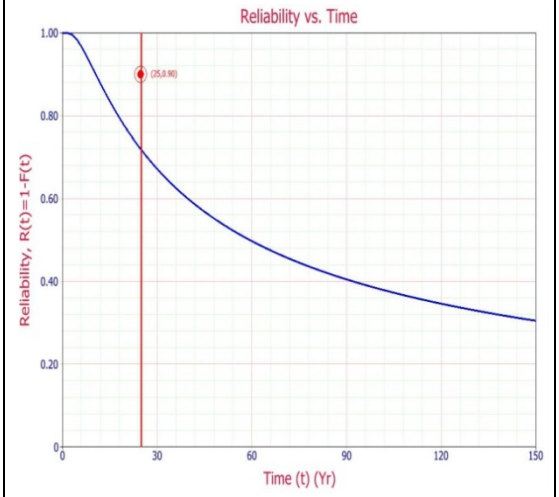
Loam/ Clay Loam	W 6X12	
	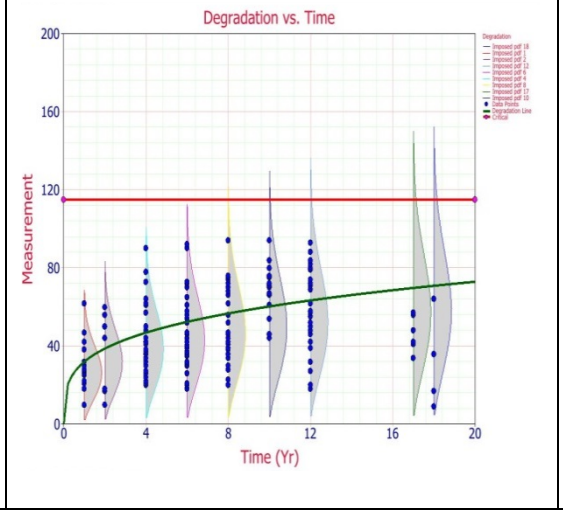	

Other	W 6X7	
	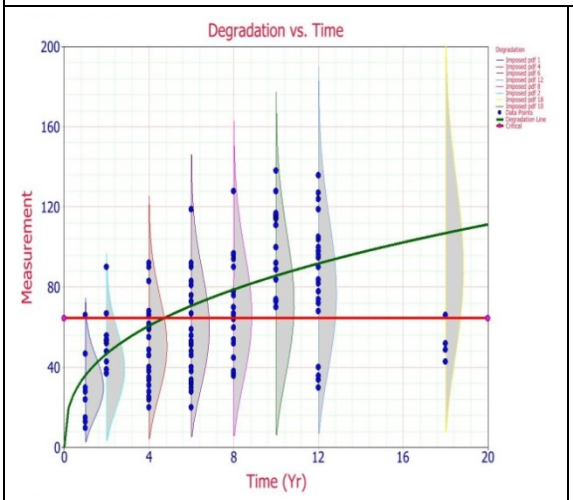	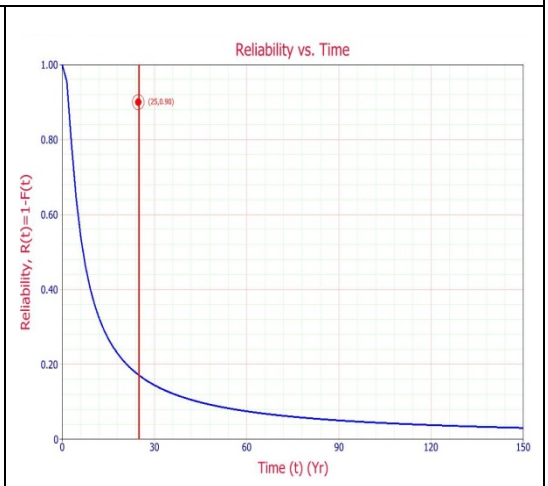
Other	W 6X9	
	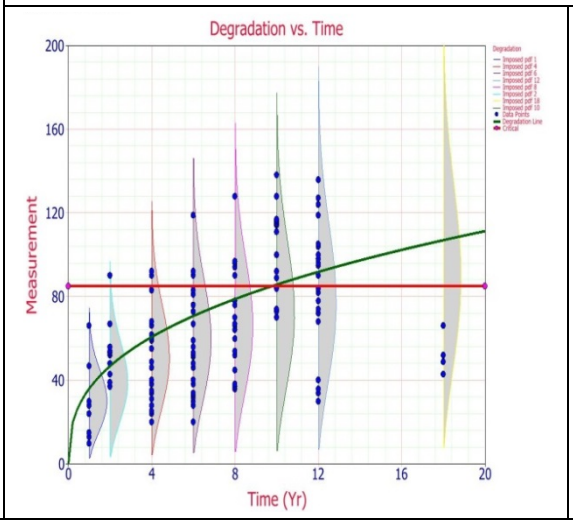	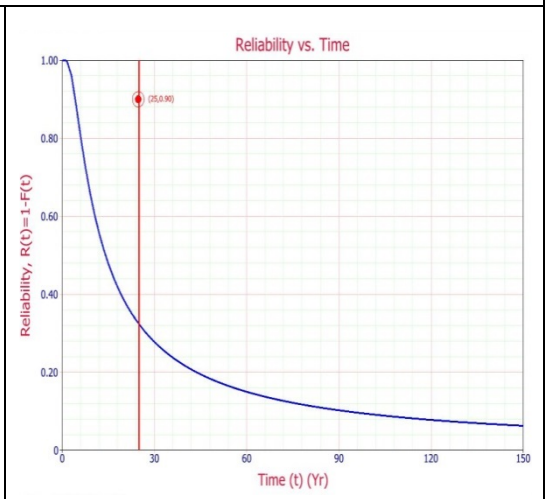
Other	W 6X12	
	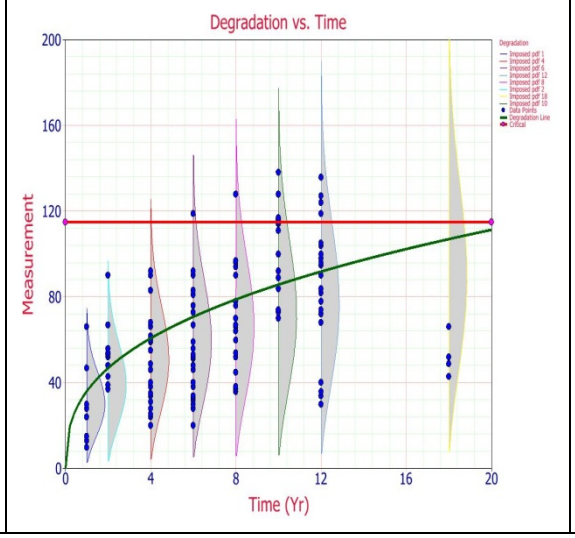	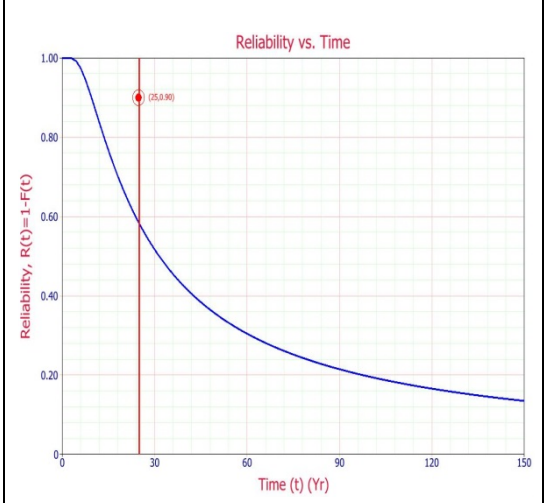

Sandy Loam	W 6X7	
	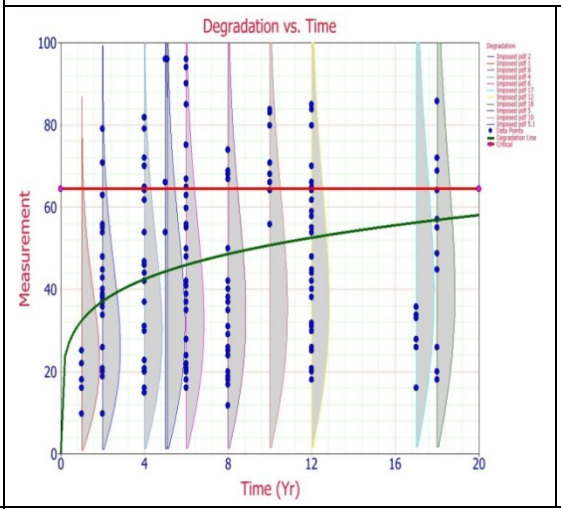	
Sandy Loam	W 6X9	
	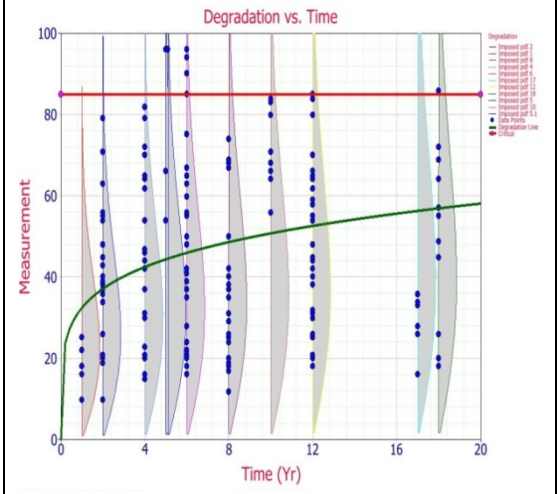	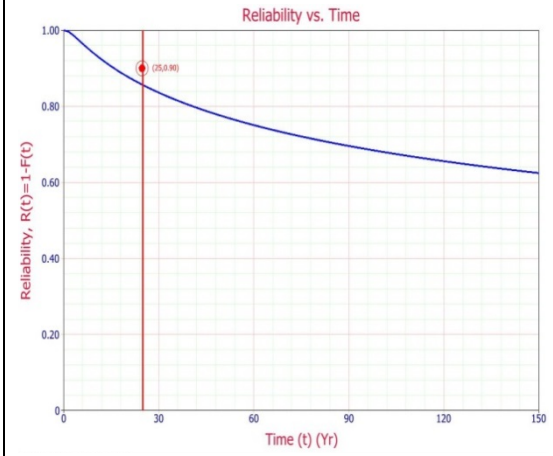
Sandy Loam	W 6X12	
	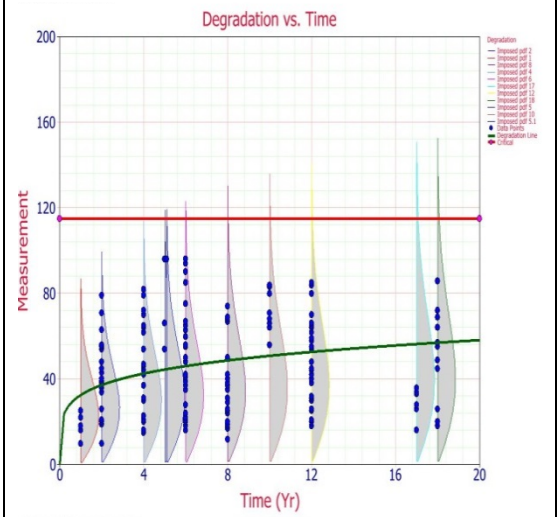	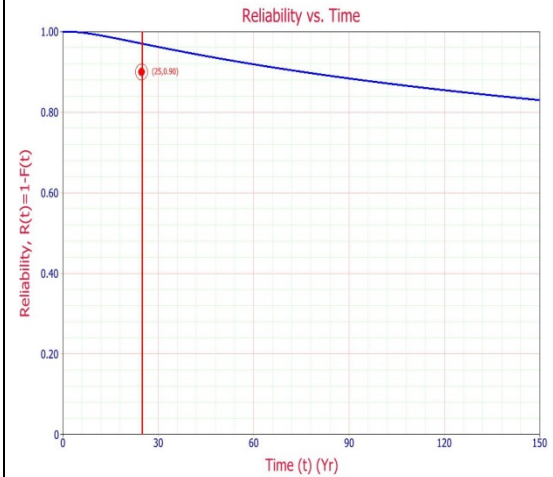

Silt Loam	W 6X7	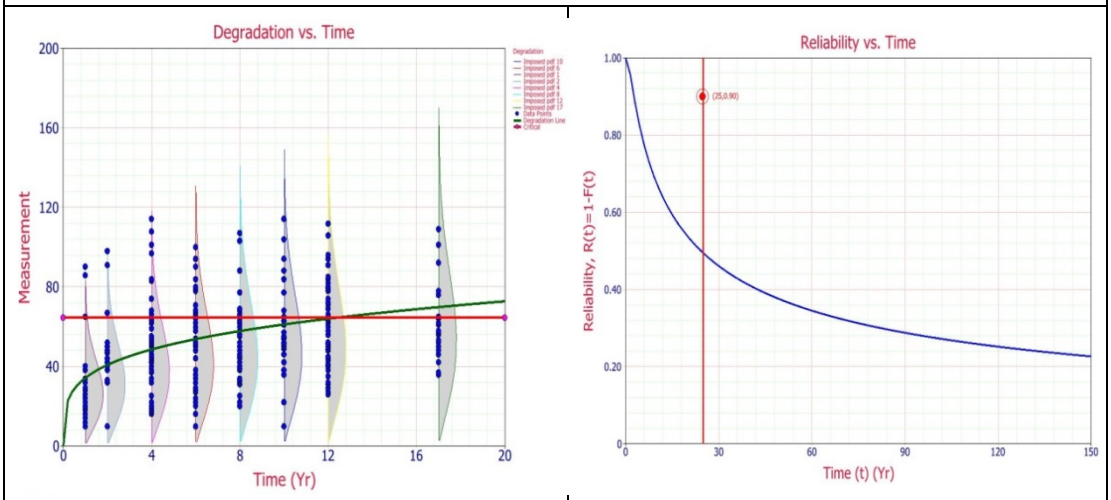
Silt Loam	W 6X9	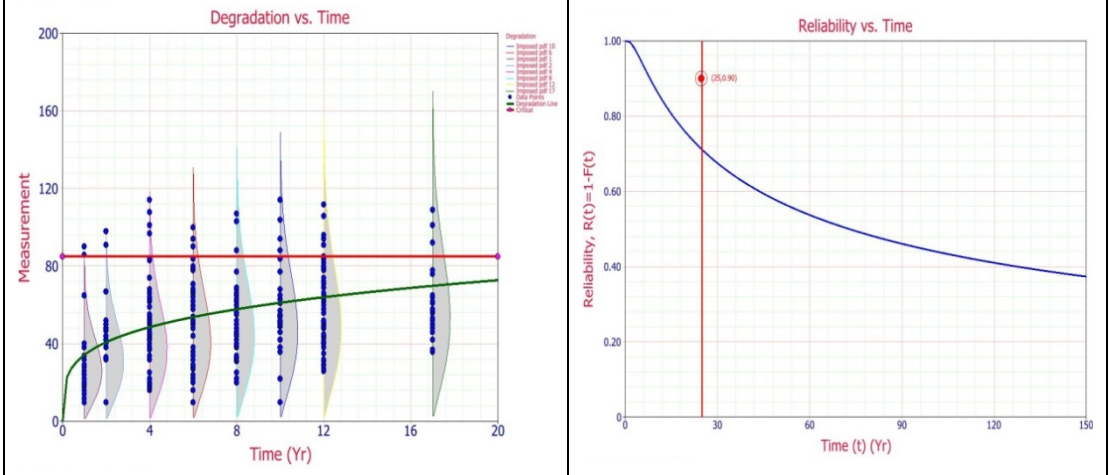
Silt Loam	W 6X12	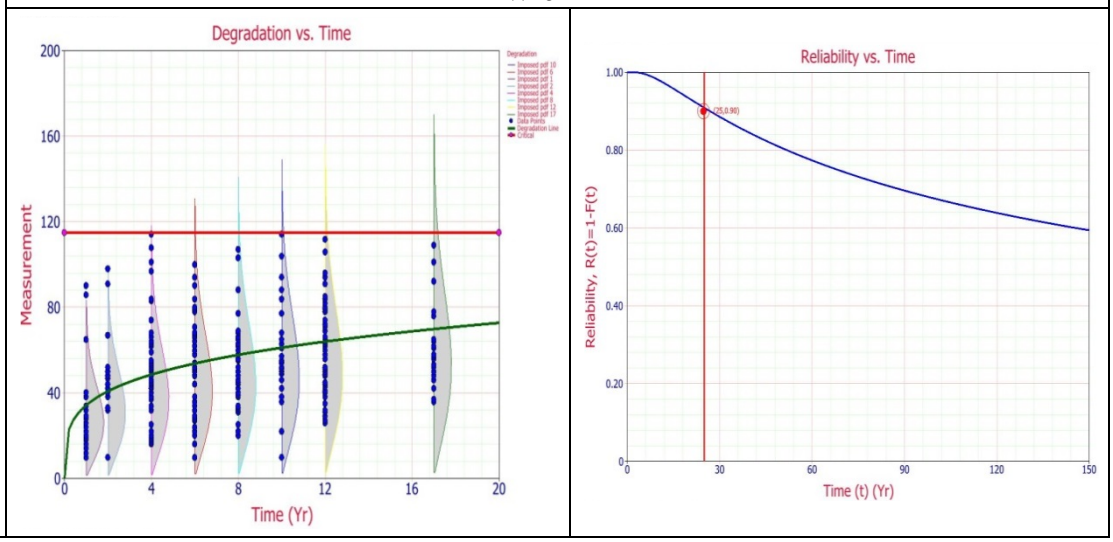

Table 38. Stochastic Models per Soil Internal Drainage

Very Poor	W 6X7	
	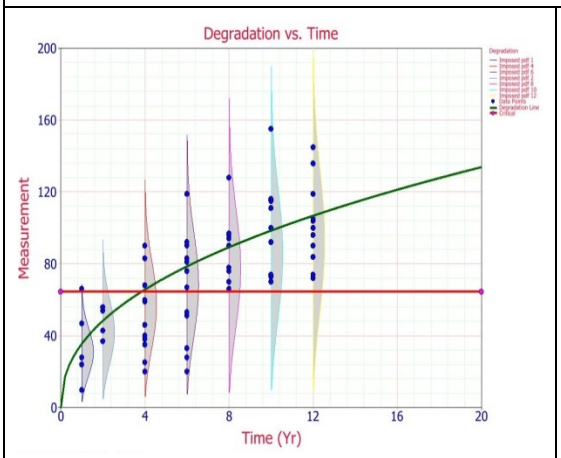	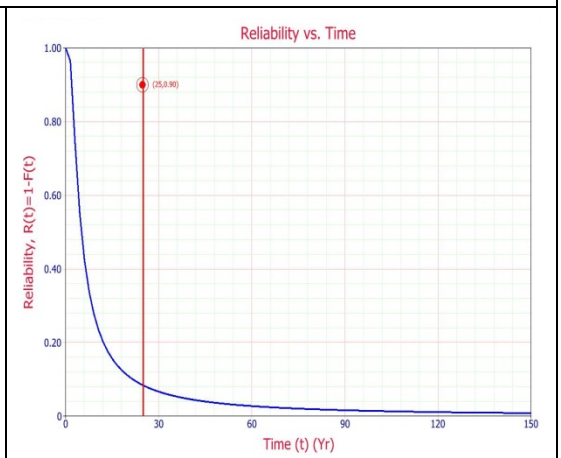
Very Poor	W 6X9	
	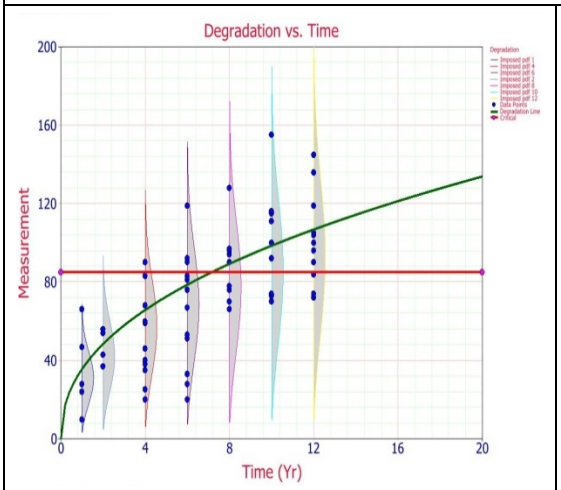	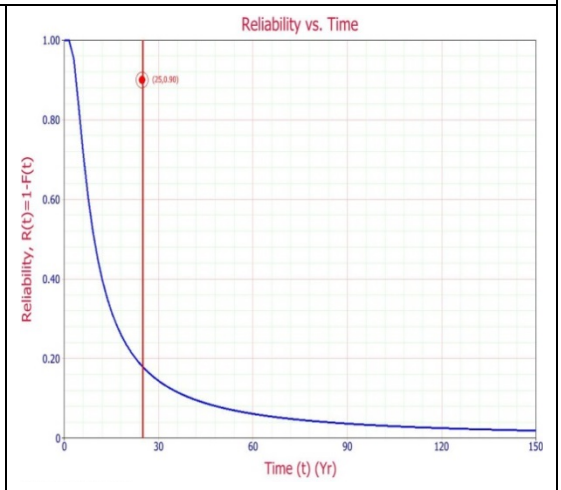
Very Poor	W 6X12	
	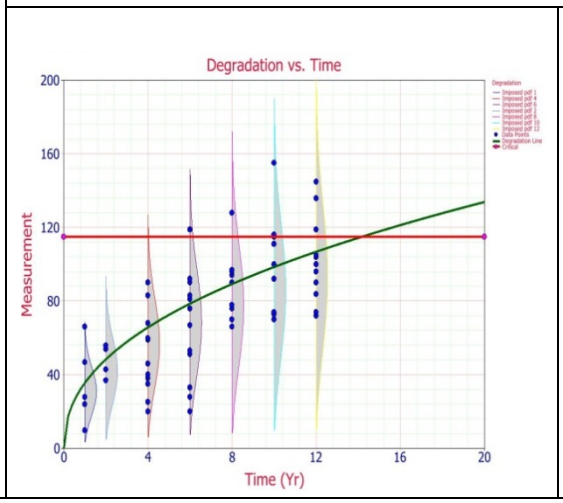	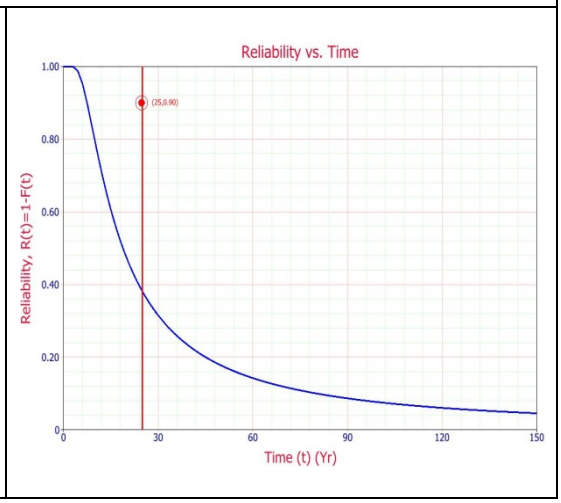

Poor	W 6X7	
	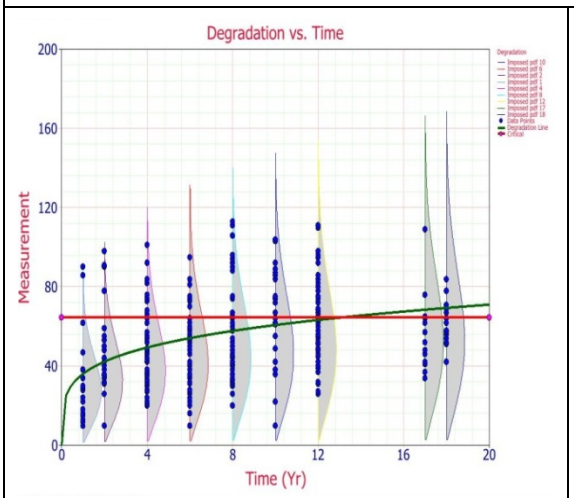	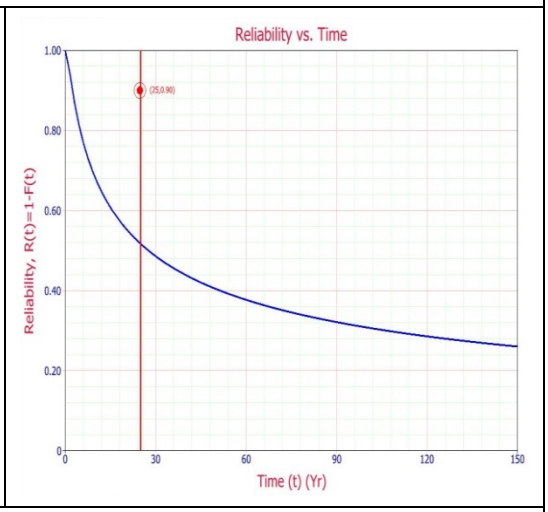
Poor	W 6X9	
	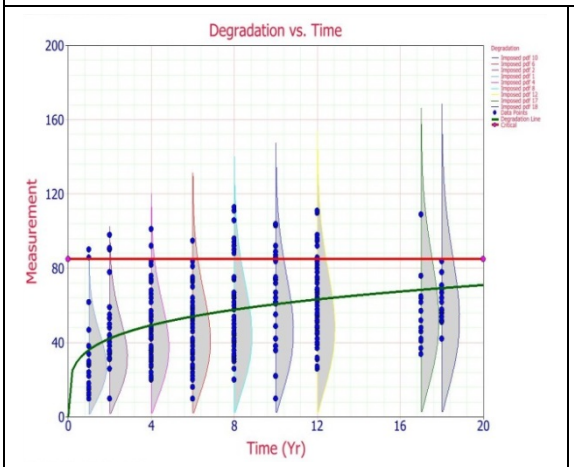	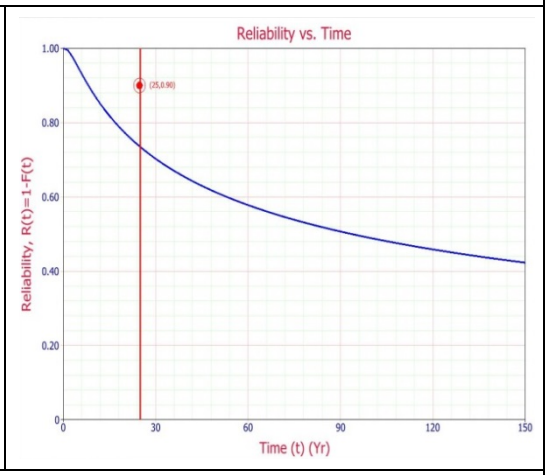
Poor	W 6X12	
	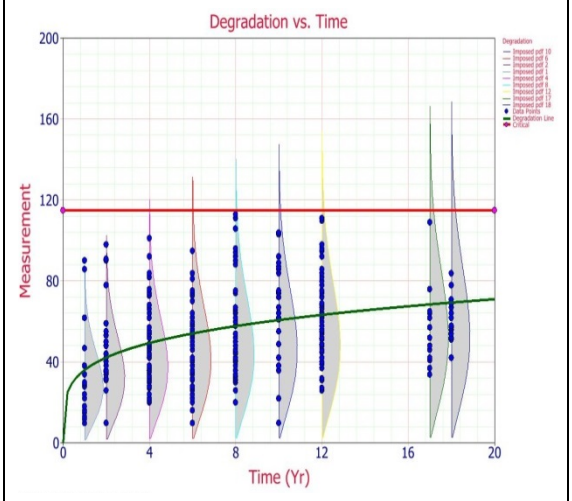	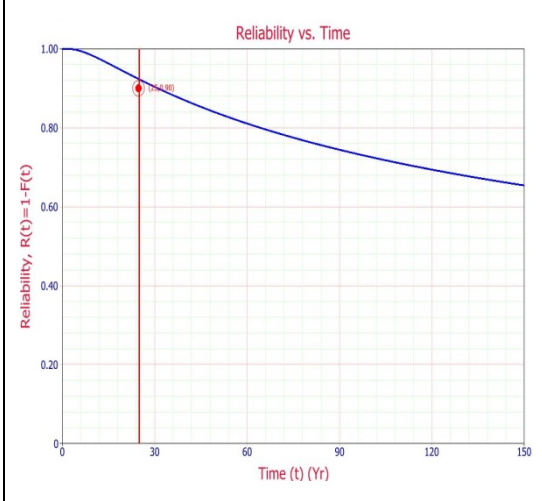

Good	W 6X7	
	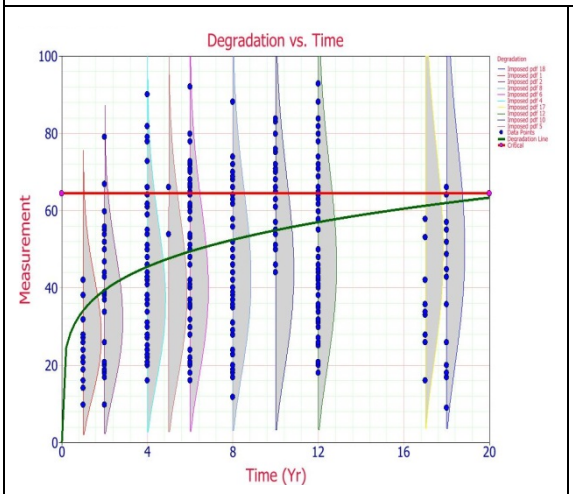	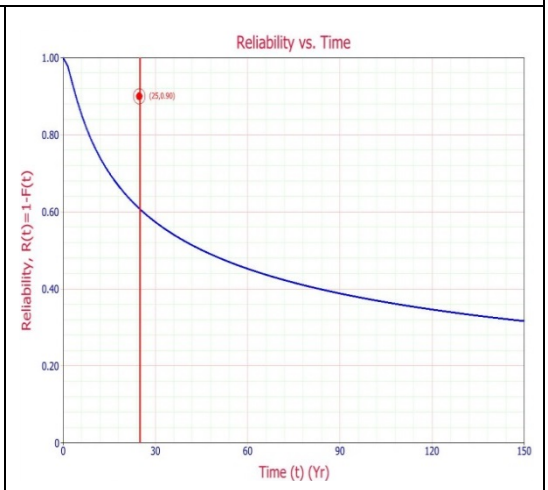
Good	W 6X9	
	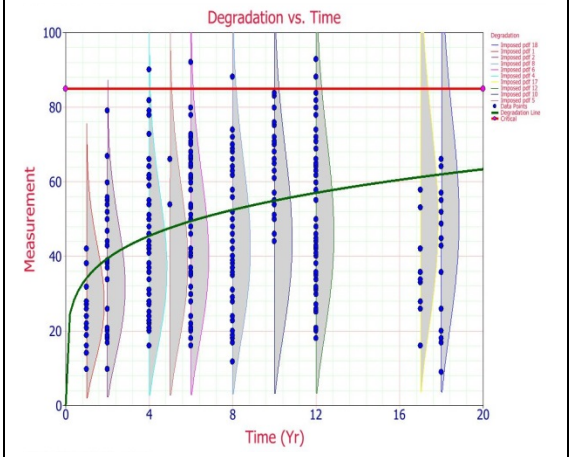	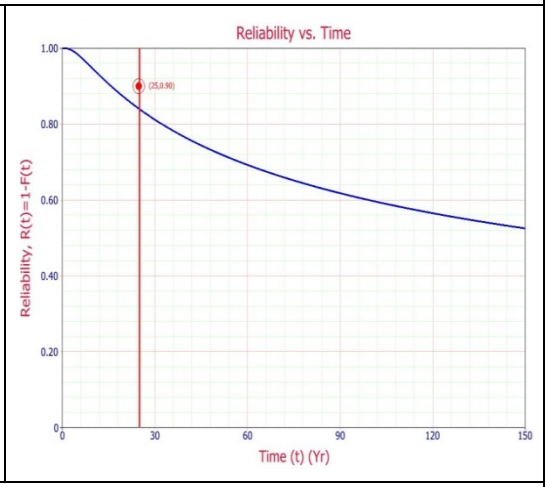
Good	W 6X12	
	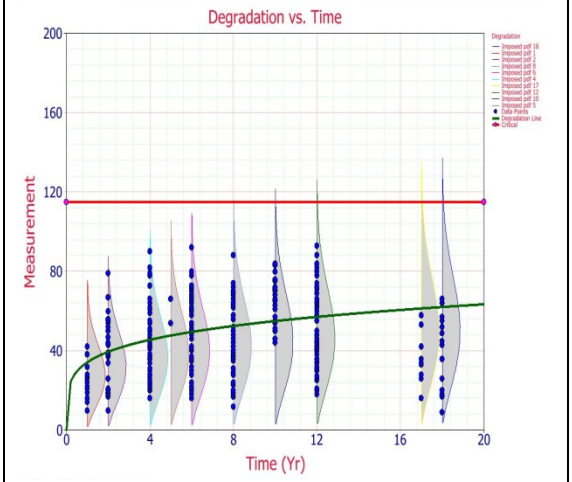	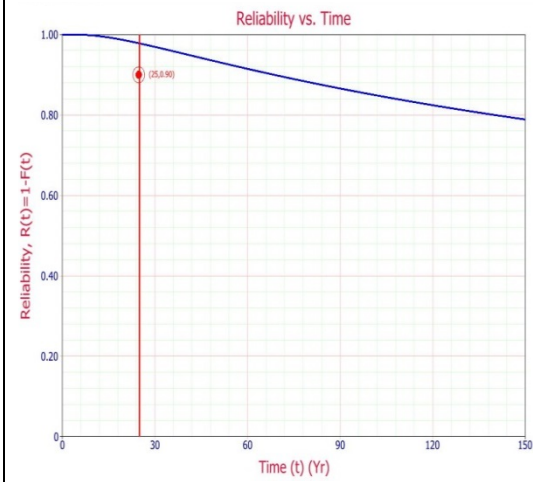

Fair	W 6X7	
	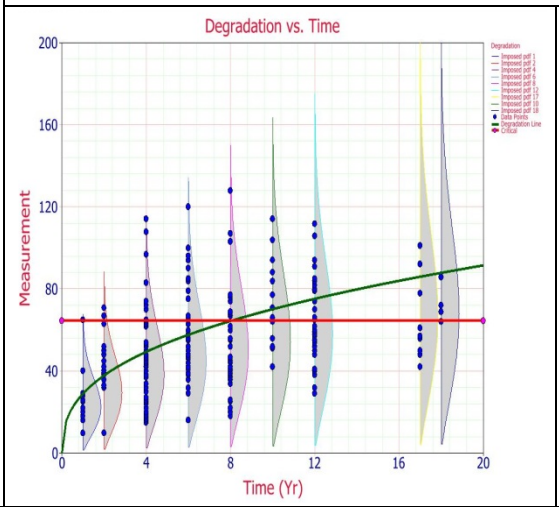	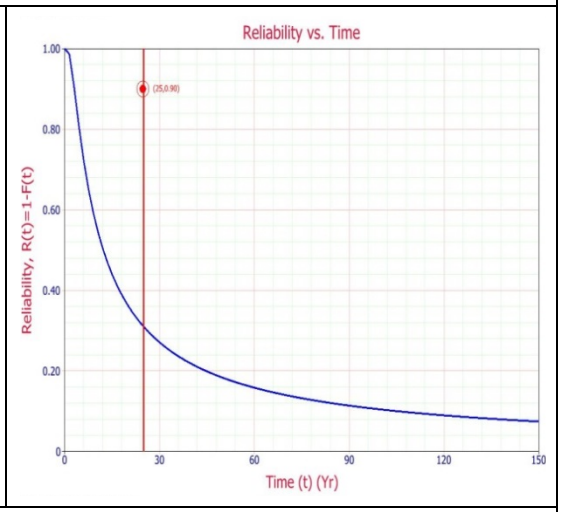
Fair	W 6X9	
	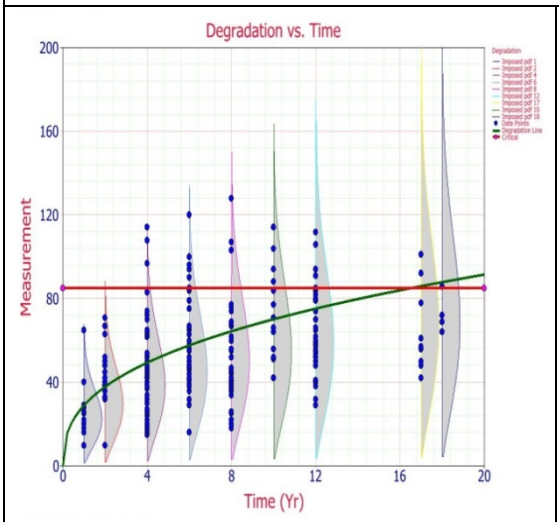	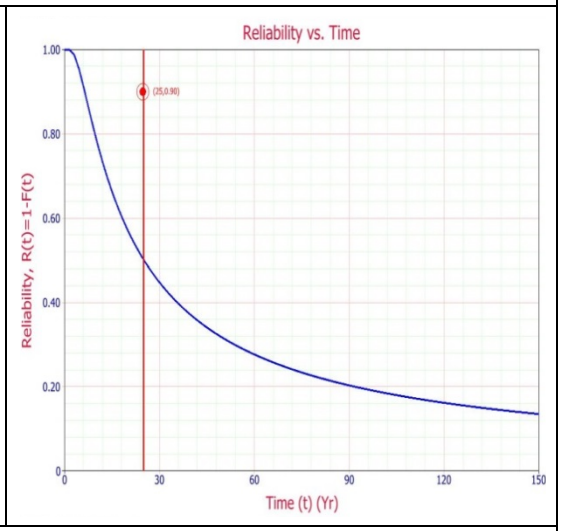
Fair	W 6X12	
	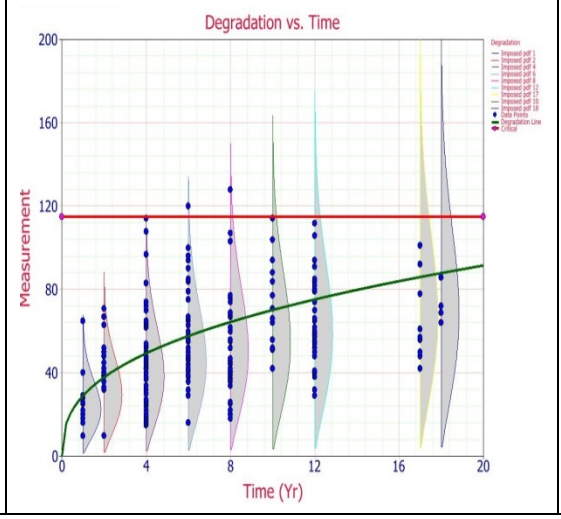	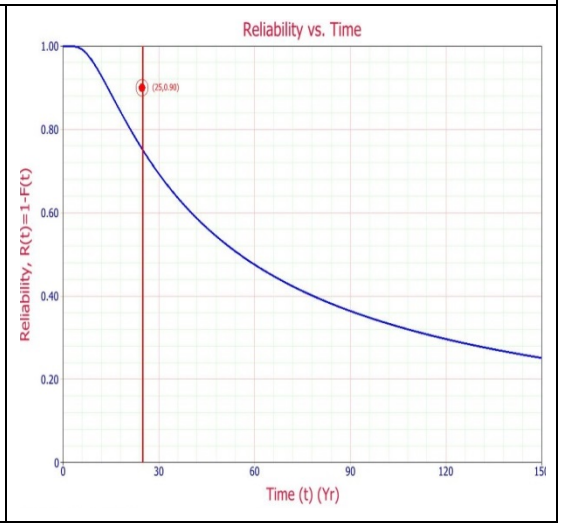

Table 39. Stochastic Models per Soil Aeration

Very Poor	W 6X7	
	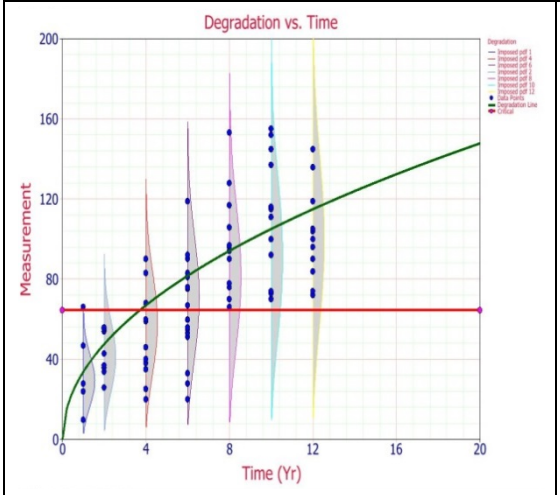	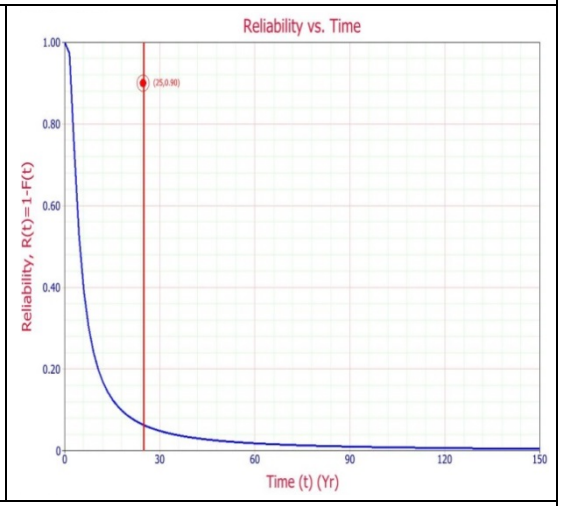
Very Poor	W 6X9	
	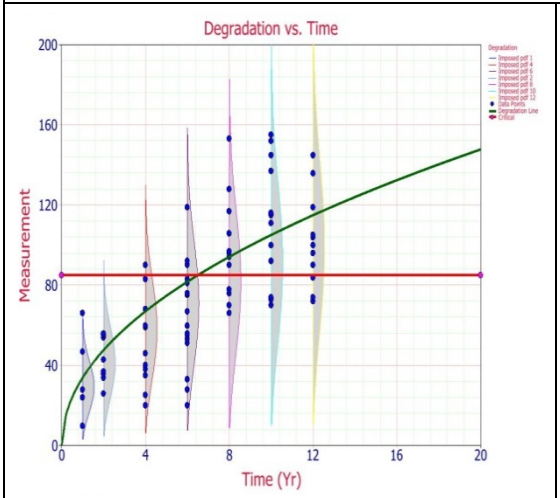	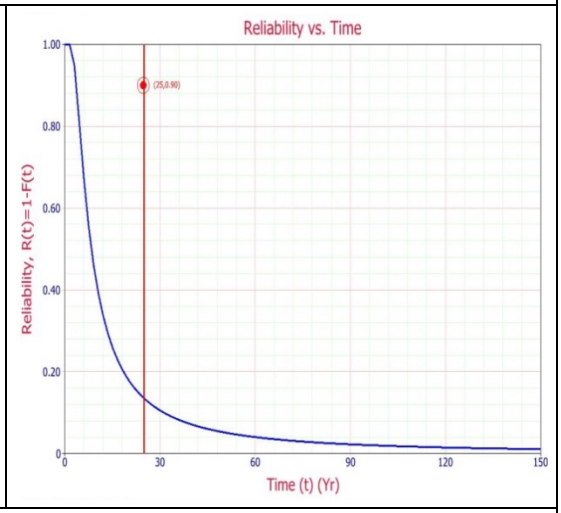
Very Poor	W 6X12	
	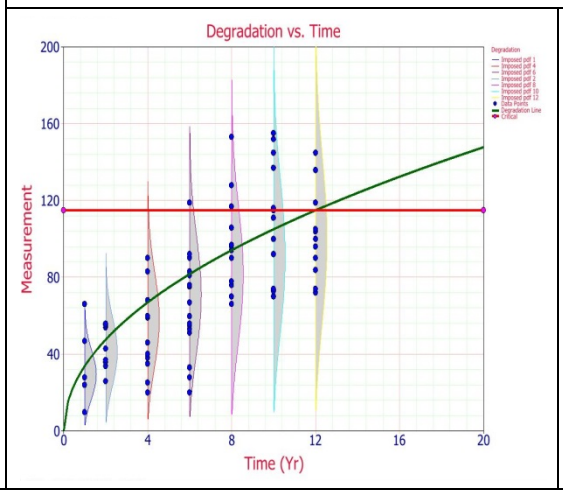	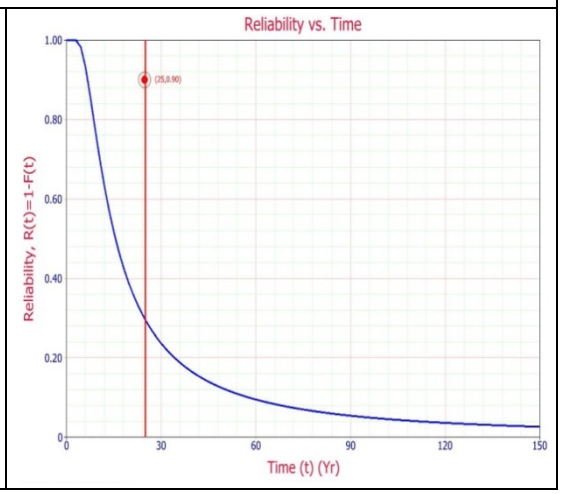

Poor	W 6X7	
	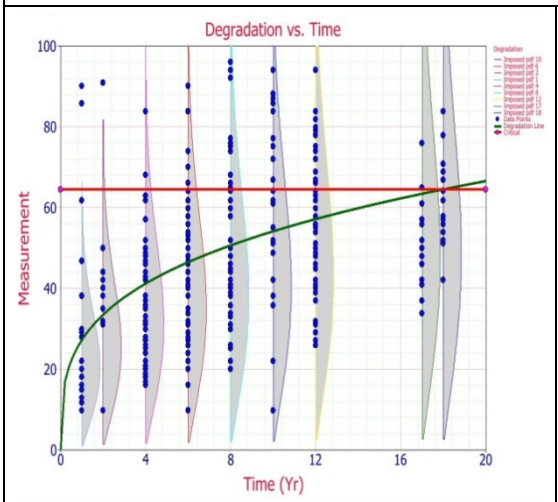	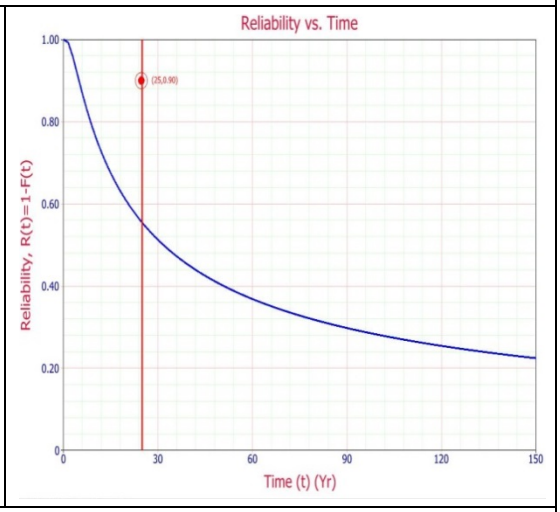
Poor	W 6X9	
	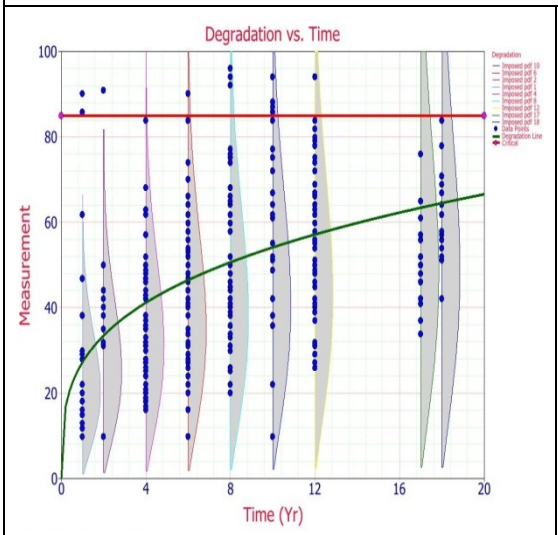	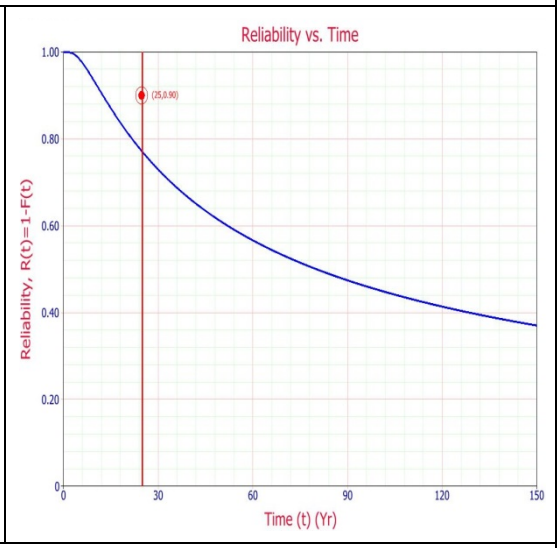
Poor	W 6X12	
	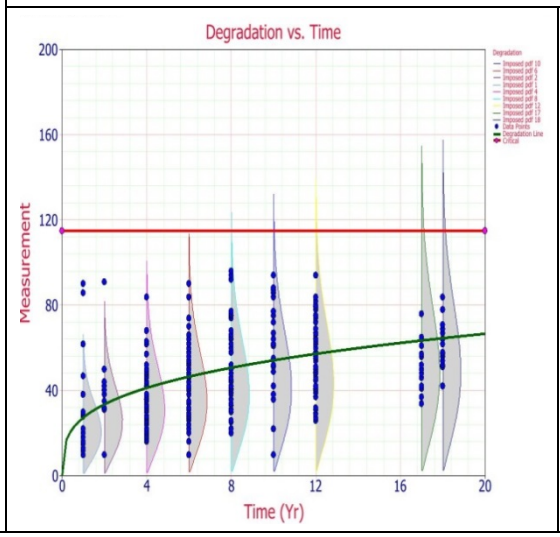	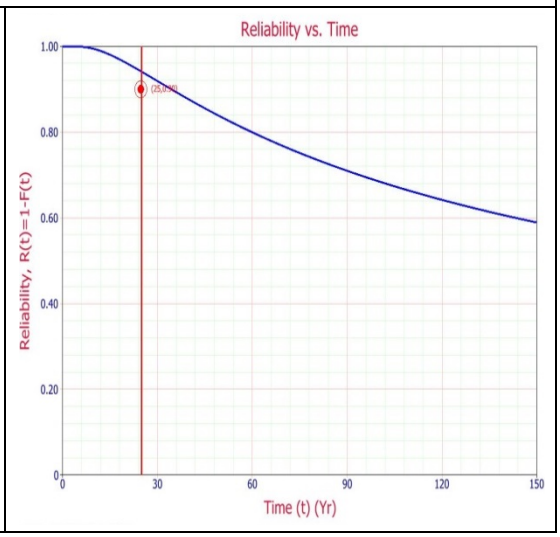

Good	W 6X7	
	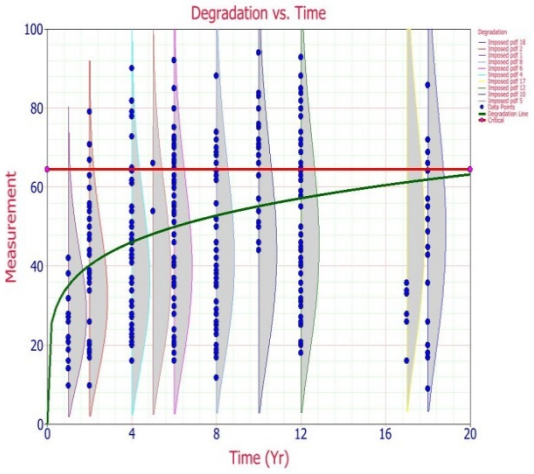	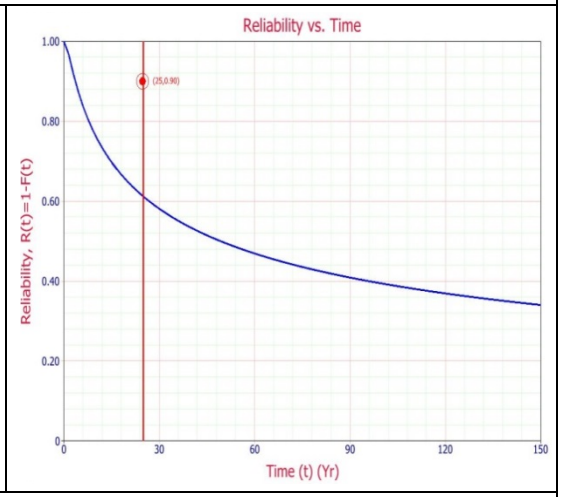
Good	W 6X9	
	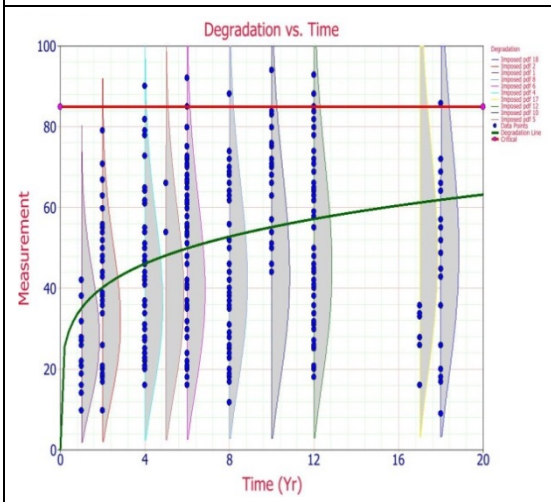	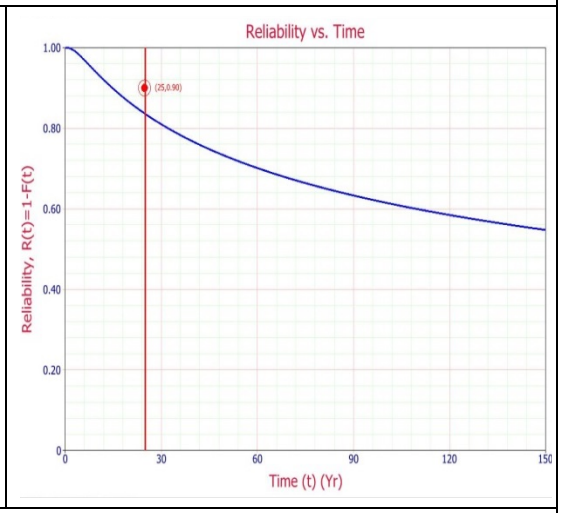
Good	W 6X12	
	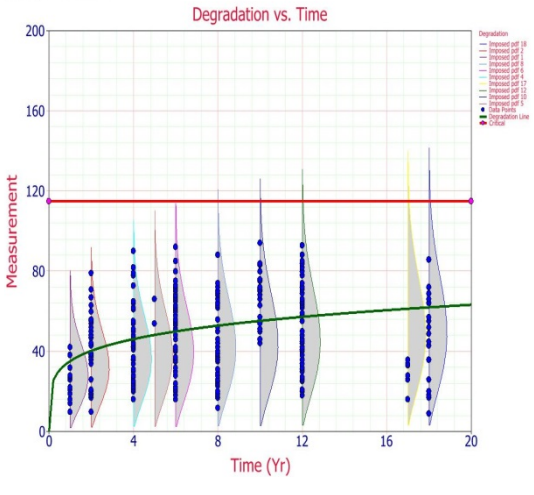	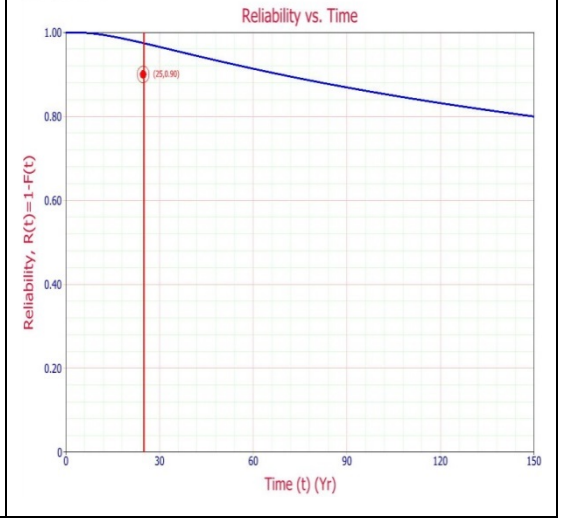

Fair	W 6X7	
	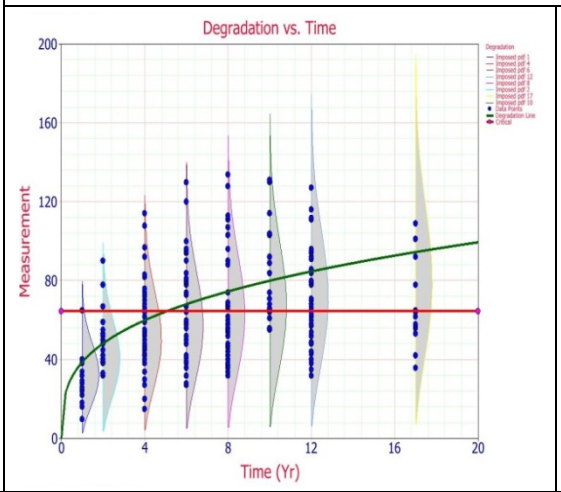	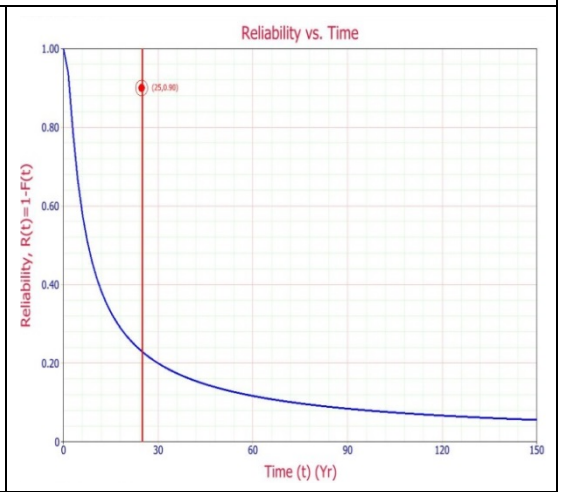
Fair	W 6X9	
	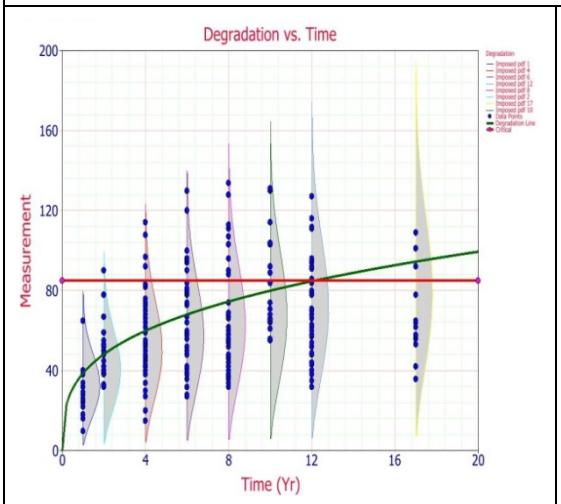	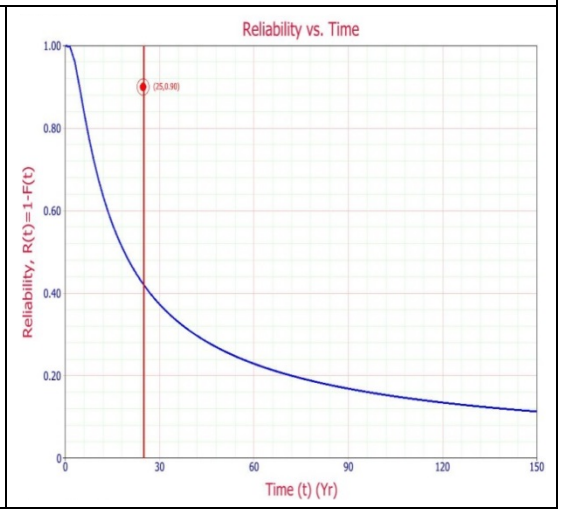
Fair	W 6X12	
	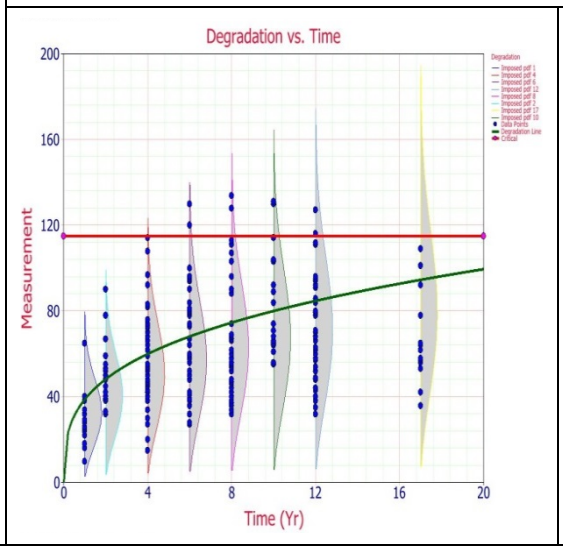	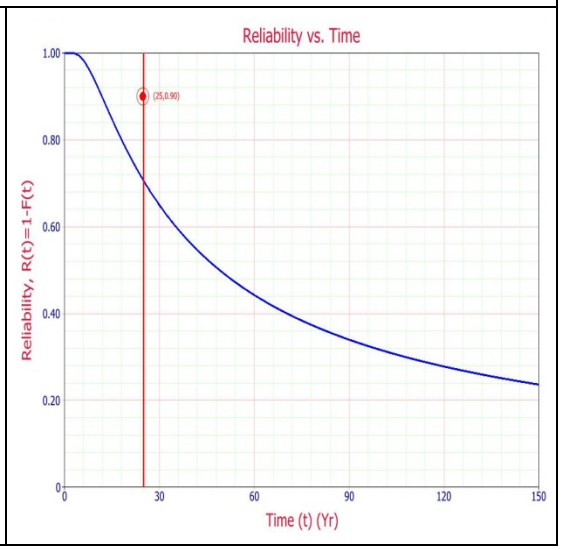

Table 40. Stochastic Models per Soil Chemical Groups

Inorganic Oxidizing Acid	W 6X7	
	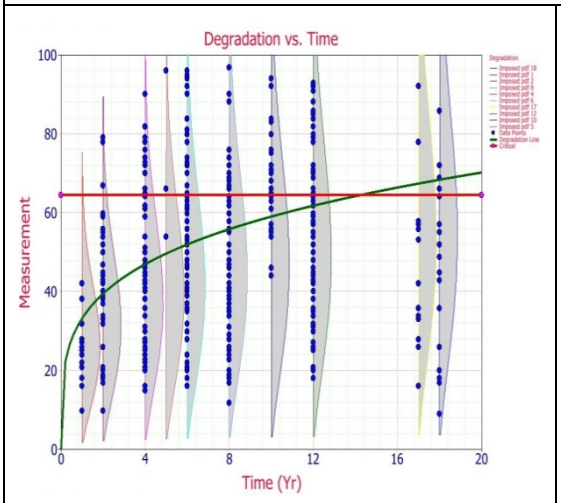	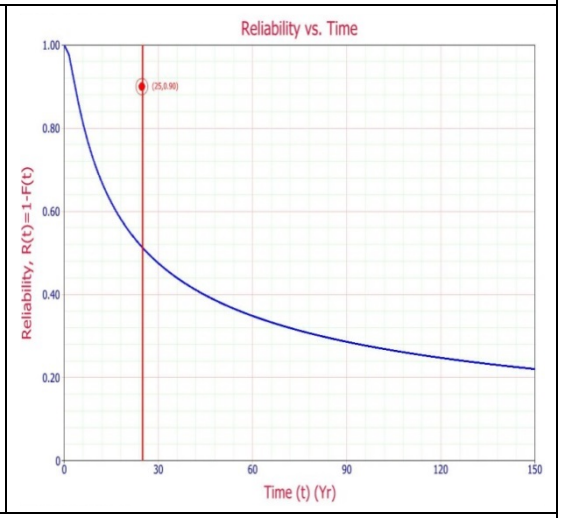
Inorganic Oxidizing Acid	W 6X9	
	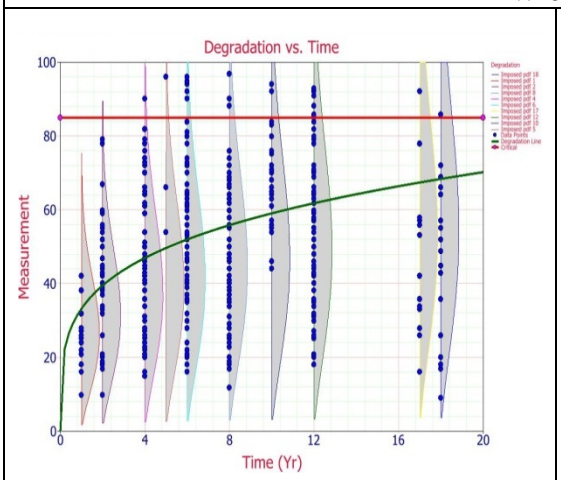	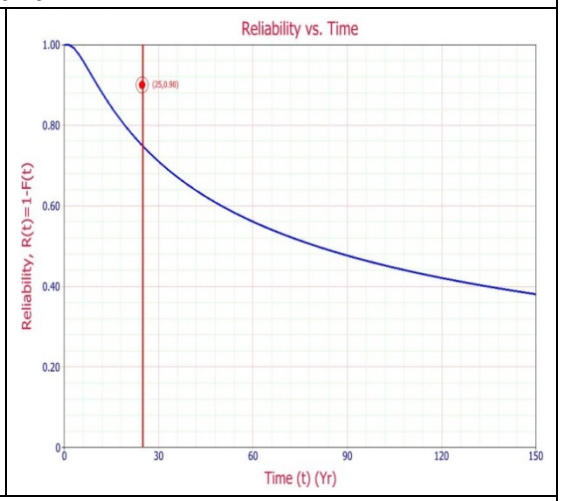
Inorganic Oxidizing Acid	W 6X12	
	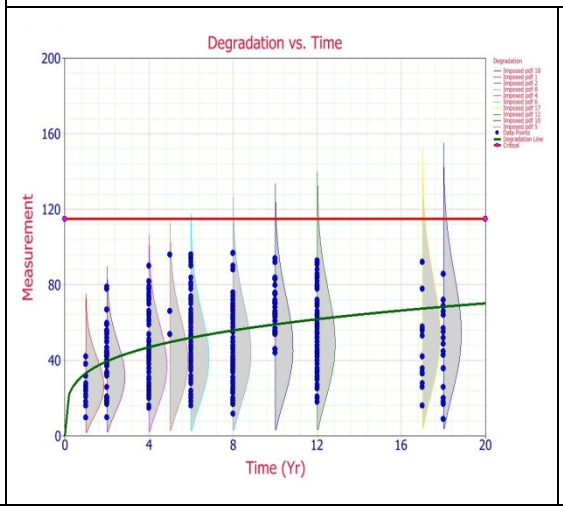	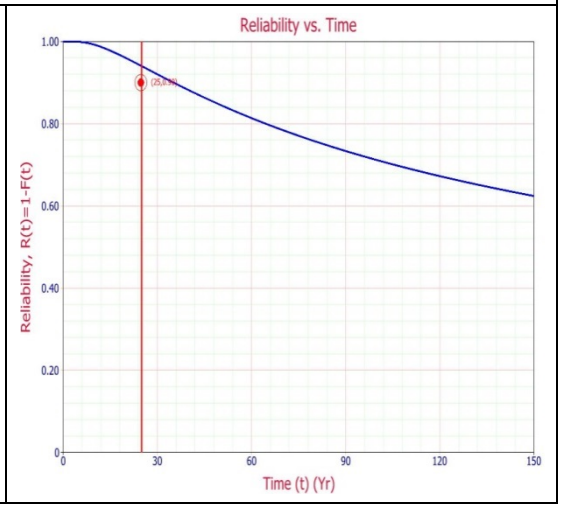

Inorganic Oxidizing Alkaline	W 6X7	
	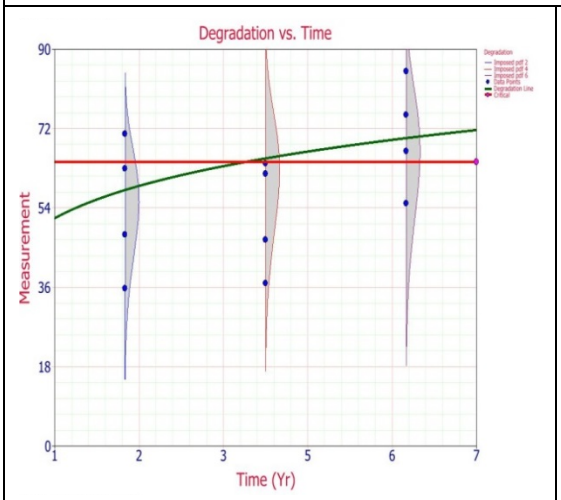	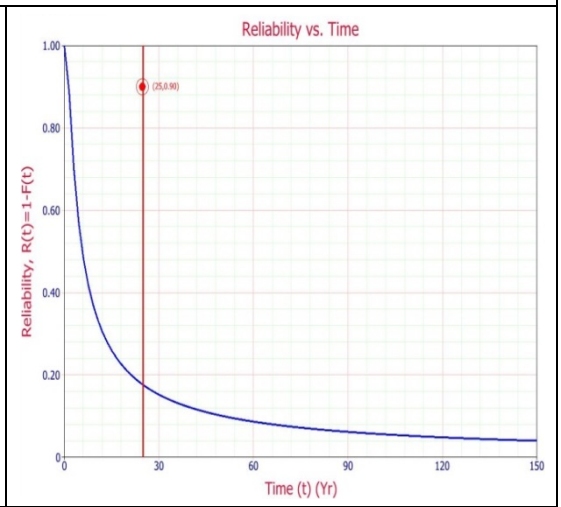
Inorganic Oxidizing Alkaline	W 6X9	
	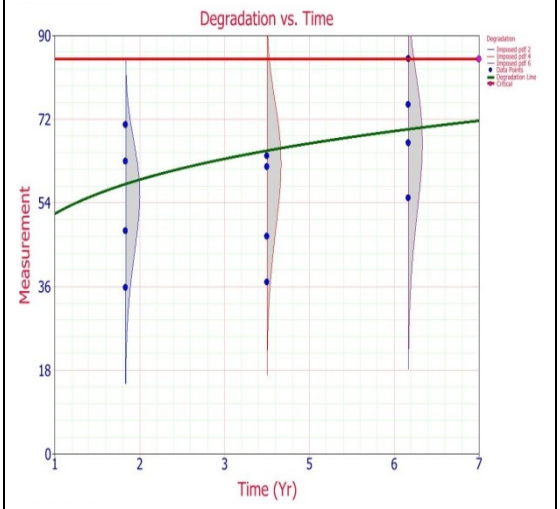	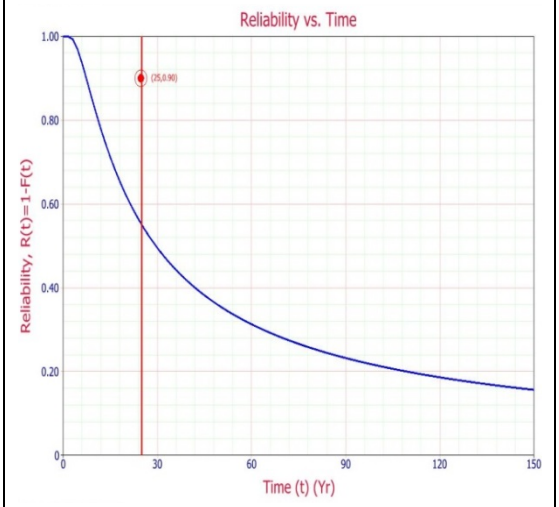
Inorganic Oxidizing Alkaline	W 6X12	
	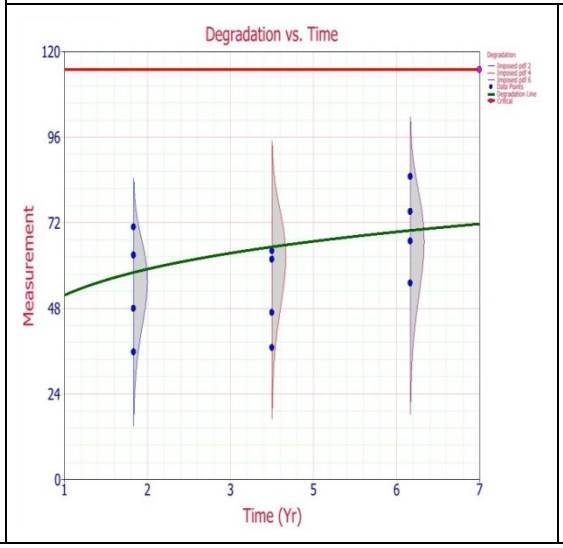	

Inorganic Reducing Acid	W 6X7	
	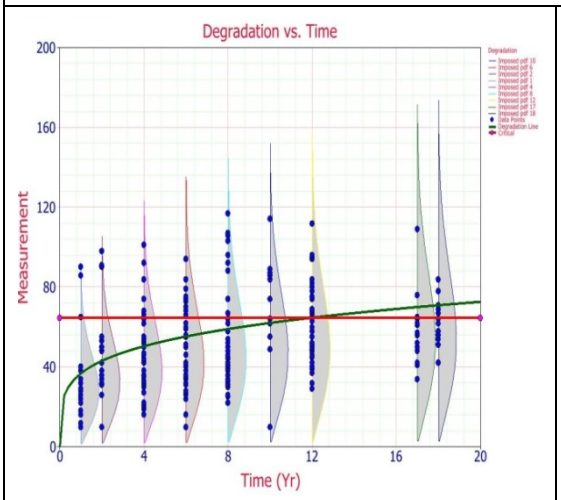	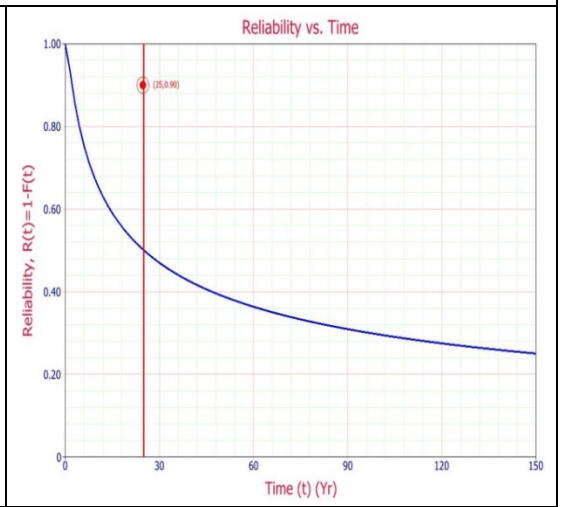
Inorganic Reducing Acid	W 6X9	
	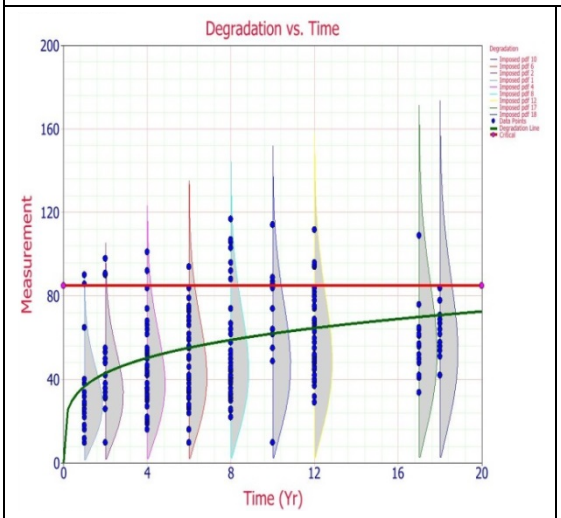	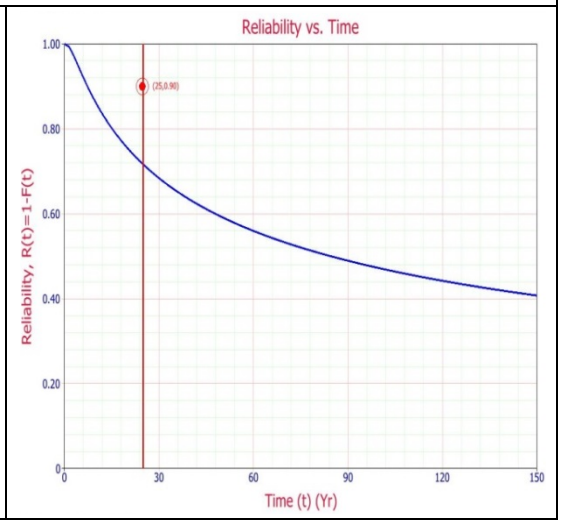
Inorganic Reducing Acid	W 6X12	
	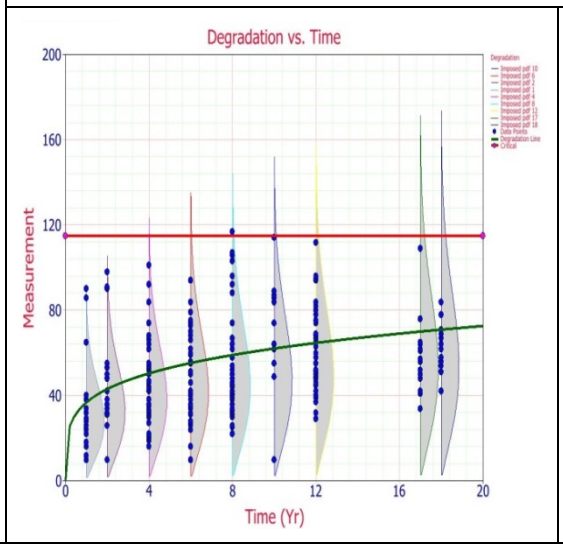	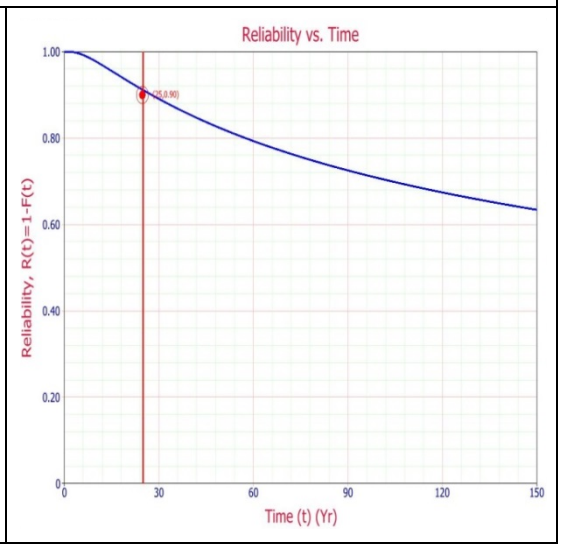

Inorganic Reducing Alkaline	W 6X7	
	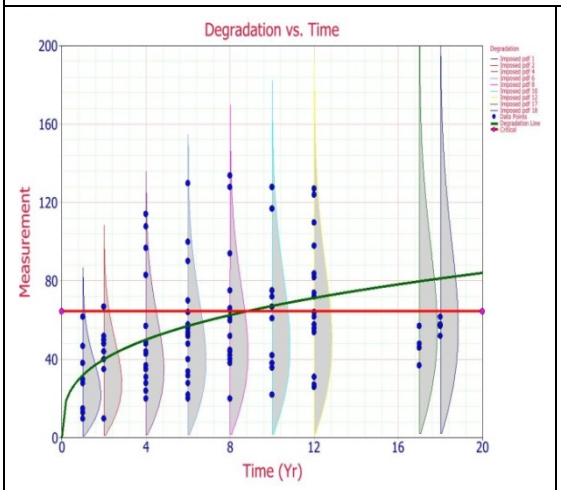	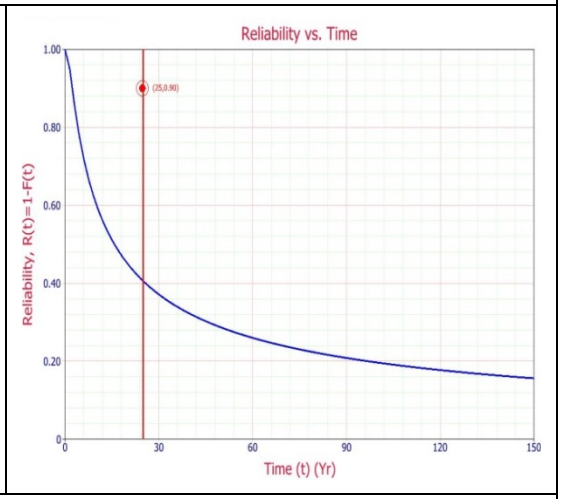
Inorganic Reducing Alkaline	W 6X9	
	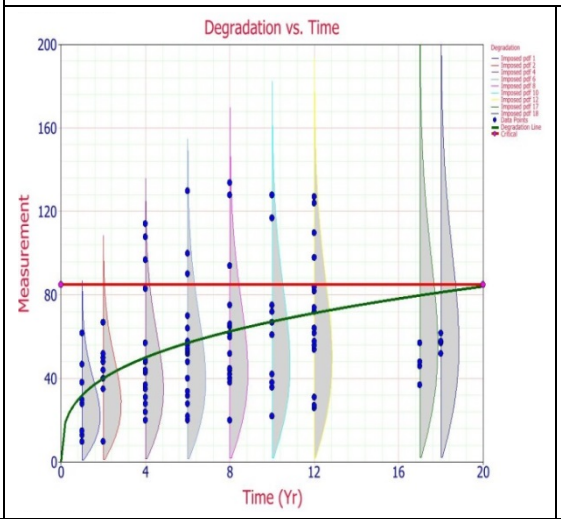	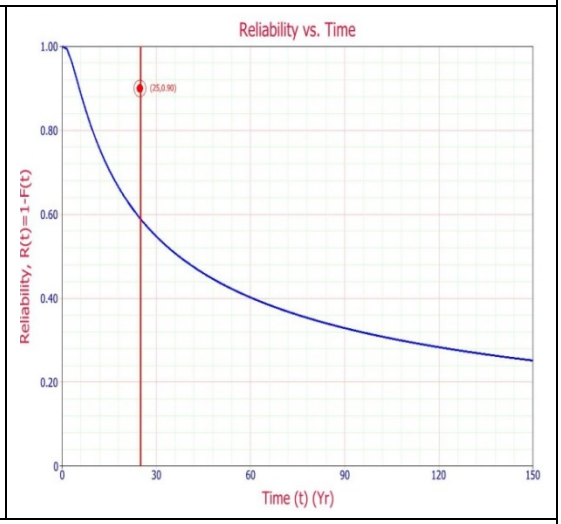
Inorganic Reducing Alkaline	W 6X12	
	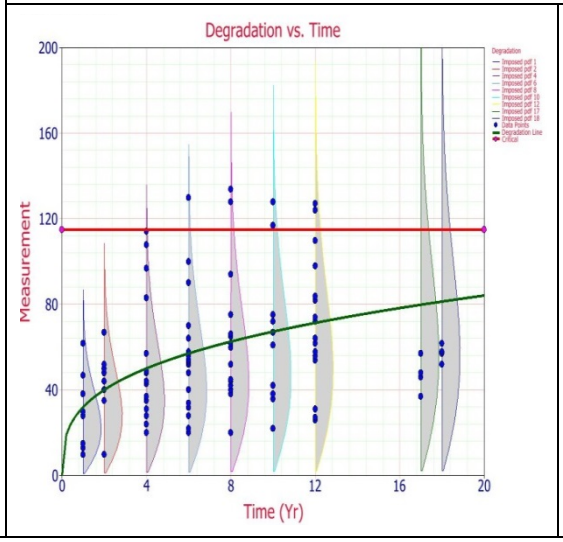	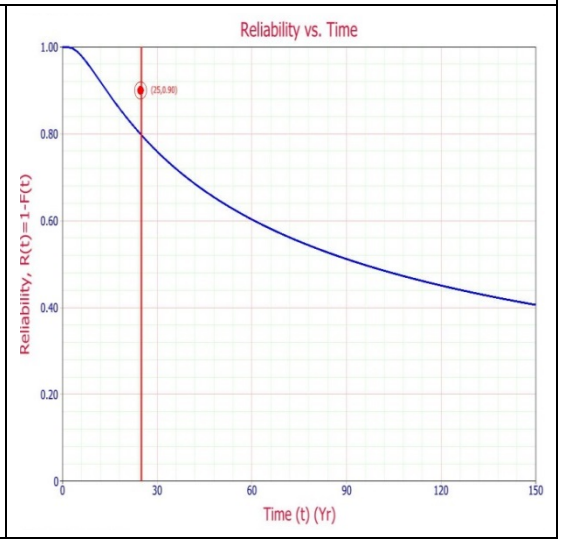

Organic Reducing Acid	W 6X7	
	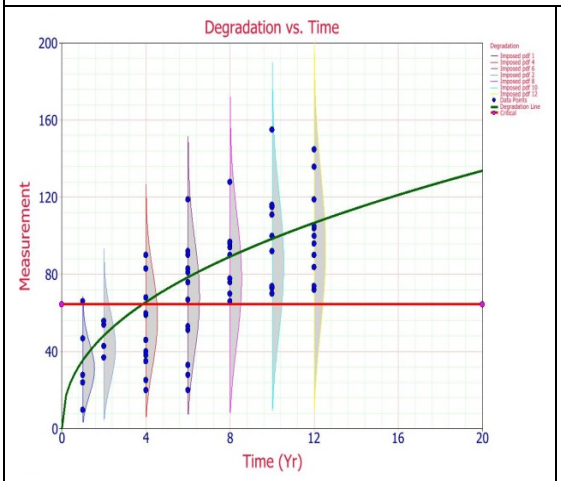	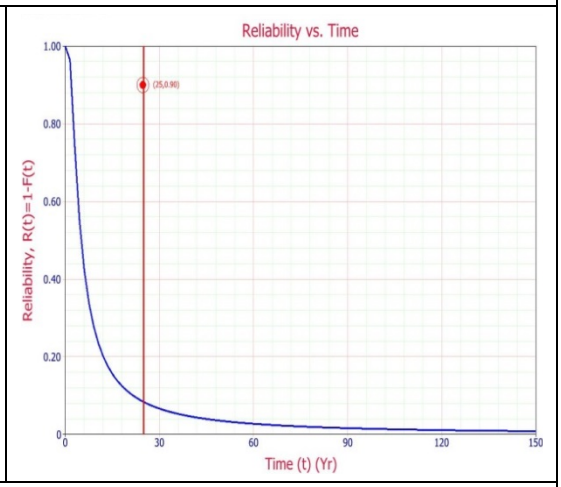
Organic Reducing Acid	W 6X9	
	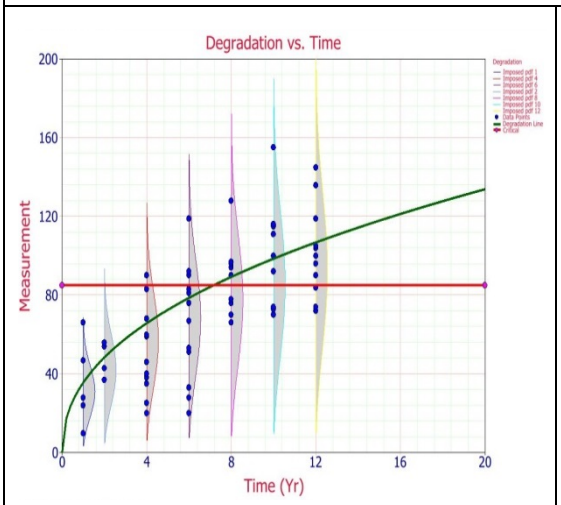	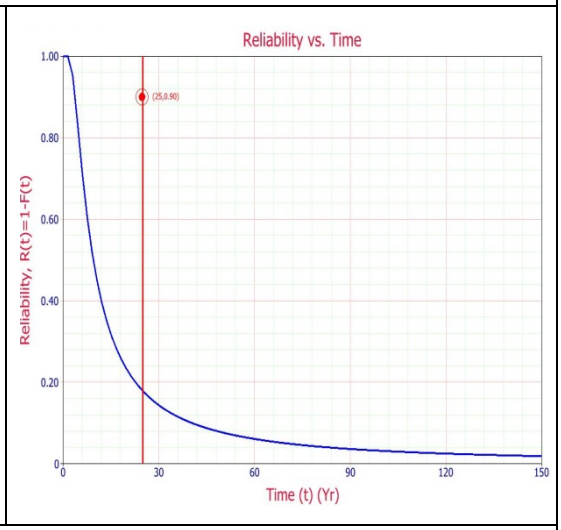
Organic Reducing Acid	W 6X12	
	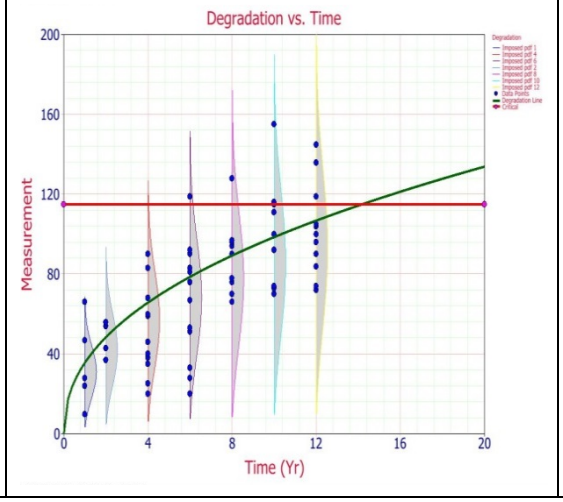	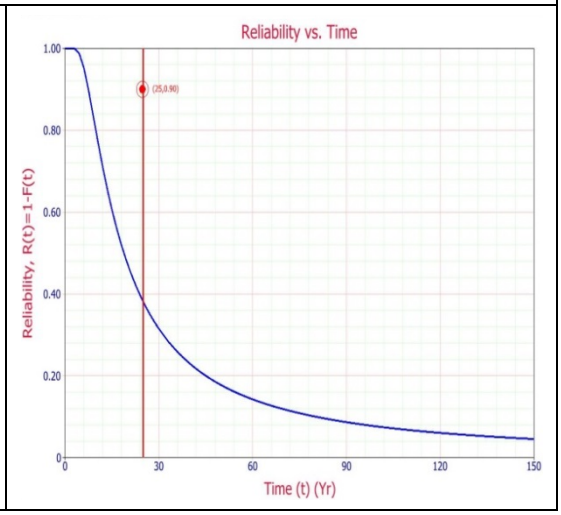

A.3. SUMMARY

In this appendix, two approaches were presented to assess the corrosion rate and the penetration depth due to underground corrosion. While the long-term corrosion rates can provide a guideline for corrosivity of a soil, the penetration depth assessed through a stochastic random process quantifies the evolution of the posts degradation over time. An analysis for the corrosion rate and penetration depth was performed for different classifications of soil and beam types.

APPENDIX B

SAMPLE SIZE CALCULATION

Power analysis is the process for determining the sample size for a research study. While there is no determinative way to determining the sample size for every research situation, power analysis involves a number of simplifying assumptions to cover all of the contingencies. This section was developed using the G*Power tool (Faul et al. 2007).

To begin, the program should be set to the F-family of tests, to a Special Multiple Regression, and to the 'A Priori' power analysis necessary to identify sample size. To complete the analysis, the following values are needed:

- The alpha level: also known as the p-value, measures the compatibility of data with the null hypothesis. A low alpha level suggests that a sample provides enough evidence that you can reject the null hypothesis for the entire population. A common value of alpha is 0.05 (Montgomery and Runger 2010).
- The power: is the conditional probability of failing to reject the null hypothesis when it is false. By convention, a power value of 0.80 or higher is desired (Ellis 2010).
- The effect size: is a quantitative measure of the correlation strength between regression coefficient. Out of the different measures of effect size, Cohen's f^2 is the most popular to use in the context of multivariate linear regression. By convention, f^2 effect sizes of 0.02, 0.15, and 0.35 correspond to *small*, *medium*, and *large*, respectively (Cohen 1988).
- The number of predictors: the total number of predictors or independent variables in the model, not including the regression constant. In our case, the predictors vary between one and five, i.e.: resistivity, pH level, redox potential, sulfates, and chlorides.

In this section, power analysis for multiple regression models with different number of predictors and assumptions are considered in order to determine the minimum required sample size of the proposed approach so the resulting model holds a minimum power of 0.80 at a confidence level of 95%.

Table 41 shows the minimum required sample sizes for:

- An alpha level of 0.05
- A power of 0.80
- Small (0.02), medium (0.15), and large (0.35) effect sizes
- Number of predictors varying between 1 and 5.

Table 41. Calculated Minimum Required Sample Sizes under Different Assumptions

Alpha level	Power	Effect size	Number of predictors	Minimum required sample size
0.05	0.80	0.02	1	395
0.05	0.80	0.02	2	485
0.05	0.80	0.02	3	550
0.05	0.80	0.02	4	602
0.05	0.80	0.02	5	647
0.05	**0.80**	**0.15**	**1**	**55**
0.05	**0.80**	**0.15**	**2**	**68**
0.05	**0.80**	**0.15**	**3**	**77**
0.05	**0.80**	**0.15**	**4**	**85**
0.05	**0.80**	**0.15**	**5**	**92**
0.05	0.80	0.35	1	25
0.05	0.80	0.35	2	32
0.05	0.80	0.35	3	36
0.05	0.80	0.35	4	40
0.05	0.80	0.35	5	43

While there is no definitive rule for the assumption to consider in power analysis, a medium effect ($f^2 = 0.15$) is the most relevant since a large effect is unrealistic for most

interventions and a small effect is often judged to be not very meaningful. Several factors impact the corrosion rate; however, an analysis of the existing data shows resistivity to explain the largest percentage of variation in corrosion rate.

APPENDIX C

ZINC QUALITY ANALYSIS

The hot-dip galvanized coating is intended for products fabricated into their final shape that will be exposed to corrosive environmental conditions. The coating grade is defined as the required thickness of the coating and is given in microns or mils. To comply with the corrosion protection guidelines, *First Solar* requires all the materials to meet the ASTM A123 specification, which provides the minimum coating thickness requirements. The specification procedure is illustrated in Figure 66 and consists of the following:

1. Select 3 random samples from each coating lot
2. Divide each sample into 3 specimen areas
3. Take 5 thickness readings on each specimen and calculate the average
4. Specimen average must be equal to one coating grade (2.6 mils) below the required grade (3 mils)
5. Sample average must be equal to coating grade (3 mils)

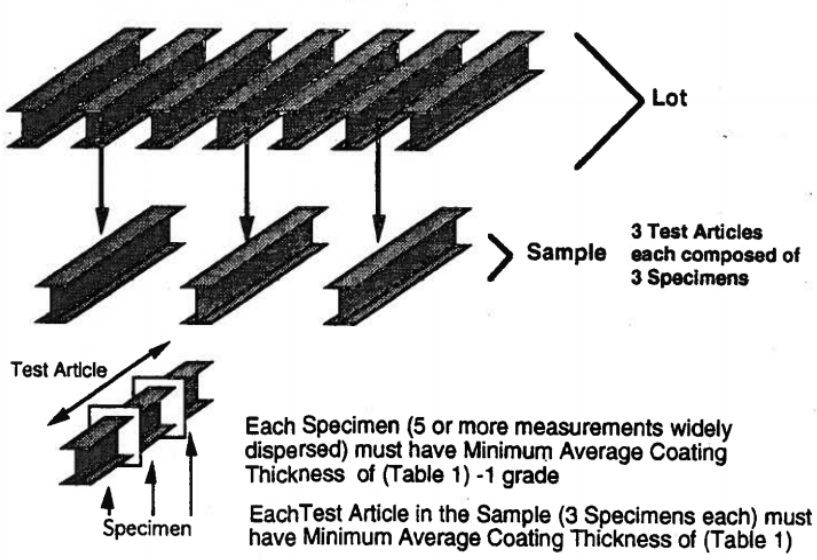

Figure 66. ASTM A123 Procedure

APPENDIX D

SUPPLIERS DATA

Table 42. Supplier # 1 Data

Criteria	PVC	LDPE	PE	HDPE	PP	PUR	Nylon	EPDM	XLPE	CPE	TPE-E	TPE-O	Teflon	Silicon Rubber	Natural Rubber
Abrasion resistance	1.5	3	2	4	2.5	5	4	3	2.5	3.5				1	
Acid resistance	3.5	3.5	3.5	4	4	2	2.5	3.5	3.5	3				2.5	
Alcohol resistance	3.5	4	4	4	4	2	1	1	4	3.5				3	
Alkali resistance	3.5	3.5	3.5	4	4	2	4	3.5	3.5	3				2.5	
Benzol resistance	1.5	1	1	1	1.5	2	3	2	2	2				1	
Degreaser solvents	1.5	3	3	3	1	2	3	1	2	1				2	
Electrical properties	2.5	4	4	4	4	1	1	4	4	2.5				3	
Flame resistance	4	1	1	1	1	1	1	1	1	3				2.5	
Gasoline resistance	1	3.5	3	3.5	1.5	2	3	1	2	2				1.5	
Heat resistance	3.5	3	3	4	4	3	4	4	3	4				5	
Low temperature flexibility	1.5	4	4	4	1	3	3	3.5	5	2				5	
Nuclear radiation resistance	2	3.5	3	3.5	2	2	3	3	4	3				4	
Oil resistance	2	3.5	3	3.5	2	4	4	1	3	3.5				2.5	
Oxidation resistance	4	4	4	4	4	4	4	4	4	4				4	
Ozone resistance	4	4	4	4	4	4	4	4	3	3.5				5	
Underground burial	1.5	3	2	4	4	3	1	4	4	4				3	
Water resistance	2.5	4	4	4	4	2	1.5	3.5	3.5	3.5				3.5	
Weather, sun resistance	3.5	4	4	4	4	3	4	4	3	4				5	

Legend: *1: Poor 2: Fair 3: Good 4: Excellent 5: Outstanding*

Table 43. Supplier # 2 Data

Criteria	PVC	LDPE	PE	HDPE	PP	PUR	Nylon	EPDM	XLPE	CPE	TPE-E	TPE-O	Teflon	Silicon Rubber	Natural Rubber
Abrasion resistance								3.5						1	
Acid resistance								3						2.5	
Alcohol resistance															
Alkali resistance															
Benzol resistance															
Degreaser solvents															
Electrical properties								3						3	
Flame resistance								1						2	
Gasoline resistance								1						2.5	
Heat resistance								4						4	
Low temperature flexibility								3.5						4	
Nuclear radiation resistance															
Oil resistance								1						2.5	
Oxidation resistance															
Ozone resistance								1						4	
Underground burial															
Water resistance								4						2.5	
Weather, sun resistance								4						4	

Legend: *1: Poor 2: Fair 3: Good 4: Excellent 5: Outstanding*

Table 44. Supplier # 3 Data

Criteria	PVC	LDPE	PE	HDPE	PP	PUR	Nylon	EPDM	XLPE	CPE	TPE-E	TPE-O	Teflon	Silicon Rubber	Natural Rubber
Abrasion resistance	3		3		4	4	4				4	4	4	2	
Acid resistance															
Alcohol resistance	1		3		3	3	4				2	2	4	3	
Alkali resistance															
Benzol resistance															
Degreaser solvents															
Electrical properties															
Flame resistance															
Gasoline resistance	1		3		3	3	3				1	1	4	3	
Heat resistance															
Low temperature flexibility															
Nuclear radiation resistance															
Oil resistance															
Oxidation resistance	4		1		1	1	1				3	3	4	2	
Ozone resistance															
Underground burial															
Water resistance															
Weather, sun resistance	4		4		4	4	4				4	4	4	4	

Legend: *1: Poor 2: Fair 3: Good 4: Excellent 5: Outstanding*

Table 45. Supplier # 4 Data

Criteria	PVC	LDPE	PE	HDPE	PP	PUR	Nylon	EPDM	XLPE	CPE	TPE-E	TPE-O	Teflon	Silicon Rubber	Natural Rubber
Abrasion resistance	2.5	3	1	4	2.5	5	4			4.5			4		
Acid resistance	3.5	3.5	3.5	4	4	2	1.5			4			4		
Alcohol resistance	1.5	4	4	4	4	2	1			4			4		
Alkali resistance	3.5	3.5	3.5	4	4	2	4			4			4		
Benzol resistance	1.5	1	1	1	1.5	2	3			3.5			4		
Degreaser solvents	1.5	3	3	3	1	2	3			4			4		
Electrical properties	2.5	4	4	4	4	1	1			4			4		
Flame resistance	4	1	1	1	1	1	1			4			5		
Gasoline resistance	1	3.5	3	3.5	1.5	2	3			4			4		
Heat resistance	3.5	3	3	4	4	3	4			4			5		
Low temperature flexibility	2	4	4	4	1	3	3			4			5		
Nuclear radiation resistance	2	3.5	3	3.5	2	3	2.5			5			2		
Oil resistance	2	3.5	3	3.5	2	4	4			4			5		
Oxidation resistance	4	4	4	4	4	4	4			4			5		
Ozone resistance	4	4	4	4	4	4	4			4			4		
Underground burial	2	3	3	4	3	3	1			4.5			4		
Water resistance	2.5	4	4	4	4	2	1.5			5			4		
Weather, sun resistance	3.5	4	4	4	4	3	4			4			5		

Legend: *1: Poor 2: Fair 3: Good 4: Excellent 5: Outstanding*

Table 46. Supplier # 5 Data

Criteria	PVC	LDPE	PE	HDPE	PP	PUR	Nylon	EPDM	XLPE	CPE	TPE-E	TPE-O	Teflon	Silicon Rubber	Natural Rubber
Abrasion resistance	2.5			4	2.5			3.5	2.5	3.5	5	5			
Acid resistance	3.5			4	4			3.5	3.5	4	2	2			
Alcohol resistance	3.5			4	4			1	4	3.5	2	2			
Alkali resistance															
Benzol resistance															
Degreaser solvents															
Electrical properties	2.5			4	4			4	4	2.5	1	1			
Flame resistance	4			1	1			1	1	3	1	1			
Gasoline resistance	1			3.5	1.5			1	2	2	2	2			
Heat resistance	3.5			4	4			4	3	5	3	3			
Low temperature flexibility	2			4	1			3.5	5	2	3	3			
Nuclear radiation resistance															
Oil resistance	2			3.5	2			1	3	3.5	4	4			
Oxidation resistance	4			4	4			4	4	4	4	4			
Ozone resistance	4			4	4			4	3	3.5	4	4			
Underground burial															
Water resistance	2.5			4	4			3.5	3.5	3.5	2	2			
Weather, sun resistance	3.5			4	4			4	3	4	3	3			

Legend: *1: Poor 2: Fair 3: Good 4: Excellent 5: Outstanding*

Table 47. Supplier # 6 Data

Criteria	PVC	LDPE	PE	HDPE	PP	PUR	Nylon	EPDM	XLPE	CPE	TPE-E	TPE-O	Teflon	Silicon Rubber	Natural Rubber
Abrasion resistance	2.5	3	2	4	2.5	5	4	3	2.5	4.5	4	2	3.5	2	4
Acid resistance	3.5	3.5	3.5	4	4	2	1.5	3.5	3.5	4	2	3	4	2.5	2.5
Alcohol resistance	1.5	4	4	4	4	1.5	1	1	4	4.5	4.5	4.5	4	3	3
Alkali resistance	3.5	3.5	3.5	4	4	2	4	3.5	3.5	4	2	3	4	2.5	2.5
Benzol resistance															
Degreaser solvents															
Electrical properties															
Flame resistance	4	1	1	1	1	1	1	1	2.5	4	2	2.5	5	2.5	1
Gasoline resistance															
Heat resistance	3.5	3	3	4	4	3	4	4	3	4	4	4	5	5	2
Low temperature flexibility	1.5	4	4	4	1	3	3	3.5	5	4	4	4	5	5	3
Nuclear radiation resistance															
Oil resistance	2	3.5	3	3.5	2	4	4	2	3	4	4	2	5	2.5	1
Oxidation resistance	4	4	4	4	4	4	4	3	4	4	4	4	5	4	2
Ozone resistance	4	4	4	4	4	4	4	4	4	4	4	4	4	5	1
Underground burial															
Water resistance	2.5	4	4	4	4	2.5	1.5	3.5	3.5	4	4	4	4	3.5	3.5
Weather, sun resistance	3.5	4	4	4	4	3	4	4	3	4	4	4	5	5	2

Legend: *1: Poor 2: Fair 3: Good 4: Excellent 5: Outstanding*